TEAR FILM STRUCTURE OF THE CONTACT LENS WEARER

BY

JEAN-PIERRE CHARLES FRANÇOIS GUILLON

A THESIS SUBMITTED FOR THE DEGREE

OF DOCTOR OF PHILOSOPHY

THE CITY UNIVERSITY, LONDON

DEPARTMENT OF OPTOMETRY
AND VISUAL SCIENCE
CITY UNIVERSITY
LONDON

DEPARTMENT OF CONTACT
LENSES AND PROSTHESIS
MOORFIELDS EYE HOSPITAL
LONDON

OCTOBER 1987

A MES PARENTS

POUR AVOIR FAÇONNE MES RÊVES

D'UNE SI BELLE MANIERE

CONTENTS

LIST OF ILLUSTRATIONS 6

LEGEND OF TABLES 15

ACKNOWLEDGEMENTS 17

DECLARATION 18

ABSTRACT 19

CHAPTER 1 20

INTRODUCTION

CHAPTER 2 23

THE FUNCTION AND STRUCTURE AND STABILITY

OF THE PRE-OCULAR TEAR FILM

2.1 - Functions of the Tear Film 23

2.2 - The Lacrimal System 31

2.3 - Innervation of the Lacrimal System 48

2.4 - Basal Tear Film Physical Characteristics 52

2.5 - The Tear Film Structure 59

2.6 - Corneal Epithelium Wetting 70

2.7 - Stability of the Tear Film 72

CHAPTER 3 82

CURRENT CLINICAL TECHNIQUES TO STUDY THE TEAR FILM

3.1 - Introduction 82

3.2 - Biomicroscopical Examination 82

3.3 - Use of Staining Agents 96

CHAPTER 4 102

THE CONTACT LENS INTERACTION WITH THE TEAR FILM

4.1 - Introduction 102

4.2 - Physical Effect of the Contact Lens on the Tear Film 103

4.3 - Changes in the Tear Film and on Lacrimation 107

4.4 - Wetting of a Contact Lens Surface 110

4.5 - Effect of Soft Lenses on the Tear Film 114

4.6 - Conclusion 117

CHAPTER 5 119

EXPERIMENTAL ARRANGEMENT TO OBSERVE AND PHOTOGRAPH THE PRE-CORNEAL, PRE-LENS TEAR FILM AND CORNEAL SURFACE

5.1 -. Introduction 119

5.2 - High Magnification Photography Instrumental Arrangement 121

5.3 - Low Magnification Instrumental Arrangement 132

5.4 - Instrumentation for Observation and Photography of the Mucous Layer on the Cornea and Contact Lenses 143

5.5 - Methods of Examination 154

CHAPTER 6 161

METHOD FOR THE MEASUREMENT OF TEAR FILM THICKNESS AND ITS CONSTITUENT PHASES

6.1 - Wave Theory of Light 161

6.2 - Conditions of Interference 162

6.3 - Thickness Measurement By Interferometry 176

6.4 - Application To The Experimental Technique 204

CHAPTER 7 231

EXPERIMENTAL RESULTS AND ANALYSIS

7.1 - Experimental Study 1: Pre Ocular Tear Film Lipid Layer 231

7.2 - Experimental Study 2: Pre-Soft Lens Tear Film 257

7.3 - Experimental Study 3: Pre-Rigid Contact Lens Tear Film 266

7.4 - Experimental Study 4: Mucous Layer Photography On The Corneal And On Contact Lens Surfaces 316

CHAPTER 8 331

DISCUSSION

8.1 - Experimental Study 1: Pre-Ocular Tear Film Lipid Layer 331

8.2 -. Lipid Thickness And Structure Evaluation 338

8.3 - Experimental Study 2: Pre-Soft Lens Tear Film 341

8.4 - Experimental Study 3: Pre-Rigid Contact Lens Tear Study 346

8.5 - Experimental Study 4: Mucous Layer Photography On The Corneal And On Contact Lens Surfaces 351

CHAPTER 9 358

CONCLUSION

LIST OF ILLUSTRATIONS

CHAPTER TWO

Fig 2.1 : Concentration of Oxygen in the Cornea: Open Eye Situation

Fig 2.2 : Concentration of Oxygen and Carbon Dioxide in the Cornea: Closed Eye Situation

Fig 2.3 : Tentative Mechanism for Removal of Lipid Contaminated Mucous Layer

Fig 2.4 : Sites of Origin of Tear Film Components

Fig 2.5 : Diagrammatic Representation of Secretory Glands in the Human Eye Lid

Fig 2.6 : Rigidity of Surface Over Lacrimal Prism

Fig 2.7 : Schematic Diagram of the Tear Film Boundary

Fig 2.8 : Lacrimal Drainage System

Fig 2.9 : The Post-ganglionic Pathway of Parasympathetic Lacrimal Secreto-motor Neurons

Fig 2.10 : Trilaminar Structure of the Pre-corneal Tear Film

Fig 2.11 : Mechanism of Dry Spot Formation

Fig 2.12 : Meniscus Induced Thinning of Tear Film

CHAPTER FIVE

Fig 5.1 : Nikon AS-1 Non-Contact Endothelial Camera

Fig 5.2 : Schematic Representation of the High Magnification Illumination and Observation System

Fig 5.3 : Illumination System for the High Magnification Experimental Set-up

Fig 5.4 : Observation System for the High Magnification Experimental Set-up

Fig 5.5 : Outline of Fringes for Analysis of Photographs

Fig 5.6 : Illumination System for the Low Magnification Experimental Set-up: Frontal View

Fig 5.7 : Illumination System for the Low Magnification Experimental Set-up: Lateral View

Fig 5.8 : Clinical Arrangement of the Low Magnification Experimental Set-up: Naked Eye Observation

Fig 5.9 : Clinical Arrangement of the Low Magnification Experimental Set-up: Slit-lamp Observation

Fig 5.10 : Cross-section Arrangement of Low Magnification Photography Set-up

Fig 5.11 : Clinical Arrangement of the Low Magnification Photography

Fig 5.12 : Scleral Lens for Mucous Observation: Frontal View

Fig 5.13 : Scleral Lens for Mucous Observation: Cross-section

Fig 5.14 : Scleral Lens for Mucous Observation: Clinical Set-up

Fig 5.15 : Nikon Bio-differential Interference Microscope

Fig 5.16 : Schematic optical system of Nikon bio-differential Interference Microscope

CHAPTER SIX

Fig 6.1 : Propagation of Wave Motion

Fig 6.2 : Destructive Interference of Two Identical Beams in Opposition of Phase

Fig 6.3 : Optical Arrangements to produce Young's 'Wavefront Splitting' Interference

Fig 6.4 : Effect of the Position of the Screen on the Shape of the Interference Pattern

Fig 6.5 : Interference Fringe Formation by a Parallel Sided Plate in Air

Fig 6.6 : Measurement of Path Difference in a Parallel Sided Plate

Fig 6.7 : Interference Fringe Formation by Reflection in a Thin Wedge

Fig 6.8 : Optical Layout of Newton's Ring in Air

Fig 6.9 : Interference Fringes in White Light: Production of White Continuum

Fig 6.10 : Spectral Composition of White Continuum

Fig 6.11 : Diagrammatic Representation of Interference Order Overlap in White Light

Fig 6.12 : Width of a Spectral Line

Fig 6.13 : The Effect of Imperfect Monochromatism of Light on the Interference Pattern

Fig 6.14 : Spectral Distribution of the Strobe Light Source

Fig 6.15 : Width of Principal Peak $\Delta\lambda_0$ of Strobe Light Source

Fig 6.16 : Distribution and Spread of Interference Fringes overlap with Increasing Layer Thickness

Fig 6.17 : Production of White Continuous Background by Main Band of Emission of Light Source

Fig 6.18 : Variation of Reflectivity with Thin Film Structures: Lipid Layer

Fig 6.19 : Variation of Reflectivity with Thin Film Structures: Aqueous Phase

CHAPTER SEVEN

Fig 7.1 : Pre-ocular Tear Film Marmoreal Lipid Pattern:
Original Magnification (x9.6)
Photograph Magnification (≈95)

Fig 7.2 : Pre-ocular Tear Film Marmoreal Lipid Pattern:
Original Magnification (x32)
Photograph Magnification (≈300)

Fig 7.3 : Pre-ocular Tear Film Contaminated Lipid
Pattern: Original Magnification (x9.6)
Photograph Magnification (≈95)

Fig 7.4 : Pre-ocular Tear Film Flow Lipid Pattern:
Original Magnification (x9.6)
Photograph Magnification (≈95)

Fig 7.5 : Pre-ocular Tear Film Amorphous Lipid Pattern:
Original Magnification (x9.6)
Photograph Magnification (≈95)

Fig 7.6 : Pre-ocular Tear Film Coloured Fringe Lipid
Pattern: Original Magnification (x9.6)
Photograph Magnification (≈95)

Fig 7.7 : Pre-ocular Tear Film Lipid Pattern
Combination 1: Original Magnification (x2)
Photograph Magnification (≈20)

Fig 7.8 : Pre-ocular Tear Film Lipid Pattern
Combination 2: Original Magnification (x2)
Photograph Magnification (≈20)

Fig 7.9 : Pre-ocular Tear Film Abnormal Lipid Clumping:
Original Magnification (x9.6)
Photograph Magnification (≈200)

Fig 7.10 : Pre-ocular Tear Film Localised Lipid Break-up:

Original Magnification (x9.6)

Photograph Magnification (≈200)

Fig 7.11 : Pre-ocular Tear Film Lipid Pattern Change with

Reduced Lid Aperture: Open Eye:

Original Magnification (x9.6)

Photograph Magnification (≈95)

Fig 7.12 : Pre-ocular Tear Film Lipid Pattern Change with

Reduced Lid Aperture: Partial Lid Closure

Phase 1

Fig 7.13 : Pre-ocular Tear Film Lipid Pattern Change with

Reduced Lid Aperture: Partial Lid Closure

Phase 2

Fig 7.14 : Pre-ocular Tear Film Lipid Spreading Sequence

Immediately After Secretion:

Original Magnification (x9.6)

Photograph Magnification (≈95)

Fig 7.15 : Pre-ocular Tear Film Lipid Spreading Sequence

1 Blink After Secretion:

Original Magnification (x9.6)

Photograph Magnification (≈95)

Fig 7.16 : Pre-ocular Tear Film Lipid Spreading Sequence

2 Blinks After Secretion:

Original Magnification (x9.6)

Photograph Magnification (≈95)

Fig 7.17 : Pre-ocular Tear Film Lipid Spreading Following

Forceful Meibomian Gland Expression:

Original Magnification (x9.6)

Photograph Magnification (≈95)

Fig 7.18 : Pre-ocular Tear Film Lipid Break-up Following Eye Drop Instillation:

Original Magnification (x9.6)

Photograph Magnification (≈95)

Fig 7.19 : Pre-soft Lens Tear Film Low Magnification Combination Lipid Pattern:

Original Magnification (x2)

Photograph Magnification (≈20)

Fig 7.20 : Pre-soft Lens Tear Film:

Original Magnification (x32)

Photograph Magnification (≈300)

Fig 7.21A: Pre-soft Lens Tear Film Localised Dry Spot Formation: Original Magnification (x32)

Photograph Magnification (≈300)

Fig 7.21B: Diagrammatifc Outline of Pre-soft Lens Tear Film Localised Dry Spot Formation:

Original Magnification (x32)

Photograph Magnification (≈300)

Fig 7.22 : Pre-PMMA Lens Tear Film Drying Sequence Phase 1: 2 Second Post Blink:

Original Magnification (x9.6)

Photograph Magnification (≈95)

Fig 7.23 : Pre-PMMA Lens Tear Film Drying Sequence Phase 1: Outline of Fringes 4 to 14

Fig 7.24 : Pre-lens Tear Film Drying Sequence Phase 1: Sectional Analysis Thickness Profile

Fig 7.25 : Pre-lens Tear Film Drying Sequence Phase 1: Sectional Analysis Drying Angle

Fig 7.26 : Pre-PMMA Lens Tear Film Drying Sequence Phase 1: Summary of Results

Fig 7.27 : Pre-PMMA Lens Tear Film Drying Sequence Phase 2:
Original Magnification (x9.6)
Photograph Magnification (≈95)

Fig 7.28 : Pre-PMMA Lens Tear Film Drying Sequence Phase 2:
Outline of Fringes 0 to 6 and
Associated Aqueous Thicknesses

Fig 7.29 : Pre-PMMA Lens Tear Film Thickness Profile

Fig 7.30 : Pre-PMMA Lens Tear Film Drying Sequence Phase 3:
Original Magnification (x9.6)
Photograph Magnification (≈95)

Fig 7.31 : Pre-PMMA Lens Tear Film Drying Sequence Phase 3:
Outline of Fringes 0 to 6.

Fig 7.32 : Pre-PMMA Lens Tear Film Drying Sequence Phase 4:
Original Magnification (x9.6)
Photograph Magnification (≈95)

Fig 7.33 : Pre-PMMA Lens Tear Film Drying Sequence Phase 4:
Outline of Fringes 0 to 7

Fig 7.34 : Pre-PMMA Lens Tear Film Drying Sequence Phase 5:
Original Magnification (x9.6)
Photograph Magnification (≈95)

Fig 7.35 : Pre-PMMA Lens Tear Film Drying Sequence Phase 5:
Outline of Fringes 0 to 4

Fig 7.36 : Pre-PMMA Lens Tear Film use of Wetting Solution:
Original Magnification (x9.6)
Photograph Magnification (≈95)

Fig 7.37 : Pre-PMMA Lens Tear Film use of Wetting Solution:
Outline of Fringes 0 to 19

Fig 7.38 : Pre-PMMA Lens Tear Film use of Wetting Solution:
Summary of Results: Thickness and Drying
Angle

Fig 7.39 : Pre-Lens Tear Film Low Wetting Angle Material

Drying Sequence Phase 1:

Original Magnification (x9.6)

Photograph Magnification (≈95)

Fig 7.40 : Pre-lens Tear Film Low Wetting Angle Material

Drying Sequence Phase 1:

Aqueous and Lipid Coverage

Fig 7.41 : Pre-lens Tear Film Low Wetting Angle Material

Drying Sequence Phase 2:

Original Magnification (x9.6)

Photograph Magnification (≈95)

Fig 7.42 : Pre-lens Tear Film Low Wetting Angle Material

Drying Sequence Phase 2: Outline of

Fringes 1 to 31 and Lipid Outline Left

Side of Photograph

Fig 7.43 : Pre-lens Tear Film Low Wetting Angle Material

Drying Sequence Phase 2: Outline of Fringes

and Lipid Layer Right Side of Photograph

Fig 7.44 : Pre-lens Tear Film Low Wetting Angle Material

Drying Sequence Phase 2: Area C of Fig 7.43

Outline of Fringes 7 to 17 and

Results of Measurement

Fig 7.45 : Pre-lens Tear Film Low Wetting Angle Material

Drying Sequence Phase 2: Area D of Fig 7.43

Outline of Fringes 6 to 21 and

Results of Measurement

Fig 7.46 : Pre-rigid Lens Tear Film Thickness Profile 1:

Low Wetting Angle Material

Fig 7.47 : Pre-lens Tear Film Low Wetting Angle Material Drying Sequence Phase 3: Original Magnification (x9.6) Photograph Magnification (≈95)

Fig 7.48 : Pre-lens Tear Film Low Wetting Angle Material Drying Sequence Phase 3: Outline of Fringes 1 to 25 and Lipid Outline

Fig 7.49 : Pre-lens Tear Film Low Wetting Angle Material: Drying Angle Sequence Phase 3: Sectional Analysis of Thickness and Drying Angles

Fig 7.50 : In-vivo Photography of the Mucous Layer on the Cornea: Normal Eye

Fig 7.51 : Diagrammatic Outline of In-vivo Photography of the Mucous Layer on the Cornea: Normal Eye

Fig 7.52 : In-vivo Photography of the Mucous Layer on the Cornea: Dry Eye Symptoms

Fig 7.53 : Diagrammatic Outline of In-vivo Photography of the Mucous Layer on the Cornea: Dry Eye Symptoms

Fig 7.54 : Photography of the Mucous Layer on Soft Contact Lenses

Fig 7.55 : Diagrammatic Outline of Photography of the Mucous Layer on Soft Contact Lenses

CHAPTER EIGHT

Fig 8.1 : Diagrammatic Structure of Lipid Layer Thickness Range

Fig 8.2 : Diagrammatic Structure of Mucous Layer Appearance

Fig 8.3 : Diagrammatic Structure of Pre-soft Lens Tear Film

Fig 8.4 : Diagrammatic Structure of Pre-rigid Lens Tear Film

LEGEND OF TABLES

CHAPTER 2

TABLE 2.1 Summary of evaporation rates of tears from the rabbit and human cornea.

TABLE 2.2 Summary of tear volume values.

TABLE 2.3 Summary of tear film thickness values.

TABLE 2.4 Summary of tear flow values.

TABLE 2.5 Summary of tear break-up time measurements.

CHAPTER 6

TABLE 6.1 Newton's scale of colours and associated phase differences and corresponding layer thicknesses.

TABLE 6.2 Destructive interference in aqueous tears for λ = 400 nm.

TABLE 6.3 Destructive interference in aqueous tears for λ = 550 nm (yellow).

TABLE 6.4 Destructive interference in aqueous tears for λ = 700 nm (red).

TABLE 6.5 Range of successive orders of destructive interference for a source distribution $\Delta\lambda$ (400nm to 700 nm).

TABLE 6.6 Constructive interference in aqueous tears for λ = 400 nm.

TABLE 6.7 Constructive interference in aqueous tears for λ = 555 nm (yellow).

TABLE 6.8 Constructive interference in aqueous tears for λ = 700 nm (red).

TABLE 6.9 Range of successive orders of constructive interference for a source distribution Δ λ (400nm to 700nm).

TABLE 6.10 Constructive interference in aqueous tears for λ = 445nm.

TABLE 6.11 Constructive interference in aqueous tears for λ = 465nm.

TABLE 6.12 Constructive interference in aqueous tears for λ = 480nm.

TABLE 6.13 Range of successive orders of constructive interference for a source distribution Δ λ (445nm to 480nm).

TABLE 6.14 Range of successive orders of constructive interference for a source distribution Δ λ (480nm to 700nm).

CHAPTER 7

TABLE 7.1 Pre-lens tear film drying sequence phase 1: relative position of fringes along CE and BD

TABLE 7.2 Use of wetting solution: film thickness and drying angle

TABLE 7.3 Low wetting angle material phase 1: tear film thickness and drying angles

TABLE 7.4 Low wetting angle material phase 2: tear film thickness and drying angles

TABLE 7.5 Pre-lens tear film low wetting angle material drying sequence phase 3

ACKNOWLEDGEMENTS

I am most grateful to my supervisors Mr R M Pearson for the enthusiasm he has shown and the constructive criticism and encouragement he has given throughout this research and to Professor M Ruben for initiating this study, and for his constant and patient support and acute clinical advice.

I record my thanks to the Board of Governors of Moorfields Eye Hospital for permission to carry out the clinical work in the Contact Lens and Prosthetics Department under the direction of Professor M Ruben.

I greatly appreciate the assistance given to me by the following people: my brother Michel for all his help; Mr Hans Bleshoy for his clinical and experimental assistance; my colleague Judith Morris - my most 'colourful' contact lens subject; Mrs Maria Silva Durand and Miss Roseline Guy for the production of some photographs and Miss Veronica Mapstone for her secretarial assistance.

Finally, thanks to Beatrice for typing the manuscript and her support and encouragement during the last two years.

I hereby grant powers of discretion to the City University librarians to allow this thesis to be copied in whole or in part without further reference to me. This permission covers only single copies made for study purposes, subject to normal conditions of acknowledgement.

ABSTRACT

New techniques are proven in this thesis which allow the visual examination of the tear film on the cornea and on different types of contact lenses. The techniques are as follows:

1. A high magnification technique of photography using the biomicroscope and crossed polarised light, allows the measurement of tear film layer thicknesses and on the surface of rigid contact lenses and 'in-vivo receding contact angle'.

2. A low magnification technique of photography allows the recording and the analysis of the superficial layers of the tear film over a wide area of the eye and contact lens surface.

3. A clinical instrument has been designed for the routine clinical observation of the tear film. It permits the visual measurement of the tear film break-up time (BUT) without the use of fluorescein.

4. A unique technique of in-vivo photography of the mucous coverage of the corneal epithelial surface and contact lens surfaces is presented. Such techniques improve the understanding of surface wettability problems.

As a result of this work the appearance of the normal lipid layer of the pre-ocular tear film has been classified into seven grades within a thickness range of 0.02μm to 0.58μm. As well as the normal, two examples of abnormal lipid layers are described.

The manner by which Meibomian gland secretion occurs and performs its role in the tear film is illustrated and analysed. Forced gland secretion by pressure induced localised lipid thickness increase. Eyelid closure was seen to compress the lipid film and instillation of saline broke up the lipid film.

It can be seen that the pre-soft lens tear film usually possesses a thin superficial lipid layer and an aqueous phase of limited dimensions.

On the other hand the pre-PMMA rigid contact lens tear film rarely possesses a visible superficial lipid layer and its aqueous layer measured 1.5μm on average. The addition the 'wetting' solution acts on the thickness of the aqueous phase which increases to 2.5μm and supports a minimal lipid layer.

The use of contact lens materials of better wettability permits the formation of films of increased thickness (up to 5.5μm) with a visible superficial lipid layer which was seen to stabilise the film and retard its drying. The main differences in mucous coverage are described as follows. At the level of the basal layer of the tear film the mucous coverage takes a continuous undulated form on the corneal epithelium but a discontinuous sporadic distribution on soft lenses decreasing to sporadic occurrence on rigid lenses.

Finally, because of the acquisition of the quantitative results, new infra-structures of the pre-lens tear film for soft and rigid lenses are proposed.

CHAPTER 1

INTRODUCTION

SCOPE OF PRESENT INVESTIGATION

Contact lenses made of different plastic material are worn by many people for long periods without causing gross ocular tissue abnormality. One of the reasons that good tolerance is possible is due to the role of the tears.

The role of the pre-ocular tear film (POTF) is manyfold. These diverse functions are influenced by numerous factors that must be looked at in detail, such as the production of tears by the lacrimal system, the drainage of tears from the ocular surface, the tear flow production rate and the evaporation rate. Also of primordial importance is the structure of the pre-ocular tear film with its different layers and their inter-relationship that dictates its physical properties and, in particular, its stability. The latter has been reported to have an essential role in achieving comfortable and problem-free contact lens wear of all types.

The tear film must provide a full and stable coverage of the surface of contact lenses and this should be achieved by forming a trilaminar fluid structure similar to that present in the pre-ocular tear film. The reduced stability of the tear film present at the surface of contact lenses could possibly be caused by the

inadequate formation of one or more of its individual layers.

Only a few studies have been concerned with the investigation of those separate layers and no clinical test has been developed to observe their structure and measure their thickness. The purpose of this study is, therefore, to:

a) Present three new research techniques that have a clinical application in the observation and photography of the pre-ocular, pre-lens tear film and the corneal surface.

b) Define a method for analysis of the experimental results based on the theory of interference fringe production and its application to the measurement of tear film thickness and structure.

c) Investigate the different types of the normal and abnormal pre-ocular tear film, study the spreading of Meibomian secretion and its behaviour during eye closure.

d) Investigate the pre-lens tear film (PLTF) structures found on soft lenses and the effect of evaporation and drying.

e) Study the tear film formation on PMMA rigid corneal lenses and its drying process. The effect of improved wetting conditions will be studied by the use of a 'wetting' solution and that of material with a low wetting angle.

The investigative technique used to date all alter the tear film in some way, therefore, more refined techniques are necessary.

f) To describe a system enabling the in-vivo observation and photography of the mucous layer on the cornea and on soft lens surfaces.

It will be used for future work necessary to further the understanding of the mechanism regulating the proper wetting of biological and artificial surfaces.

CHAPTER 2

THE FUNCTION AND STRUCTURE AND STABILITY OF THE PRE - OCULAR TEAR FILM

2.1 FUNCTIONS OF THE TEAR FILM

It is necessary to understand the function of the tear film in order to be able to analyse its component parts.

The pre-ocular tear film (POTF) is the fluid structure that covers the ocular surface within the frame formed by the edges of the lids along which it takes a meniscus shape. The latter are also referred to as tear meniscus, lacrimal meniscus, rivus lacrimalis, tear prism, or tear strip. The tears or tear fluid refers usually to the secretions from the different glands that contribute to the tear film.

The POTF has a tri-laminar structure with a superficial lipid layer, an intermediate aqueous phase and a basal mucous layer (Wolff, 1946).

The chief functions of the POTF are: to provide a regular optical surface; to help to maintain corneal integrity; to remove foreign debris; to provide lubrication of the eyelids; and to carry anti-microbial agents.

2.1.1 PROVISION OF OPTICAL SURFACE

The first function of the pre-ocular tear film is to provide a surface of perfect optical quality. It compensates for the microscopic irregularities of the corneal surface and in doing so, it allows the cornea by virtue of its curvature to be the most powerful refractive surface of the eye, approximately +45 dioptres (Duke-Elder, 1938). In most cases, a stable optical surface forms because of its physical properties immediately upon eyelid opening.

2.1.2 MAINTENANCE OF CORNEAL INTEGRITY

A second role for the tear film is the maintenance of corneal epithelial integrity and transparency which is achieved by keeping the ocular surface continuously moist. It prevents the process of keratinisation and provides the medium for gaseous exchanges with the environment and satisfy the metabolic needs of the avascular cornea. The corneal epithelium relies mostly on the tear film for the supply of oxygen necessary for its proper functioning (Hill & Fatt, 1963; Fatt & Bieber, 1968). About nine tenths of the metabolic reaction requiring oxygen is confined to the epithelial layers (Polse & Mandell, 1970). Further, Fatt & Bieber (1968) have calculated the concentration of oxygen and carbon dioxide at the different corneal layers as a result of diffusion for the open eye and the closed eye situations (Figs 2.1 and 2.2). In a closed eye situation only a small amount of oxygen reaches the central part of the stroma while the corneal endothelium relies for a great

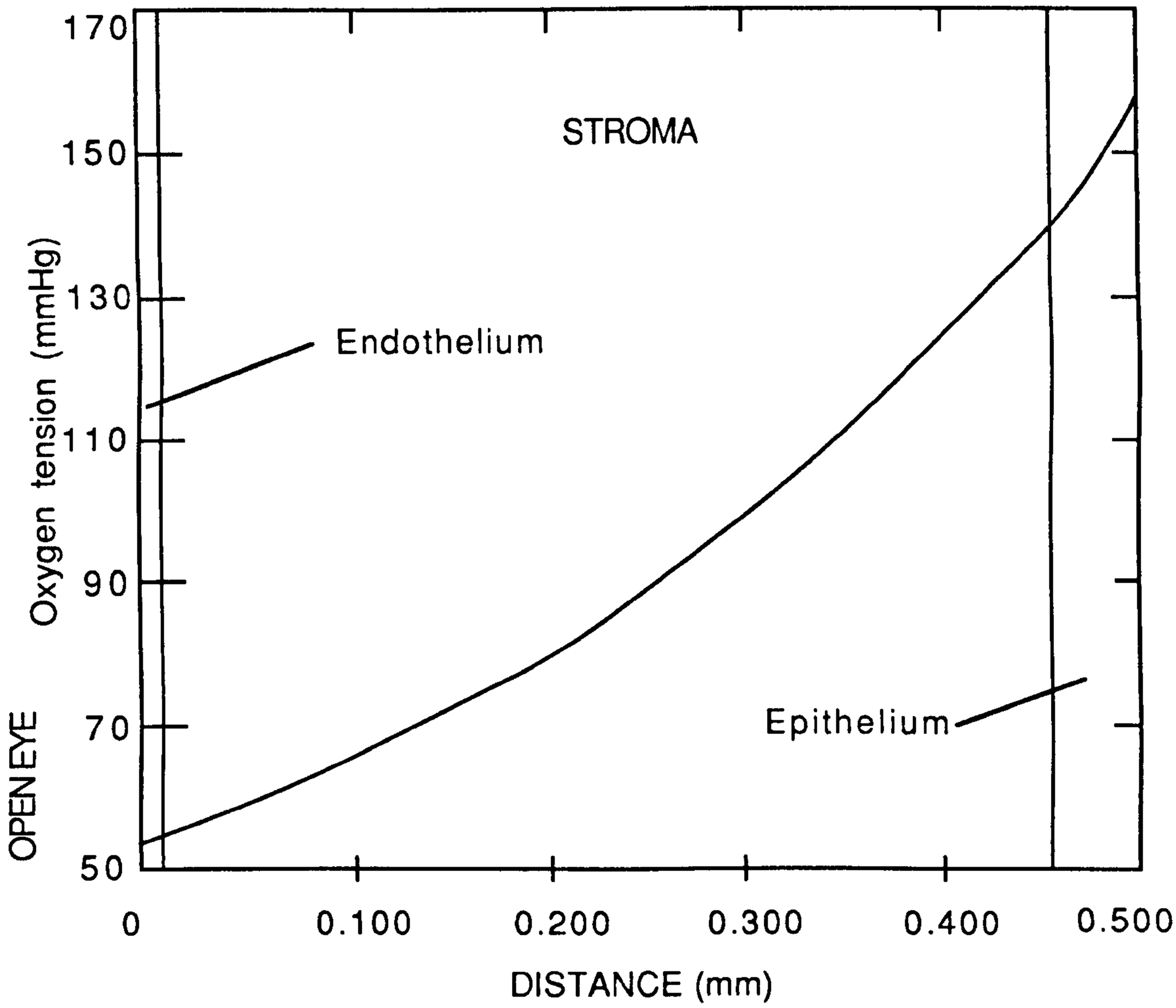

FIGURE 2.1
CONCENTRATION OF OXYGEN AND CARBON DIOXIDE IN THE CORNEA: OPEN EYE SITUATION (after Fatt & Bieber, 1968)

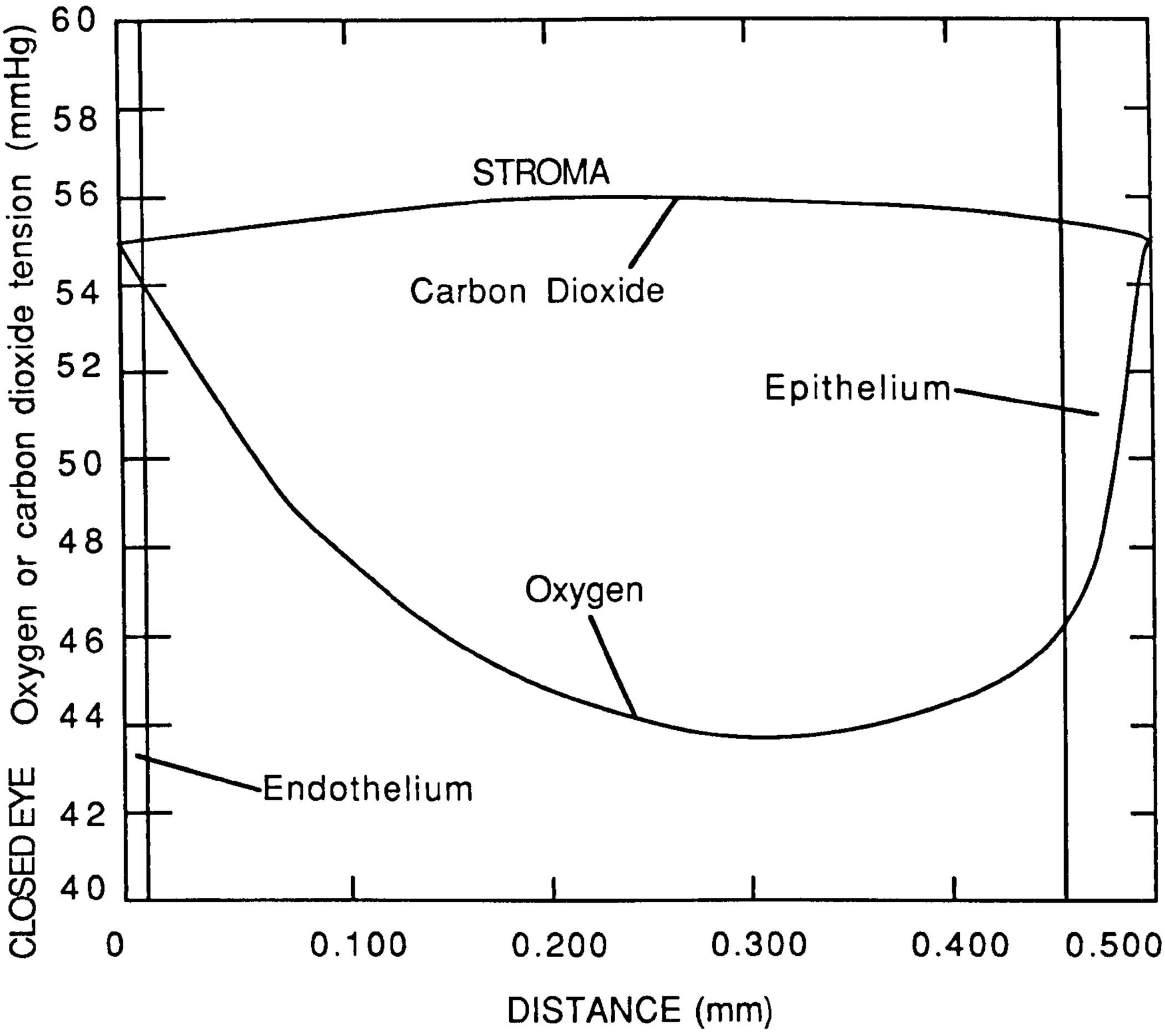

FIGURE 2.2
CONCENTRATION OF OXYGEN AND CARBON DIOXIDE IN THE CORNEA: CLOSED EYE SITUATION (after Fatt & Bieber, 1968)

part on the aqueous humour for the supply of oxygen necessary for its metabolic activity. The gaseous by-products of epithelial metabolism, mainly carbon dioxide, are in turn dissolved in the tear film and eliminated.

2.1.3 THE REMOVAL OF FOREIGN BODIES

Previous work has shown that it is due to the flow of the tears that the cell debris, resulting from the normal epithelium desquamation, are removed from the surface (Lemp, 1976). Keratinised annuclear (squamous) epithelial cells, nucleated squamous epithelial cells, cylindrical epithelial cells and leucocytes have all been found in the tear fluid (Norn, 1960). The tear film acts as a trap to dust and particles (Wolff, 1954) and during blinking it removes lipid-contaminated mucous strands which are occasionally found at its surface, producing localised areas of instability. A mechanism by which the action of the lid rolls the mucous strands to the superior and inferior palpebral fornices has been described in the normal eye (Holly & Lemp, 1977). Foreign bodies are also removed after reflex tearing by the POTF and flushed away from the ocular surface (Fig 2.3).

2.1.4 EYELIDS LUBRICATION

The examination of the POTF by the methods to be described will have to be rapid instrumentation because of eye lid movement, blinking and fluid movement.

The pre-ocular tear film plays the role of lubricant during the movement of the eyelids over the

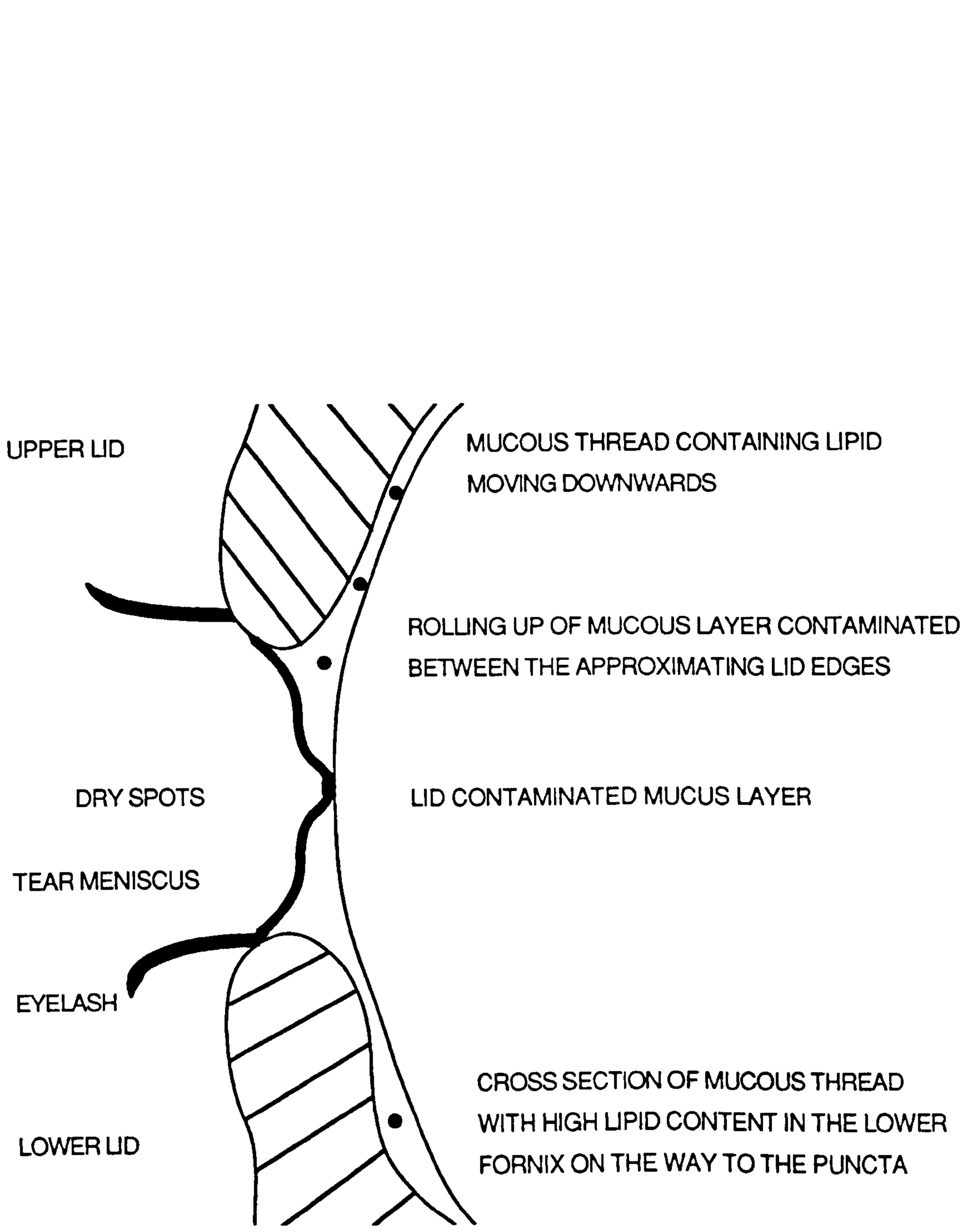

FIGURE 2.3
TENTATIVE MECHANISM FOR REMOVAL OF LIPID CONTAMINATED MUCOUS LAYER
(after Holly & Lemp, 1977)

ocular surface. The inner surfaces of the lids are in very close contact with the cornea (Kessing, 1967), at least over a small area behind the lid margins (Ehlers, 1965; Lemp et al, 1970b). A good apposition between the corneal and lid surfaces (Lemp & Holly, 1970) is necessary to allow the spreading on the ocular surface, by the action of the lid, of the conjunctival mucous produced by the goblet cells. It is supposed that there is, in fact, very little direct solid-to-solid contact during blinking and that a small amount of mucous situated at the edge of the lid will act as a lubricant during blinking.

2.1.5 PROTECTION AGAINST INFECTION

During an eye infection, some changes occur in tear composition and, production: any variation that occurs will affect the superficial appearance of the pre-ocular tear film. A method that could directly or indirectly show the effects of infection of the conjunctiva or glands of the lid would be of value.

The main bacteriolytic role in the PDTF is played by the lysozyme fraction of the tear proteins (Ridley, 1928). Lysozyme is a long chain, low molecular weight proteolytic enzyme which disrupts the 1,4-B-linkage between N-acetylmuramic acid and N-acetylglucosamine in more complex cell wall structures. Its activity is pH dependent and maximal for a pH range from 6 to 7.4. Excessive tearing, by reducing the lysozyme concentration, reduces its bacteriolytic action. This occurs during ocular pathologies associated with painful

or irritated eyes, such as, conjunctival infection. (Sapse et al, 1968) or when diluents such as eye lotions are used.

Beta lysin is another protein found in the POTF (Ford et al, 1976). It may play an important bactericidal role (Friedland et al, 1972) although this is seriously questioned by Janssen et al (1984).

The presence of lactotransferrin, a glycoprotein, probably originating in the lacrimal glands, has been reported (Liotet et al, 1980). Lactotransferrin performs an anti-microbial and anti-toxic role in tears by capturing and draining the iron necessary for the growth of many micro organisms.

Further, protection against bacterial and viral infection is provided in the POTF by the presence of various immunoglobulins which amount to 5 percent of total globulins (Allansmith, 1973; McClellan et al, 1973). Several immunoglobulins play such a role. The main function is due to secretory immunoglobulin A (SIg A). SIg A protects the surface of the mucous membranes. This secretory component is manufactured by the epithelial cells of the lacrimal gland (Franklin et al, 1973), then it mixes with acinar produced secretory component and is secreted into the lumen to bathe the conjunctival mucous surface (Tomasi, 1967) with an immunologic paint to modulate and control surface flora by agglutination and disposal of micro-organisms. Reports of the IgA content of tears vary from 17mg/100ml (McClellan et al, 1973) to 60mg/100ml (Allansmith et al, 1973).

The normal immunoglobulin G (IgG) value in tears is 14mg/100ml ±25 (range 2 - 65) (McClellan et al, 1973). Its concentration increases significantly during acute inflammation due to an increased vascular permeability. This increase in concentration may be the result of serum IgG spilling into the tears. The role of IgG as a complement fixing agent is to destroy invading micro-organisms.

IgD and IgF have also been detected in the lacrimal gland and tears (Abelson et al, 1977).

2.2 THE LACRIMAL SYSTEM

The pre-ocular tear film is a transient structure produced by the lacrimal system. Any method of visual examination that details it quantitatively and qualitatively must take into account the functions of this system. The lacrimal system can be divided into three parts:-

- A secretory part which is responsible for basic tear secretion and reflex tear secretion.
- A distributional part which allows the spreading of the tear film over the ocular surface. This is the part that will be examined.
- An excretory part which is responsible for the drainage of the tears from the ocular surface.

2.2.1 THE SECRETORY SYSTEM

i) Introduction

The lacrimal fluid bathes the ocular surface and forms what is known as the pre-ocular tear film

(POTF) and is comprised of the secretions of the lacrimal gland proper and accessory lacrimal gland tissues together with the secretions of the Meibomian glands and the mucous glands of the conjunctiva (Adler, 1965) (Fig 2.4).

ii) <u>The Lacrimal Gland Proper</u>

Physically the largest gland, it is almond in shape, conforming to the globe form of the eye. It is situated in the temporal angle of the orbit, lying under the orbital rim of the shallow lacrimal fossa between the globe and the lateral process of the frontal bone (Fig 2.5). The lateral aponeurosis of the levator tendon produces an indentation in the gland so deep that the gland appears to be composed of two separate lobes, an orbital portion lying above the aponeurosis and a palpebral portion below. The palpebral portion is in proximity of the conjunctival fornix and sometimes can be seen when pulling the upper lid outward and upward while the subject looks nasally.

The orbital lobe measures approximately 20mm x 12mm x 5mm, weighs 0.78g (Whitnall, 1932) to 0.61g (Allansmith et al, 1976) and appears as a highly vascular tissue. The basic unit of the lacrimal gland is a tubule or acinus. These acini also possess myoepithelial cells with the contractile properties of the smooth muscles. The aggregation of acini forms the lobules, several lobules are encapsulated into a sheath to make the several lobes of the glands. Each of the fifteen to forty loosely knit lobules which form the palpebral lobe

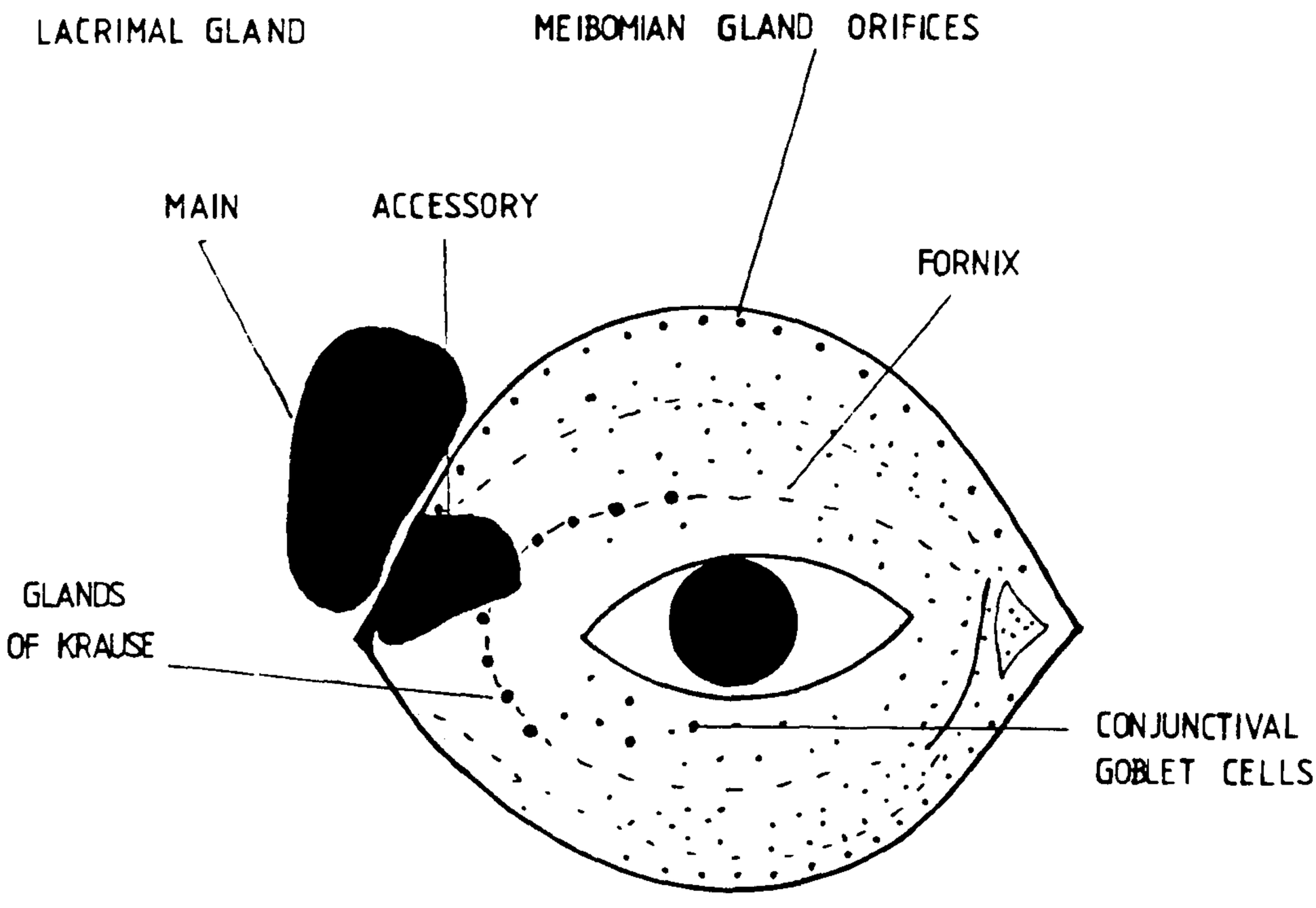

FIGURE 2.4
SITES OF ORIGIN OF TEAR FILM COMPONENTS
(AFTER TIFFANY & BRON, 1978)

DIAGRAMMATIC REPRESENTATION
OF SECRETORY GLANDS IN THE
HUMAN EYE LID:

1. Lacrimal Gland
   a. Orbital Part
   b. Palpebral Part
2. Glands of Krause
3. Meibomian Glands
4. Moll's Glands
5. Glands of Zeis
6. Sweat Glands

FIGURE 2.5
LACRIMAL GLAND PROPER

has a secretory duct which empties into the main secretory duct from the orbital lobe (Jones, 1973).

The secretory granules leave the secretory cells to empty into the lumen of the acini. They are then carried through two to eight intercallated ducts, which pass through the palpebral lobe to empty at the upper temporal fornix of the conjunctival sac. Initially, it was thought that the secretory cells of the lacrimal gland were serous in origin with a watery secretion. But more recent work (Ruskell, 1968; Allen et al, 1972; Jensen et al, 1969) has shown that some of the secretory cells present may be considered as serous and there is also evidence of some cells concerned with glycoprotein secretion. The latter cells have been shown to secrete at a much slower rate than the serous cells. According to Ruskell (1969), therefore, the lacrimal gland is considered as a sero-mucous gland.

Jones (1973) thought that the lacrimal gland was only active during reflex secretion and played no part in the basic secretion. This seems doubtful as surgical removal of the lacrimal gland to control hyper-secretion led to inadequate tear film formation and keratitis sicca (Whitwell, 1958). Golding-Wood (1954) and Ruskell (1969) have shown, respectively, in man and in monkeys that denervation or removal of the gland induces an important reduction in tear secretion. Further, Jordan & Baum (1980) suggested that there is no difference in the secretion of aqueous tears by the accessory and main glands, that both are constantly subjected to a low level of stimulation.

iii) The Accessory Lacrimal Glands

The accessory lacrimal glands of Krause, about forty of which are situated in the upper conjunctival fornix and six in the lower fornix, and the accessory glands of Wolfring, usually three adjacent to the upper margin of the tarsus with their duct openings situated at the limit of bulbar and tarsal conjunctiva are also responsible for aqueous tear production. The number of accessory lacrimal glands shows individual variations but their structure is identical to that of the main lacrimal gland with tubular acini internally lined with microvilli and surrounded by myoepithelial cells.

iv) The Mucin Secretion

The ocular mucus has been considered to be composed mainly of mucins in the form of a gel in complex with water, lipids, enzymes, proteins, carbohydrates and electrolytes (Folch et al, 1957).

The conjunctival mucin secreting goblet cells are mainly found in the area of the fornix and the plica semi lunaris and are known as Crypts of Henle. They diminish progressively in number in the area of the bulbar conjunctiva (Kessing, 1968) and their density is usually between 26 and 40 per square cm and large individual variation is present (Marquardt, 1986).

Some complementary glycoprotein might also be secreted by the conjunctival epithelial cells to form the foundation to the mucous layer (Greiner et al, 1980; Takakusaki, 1969; Dilly, 1986). Further recent evidence (Allansmith et al, 1976) suggests that all

acinar cells from the main and accessory lacrimal glands contain material that is stained positively by the periodic acid-schiff method. They, therefore, could produce glycoprotein.

v) The Oily Secretion

A) The main oily secretors are the tarsal or Meibomian glands, studied by Meibomius (1666). These tubulo-acinar glands are located within the tarsal plates in each lid: 30 to 40 in the upper lid and 20 to 30 smaller ones in the lower lid. Their orifices are situated on the inner side of the muco-conjunctival border and the act of blinking is sufficient to express their secretion on to the tear film. They are sebaceous holocrine glands.

B) The glands of Zeis and Moll are the minor oil secretors. The glands of Zeis are situated at the palpebral margin of each eyelid and are sebaceous glands. Their role seems mainly to prevent desiccation of the palpebral surface. The sweat glands of Moll are found at the root of the eye lashes and their secretion prevent the lashes from becoming brittle.

2.2.2 TEAR SPREADING SYSTEM

Ninety percent of the tear fluid contained within the palpebral fissure is found in the tear strips or tear meniscus situated along the upper and lower lid margins (Fig 2.6). After fluorescein instillation, a 'black line', visible under ultra-violet (UV) light at the edge of the meniscus, delimits the complicated multilayered structure that we know as the pre-ocular tear film from

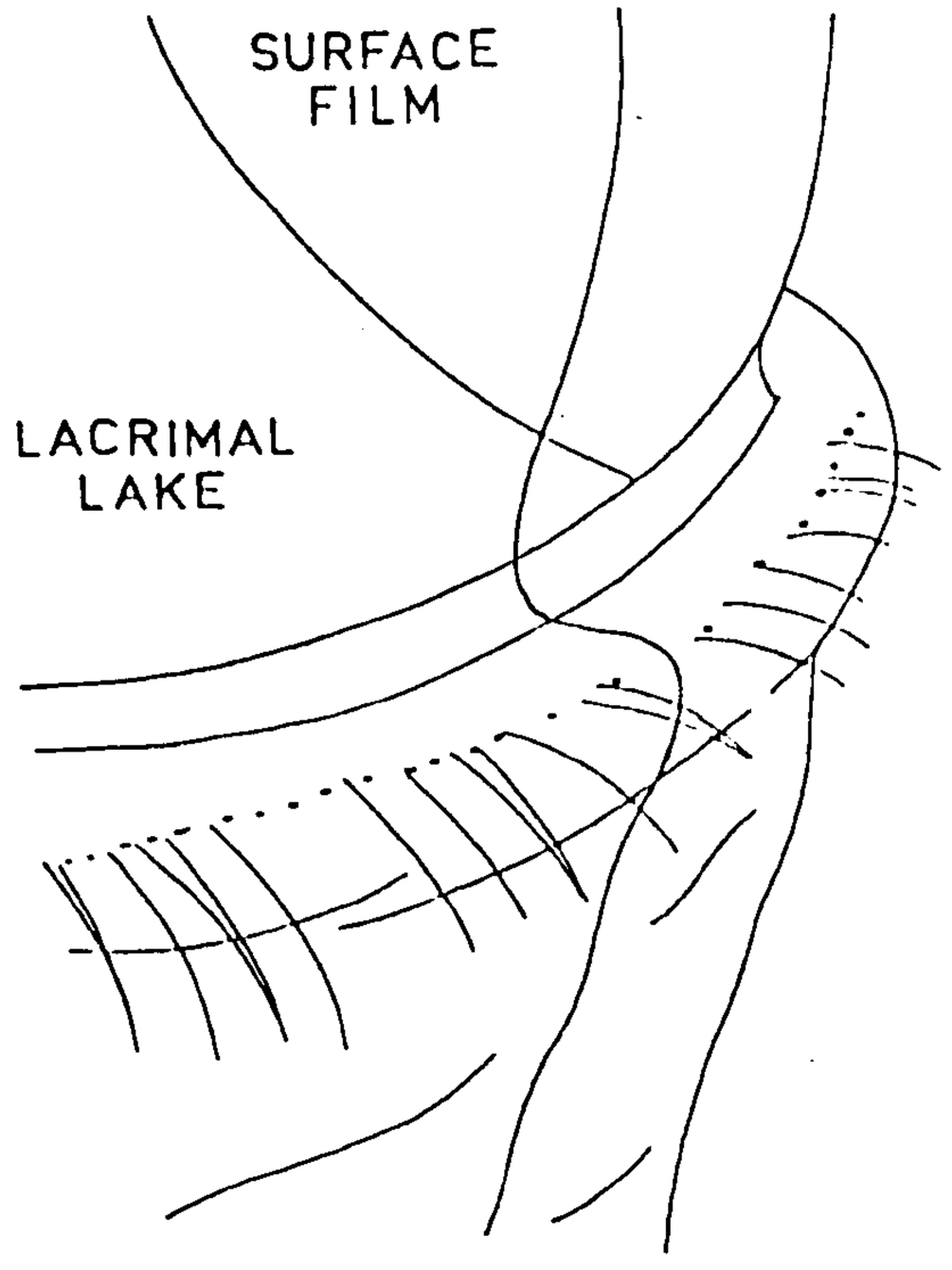

RIGIDITY OF SURFACE
OVER LACRIMAL PRISM
After McDONALD 1968

FIGURE 2.6
RIGIDITY OF SURFACE OVER LACRIMAL PRISM

the tear strips (Fig 2.7). The formation of the pre-ocular tear film is due to the physico-chemical interactions taking place during the blinking process, which initiates the spreading of the superficial lipid together with the water soluble ocular surfactant, mucin.

i) Blinking - Lid Closure

Normal Caucasian humans blink on average 12.5 times a minute (Gordon, 1951). The upper eyelid downward movement, approximates 17 to 20cm per second (Doane, 1980), and the velocity is sufficiently high so that considerable shear stresses are present at the various interfaces of the tear film during blinking.

The lipid layer does not spread under the eyelid because of its mucous coating. It cannot spread over the lid exterior surface as it is coated with a thin layer of sebaceous gland secretion which is more surface active than the Meibomian gland secretion. Thus its limited quantity allows it to be contained between the lid interspace and when they are completely closed, sandwiched between the lids and the ocular globe (Holly, 1980).

At the same time, the close apposition of the lid border induces the redistribution of the mucous layer over the ocular surface, through shear action across the thin aqueous layer. The same movement also rolls up and drags into the upper and lower fornices, the lipid contaminated mucous. These mucous strands are known to cause the tear film to break up locally (Norn, 1969a) (Fig 2.3).

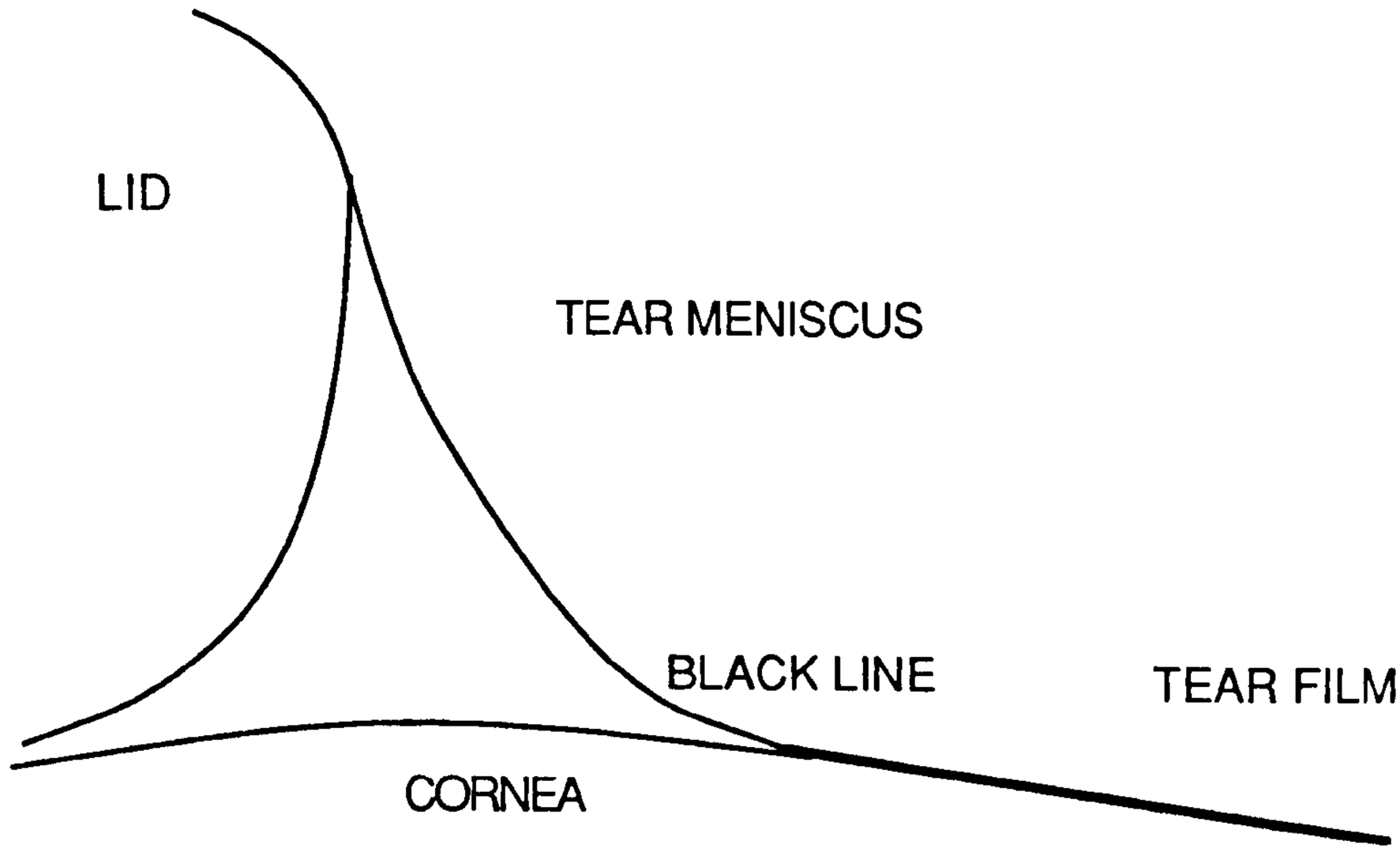

FIGURE 2.7
SCHEMATIC DIAGRAM OF THE TEAR FILM BOUNDARY
(After F.J. Holly, 1978a)

ii) Blinking - Lid Opening

As the eyelids open, at a speed approximately 8cm per second (Berger & Corrsin, 1974), a new aqueous-air interface of high surface tension is created. Immediately a mono-molecular layer of lipids is spread on the aqueous phase and is followed by the spreading of the excess lipid, together with the associated muco-proteins. This first mono-molecular layer of lipid is capable of an initial spreading rate as high as 20 to 30cm per second (Holly, 1973a). This means that the only limiting factor is the speed of elevation of the eyelid and it explains why a lipid free surface cannot be seen even using high speed cinematrographic techniques.

A secondary slower spreading motion, lasting approximately one second, can be observed in the superficial layer. It has been shown that if mucin is injected underneath a Meibomian secretion spread over saline, the film pressure increased almost threefold (Holly, 1973b). The most likely explanation is that the mucous accumulated at the edge of the eyelids is coated with Meibomian lipids and it is able to spread along the newly formed water lipid interface. This visible duplex film increases the stability of the tear film by lowering its surface tension. It also thickens the tear film by viscous drag of fluid from the marginal tear strip. This situation continues until the negative hydrostatic pressure, due to the meniscus curvature increases to a level which restricts the flow between the meniscus reservoir and the tear film, creating the localised

thinning or 'black line' delimiting the POTF (McDonald & Brubaker, 1971).

iii) Vector of Flow

The vector of flow of tear can only be seen in the superior and inferior marginal strips because the tear film itself is so thin that surface forces are greater than gravitation forces (Holly & Lemp, 1977) and no significant flow can occur in the tear film (Ehlers, 1965).

Maurice (1973) developed a technique using 2 percent by weight of lampblack suspended in saline by the addition of 0.2 percent TWEEN 20 (Atlas Chemical Industries Inc) to observe the vector of tear flow in the eye. The particles were restricted to the marginal strips. A small intermittent movement possibly representing the newly secreted tears was apparent in the superior strip. It was either lateral or nasal, in which case it disappeared into the upper punctum. A larger number of particles were seen in the lower strip and their nasal progression to the lower punctum was very rapid after a blink, but then slowed down gradually to a stop if blinking were avoided for about a minute. Repeated blinking and depletion of the marginal strip confined the particles to an irregular movement immediately after the blink or no movement at all.

The blinking action thus forces the tears within the marginal strip from the outer canthus to the inner canthus, towards the puncti, contributing to its renewal.

2.2.3 THE EXCRETORY SYSTEM

The tears leave their ocular environment through the surface of the conjunctiva, by evaporation to the atmosphere and drainage through the puncti.

i) Exchange Across the Conjuoctival Surface

Schirmer (1903) first calculated that an 8 percent tear loss in one minute was occurring by diffusion across the conjunctival epithelium. More recently, Maurice (1973) recorded a 35mv electrical potential at the conjunctival surface with the negative pole to the blood side. By calculation based on the electrical potential measured, the permeability of the conjunctiva and its surface area, he found that up to 2µl per minute or 20 percent of the PDTF could be adsorbed over the bulbar conjunctival surface.

ii) Loss by Evaporation (Table 2.1)

Ten to 25 percent of the total tear secretion is lost by evaporation depending upon external conditions such as humidity and turbulent air flow (Holly, 1973a). Mishima & Maurice (1961b) and Mishima (1965) measured the thinning rate of a rabbit cornea whose aqueous humour had been replaced by parafin to stop water flow from the aqueous humour and calculated that the standard rate of evaporation varied from 2.2 to 3.7µl/h/cm^2. This is equivalent to a tear film thickness reduction of about 0.1µm for every 10 seconds inter blink.

Hamano et al (1980c) employed a method, used in clinical dermatology, of evaporation measurements based on the diffusion law of water vapour. His results, 11.4 X 10^{-7}g/cm^2/sec, are in good agreement with the previous

EVAPORATION RATE OF TEARS FROM THE RABBIT CORNEA

MISHIMA & MAURICE (1961b)	(6µl/2.1cm²/hr)	8.0 X 10^{-7} g/cm²/sec
IWATA ET AL (1969)		10.1 X 10^{-7} g/cm²/sec
HAMANO ET AL(1980c)	(41g/m²/hr)	11.4 X 10^{-7} g/cm²/sec

EVAPORATION RATE OF TEARS FROM THE HUMAN CORNEA

HAMANO & MITSUNAGA (1982):		
NORMAL	(75g/m²/hr)	26.9 X 10^{-7} g/cm²/sec
DRY EYES	(49g/m²/hr)	15.15 X 10^{-7} g/cm²/sec
BELLDEGRUN ET AL (1985):		
NORMAL		4.29 X 10^{-7} g/cm²/sec
ABNORMAL		7.45 X 10^{-7} g/cm²/sec

TABLE 2.1
SUMMARY OF EVAPORATION RATES OF TEARS FROM THE RABBIT AND HUMAN CORNEA

measurements of Iwata et al (1969): 10.1 X 10^{-7}g/cm^2/sec. The same technique was applied to normal human eyes (Hamano & Mitsunaga, 1982) and gave a value to be equivalent to 26.9 X 10^{-7}g/cm^2/sec while dry eyes led to a lower evaporation rate of equivalent to 15.15 X 10^{-7}g/cm^2/sec which is close to that of the rabbit eye. Hamano explains the low rate in rabbits by the presence of a thick lipid layer and that of the dry eye patient by their limited tear volume and the possibility of evaporation of water from the corneal tissues through the epithelium.

Rolando & Refojo (1983) designed a goggle experiment to measure tear evaporation rate. They found that any abnormality of tear, lid, ocular structure and/or function results in an instability of the tear layer that is evidenced by an increased evaporation rate of aqueous tears (Rolando & Refojo, 1983; Rolando et al, 1983). They found that the mean evaporation rate in subjects with ocular surface abnormalities (7.45 X 10^{-7}g/cm^2/sec) was nearly twice that in a normal group (4.29 X 10^{-7}g/cm^2/sec) (Belldegrun et al, 1985). The difference in values compared to that found by Hamano & Mitsunaga may be due to difference in experimental technique. Hamano's experiment being a static method while Refojo's goggle method uses dynamic flow of air.

In the previous experiments the structure and appearance of the pre-ocular tear film was not assessed and a variation in lipid presence, thickness and contamination will have affected the results.

In the absence of the oily layer the rate of evaporation is increased 10 to 20 times (Holly & Lemp, 1977; Mishima, 1965) but a marked tear flow decrease is recorded in Sjögren's syndrome inferring that normal evaporation produces hypertonicity of the tear film (Mastman et al, 1961) in that condition.

There is a close relationship between evaporation and tear film osmolarity in keratoconjunctivitis sicca. The decrease in tear volume produce an increase in the ratio between surface area and volume increasing the effect of evaporation on the tear film osmolarity. This is also affected by the increase in tear evaporation rate in keratoconjunctivitis sicca.

iii) Tear Drainage

The drainage of tears takes place through two small orifices, the puncti lacrimalis, in apposition to the globe and in contact with the marginal tear strip at the upper and lower lid border of the inner canthus. Each punctum constitutes the opening of drainage ducts: the canaliculi. These canaliculi, run first a vertical course, then a horizontal one before joining together to form a single common duct, opening into the tear sac or lacrimal sac (Fig 2.8). The canaliculi are lined with stratified squamous epithelium but are rigid enough to produce capillary attraction. The lacrimal sac in turn opens into the naso-lacrimal duct. Both the lacrimal sac and naso-lacrimal duct are lined by columnar epithelium and possess a deep fibrous layer. The same fibres as the orbicularis muscle are attached into the lateral side of the sac. The naso-lacrimal duct opens into the inferior

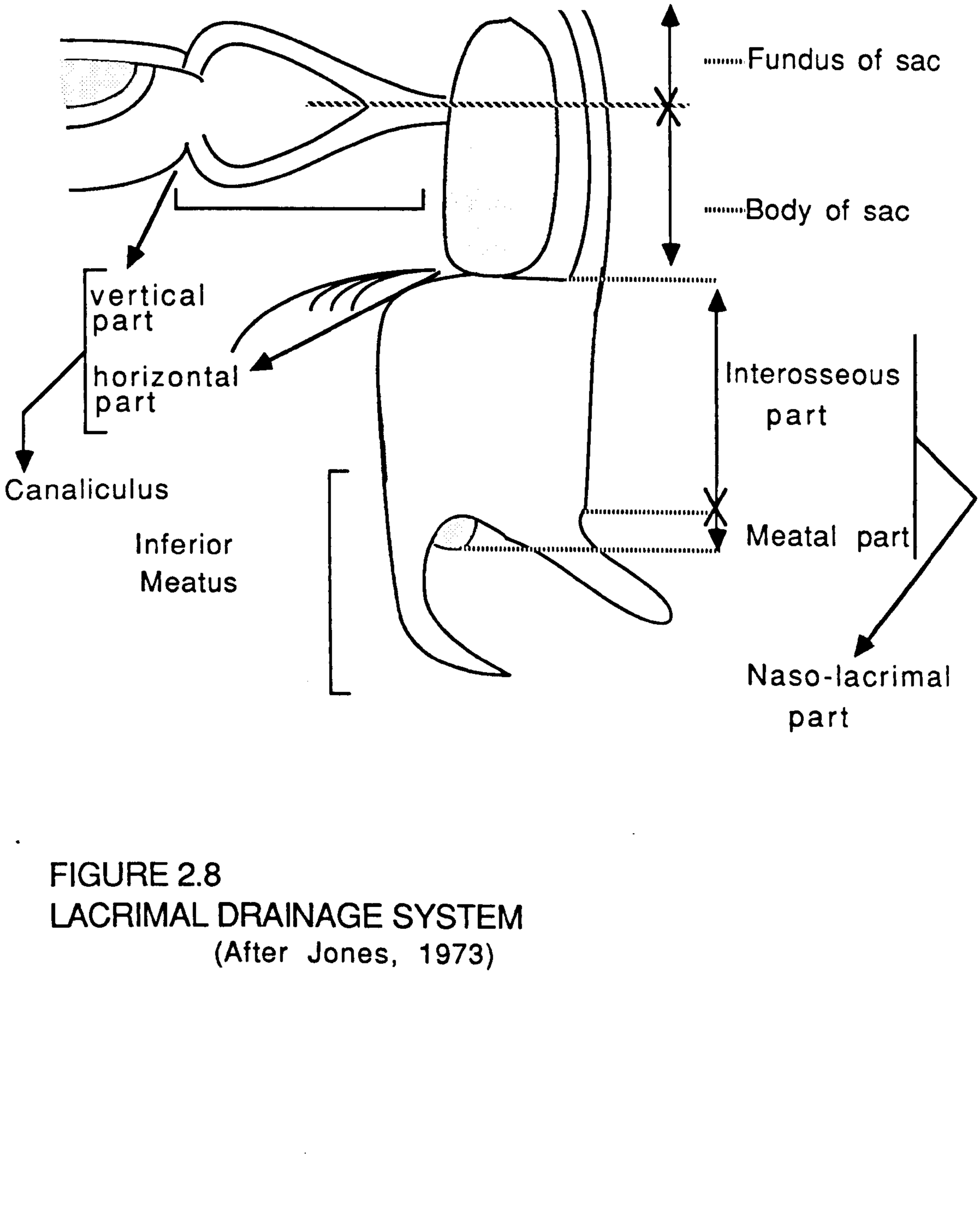

FIGURE 2.8
LACRIMAL DRAINAGE SYSTEM
(After Jones, 1973)

meatus of the nose where the tears are finally discharged as part of the nasal secretion (Jones, 1966).

The two important factors contributing to lacrimal drainage in the excretory system are:

- the compression and shortening of canaliculi lumen during eyelid closure and orbicularis muscle contraction which forces the tears toward the lacrimal sac and enhances the action of this structure.

- during blinking the contraction of the orbicularis which draws out the lateral wall of the lacrimal sac creating a negative pressure into the sac. With the relaxing of the obicularis, the sac collapses and expels the fluid towards the naso-lacrimal duct (Jones, 1966). Negative pressure in the nose during inhalation and swallowing (François and Neetens, 1973) and gravity also plays a role in emptying the sac.

2.3 INNERVATION OF THE LACRIMAL SYSTEM

The control of tear production and the interaction of the various glands is regulated through the innervation of the lacrimal system.

The secreto-motor nerve fibres responsible for the control of lacrimal secretion are issued from the facial nerve, pass with the greater petrosal nerve to the pterygopalatine (or sphenopalatine) ganglion which is connected with the maxillary nerve.

Previously, the post-ganglionic fibres were thought to pass into the maxillary nerve (Fig 2.9) reversing their course into the zygomatic nerve to join the lacrimal nerve and enter the lacrimal gland by way of

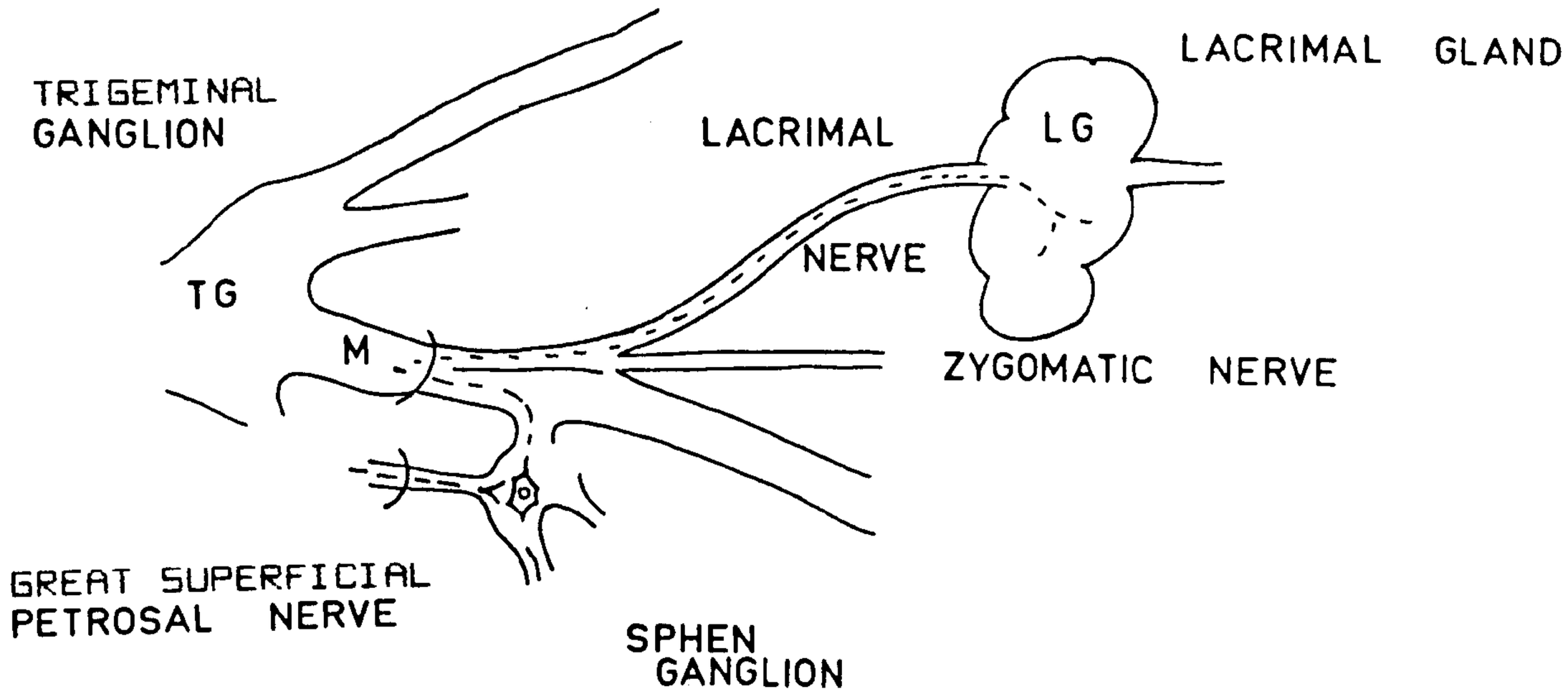

CLASSICAL VIEW

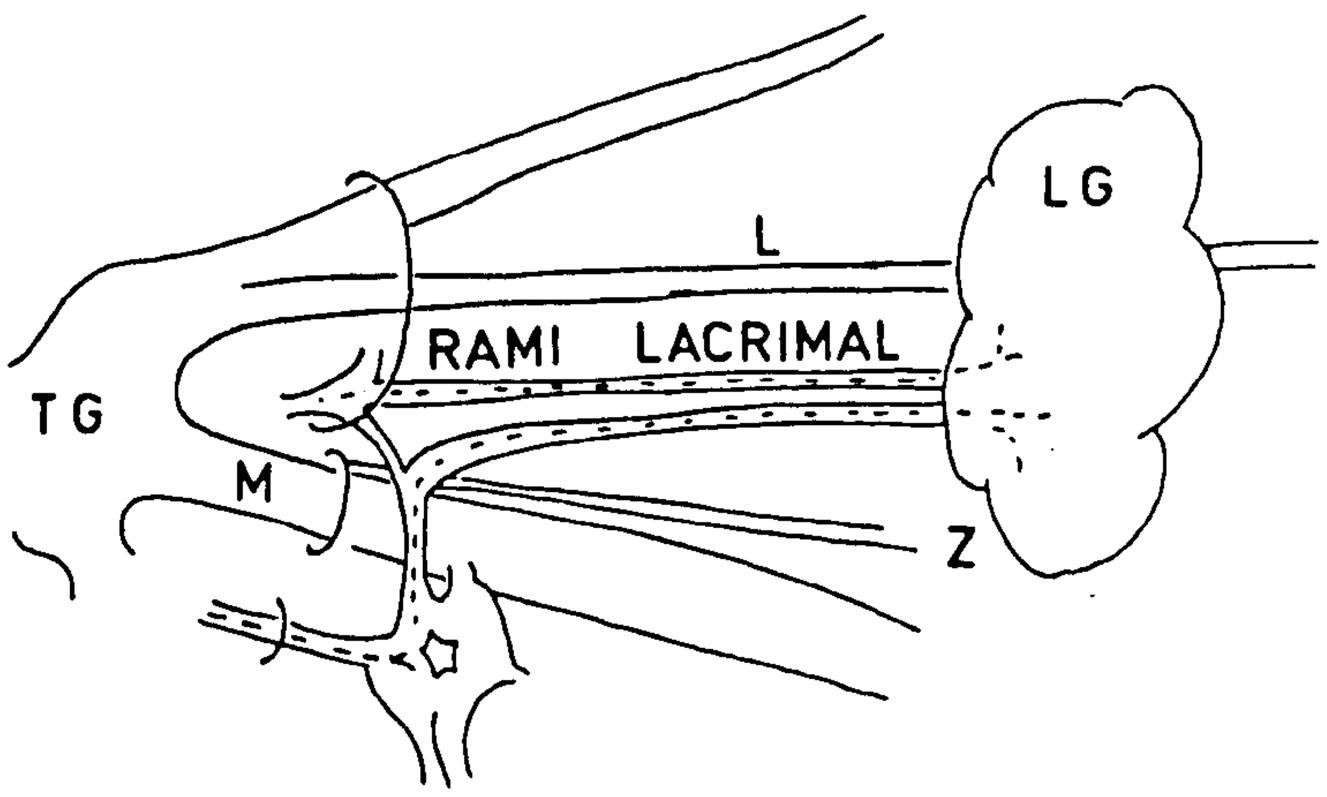

RECENT VIEW

FIGURE 2.9
THE POST-GANGLIONIC PATHWAY OF PARASYMPATHETIC LACRIMAL SECRETO-MOTOR NEURONS
AFTER RUSKELL 1971

an anostomosing branch. More recent work by Ruskell (1971), has shown the presence of rami lacrimales, fine unmyelinated nerves passing directly from the ganglion to the lacrimal gland in monkeys. It is reasonable to think that those rami lacrimales carry the post-ganglionic fibres to the lacrimal glands (Fig 2.9).

The sympathetic nerves fibres originating in the hypothalamus probably gain access to the gland as a peri-vascular plexus of the lacrimal artery. It seems that nerves and terminals of both sympathetic and para-sympathetic are present in the walls of the arterioles and capillaries in the connective tissues surrounding the acini of the glands. Few terminals even penetrate the acini and lie between the serous cells but not the mucous cells. No terminals seem to be found close to the myoepithelial cells surrounding the acini but a numerous number can be found in the ducts of the human lacrimal gland in close proximity to the myoepithelial cell present (Ruskell, 1976).

According to Ruskell (1976) the control of the lacrimal gland secretion seems to occur at two levels: an ordinary level and during hypersecretion.

- At the ordinary level, the secretion is triggered by the parasympathetic stimulation of the serous cells and the autonomous action of the mucous cells.

- During hypersecretion, the interstitial parasympathetic fibres seem to come into effect and stimulate the myoepithelium cells of the acini which

contract and produce an increased mechanical stimulation of the secretion.

The role of the sympathetic innervation has not been accurately determined, but it is possible that, as in the rabbit, it may exert a slow acting influence on the secretion through vaso-motor changes.

The afferent reflex pathway for the lacrimal gland is situated in the fifth cranial nerve and the usual reflex secretion originates from peripheral sensory stimulation of the cornea, the conjunctiva, skin or nose. If the stimulus on one side is weak, the reflex response will be unilateral but a bilateral response will follow a stonger unilateral stimulus. Reflex lacrimation from retinal stimulation will vary with the intensity of light. Psychogenic stimulation during weeping caused by emotional disturbance or various central nervous system diseases involves the frontal cerebral cortex, the basal ganglia, the thalamus and the hypothalamus and is always bilateral (Jones, 1973). The production of tears on an emotional basis is unique to humans among all vertebrates.

Little is known about the interaction between the various parts of the tear producing glands during normal and reflex secretion.

The qualitative observation of the POTF in those situations could permit the differentiation between lacrimal and Meibomian production.

2.4 BASAL TEAR FILM PHYSICAL CHARACTERISTICS

The output from the various tear glands produce a quantity of tear necessary to cover and protect the exposed ocular surface between blinks. The assessment of tear volume, pre-ocular tear film thickness and tear flow has been the subject of many studies.

2.4.1 TEAR VOLUME (TABLE 2.2)

The total tear volume found within the palpebral aperture has been estimated to be between 7µl to 10µl (Maurice, 1973) and up to 90 percent of the tear volume is found in the superior and inferior marginal tear strip, also known as lid tear meniscus. The remaining is spread over the ocular surface to form the very thin pre-ocular tear film (POTF). Norn (1965b) found that 7µl of the pre-ocular tear film occupied an ocular area of 172mm^2. From the total volume 75 percent is found in the meniscus and 25 percent in the pre-ocular tear film. The average tear volume has been estimated to be 7µl ± 2µl (Mishima, 1965) and 8.47µl ± 2.02µl (Furukawa & Polse, 1978) both using slit-lamp fluorophotometric techniques. An extra 20µl to 30µl can be held between the lids if care is taken to avoid blinking. When blinking is permitted, it appears that for a normal palpebral fissure, any amount above 10µl will be flushed out (Maurice, 1973). But, obviously, that amount will vary with the size of the palpebral fissure.

Further, it also appears that there is very little fluid in the fornices. If the lower lid, for example, is pulled away from the surface of the eye, some tear fluid

MISHIMA (1965):		
	P.O.T.F	→ 0.65 µl / cm2
	TOTAL	→ 7 µl ± 2 µl
NORN (1965):		
	MENISCUS	→ 7 µl
	TEAR FILM	→ 0.7 µl
	AREA	→ 172 mm2
MISHIMA ET AL (1966):		
	TOTAL	→ 7 µl
	MENISCUS	→ 5.25 µl
	TEAR FILM	→ 1.75 µl
FURUKAWA & POLSE (1978):		→ 8.47 µl
MAURICE (1973):		
	MAXIMUM	→ 10 µl

TABLE 2.2
SUMMARY OF TEAR VOLUME VALUES

will invade the newly created space. But when the lid is released, the tear fluid is expelled by apposition to reform the marginal tear strip. No tear reserve is present at the inner canthus which is only moist.

The average total thickness of the pre-ocular tear film (5μm to 10μm), indicates a volume of approximately 1μl for the POTF which corresponds to only a very limited amount of the total tear volume. As we have seem, most of the lacrimal fluid is found in the marginal tear strips and when fluorescein staining is used, a 'black line' can be seen extending along the corneal surface just within the lid margins. These 'black line's separate the pre-ocular tear film from the marginal tear strips, and represent an area of thinning of the tear film (McDonald & Brubaker, 1971). When fluorescein concentration is less than 10^{-6} no fluorescence occurs.

Examination of the proximity of the 'black line', showed that there was no diffusion of dye across the line and when fluid accumulates in the lower marginal strip, the line moves away from the lid margin (Maurice, 1980).

The formation of the tear meniscus depends on the balance between the negative pressure induced by its concave surface and the hydrostatic pressure due to the height of the fluid column in the meniscus (Holly, 1980) (Fig 2.6).

In the presence of a restricted amount of fluid (as in the ocular environment) an imbalance is created because the tear film cannot replenish the aspirated fluid fast enough by inter-laminal flow. The aspiration is the result of an unsaturated or 'thirsty' meniscus and

it leads to the localised thinning in the film (McDonald & Brubaker, 1971). Slit-lamp observation of the 'black line' and of the curvature of the meniscus give some information of the degree of unsaturation of the meniscus.

The smaller the radius of curvature, the more 'thirsty' the meniscus, hence when the meniscus gets larger and less curved, it gets less 'thirsty' as a larger volume of fluid is available (Holly, 1980).

The observation of lid meniscus height has been mentioned as a guide in the diagnosis of dry eye symptoms (Baum, 1973).

Lamberts et al (1979) measured the average height of the inferior tear meniscus in 86 normal eyes and found that a value greater than 0.1mm was obtained in 93 percent of the eyes studied. However, they could not find any correlation with their assessment of tear volume by Schirmer's test after topical anaesthesia. The condition of marginal tear film deficiency is usually subclinical and asymptomatic. It could be used as an indicator of poor contact lens tolerance.

2.4.2 PRE-OCULAR TEAR FILM THICKNESS (TABLE 2.3)

Initial evaluation indicated a very thin pre-ocular tear film. Fischer (1940) had found that it dried down to 0.05μm. Using a weighing technique, von Bahr (1941) obtained a thickness of 25μm by calculation. More recent studies agree to an average pre-ocular tear film thickness of 7 to 10μm. Maurice (1962) estimated the film at less than 10μm (10μm by calculation and 5.8μm to

FISCHER (1940)		
	DRYING THICKNESS	→ 0.05 µm
VON BAHR (1941)		
	RABBIT WEIGHING	→ 25 µm
MAURICE (1962)		
	CALCULATION	→ 10 µm
	WEIGHING	→ 5.8 µm to 8.8 µm
EHLERS (1965)		
	AVERAGE	→ 7 µm to 9 µm
	BLOOD CELLS	→ 7 µm
	WEIGHING	→ 10 µm
	REDUCTION WITH TIME	→ 0 sec : 8.5 µm
		→ 30 sec : 4.5 µm
NORM (1965)		
		→ 4µm
	OCULAR AREA	→ 172 mm2
MISHIMA (1965)		
	GLASS FILAMENT	→ 7.5 µm
	FLUOROMETER	→ 6.5 µm
	PRE-CORNEAL	→ 5 µm to 10 µm

TABLE 2.3
SUMMARY OF TEAR FILM THICKNESS VALUES

8.8µm by weighing). Ehlers (1965) thought it could vary between 7µm, as instilled red blood cells could move freely in the film, and 10µm by weighing small round discs of known size before and after pressing them against the cornea at different times following a blink, he also showed a decrease in thickness from 8.5µm to 4.5µm, 30 seconds after blinking. With a blink every 8 to 10 seconds, the average total thickness of the film will therefore be between 7µm and 9µm. Mishima (1965) found that the thickness of the fluid layer was uniform over the cornea 7.5µm, by a glass filament method and 6.5µm by a fluorophotometric method.

Hence, it seems that whatever the technique used there is a good agreement regarding the tear film thickness estimation to be between 7µm and 10µm at eye opening and to slowly decrease between blinks down to 4µm to 5µm.

2.4.3 TEAR FLOW (TABLE 2.4)

Tear production rate, or tear flow, is of prime importance in maintaining a normal, wet eye as tear film stability decreases with age in relation to the decrease in tear flow (Marquardt, 1982). The tear flow rate was first measured in 1903 by Schirmer and referred to as tear flow when he collected on filter paper the tear secretion of patients whose lacrimal sacs had been removed. In this way, he collected 0.5g to 0.75g over a 16 hour period which corresponds roughly to 0.6 to 0.8µl per minute. Ever since, subsequent studies have produced widely different results. These variations seem mainly

SCHIRMER (1903)	FILTER PAPER	→ 0.6 to 0.8 µl / min
FISCHER (1931)	FILTER PAPER	→ 0.3 µl / min
BALIK (1952)		→ 15 µl / min
THAYSEN & THORN (1954)		
	FILTER PAPER	→ 10 to 100 µl / min
SZMYT (1958)	FILTER PAPER	→ 13 µl / min
COCHET & AMIARD (1962)		
	PHYSIOLOGICAL	→ 1.5 ml / 24 hr
	REFLEX	→ 7 to 12 ml / 24 hr
		→ 0.6 to 0.8 µl / min
McEWEN (1962)		→ 10 µl / min
	FLUOROPHOTOMETRY	
EHLERS (1965)	REFLEX	→ 7 to 12 ml /24 hr
	PHYSIOLOGICAL	→ 1.5 ml / 24 hr
MISHIMA (1965)		→ 1.2 µl /min
NORN (1965)	COLOUR MATCH	→ 10 to 20 µl / min
MISHIMA ET AL (1966)		
	COLOUR MATCH	→ 1.2 µl / min
BRANDT & FRITSCHE (1967)		
	FILTER PAPER	→ 9.5 ml / 24 hr
EHLERS (1967)		
	CALC CELL COUNT	→ 2.4 µl /min
KIRCHNER (1964)	NOVER TEST	→0.42 to 0.92 µl / min
MISHIMA ET AL (1966)		
	FLUOROPHOTOMETRY	→ 0.2 to 2.0 µl /min
NOVER & JAEGER (1952)		
	NOVER TEST	→ 10 µl / min
	FLUOROPHOTOMETRY	
SORENSEN & JENSEN (1976)		
	RADIOACTIVE TRACER	→ 0.6 µl /min
FURUKAWA & POLSE (1978)		
	FLUOROPHOTOMETRY	
	AVERAGE	→ 1.78 µl / min
	AGE: 15	→ 2 µl / min
	(15 to 39)	→ 1.55 µl / min
	(40 to 63)	→ 0.95 µl / min
	65	→ 0.7 µl / min
LAMBERTS ET AL (1979)		
	CALC/SCHIRMER	→ 2 µl / min

TABLE 2.4
SUMMARY OF TEAR FLOW VALUES

to be due to the experimental techniques of tear collection and to the techniques of evaluation of the results.

Table 2.4 lists the results obtained with the different methods. To date, five main techniques have been used:

1. Schirmer tear test, using collection by a filter paper or cotton thread.
2. Dye dilution tests, using fluorescein.
3. Tear flow calculation techniques.
4. Slit-lamp fluorophotometry.
5. Radioactive tracers.

Reflex lacrimation may increase the tear volume present by a hundredfold (Maurice, 1980).

2.5 THE TEAR FILM STRUCTURE

The introduction of a contact lens on the ocular surface will alter the structure of the pre-ocular tear film; a detailed knowledge of this structure is necessary for analysis of appearance by a visual technique.

2.5.1 GENERAL STRUCTURE

The present thinking on the structure of the tear film is well established after Holly & Lemp (1971b) and stems from the basic description of a tri-laminar structure by Wolff (1946; 1954) (Fig 2.10). It is composed of a basal mucous layer spread on the corneal epithelial surface, an intermediate watery layer and a superficial lipid layer.

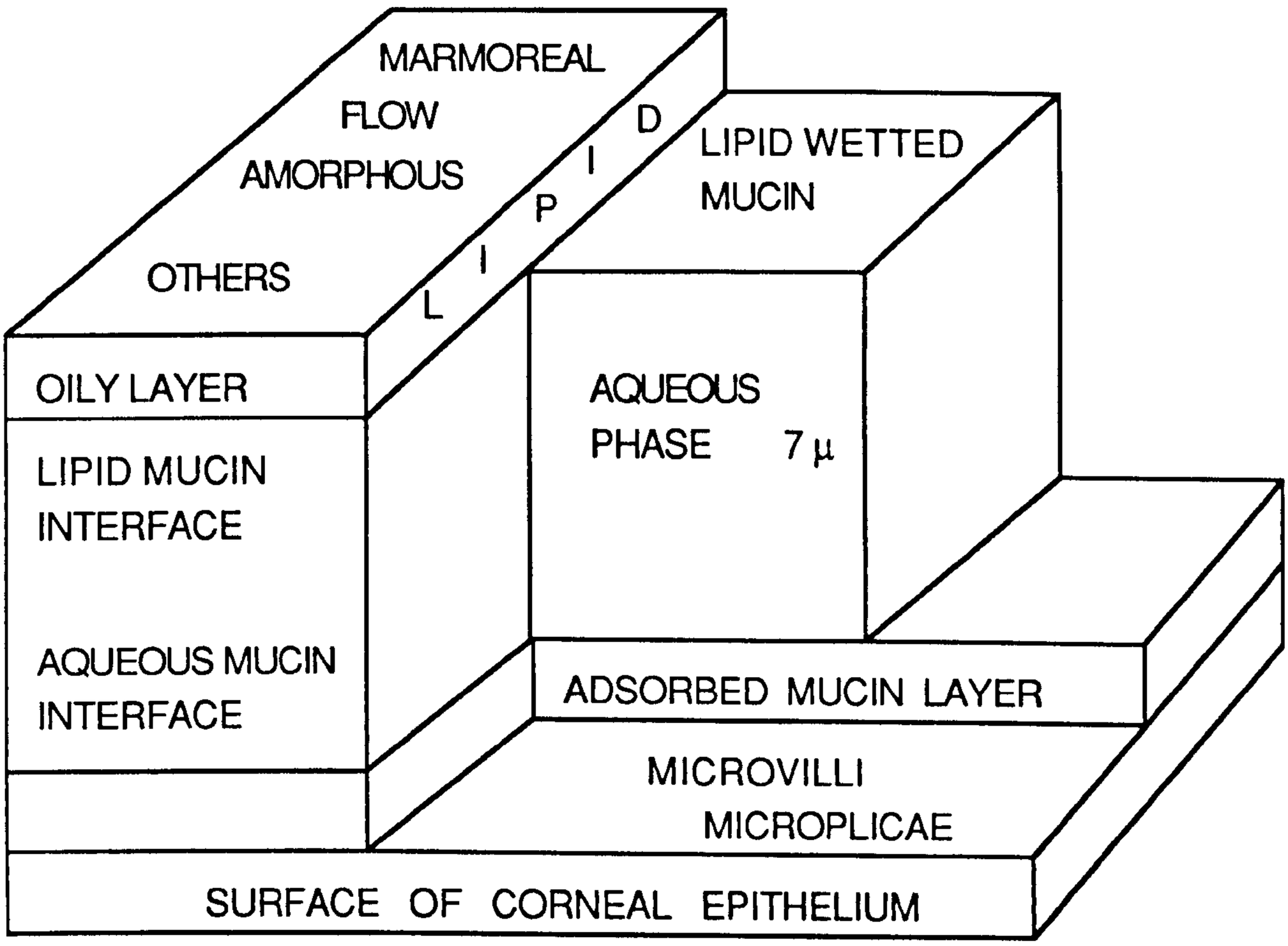

FIGURE 2.10
TRILAMINAR STRUCTURE OF THE PRE-CORNEAL TEAR FILM

The deep layer of the tear film is formed by the mucoid secretion adsorbed at the surface of the anterior membrane of the superficial squamous cells. Ehlers (1965) had earlier suggested that phospholipids of the Meibomian glands secretion were rubbed onto the corneal surface, forming a 'surface active layer'. Tiffany (1988) elaborated a six-layer model with a superficial oily layer, a polar lipid monolayer, an adsorbed mucoid layer, an aqueous layer, a mucoid layer, and a glycocalyx layer at the surface of the cornel epithelium.

2.5.2 STRUCTURE OF THE CORNEAL EPITHELIUM

The superficial part of the cornea is the stratified epithelium (50 to 90μm thick) which consists of three zones of nucleated cells.

The basal zone is formed by a single row of columnar cells (18 to 20μm height, 8 to 10μm wide) with a vertically oval shaped nucleus. The flattened base of each cell is attached to the basement membrane by hemi-desmosomes and to each other by desmosomes.

The mid-zone of the epithelium is formed by the next two to three rows of polyhedral cells, the posterior surface of which is concave to fit closely to the superior rounded part of the basal cells. Because of their thin lateral extensions, they are also known as 'wing cells'. Their nucleus becomes flattened to conform to the shape of the cell as it moves towards the surface.

The most superficial layer consists of large flattened squamous cells. They measure about 4 μm in thickness but are nearly 50μm in width. Their nuclei are

similarly flattened. The anterior membrane of those cells is thicker (6 - 7nm) than the other membranes in squamous cells (3nm only)(Tripathi, 1975).

The thicker outer layer of those superficial squamous cells provide a structural basis for the osmophilic layer of phospholipids. The outer surface of the squamous cells possess projections, microvilli (0.5 to 1µm high and up to 0.5µm thick) and microplicae (0.5µm high) which might be some remnants of the corrugated pattern of the cell borders. It has been put forward that these projections played a role in the retention of the pre-corneal tear film by increasing the area of contact as the number of microplicae are markedly reduced in dry eyes. Their exact role is not yet clearly understood but it could be nutritional.

The different cell layers represent different stages of cell development. As the cells are pushed towards the surface, they are continuously replaced by new cells, which move forward, gradually flatten and become desquamated. In this way, keratinisation never occurs in normal corneal epithelium.

The life of these surface squamous cells is short as nearly one seventh of the total population is shed daily. As it was shown by radioactively labelled cells, the time from division to desquamation for normal epithelial cells was less than one week (Hanna & O'Brien, 1960).

However, following superficial corneal injury, the healing process is much more rapid, first by pseudopodial migration of neighbouring basal cells and movement of

adjacent cells to cover the wounded area but also by a very increased epithelial cell mitosis rate.

2.5.3 THE INNER MUCOUS LAYER

Blumcke & Morgenroth (1967) demonstrated the presence of a lipid and protein layer on the epithelial cell surface by electronmicroscopy. This was challenged by Holly (1973b) who found a 200 Ångstroms to 400 Ångstroms thick mucin layer (0.02 to 0.04µm) coating the epithelial cell surface.

More recently Nichols et al (1985) demonstrated a mucous layer of 1µm thickness on guinea pig corneas.

The conjunctival goblet cells, by their significant output and their strategic location, are thought to be the main source able to supply this mucous layer, periodically renew it and remove as well the lipid contaminant in the form of mucous strands. But some complementary glycoprotein might be secreted by the conjunctival epithelial cells to form the foundation to the mucous layer (Takakusaki, 1969; Ehlers et al, 1972; Greiner et al, 1980). These glycoproteins have a cross-link arrangement which is the basis for the formation of the mucous strands.

The main macromolecular component of mucous secreted by the epithelial cells consists of glyco-protein. They are carbohydrate protein complexes characterised by the presence of hexosamine, hexose and sialic acid (Van Haeringen, 1981).

Great individual variations, however, occur in the composition of carbohydrates and protein components.

The glycoprotein molecule has many sites where chemical bonds can be formed. These sites lock on other sites located on the corneal epithelium, creating a mucin surface (Doughman, 1977). Glycoproteins are rod-shaped molecules with a protein at the core and carbohydrate side chains. These molecules are surface active substances since they have both polar and non-polar segments. According to Holly et al (1977) the non-polar segments can align with the lipid surface of the corneal epithelial cell membrane and their polar segments render them soluble in the aqueous phase of the tear film. On the other hand this may not be sufficient evidence that the lipid surface of the cell membrane is necessarily hydrophobic, because the polar and charged group are exposed but not the hydrocarbon region of the lipid chains.

The mucous is discharged from the goblet cell and swells in the conjunctival fluid where it becomes filiform. When these fibrils become detached from the cells, they move with the tear flow. The mucous envelops foreign bodies and its lipid contaminants, and gather over the entire length of the fornix. Usually, a larger mucous strand is found at the inferior fornix and a smaller one at the superior fornix. The occurrence of mucous thread is increased in some pathological conditions such as: keratoconjunctivitis, vernal-conjunctivitis and acute infectious conjunctivitis.

Norn (1972) found that the mucous fibrils in the mucous thread could be stained by PAS reagent and also by alcian blue suggesting that they consist of acid mucopolysaccharides. Greiner et al (1982) observed, by

electron microscopy, 20 biopsy specimens of human conjunctival epithelial surfaces and its associated mucous. They found that three morphological mucous types existed: strands, sheets and granules. They thought that the mucous sheets may result from the flattening of the thick mucous strand by the shearing action of the upper eyelid. The mucous granules may be due to the dehydration and fractures of mucous sheets and strands.

2.5.4 THE AQUEOUS PHASE OF THE TEAR FILM

The aqueous phase accounts for over 90 percent of its thickness and contains 98.2 percent water and 1.8 percent solids (Ridley & Sorsby, 1940). This phase originates from the main lacrimal glands and the accessory lacrimal glands of the conjunctiva. The solutes in the aqueous phase consist mainly of inorganic electrolytes and low and high molecular weight organic substances. The organic substances of low molecular weight are glucose, urea and amino acids. The organic constituents of high molecular weight are the tear proteins (albumin, globulin, and lysozymes). The main inorganic electrolytes in the aqueous phase are: sodium, potassium, calcium, chloride, bicarbonate and carbonate ions (Biological Data Handbook - Tears, 1974).

The sodium concentration in tears (145mg/ml) is similar to that in serum, but the potassium concentration (16 to 24mg/ml) is three to five times higher in tears than in serum; their role is essential in the osmotic regulation of the intracellular and extracellular spaces. The chloride concentration (128 to 144mg/ml) is slightly

higher than in serum, and its role is linked with sodium and potassium in osmotic regulation (Botelho, 1964).

The bicarbonate concentration (26mg/ml) seems to be involved with the pH regulation. It plays a role in the buffering action of tears, keeping the pH near isotonicity 7.45, with a range from 7.14 to 7.82 (Carney & Hill, 1976) a more acidic pH 7.25 is found following prolonged lid closure (Carney & Hill, 1979).

The other ions found in lower concentration, calcium, seem to be independent of tear action production (0.4 to 1.1mg/ml).

The osmotic pressure of the tear film is about 305mosm/kg, or equivalent to 0.95 percent Nacl (Gilbard et al, 1978; Terry & Hill, 1978). A 5 percent difference in osmolarity is found between tears collected at the lid margin and those collected in the conjunctival fornix, the lower values around 290mosm/kg are closer to that of the serum (Mishima et al, 1971). If the tear film is hypotonic, as in excessive tearing, water will enter the corneal epithelium and cause it to become oedematous (Carney and Jacobs, 1984). With hypertonic tears, water is drawn into the tear film causing a decrease of epithelium hydration. In keratoconjunctivitis sicca, high osmotic values have been demonstrated and it may be due to an imbalance between evaporation and the decreased tear production in this disease. Osmotic pressure is sensitive to changes in tear flow and reflex stimulation of tears. For example, in early adaptation to contact lenses reflex lacrimation results in a decrease in electrolytes and in total protein. The resulting

relative hypotonicity may account for the epithelium oedema, often seen in the early stages of contact lens adaptation (Callander & Morrison, 1974).

Holly (1973b) has assumed that the structure of this aqueous layer was similar to that of most polymer solutions possessing solute molecules with high axial assymetry. He has divided the phase into a superior dilute phase, where the molecules have complete rotational freedom and a lower more concentrated phase or coacervate (Fig 2.10). It is possible that part of the dilute mucin phase might originate directly from the lacrimal gland secretion (Ruskell, 1969). Maurice (1973) suggested that some contribution to the aqueous layer of the tear film occurs through an outwardly directed osmotic flow through the cornea and the conjunctiva which is induced by the hyperosmolarity of the tear film due to evaporation between blinks.

2.5.5 SUPERFICIAL LIPID LAYER

The presence of an oily layer had been optically detected by observation of surface interference patterns seen in specular reflection by Vogt as early as 1921 and first photographed by Fischer (1928). Many papers since then have dealt with this phenomenon (McDonald, 1969; Brauninger et al, 1972; Hamano et al, 1980a; Josephson, 1983). Several authors have shown that this oily layer is derived from the tarsal Meibomian glands and that the dynamic stability of the tear film is markedly changed by Meibomian gland dysfunction (Ehlers, 1965; Korb & Henriquez, 1980; Henriquez & Korb, 1981).

Analysis of this secretion using thin layer chromatography (Nicolaides, 1986) has shown it to be a lipid material containing a high proportion of cholesterol esters and other ester waxes. It has a moderate content of free cholesterol and a low content of free fatty acid. It is quite unlike any of the other lipid secretions produced by the skin and is akin to the vernix caseosa of the neonate. It differs from the sebum in being virtually free from triglyceride which forms approximately 45 percent of sebum (Keith, 1967). Its structure is that of a duplex film where the cholesterol esters form the outer layer and the remaining constituents form an inner molecular film overlying the superior dilute phase of the aqueous layer (Norn, 1963).

The functions of the lipid layer are two-fold. Firstly this layer prevents lacrimal evaporation, and secondly it maintains an optically homogenous tear film surface (Mishima & Maurice, 1961a, 1961b; Andrews, 1973; Records, 1979). Both these functions have been extensively investigated and all in-vivo experiments support these conclusions (Mishima & Maurice, 1961a, 1961b; Iwata et al, 1969; Sorensen & Jensen, 1977, 1979).

Observations of particle movements within this layer when viewed under moderate levels of angular magnification (x35) enable relatively straight-forward detection and have led Ehlers (1965) to describe its properties and also to note the appearance of amorphous superficial figures or strands which were transient, changeable, altered by blinking and occasionally provoked by pressure on the lid margins.

McDonald (1969) has shown that the appearance of Newton's colour fringes in the lipid layer is directly related to the thickness of the film. He suggested that a grey appearance of varying shades corresponded to a lipid layer thickness of less than 0.1μm and that compression of the film during blinking (lid aperture reduction) led to an increase in thickness from 0.1μm to 0.17μm. This increase was found to correspond to the successive appearance of red, orange, yellow, green and blue fringes forming the first order of spectral interference colours. The observation of a complete spectrum of the second order of interference colours was found to occur when the superficial lipid layer was 0.52μm or greater. These observations enabled McDonald to conclude that the average lipid layer was between 20 and 72 molecules thick (0.1μm to 0.37μm). Unfortunately, these results are in error due to incorrect refractive index calculations and have been widely quoted, the latest reference being Josephson (1983). A more precise interpretation of the interference colours and their associated thicknesses should take account of the relevant refractive indices of the layer previously omitted (Guillon & Guillon, 1984; Olsen, 1985; Tiffany, 1986).

Hamano et al (1979a; 1982), using a wide field bio-differential microscope, have classified the lipid appearance into three main categories:

a) A marmoreal (marble-like) pattern consisting of patchy structures of dark and light parts rather like a meshwork.

b) A flow pattern having a regular, almost smooth, stream-like structure of bright appearance.

c) An amorphous pattern having no discernible structure whatsoever.

The first pattern was reported to be found in 90 percent of normal eyes.

2.6 CORNEAL EPITHELIUM WETTING

Because of the phospholipid component of the cells membrane, the epithelial surface is relatively hydrophobic when wiped dry, it is not wettable by aqueous tear. Mucin plays the role of a wetting agent to the corneal surface (Holly & Lemp, 1971a). This hydrophobicity could be artefactual (Cope et al, 1986).

2.6.1 BASIC PRINCIPLES

The relationship between a surface and a gas and a liquid is characterised by the fluid contact angle with the solid. It is the angle at which the liquid meets the solid's surface. The surface molecules of a fluid volume are attracted internally by the cohesive forces of the bulk of the fluid which is greater than the attractive force of the molecule of the vapour adjacent to the surface. In weightlessness a small fluid volume will take the shape of a perfect sphere, on a surface it will tend to keep this shape and form a droplet. The exact shape of a fluid droplet will depend on the surface forces present at the solid, fluid and gas interface. The contact angle is that found between the solid surface and the tangent to the edge of the droplet surface. A

high contact angle demonstrates the inability for the liquid to wet the surface; a low contact angle shows an increased affinity for the surface; zero angle corresponds to complete wettability.

The critical surface tension (CST) of a liquid is the measure of the force necessary for the liquid to completely wet a given surface.

In order for water to cover a surface, the CST of the water must be equal to or lower than the CST of that surface.

2.6.2 CORNEAL WETTABILITY

Little is known of the exact nature and structure of the advocated mucous coverage of external ocular structures. Up to now all the research work on corneal wettability has relied on the application of techniques used in surface chemistry.

The CST of rabbit and bovine corneal surface (cleansed by rinsing) is 28dynes/cm (Holly and Lemp, 1971a). The same result is obtained when lipids from meibomian secretion are spread on corneal epithelium.

The contact angle of physiological saline on cleansed cornea was found to be 50 degrees (Lemp et al, 1970b).

The surface tension of water is 72dynes/cm. The mucous secretion acts in two ways. It first dissolves in the tear fluid to reduce its CST from 70 to 38dynes/cm, and by spreading on the corneal surface it elevates its CST to 40dynes/cm.

In this way the aqueous phase has a lower critical surface tension than that of the mucin-coated epithelium and all the requirements for corneal wetting are met and the contact angle is zero degrees.

Because in the tear film there is no free aqueous interface, mucin has to lower the film surface tension indirectly by lowering the tension of the superficial lipid layer. Furthermore, the mucous layer coating the epithelium is able to maintain the interfacial tension at a low value by removing the lipid contaminants which continually bombard the epithelium surface (Holly & Lemp, 1977).

These early results are increasingly being challenged because of the destructive nature of the solutions used in the experiments (Cope et al, 1986).

The development and use of non invasive techniques of observation of the mucous coverage will allow a better understanding of wetting properties of corneal and contact lens surfaces.

2.7 STABILITY OF THE TEAR FILM

2.7.1 BREAK-UP OF NORMAL TEAR FILM (TABLE 2.5)

The pre-ocular tear film in humans does not remain stable for long periods of time (Holly, 1981a). When blinking is prevented, the tear film ruptures within 15 to 40 seconds, dry spots appear over the cornea (Lemp & Hamill, 1973) and the tear film decreases in thickness by around 10 percent through evaporation. A duplex lipid film is seldom stable for long period of time some of the

NORMAL

NORN (1969b)	RANGE	→ 3 sec to 25 sec
LEMP & HAMILL (1973)	TOTAL	→ 100 eyes
	RANGE	→ 10 sec to >45 sec
		→ 15 sec to 34 sec
FORST (1976a)	TOTAL	→ 238 eyes
	AVERAGE	→ 14 sec
	RANGE	→ 4 sec to 54 sec
	CRITICAL	→ 5 sec to 7 sec
KAME ET AL (1976)	TOTAL	→ 80 eyes
	AVERAGE	R.E. → 15.27 sec
		L.E. → 14.57 sec
	RANGE	→ 3 sec to 20 sec

TABLE 2.5
SUMMARY OF TEAR BREAK-UP TIME MEASUREMENTS

superficial lipids will migrate to the epithelium interface, there it contaminates the adsorbed mucin layer creating areas of high interfacial tension and converting it into a hydrophobic surface (Fig 2.11). This process will be accelerated by local thinning of the tear film, induced by the surface tension gradients in the superficial lipid layer, or by gross irregularity in the epithelial surface (Fig 2.12). The tear film in those areas becomes unstable forming non-wettable areas of gradually increasing size. The measurement of the break-up time (BUT) will be considered in Chapter 3.

2.7.2 TEAR FILM ABNORMALITIES

The detection and differentiation of tear film abnormalities can be improved by non-invasive observation technique.

The definition of an abnormal tear film and its causes have been often reviewed by many authors (Bron, 1985; Holly & Lemp, 1977).

The following signs are considered to be of importance by these authors as a basis for the adequate diagnosis of an abnormal tear film:-

- a scanty or uneven meniscus
- the presence of excessive particulate matter
- the rupture of the tear film prior to a subsequent blink
- the production of hyperosmotic tears
- the abnormality or absence of the superficial lipid layer

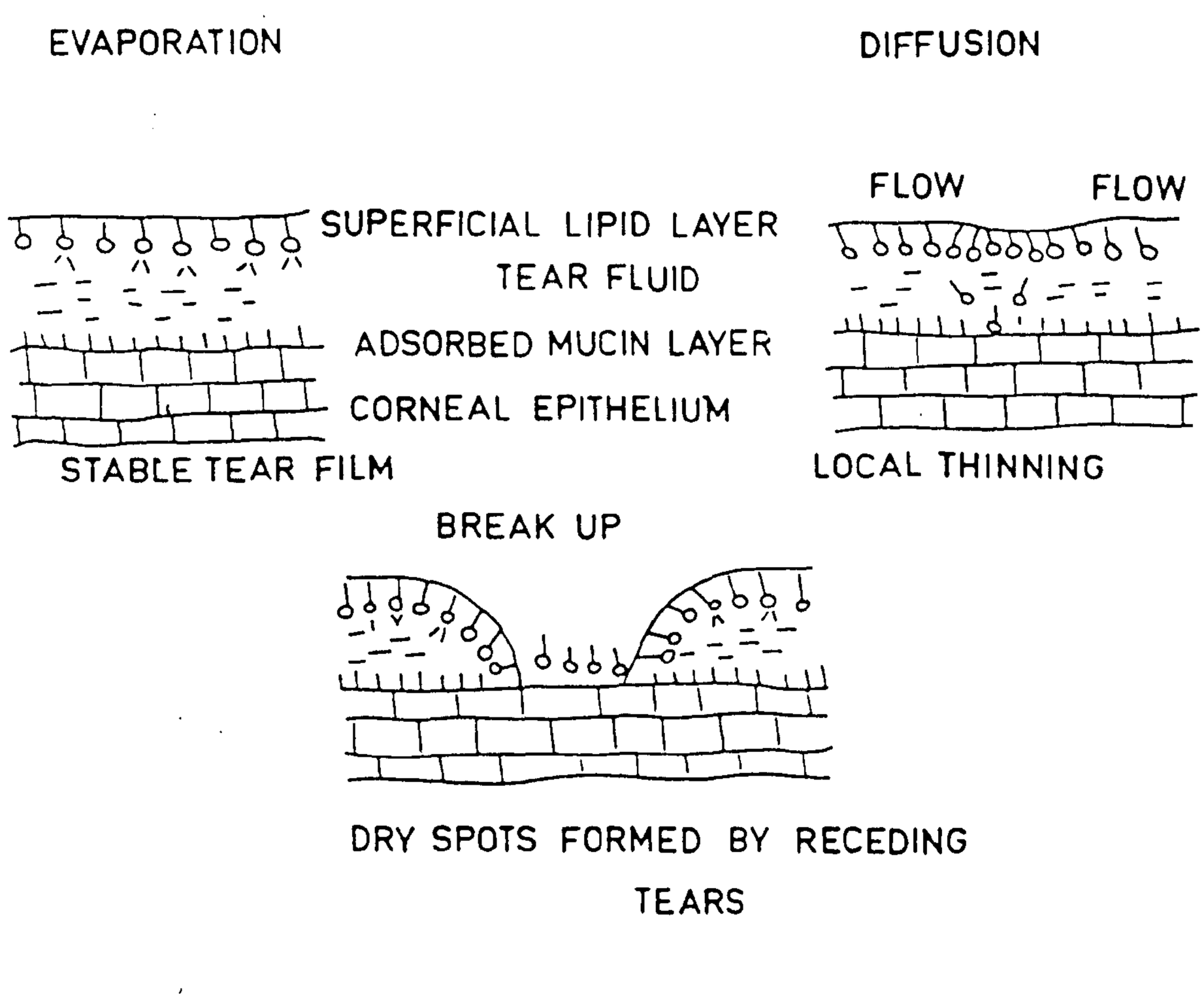

FIGURE 2.11
MECHANISM OF DRY SPOT FORMATION
(After Holly, 1973b)

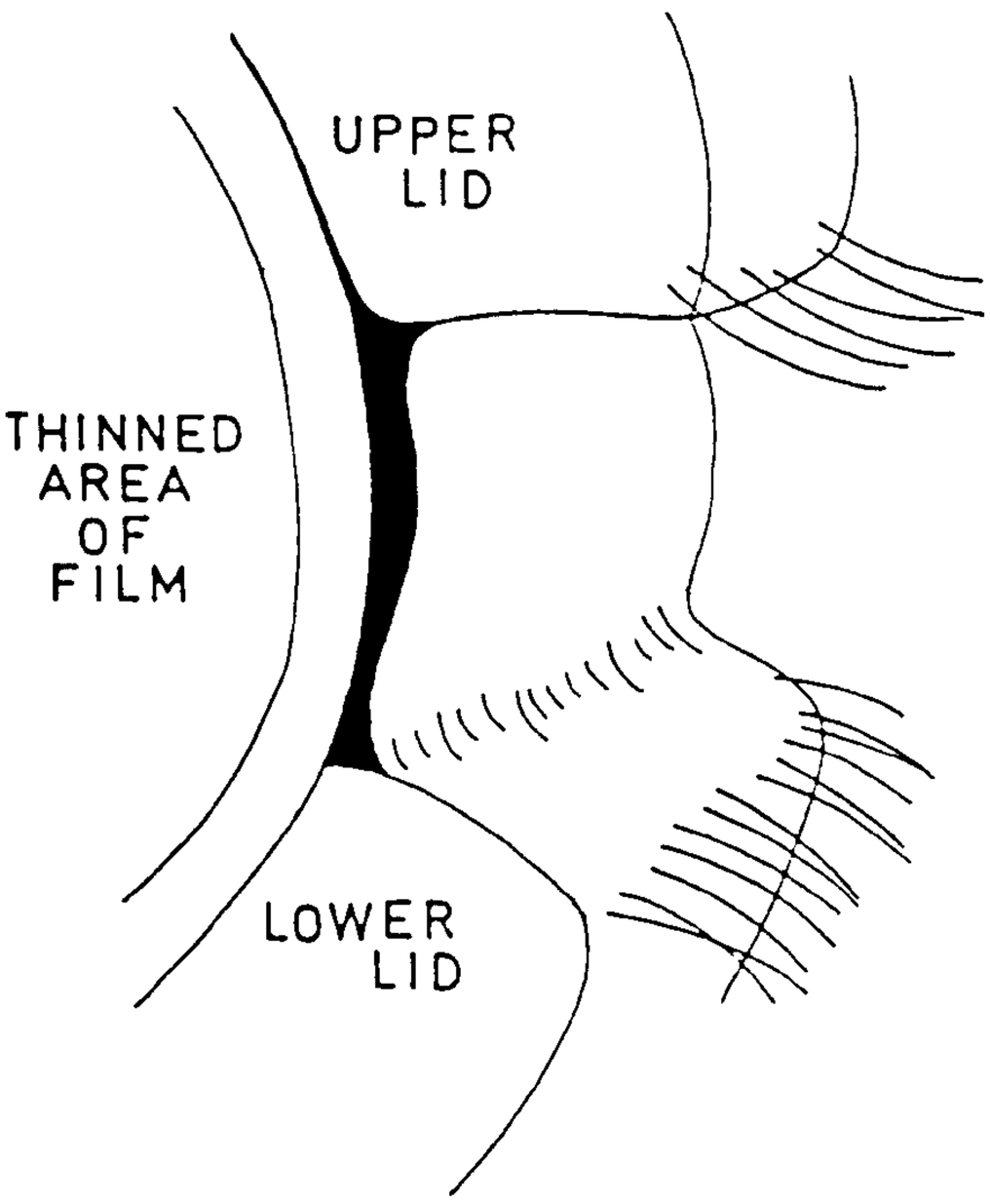

FIGURE 2.12
MENISCUS INDUCED THINNING OF TEAR FILM
(After McDonald & Brubaker, 1971)

- an abnormal or inadequate mucous layer

- the presence of an epithelial surface disorder.

The factors leading to the production of an abnormal tear film are numerous and include the following:-

- an insufficient lacrimation

- an increased evaporation and a low tear turnover rate

- an increased polarity of the meibomian secretion

- an abnormal tear protein composition

- an inadequate blink behaviour

- an inadequate mucous supply and mucous layer

- a primary ocular surface disorder.

Some of those signs can be detected as a matter of routine clinical observation using non-invasive techniques or simple tests available to the practitioner.

i) <u>Abnormal Meniscus</u>

A scanty or uneven meniscus is seen as an irregular reflection originating from its very small curvature bordering the lid edge when using direct illumination. An uneven border line and a height less than 0.1mm combined with a sharp definition of its black line separating it from the tear film, are signs of abnormality. Localised tear film break-up originating from this meniscus border is increased in these cases. An increased curvature is a sign of reduced volume (below 2.9µl) but also of reduced hydrostatic pressure which encourages movement of fluid from the pre-ocular tear film, the meniscus and induces localised disruption.

ii) Particulate Matter

The presence of excessive particulate matter in the POTF and meniscus when viewed with high and low magnification is abnormal. This particulate matter often consist of mucous strands of increased length formed by mucous dislodged from the epithelial surface and mixed with superficial lipid layer. In Filamentary Keratitis these strands will be strongly attached to the surface epithelial cells.

Increased cellular debris is indicative of surface damage when observed in contact lens wear or in conjunction with the use of preservatives and in response to conjunctival inflammation (Bron et al, 1985). Keratoconjunctivitis Sicca (KCS) patients exhibit a quantifiable increase in cellular debris in the tear film following rapid desquamation of damaged cells.

iii) Break-Up

The observation of the rupture of the POTF before a subsequent blink and its measurement in the most commonly used test of tear film stability.

Reduced break-up time (BUT) or limited ocular surface wetting measured with or without fluorescein instillation is one of the main signs of an abnormal tear film

Lipid Layer - the abnormality qr absence of the superficial lipid layer or its contamination has been observed repeatedly since McDonald first introduced the concept (Hamano et al, 1980a; Josephson, 1983; and Guillon, 1982).

The abnormality of the lipid layer is caused by:-

- an abnormal blockage of the secretion ducts (according to Norn 1985, more than 56% blocked ducts is considered abnormal)
- the poor apposition of the lid margin or an abnormal position of the strand orifices
- the contamination by skin lipid and/or make-up and skin lotions
- the presence of blepharitis or facial skin disorders
- contamination by excessive or denaturated mucous discharge.

Destabilisation of the tear film also occurs with changes in lipid composition. Such an increase in free fatty acid or triglyceride or an abnormal ratio of its polar and non-polar components which is the parameter on which depends the duplex lipid film formation.

- the presence of a meibomianitis has been also associated with aqueous deficiency in some cases (McCulley and Sciallis, 1977).

- an abnormal or inadequate mucous layer contains coarse hydrophobic strands of mucous accumulated when the mucous supply cannot keep up with accelerated mucous loss induced by increased lipid contamination, deranged mucous-lysozyme interaction (Lee et al, 1981) or increased exfoliation of surface cells.

In keratoconjunctivitis sicca (KCS) the mucous content of the tears shows abnormal precipitation pattern (Rolando et al, 1986). The density of the Goblet cells may be diminished and the subsurface mucous vesicles of

the epithelial surface thought to contribute to the process of mucous layer formation are absent (Dilly & Mackie, 1981).

Mucous glycoprotein deficiency is usually inferred indirectly by the observation of reduced BUT in the presence of normal aqueous secretion.

Benjamin et al (1984) have shown indirectly the presence of a mucous layer by its effect on the surface wettability of contact lenses. New techniques based on in-vivo non-invasive direct observation and photography of the mucous layer on the corneal surface and on different types of contact lenses are showing some difference in its structure and thickness in different cases (Guillon, 1986).

- the presence of an epithelial surface disorder can directly cause a tear film abnormality, originated by loss of mucous glycoprotein, decrease in conjunctival goblet cell density followed by a rapid exfoliative process of surface cells and keratinisation.

Insufficient lacrimation - the two main causes of bilateral aqueous deficiency are keratoconjunctivitis sicca (KCS) and Sjögrens syndrome. Sjögrens syndrome is a disorder including dryness of the eyes and the mouth and is often associated to a connective tissue disorder such as rheumatoid arthritis. KCS is an age-related syndrome occuring commonly in the fifth and sixth decade of life, as some evidence points to a deterioration and atrophy of the lacrimal acinar and duct tissue Damato et al, 1984) and affecting women more than men as it has often been related to hormonal imbalance (Holm, 1949).

Bron (1985) has drawn a very good resume of the history of the occurrence of KCS. It seems to start with infiltration and atrophy of the lacrimal gland combined with a certain degree of inflammation. The ensuing reduction in tear flow reflected in a limited meniscus and tear film volume combines with an increase in evaporation rate to produce an hyperosmolarity, inducing the familiar symptoms of discomfort and the first signs of abnormal cellular responses.

The alteration in mucous production, spreading and its accelerated denaturation reduces the wettability of the epithelial surface and induces the deterioration of the surface epithelial cells which are more rapidly desquamated and appear as debris in the tear film.

The reduction in tear film stability may account for some of the conjunctival and corneal damage observed.

KCS patients often show signs of ocular inflammation such as conjunctival redness, blepharitis or meibomian disease and can be vulnerable to recurrent corneal ulceration, vascularisation and possible corneal scarring. The signs and symptoms of instability resulting from all kinds of tear film abnormalities can be detected and monitored by the non-invasive techniques to be presented in this thesis.

As seen, the formation of the pre-ocular tear film relies on a variety of factors.

CHAPTER 3

CURRENT CLINICAL TECHNIQUES TO STUDY THE TEAR FILM

3.1 INTRODUCTION

A large number of clinical, experimental and research techniques have been developed to study the tear film and its different components.

This chapter is a review of the relevant techniques that can be applied to the clinical examination of the tear film. They can be separated into two groups:

1) those involving a biomicroscopical examination
2) those making use of ophthalmic stains.

3.2 BIOMICROSCOPICAL EXAMINATION

3.2.1 INTRODUCTION

The routine biomicroscopic examination provides invaluable information of a non-invasive nature when directed to the appearance of the tear meniscus, that of surface interference phenomena, and that of superficial particulate movement. With a specially designed set-up the measurement of break-up time (NIBUT) can be achieved without the use of fluorescein (Mengher et al, 1985a; Guillon, 1985; Guillon, 1986).

3.2.2 OBSERVATIONS OF THE TEAR MENISCUS

The tear meniscus forms along the lower and upper lid. Each meniscus is limited on the lid margin side by the muco-cutaneous junction situated just behind the Meibomian gland orifices. On the corneal side it is separated from the pre-ocular tear film by a localised thinning known as 'black-line' when the film is stained with fluorescein (Holly, 1978a).

The lower meniscus is easier to examine for regularity, height, width and curvature. Holly & Lemp (1977) assessed its width to be approximately 1mm and suggested that a scanty appearance or area of discontinuity were signs of an aqueous tear deficiency or lipid abnormality.

Taylor (1980) suggested that the meniscus should be described qualitatively as intact, non-intact or temporally non-intact.

Although a few authors (Klein, 1949; Wright, 1971; Baum, 1973) proposed the evaluation of the tear meniscus as an assessment of the tear flow. Lamberts et al (1979) found that the tear meniscus height in normal eyes varied between 0.3mm and 0.1mm in 92% of his 86 observations and that no correlation was found between tear meniscus height and Schirmer test with and without anaesthesia.

Terry (1984) concluded that a tear meniscus height inferior to 0.3mm is an indication of dry eye.

The reflection of a light beam moved vertically across the meniscus gives an assessment of its curvature (McDonald, 1969). The normal meniscus should have a convex surface near the corneal side, a concave surface

centrally and a convex curve in its contact with the eyelids. When the lower meniscus is illuminated in a downward fashion by a beam of light the reflection should show a 'with' movement in the convex zone followed by an 'against' movement in the concave zone. When these movements are absent, a low surface tension at the meniscus is suspected.

3.2.3 OBSERVATION OF INTERFERENCE PHENOMENA

Observation of surface phenomena of the tear film have been carried out soon after the creation of the slit-lamp biomicroscope. Only over the past few years, has photography of these phenomena been possible. The following is a short history of the progression of this technqiue.

Historically, the interference phenomena visible at the surface of the cornea were first described by Vogt (1921).

Marx (1921) described the formation of dry spot on the cornea occurring on average every 60 seconds and suggested that the thickness of the tear film could be estimated from the dispersion of colours.

Koby (1924) photographed the zone of specular reflection of the cornea and reported the presence of dust and irregularities of surface.

Meesmann (1927) also noted the presence of surface spectral colours in the tear film.

Fischer (1928) gave a general description of the pre-corneal layer of liquid from photographs of the light reflection from the corneal surface.

Fischer (1940) mentioned that the tear film dries down to a thickness of 0.05µm, a number probably achieved by analysis of interference fringes.

Wolff (1946) mentioned the presence of oil drops seen in the rivus lacrimalis.

Edmund (1951) presented measurements of the corneal gloss produced from light reflected from the corneal surface.

Ehlers (1965) in his extensive dissertation describes his biomicroscopical examination of the pre-corneal film, the presence of embedded particles and various colour dispersion phenomena visible in the portion lying slightly outside the direct "mirror zone" formed by the light reflected from the cornea. The surface particles are shown to move as an integrated whole when the lower lid is carefully displaced upward over the bulbus. He observed some amorphous or diffuse phenomena consisting of superficial figures or strands of varying appearance giving to the surface the resemblance of a tarnished, dirty or greasy metal surface with spots of reduced gloss. These were transient in nature and altered by blinking and sometimes the dull zones formed stripes, usually vertical and in a few cases parallel. Ehlers concluded that these phenomena could be due to small droplets of secretions just discharged from the Meibomian gland.

McDonald (1969) studied extensively the surface phenomena of the tear film on the eye, on contact lenses, in human and in the rabbit. First with a self inspection technique using a concave microscope mirror placed on an

x-ray viewing box but mainly with the biomicroscopic observation of the reflection of a fluorescent light or a gooseneck lamp suitably placed close to the cornea. He observed the spectral interference patterns visible in front of the virtual image of the lamp. He concluded that the grey background observed corresponded to a surface layer not thick enough to cause interference (less than 1000 Ångstroms), that the first order of spectrum of interference was present for thicknesses between 1000 Ångstroms and 1750 Ångstroms and that a second order spectrum of colours corresponded to a layer thickness between 1750 Ångstroms and 5200 Ångstroms.

He suggested that these interference patterns were confined to the oily layer which varied on average between 1000 Ångstroms and 3700 Ångstroms. As a monolayer of fatty acid measures on average 25 to 30 Ångstroms, this corresponded to a 72 molecules thick layer in its thickest part and a 20 molecules thick layer in its thinnest part. McDonald showed the origin of the oily layer to come from the orifices of the Meibomian glands. Their secretion was increased by everting the upper lid or by rubbing of the eyes as it probably massages the glands causing them to empty on the tear surface.

In some cases he noted the presence of fractures in the oily layer and interpreted them as breakdown of the viscosity of the oily layer. His observation on the rabbit showed a surface of different shades of 'grey with movable whorls' suggesting an oil cover of variable thickness while partial lid closure causes the successive

appearance of the first and second order of interference colours. The same observation was made during normal or partial blink with a continuity in the oily layer appearance between the 'lacrimal lake' and the 'lacrimal prism'.

McDonald also described a 'crumpling effect' visible during blink in the presence of a very thin oily layer and a 'pleated drape effect' visible in the same circumstances when the oily layer is squeezed between the lids.

His observations of interference phenomena on contact lenses placed in a rabbit's eye or in human eye revealed a full thickness tear film interference pattern consisting of five or more orders of spectra whose colours swept rapidly across the surface and then receded to extinction. This represented thicknesses from 11,000 Ångstroms to 1000 Ångstroms near the edge of the drying tear film. This rapid drying on the front of a contact lens was attributed to the three following possibilites:

i) the pre-lens tear film may have an oil film more permeable or more expanded that the normal cornea

ii) normal tear film renewal from behind or from the periphery may be inhibited by the contact lens

iii) the better wetting properties of the corneal epithelial surface may be a factor in the rate of surface drying.

When a microscopic area dries it acts as a nucleus from which the tear film recedes. These dry areas then resist rewetting and dry faster than the adjacent

surfaces suggesting that they have a lower surface tension.

Clark & Carney (1971) had shown by theoretical analysis and reflectometry measurement that most of the reflection originated from the oily layer present at the anterior surface of the film.

Clark (1973) used interferometric techniques to measure the anterior surface topography and thickness variation of the pre-corneal film. He observed thickness gradients in the oily layer of the pre-corneal tear film as great as 2 mrad (miliradians) and its thickness to be around 0.1 μm. The use of a hard corneal contact lens was necessary to provide a sufficiently large refractive index difference between the tear fluid and the underlying surface to record interference fringes formed across the whole depth of the liquid. They managed to photograph sodium light fringe patterns formed in the pre-lens tear film thickened by wetting solutions and later after thinning by evaporation, but no measurements were given.

Norn (1979) devised a semi-quantitative method of measurement of the lipid layer by observation of the reflection from a ground matt glass plate mounted in front of a slit-lamp mirror.

If a red petrol-like pattern appears on the pre-corneal tear film when the eyes are fully opened the fatty layer has maximal thickness (greater or equal to 200 nanometers). If the film is colourless, the patient is asked to slowly close their eye until the interference

phenomenon shows, for example, if the width has to be halved, the layer is then 100nm.

In this way, by relating the palpebral aperture when the interference occurs to that of the patient's normal palpebral aperture it is possible to calculate semi-quantitatively the thickness of the fatty layer.

That technique can be used clinically but the calculations used, the measured variable and the irregular nature of the lipid layer will limit its precision but on 206 normal persons an average thickness of 102± 3nm was found, only 5 percent showed maximum layer (equal to or greater than 200nm) and 8 percent a minimal layer (equal to or less than 17nm corresponding to a palpebral fissure equal to or greater than 2mm)

A maximum thickness was noted on awakening and took 20 to 60 minutes to stabilise, and was independent of age, sex and break-up time (BUT). An increased thickness is found in chronic blepharitis (129± 8nm), in acute infectious conjunctivitis (164± 7nm) and all conditions complicated by bacterial infection.

It is possible that reflex tearing in those conditions induce an increased reflex production of lipid.

Hamano et al (1980b) used their biodifferential interference microscope on normal rabbit and human tear films, also in the cases of palpebral entropion, trichiasis, superficial keratitis, erosion, ulcers, epithelial desquamation and Sjögren's syndrome. In the case of a contact lens they remarked that the gas permeable hard lenses had a better wettability than PMMA

lenses but rapid contamination by mucous or protein was a problem. They expressed the view that 3 and 9 o'clock staining of the cornea in rigid lens wearers was due to tear film break-up occurring repeatedly in the same area bordering the contact lens.

A better surface wettability was expected from soft lenses but increased rate of water evaporation was noted in ultra-thin lenses and in lenses made of high water content material.

Their first instrument was not designed for the examination of curved surfaces and the image suffered from the presence of diagonal band of colour inherent to the optic of the system that was spoiling the information from the photograph.

Later, an even field microscope was designed to solve this problem (Hamano et al, 1982).

Haberich & Lingelbach (1981) used an opaque truncated retro-illuminated cone to illuminate the tear film and observe the interference fringes in the lipid layer through a hole at the centre of the cone. The method consists in a combination of the interference and Schlieren optic technique.

From these observations Haberich (1982) proposed that the break-up of the tear film is not due to localised thinning of the tear film and contamination of the basal mucous layer by lipid as suggested by Holly (1973b), but originates from breaks in the integrity of the epithelial membrane of the superficial cells. When the lipid layer of the membrane breaks, it induces an increase in water inflow towards the cell and a

transpolarisation of its surface due to the loss of its lipophile properties. Both factors cause the breakdown of the tear film and in this context a lack of mucine is not a necessary requirment.

The proposed structure for the pre-ocular tear film states that the interspace between the lids and the bulb (fornix conjunctiva) contains only an aqueous solution of dissolved mucins with a 'proper' mucin layer only present within the palpebral aperture.

Further, when a contact lens is inserted the mucin layer is not present at the surface of the lens which is only covered by the aqueous tear liquid and a superficial lipid film.

Both theories and structure are doubtful as they seem to go against the accepted theories based on the need of the natural wetting agent (mucin) to efficiently form a pre-ocular and pre-lens tear film.

Guillon (1982) described his technique of high magnification observations of tear film layers under polarised light with photographs of irregular lipid layer and dust particles at the surface of the pre-ocular tear film. The pre-soft lens tear film is shown to be unstable in the presence of surface deterioration and deposits with rapid break-up and drying in localised areas. On corneal contact lenses the absence of a lipid layer is noted as the assessment of interference fringes within the aqueous phase leads to a measurement of pre-lens tear film thickness of 1.5μm. The presence of a lipid layer surrounding the lens is assessed to be due to the barrier effect of the contact lens edge.

Kilp et al (1982) used a reflecting microscope at high magnification but also differential interference contrast microscopy to study the surface irregularities of the tear film. They related subjective symptoms to isolated disturbances of the lipid phase which formed small droplets separated by dark areas of reflection identified as discontinuities in the duplex lipid film. In cases of decreased aqueous phase or abnormal mucin production an accumulation of lipid occurs at the surface as they are no longer drained away and their spreading is no longer insured. They also noted the presence of small dark granulations (believed to be the product of the interaction of lipid with mucins and surface active proteins) situated below the normal lipid film.

Josephson (1983) described a technique for the observation of the lipid layer of the pre-ocular tear over the bulbar conjunctiva near the temporal border of the limbus. He noted that the specular reflection over the cornea can also be used and that ground glass or a piece of polaroid filter can be used in front of the light to decrease the illumination.

The system was also linked to a video-camera for dynamic recording.

He noted the various shades of grey visible at the surface of the normal lipid film, the appearance of tarnished metallic surface of reduced gloss and that of greasy flakes or membranes or of parallel zones of a transient and inconsistent nature between blinks. Small fat globules were sometimes visible specially during Meibomian gland expression by digital pressure and the

break-up of the lipid layer is described in the formation of pale grey islands with sharply defined borders. He concluded that the use of this technique should give information to indicate the potential for successful contact lens wear and to aid in the analysis of patient symptoms.

Lydon & Guillon (1984a) described a technique of wide field in the photography of the lipid layer of the pre-ocular at 1 to 1 or 2 to 1 magnification.

Knoll & Walters (1985) used a modified Bausch & Lomb keratometer to photograph the changes in the specular reflection from the anterior surface of the tear film formed on hard gas permeable and hydrogel lenses.

In hydrogel lenses the drying sequence reveals successively the oily layer interference colours, the appearance of granules increasing with time, the aqueous layer interference colours, an 'orange-peel' appearance and Transient BAS-relief Features (TBF).

In rigid gas permeable lenses the drying sequence reveals successively the oily layer interference colours, the appearance of granules increasing with time, the aqueous layer interference colours, an evaporation front, and the presence of residues.

Olsen (1985) used a slit-lamp photometer to measure the reflectivity of the corneal reflex at 2 selected wavelengths (500 and 700 nm at 20 degrees incidence) on 10 normal subjects. His finding 4.06 percent ± 0.83 percent and 3.16 percent (±0.79 percent) are consistent with a model of the oily layer acting as thin dielectric film with a thickness of 40 nm. It is

possible that this value corresponds to the marmoreal appearance of the lipid layer which is present in the majority of subjects.

Besides the extensive work of McDonald, none of the studies have associated the appearance of the tear film and a scientific analysis of the interference colours for precise thickness measurement.

3.2.4 OBSERVATION OF PARTICULATE MOVEMENT

McDonald (1969) evaluated the speed of movement of the tear film by observation of the movement of particles found at its surface such as mucous strands, dust, air or lipid bubbles or desquamated cells.

These observations allow the classifications of the viscosity of the tears as the inverse of the speed of flow of particles. A reduced viscosity will qualify a fast movement of particles and a high viscosity a slow movement of particles. Practice and numerous observations will be necessary to assess the normal velocity and the related subjective measurement of viscosity.

Schuller et al (1972) and Hill (1981) found a good correlation between this method and tear viscosity measurements. Hill (1981) suggested that the viscosity rating tests can help in identifying the prospective wearer prone to contact lens deposition.

3.2.5 NON-INVASIVE BREAK-UP TIME (NIBUT)

Following an original design by Lamble et al (1976) Mengher et al (1985a) developed a non-invasive

technique for the assessment of pre-corneal tear film break-up time without the use fluorescein. Their method is based on observing changes in the specular image of a grid pattern projected onto the open eye. A distortion of the grid line represents local thinning and its discontinuity represents a break in the tear film. The time taken for the appearance of the first discontinuity in the grid pattern is taken as a measure of the tear film break-up.

Patel et al (1985) observed the first catoptic image produced by a Bausch and Lomb keratometer and measured the time taken for that image to become diffuse as tear thinning time (TTT). Tear thinning time was also measured 3 minutes after fluorescein instillation as well as break-up time (BUT) immediately after instillation. They found on average TTT of 18.0± 6.5 seconds, a reduction of 3.6 seconds due to instillation of fluorescein while BUT showed greater values (22.7± 6.8 seconds) which may be due to the immediate effect of fluorescein on the tear film.

Mengher et al (1985a) reported NIBUT in normal population of 47.9± 5.3 seconds for the right eye (range 4 - 214 seconds) and 35.1± 3.2 seconds for the left eye, (range 4 - 150 seconds).

They found 62 percent of observations to be greater than 20 seconds in normal subjects compared to 37 percent in dry eye patients, 33 percent of which exhibited a NIBUT inferior to 5 seconds.

They also showed that fluorescein instillation decreased significantly tear film stability as

64.7 percent of NIBUT measured after instillation were below 30 seconds compared to 80 percent in the control eyes. Ten to twenty minutes were necessary for recovery of tear film stability following fluorescein instillation (Mengher et al, 1985b).

3.3 USE OF STAINING AGENTS

3.3.1 STAINS IN CLINICAL PRACTICE

A great variety of stains have been employed in the study of the tear film and in routine clinical ophthalmological, optometric and contact lens practice. Their main purpose is to detect areas of epithelial irregularity (punctate staining), degenerated or dead cells. Some tests (BUT - Colorimetric test) make use of stains to study the stability of the tear film. The most popular staining agent used routinely is sodium fluorescein, and to a lesser extent Rose Bengal. Their uses will now be surveyed.

3.3.2 USE OF SODIUM FLUORESCEIN

Fluorescein is a water soluble dye which takes a yellow-green colouration that can be excited by illumination by near U.V. light such as that produced by 'cobalt blue' glass. A few factors affect the fluorescence of fluorescein, in particular the concentration and the pH of the solution. The fluorescein accumulates in the intercellular spaces produced by discontinuity in the corneal epithelium. The thickness of the tear film and its integrity can be

assessed by the intensity of the colouration over the ocular surface.

3.3.3 MEASUREMENT BY BREAK-UP TIME

The tear film break-up time (BUT) was proposed by Norn (1969b) as corneal wetting time. A moistened fluorescein strip is applied to the bulbar conjunctiva and after two or three blinks to spread the fluorescein evenly, the tear film is viewed with the help of a blue filter in front of the illumination system of the slit-lamp biomicroscope. When a dark area appears in the uniform colouration, it represents the rupture of the tear film and the time elapsed since the last blink is recorded as break-up time (BUT).

Norn (1969b) found a BUT mean value of 30 seconds but a large coefficient of variation (31 percent) also reported by Vanley et al (1977) and Forst (1976a) shows the need for repeated measurements although this is disputed by Lemp & Hamill (1973) and Rengstorff (1974). A BUT inferior to 10 seconds usually reveals an anomaly of the pre-ocular tear film. If the film ruptures repeatedly in the same spot a superficial epithelial abnormality must be suspected (Lemp et al, 1970a).

If it occurs near the meniscus, the thinning induced by its proximity might be the cause (McDonald & Brubaker, 1971). alternatively, a half blinker will favour break-up over the inferior part of the inferior surface.

3.3.4 VARIATION IN MEASUREMENTS OF BREAK-UP TIME

Many factors affect the measurement of the tear film break-up time (BUT).

Those reducing the BUT include the use of local anaesthetic, the use of benzalkonium chloride (BAK) as a preservative agent, the use of certain ointments, the presence of air convection during testing, forced blink before measurement or holding the lids forcibly open during measurements.

Those increasing the BUT are the instillation of mucomimetics (Holly 1978a) and other eye drops enhancing tear film stability and a decrease in fluorescein concentration which optimum value should be 0.5 percent (Forst, 1978).

Various methods, concentration and volume of fluorescein have been suggested; Norn (1983) used 10µl of 0.125 percent, Forst 0.5 percent, Stodtmeister et al (1983) 1µl of 5 percent fluorescein.

The main problem with the break-up time measurement is its invasive nature. When it is used in a routine clinical situation, involving moist impregnated strips, too many variables are not controlled; concentration, pH variation in the case of fluorescein solution, the size of the instilled drops and the preservative use are probably the main source of error.

It is useful for detection of the abnormally low BUT. The fluorescein dyes the aqueous phase of the tear film and has little effect on the lipid layer or the mucous layer. In view of the finite size of that aqueous

phase it seems that the minimal amount of unpreserved dye in an adequate concentration instilled in precise volume will improve the repeatability of the test, in cases of controlled research situations.

Marquardt et al (1986) advocated an improved technique of break-up time measurement: the instillation of a fixed amount of fluorescein (1 or 2 microlitres of a 5% sodium-fluorescein solution by a laboratory pipette) and the use of a barrier yellow filter (Schott-filter OG 530) will increase the contrast for the fluorescein.

3.3.5 FLUORESCEIN AND CONTACT LENS FITTING

The popularity of fluorescein in contact lens fitting is due to its many uses. It serves to assess the fit of rigid corneal lenses, silicone rubber and scleral lenses as well as verify their effect on the corneal epithelium. It is the only means of imaging the post-lens tear film, its thickness and morphology. Large molecular fluorescein (fluorexon) is available for use in soft lens fitting.

The use of BUT as an aid to contact lens fitting has been studied by Forst (1976b) who predicts that a value above 10 seconds should ensure good contact lens tolerance, a result between 10 and 6 seconds might be accompanied by front lens surface drying and 3 and 9 o'clock staining while BUT below 6 seconds will probably prohibit successful contact lens wear.

Lowther & Hilbert (1975) and Koetting (1976) studied the relationship between BUT and soft lens

deposition and the latter work showed that in low BUT values under 10 seconds, 35 percent of the lenses became unwearable.

The drawback of fluorescein use in tear film assessment in contact lens wear is, again, its invasive nature that can be heightened in the case of a rigid pre-lens tear film of minimal thickness. Any variation of fluid volume in the ocular environment may alter both the delicate balance between the lens meniscus at the pre-lens tear film, and affects its structure and measurement.

Non-invasive techniques of examination appears to be the better choice.

3.3.6 USE OF ROSE BENGAL STAINING

Rose Bengal is a water soluble dye which stains degenerated, and dead cells and mucous fibrils (Norn, 1972). It produces a punctate colouration along the lacrimal rivus which is probably due to pronounced cell degeneration in this area and is known a Marx' line. One percent Rose Bengal is preferred as the irritation increases with higher concentrations.

In contact lens wear the main use of Rose Bengal is to assess superficial damage during fitting or after prolonged wear. The uses of other various stains and their combinations have been extremely well documented by Norn (1983) but have found little acceptance by the contact lens fitting population at large.

As seen most of the tests used in a clinical situation affect either the production, the volume or the structure of the tear film it tries to assess. The routine assessment of the tear film will benefit from a technique relying solely on observation.

CHAPTER 4

THE CONTACT LENS INTER-ACTION WITH THE TEAR FILM

4.1 INTRODUCTION

When a contact lens (hard or soft) is inserted in the eye, it disturbs the delicate balance of the tear film environment and affects the physiology of the ocular surface. Some temporary variations in tear composition and in production occur and the superficial fluid forces present in the tear film are altered. Contact lens materials with adequate surface wetting properties and improved oxygen permeability are in use nowadays. But the long term wear of contact lenses is accompanied by alterations to the lens surface qualities and accumulation of deposits from the tear film. These will be detrimental to the formation of an effective pre-lens tear film and will decrease contact lens tolerance.

A successful contact lens must meet five basic criteria. These are:

- provision of sufficient atmospheric oxygen to the corneal epithelium to allow normal corneal metabolism to take place.

- exertion of minimal bearing or pressure on the corneal epithelial surface.

- a fit that allows flushing of epithelial debris and centration that permits excellent, crisp visual characteristics on blinking.

- minimal interference with lid-globe congruity so that negative pressure inducing tear menisci will be prevented.

- possession of a stable anterior surface tear film.

4.2 PHYSICAL EFFECTS OF THE CONTACT LENS ON THE TEAR FILM

4.2.1 FLUID FORCES

The first change occurring on the insertion of a rigid contact lens is the immediate thinning effect on the surrounding tear film. A meniscus forms around the lens edge and draws fluid from its surrounding due to its unsatiated negative pressure (Holly, 1978b) and a 'black line' can be observed around the contact lens (Holly, 1973a) similarly to that found adjacent to the tear meniscus along the lid edges (McDonald & Brubaker, 1971). The intensity of the meniscus induced thinning depends also upon the thickness of the surrounding film and the area adjacent to the thinning is regularly the site of tear film fracture particularly when high powered lenses are used which adversely affect the lid-globe congruity.

A corneal contact lens is held in place by a balance of forces. The main force that holds the lens against the cornea is the fluid force produced by the tear layer (Lowther & Hill, 1967). This force is determined by the physical characteristics of the tear layer and by the geometry relationship between the posterior lens curvature and the cornea (Poster, 1964).

The surface tension of the tear film is manifested by the concave tear meniscus surrounding the edge of the lens indicating that the pressure of the post-lens tear film is inferior to the atmospheric pressure (Yorke, 1971). Kikkawa (1970) measured the radius of the meniscus at the top of the lens to be 0.008 to 0.003 cm. Townsley (1972) found a smaller radius at the top (0.006cm) and a larger radius at the bottom (0.025cm) with the lens edge 0.156cm away from the cornea. The difference in radius is due to pressure differences caused by the height of the column of tear fluid behind the lens. Forst (1981) measured a radius of 0.7mm for a contact lens with a normal edge (edge level 0.12mm) and 0.4mm for a contact lens with a flattened edge (edge level 0.25mm). He noted from photographic evidence that parallel fitted lenses recentred faster than a flatter fitted lens and that centration was independent of the peripheral capillary force, therefore the edges of lenses should be shaped to satisfy physiological requirements such as absence of irritation to the lids, good mobility of the lens and good pumping effect. If the axial edge clearance of the contact lens is excessive (greater than about 120μm) then a negative pressure inducing meniscus will result so further compromising the integrity of the epithelium immediately beneath (Guillon et al, 1983).

Fortunately if adequate axial edge clearances (80 to 100μm) are utilised a functional tear meniscus will result and this in association with the flexibility and resiliency of the normal eyelid will minimise the lid-globe congruity interference so that most of the

associated symptoms such as lens drying and 3 and 9 o'clock staining (peripheral epithelial staining) can be eliminated (Holly, 1981b).

Mackie (1970) pointed out that when the lids are drawn back the lens will not decentre over the limbal region in most cases because there is a tendency for the lens to be drawn back to the optical zone by the negative pressure due to the geometrical relationship between the lens and the cornea.

4.2.2 LID FORCES & LID-GLOBE CONGRUITY

By virtue of their finite thickness contact lenses interfere with the congruity of the eyelids and the globe (Lemp & Holly, 1970). This is particularly true of the upper lid, when a contact lens either contacts the lid margin or rides constantly underneath the lid.

The lid movement during blinking show a rotary motion in a downward and nasal direction, strong enough that in some cases a corneal lens can be rotated more than 90 degrees in one lid movement (Forst, 1976b). The lens also tends to move with the lid during the downward phase of the blink and upward as the upper lid is raised (Mandell, 1977; Hayashi & Fatt, 1980). It is also known (Forst, 1981) that positive lenses sometimes are pressed down by the upper lid and negative lenses stick to the upper lid. In the case of high riding lenses, when the lens meniscus comes into contact with the lid tear meniscus, the hydrostatic pressures will be equalised by tear flow towards the meniscus possessing lower pressure. When the upper lid covers part of the lens a pre-lens

meniscus will be present favouring the unobstructed tear spreading over the lens surface. However the positioning of the lens leads to interference of mucous spreading and associated tear film instability (Holly, 1981b).

When the lens is free from the lid influence gravity becomes the force behind its movement and a lens with a greater mass (ie. high plus, aphakic lenses) will be pulled downward with a greater force. In this case the lens is controlled in position by the opposite forces of gravity and the fluid forces.

4.2.3 TEAR EXCHANGE UNDER A RIGID CONTACT LENS

It has long been understood that in order to maintain normal corneal metabolism a certain minimal level of oxygen tension at the corneal epithelial surface must be obtained (Smelser & Ozanics, 1952; Polse & Mandell, 1970; Mandell & Farrell, 1980). If this level fails to be realised corneal hydration changes occur leading to significant corneal oedema (White & Miller, 1981).

During the downward lid movement, tears are forced upwards between the lens and the cornea through a channel formed by the peripheral curve. This is aided by the formation of an inferior tear prism of greater size when the upper lid passes over the top portion of the lid and lifts the lower lens edge slightly from the cornea. The tear behind the lens will be forced out by the side with each blink. Cucklanz & Hill (1969) found for one set of lens conditions that approximately 20% of the tears behind the lenses were exchanged. One way to represent

the oxygen need of the cornea is the use of equivalent oxygen percent (EOP) which expresses each oxygen tension as a percentage of atmospheric oxygen where the range is 0 to 21 percent at sea level. To avoid corneal oedema a contact lens system should provide at least 7.5 percent EOP during dynamic conditions at the contact lens interface. With regard to the wearing of optimally fitted polymethylmethacrylate (PMMA) corneal contact lenses it has been shown that the tear pump produced by lens movement on blinking provides between 1 and 3 percent equivalent oxygen and that the use of an enhanced wetting material will produce not more than a further 1 percent increase in the equivalent oxygen available (Mandell, 1982; Hill et al, 1973; Hill & Bailey, 1978).

4.3 CHANGES IN THE TEAR FILM & ON LACRIMATION

When a contact lens is first worn by an unadapted subject various lacrimal and ocular changes occur. Some of these changes still exist after the physiological process of contact lens 'adaptation', others are short-lived. The blinking pattern is altered as is the level of tear production and composition of the tear fluid.

4.3.1 EFFECT ON BLINKING

Abelson & Holly (1977) have found that 80 percent of all blinks were complete (when the upper eye lid covers more than two thirds of the cornea), 17 percent were incomplete (less than two thirds) and 2 percent were twitch blinks (small movements of the upper eye lid).

Reading has been shown to reduce the frequency and

completeness of blinking (Doane, 1980).

i) Stability on Blinking

It has been shown that any rigid contact lens must possess an extremely high level of stability so that it can resist significant deformation due to lid pressure found on blinking. If an inadequate level of stability is present two basic phenomena will occur. Firstly, the lens will deform to take up the shape of the cornea which it overlies so leading to poor visual acuity and a decrease in lens mobility (Holly, 1981b; Lydon & Guillon, 1984b). Secondly, there will be a consequential reduction in tear flow beneath the lens leading to the reduction of oxygen supply, the increase of toxic metabolic by-product accumulation and the increase in debris entrapment between the lens and cornea (Holly, 1981b; Mandell, 1982).

Eventually both factors will lead to significant physiological complications and may be the cause of cessation of lens wear.

ii) Effect on Blink Rate and Motion

On the first day of rigid lens wear a period of accelerated blinking occurs during approximately one hour, and is characterised by lid closure with maximum force. The blinking rate decreases to a level slower than normal and closure occurs with minimal force during the following phase lasting from three to five hours. A recovery towards normal blink frequency should occur during the adaptation period (Mandell, 1977).

An excessive proportion of incomplete blinks can cause a variety of ocular problems. In hard lens wearers

it induces 3 and 9 o'clock staining and increased surface deposits and inadequate tear exchange leads to oxygen deprivation (Fatt & Hill, 1970). In soft lens wearers it may lead to lens dehydration, increased lens surface deposits and inferior punctate corneal staining (Kline et al, 1979) while accumulation of debris beneath the lens can induce subepithelial infiltrates in extended wear (Zantos & Holden, 1978).

In well adapted rigid contact lens wearers an increase in blink rate from 15.5 blinks per minute to 23.2 blinks per minute was found by Hill & Carney (1984) who showed a decrease in the frequency of occurrence of long interblink period. They also found (Carney & Hill, 1984) that the same blink rate increase existed in soft lens wearers (from 12.1 blinks per minute to 20.3 blinks per minute).

Some subjects will develop a reduced blink motion and frequency and will need training to alleviate the related symptoms.

Collins et al (1987) have shown that blinking exercises can benefit contact lens wearers that have a high proportion of incomplete blinks and they may improve blinking performance to the extent that associated symptoms can be minimised or overcome. But the possible transient nature of the improvement may necessitate periodic repetition of the exercise program.

4.3.2 EFFECT ON LACRIMATION & TEAR COMPOSITION

An increase in tear production accompanied by the reduction in tear tonicity level following the insertion

of a contact lens. Mandell & Harris (1968) postulated that these lacrimal changes occurring during the adaptation period induce a corneal thickness increase of 1 percent up to 3 percent (Harris & Mandell, 1969).

The increase in tear flow is reflected in the sharp drop in tear salt levels. Tear sodium concentration (Hill, 1975) and tear chloride concentration (Schmidt et al, 1977) have been shown to fall on the day of issue of a lens and to recover their normal level over a period of around ten days.

Similarly, the total protein level of the tears reflects the same pattern (Hill & Uniacke, 1969) and may represent the dilution effect of increased lacrimation.

This corneal thickness increase, caused by water movement into the cornea, is followed by a recovery and a decrease in tearing induced by the neural adaptation of the receptors in the lid margins to stimulation by a contact lens (Lowther & Hill, 1968).

4.4 WETTING OF A CONTACT LENS SURFACE

Intuitively it would seem reasonable to suggest that the wetting characteristics of a given material would have a pronounced influence on the PLTF stability. However until present time all attention on wettability has been directed towards in-vitro measures and no obvious link between in-vitro and in-vivo performance has been uncovered.

Several techniques are available for the measurement of wetting angles, the two most widely available being the captive bubble technique (CBT)

(Poster et al, 1978a; Poster et al, 1978b) and the sessile drop technique (SDT) (Walker, 1982), the latter being the more widely utilised due to its inherent simplicity. It is most important to appreciate that the measured wettability of a material is not solely dependent upon the nature of the material. It will also depend upon the following:-

- the physical nature of the surface of the material under test.

- the nature of the liquid.

- whether the liquid drop has advanced or receded across the surface.

- the atmospheric conditions

- the consistency of the experimenter.

Indeed, so influenced by the above are the measurements, that if the conditions of the test are not explicit, the results are meaningless (Walker, 1982; Cordrey, 1984).

To measure contact angles a drop of liquid is applied to the surface in a controlled manner and the angle of a tangent to the drop in its equilibrium position is recorded. As the angle decreases so the wettability of the surface increases. Measures are made for both advancing and receding conditions.

Fatt (1984) mentions that the surface problem of the contact lens in the environment of the eye is complex and there is the need for standardised methods of contact angle measurement together with some kind of quantitative or even semi-quantitative evaluation of lens performance of the eye. He measured the contact angle of a PMMA lens

by the sessile drop method using first a new lens which had been cleaned and soaked overnight. The contact angle of 73 degrees was found. The same lens treated with a wetting solution and rinsed under the tap gave a measurement of 13 degrees. When the lens was worn for 2 hours and 12 hours, a value of 44 degrees was obtained in both cases.

To explain these variations Fatt relies on the early work of Langmuir (1934) & Blodgett (1935) on the deposition of monomolecular layers on a solid surface. When a wetting solution is applied to the lens, a layer of molecules is left behind in which the non-polar heads adhere to the surface. The polar attracting tails are forming a surface on which water is more easily spread than on the PMMA surface and lower contact angle values can be measured. When the lens is worn a monolayer of lipid is deposited on the lens surface by the downward movement of the lid and a second layer is deposited when the lid goes up. The process is repeated with each blink until the adherence of an additional layer is too weak to hold onto the underlying multilayer. The increase in contact angle measurement to 44 degrees may represent a surface covered with a multilayer of tear lipid and mucin. Point to point variation on the lens surface may be attributed to variation in thickness or structure of this layer.

In their very elegant work Benjamin et al (1984) have adopted the relative sessile contact angle (RSCA) technique to an in-vivo situation when the eye of an adapted rigid contact lens wearer was positioned in front

of a photo-biomicroscope such that the cornea was pointed upwards. One microlitre drop of distilled water was placed near the vertex of the anterior contact lens curve prior to blinking. The subject was allowed to blink once after drying of the anterior lens surface by evaporation. A sessile contact angle (in-vivo RSCA) showed an abrupt contact angle decrease (wettability increase) after only one blink. The variation found in the following blinks were not significant. This reduction of in-vivo contact angle was attributed to the establishment of mucin layers on the surface of the lenses. Provided that the subject has adequate tear quality to permit contact lens wetting, the in-vivo wetting of polymer surfaces was achieved regardless of material hydrophilicity.

Benjamin et al (1986) using the same technique on four different types of rigid lens postulated that some surface deposits incurred during wear may disrupt the mucin coating on rigid polymer surfaces and reduce the camouflage action that this layer exerts on the hydrophobic nature of these lenses in the eye.

It is noticeable that without exception all of the latest generation of rigid gas permeable materials are claimed to have excellent wetting properties. However clinically rigid low wetting angle materials such as BP Flex and Paragon 18 have been found to be of no significant benefit by some authors whilst others have found sufficient improvement to warrant total replacement of regular PMMA (Dickinson, 1973; Dickinson, 1978; Kress, 1978; Masnick, 1979; Sarver et al, 1977).

Large variation exists in the in-vitro measurement of contact lens surface wetting properties. Those measured values bear little relation to the 'in-eye' situation. There is the need for a technique that can be used during contact lens fitting and after care and give an adequate evaluation of wettability by tear film structure and thickness analysis.

4.5 EFFECT OF SOFT LENSES ON THE TEAR FILM

The improved comfort provided by the soft lens will limit the adaptive effects on lid margin and corneal sensitivity and its related variation of lacrimation and tear fluid component that are seen in rigid contact lens wear.

Some evidence shows variation of water content and diameter linked to the tear pH and a possible hypertonic shift in the lens environment (Masnick & Holden, 1972; Poster & Skolink, 1974) but Carney & Hill (1976), on the contrary, showed a small but significant adherence shift between pre-fitting and post-dispensing periods and these shifts should not alter the refractively dependent parameter of a new lens.

4.5.1 CHANGE ON INSERTION OF SOFT LENS IN THE EYE

When a soft lens is taken out of a vial, it is usually at room temperature (20° Centigrade). When placed on the eye the temperature rises almost immediately to that of the corneal surface (35 degrees Centigrade). This induces a decrease in water content of the lens of 1 percent for a 38 percent water content

lens, 2 percent and 3 percent decreases for 55 percent and 75 percent water content lenses respectively. This loss solely due to temperature difference will take from 10 to 20 minutes for a thin high water content lens and up to one hour for thick low water content lenses (Fatt, 1984).

Further decrease in water content of soft lenses occurs during the initial period of wear and is possibly due to the effect of evaporation leading to a steepening of the base curve during lens dehydration (Andrasko, 1983) and apparent lens tightening (Martin & Holden, 1983). Some authors (Andrasko, 1983; Hamano et al, 1979b) suggest that thinner lenses show a greater dehydration while (Kohler & Flanagan, 1985) suggest otherwise, while Wechsler et al (1983) concluded that high water content hydrogel lenses lose a smaller percentage of their water than low water content contact lenses while being worn, but high water content lenses lose more water by weight than do low water content lenses. This loss occurring mostly in the first few minutes following insertion and stabilises within one hour.

In an environment of low relative humidity it will lead to greater loss of lens water content; from 37 percent to 30 percent and from 70 percent to 56 percent for a relative humidity of 18 percent.

If areas of poor wettability exist at the surface or if the tear film is unstable enough to produce dry areas then water evaporation from the surface will occur. it will be replaced by fluid coming from the posterior

surface and through the matrix of the lens. This will produce a gradient of water content in the lens at a right angle from the surfaces.

To limit the effect of evaporation a thick and stable tear film with a superficial lipid layer must exist at the surface of the lens. The more hydrophilic the surface, the more stable the pre-lens tear covering becomes. None of the hydrogels used for contact lenses are completely water wettable and their advancing contact angle is not zero (Holly, 1981b).

Further the water content per-se does not reflect water wettability and hydrogels with a polymer matrix of a given chemical composition show decreasing water wettability with increasing water content produced by decreasing crosslink density. On the other hand, for hydrogels of the same water content the water wettability will change according to the hydrophilicity of the polymer forming the gel matrix.

For the above reasons, high water content hydrogels are not necessarily more wettable than low water content lenses (Holly 1979).

The water content is a parameter of the bulk of the lens which does not necessarily reflect its surface composition. Hydrogel surfaces are also capable of hydrophilic-hydrophobic formation due to the segmented mobility of the surface polymer chain (Holly, 1981b).

As dry spots form on the surface of the lens the areas exposed to air will become rich in hydrophobic groups (methyl groups) while the areas exposed to fluid will accumulate hydrophilic groups (hydrogel groups).

For a given matrix the higher the water content the higher the segmental chain mobility of the polymer matrix is at the interface.

This mobility permits the outward rotation of the hydrophobic groups (methyl groups) when exposed to air or to a non-polar liquid conveying a certain degree of hydrophobicity to the surface.

All the above, when considered in the light of a possible unstable tear film and the adsorptions of proteins and possibly lipids that takes place almost immediately upon lens insertion creates a complicated clinical picture. In the adverse conditions, denatured protein merely contaminated by lipids may accumulate on the lens surface and limits the beneficial effects of mucous glycoprotein adsorption. This will be associated with rapid pre-lens tear film break-up where the lens surface is alternately exposed to air or aqueous tear between blinks. This condition may alter the bio-compatibility of the lens surface, increase the occurrence of deposits and coating and the possible adherence of antigens which Allansmith (1986) denounces as the cause to immunological reactions seen as Giant Papillary Conjunctivitis (GPC).

4.6 CONCLUSION

It must be remembered that often the benefits of increased oxygen transmissibility are counter balanced by other characteristics of the lens material that may be undesirable eg. poor wetting, unacceptable levels of

batch variation, marked hydration changes, poor surface hardness and so on (Mandell, 1982).

In order to fully utilise the beneficial aspects of significantly oxygen permeable rigid materials, it is of great importance not only to maximise the oxygen transmission characteristics of the material but also to maximise the tear pump mechanism since use of the combined attributes of tear pumping and significant gas transmission is likely to be the only method of ensuring the minimal disturbance of corneal metabolism necessary for optimal contact lens wear (Lydon & Guillon, 1984b).

Therefore the design of a rigid lens is of great importance, so that the adverse mechanical, visual and physiological effects of the lens material can be minimised.

The adverse effects associated with long term low levels of oxygen deprivation include corneal swelling (White & Miller, 1981), corneal sensitivity loss (Millodot, 1981), corneal shape change leading to irregular corneal astigmatism and distortion (Levenson, 1983; Rengstorff, 1981) and epithelial integrity loss (Bergmanson & Chu, 1982; Farris et al, 1971), all of which can be wholly or partly resolved using significantly gas permeable materials possessing adequate wetting properties (Mandell, 1981; Finnemore & Korb, 1980; Lowther, 1981; Lowther & Paramore, 1982).

CHAPTER 5

EXPERIMENTAL ARRANGEMENT TO OBSERVE AND PHOTOGRAPH THE PRE- CORNEAL, PRE- LENS TEAR FILM AND CORNEAL SURFACE

5.1 INTRODUCTION

The usefulness of the techniques relying on specular reflection photography has been limited for a number a reasons:

- they have only been used for high magnification observation of very small areas and failed to visualise large areas of the tear film.

- they have mainly been applied to the study of the superficial lipid layer and in a very limited way to the pre-contact lens tear film.

- they have used solely white light illumination and failed in adequate analysis of interference fringes.

- they have never been applied to the photography of the inner mucous layer of the tear film.

The aim of this thesis is to design techniques which enable visualisation and precise measurement of all component layers of the tear films forming on the cornea and on contact lenses.

This thesis describes three complementary techniques to achieve the observation and photography of the structures and integrity of the pre-ocular and pre-lens tear films without the use of fluorescein.

The first uses high magnification crossed polarised photography to study in detail the appearance and the kinetic behaviour of the superficial tear film structures. That is the lipid layer of the pre-ocular tear film and the lipid and aqueous layers of the tear films forming on the surface of soft and rigid contact lenses.

The second technique uses low magnification (x1 to x2 linear magnification) and a specialised instrument specifically designed to make the tear film visible over a large area of the cornea and contact lenses to enable the study of the overall formation, behaviour and stability of the tear film and the measurement of the "real" break-up time without use of stains.

The third technique uses very high magnification and a custom designed scleral lens to photograph 'in-vivo' the basal mucous coating of the corneal and contact lens surfaces. This has not been achieved before by a non-contact technique.

These techniques are used in four experimental studies. The photographs obtained are interpreted using the adequate mathematical formulae deriving from the physics of interference to obtain the tear layer thickness measurements.

These calculations have not been previously employed and full details and formulae as well as their assorted reference tables are presented in Chapter 6. The following text is limited to a description of the three experimental arrangements.

5.2 HIGH MAGNIFICATION PHOTOGRAPHY INSTRUMENTAL ARRANGEMENT

5.2.1 GENERAL DESCRIPTION

A Nikon As-1 non-contact endothelial camera (Fig 5.1)(Nikon UK Ltd) is used in conjunction with two polarising filters, one in front of the illumination system, the other used as an analyser before the observation system. By rotation of the analyser at an angle approaching 90 degrees from the axis of the polariser (fig 5.2) it is easy to control the amount of light entering the observation system. This also eliminates background noise giving a sharper definition to the image and increases the coherence of the light photographed after specular reflection.

5.2.2 ILLUMINATION SYSTEM (Figure 5.3)

The light source is a 6 volt/30 watt halogen lamp coupled with a 280 volt/500 watt electrical zenon flash tube for photography with a choice of five adjustable levels of light intensity via the power control box with a re-charging time from 1 to 4 seconds depending upon the flash output used.

The emerging parallel beam is controlled by a slit diaphragm and an aperture diaphragm along its path.

The specific output and spectral distribution of the xenon light source is studied at length in Chapter 6.

A holder for the polarising filter has been designed to fit on the slit lamp mounting.

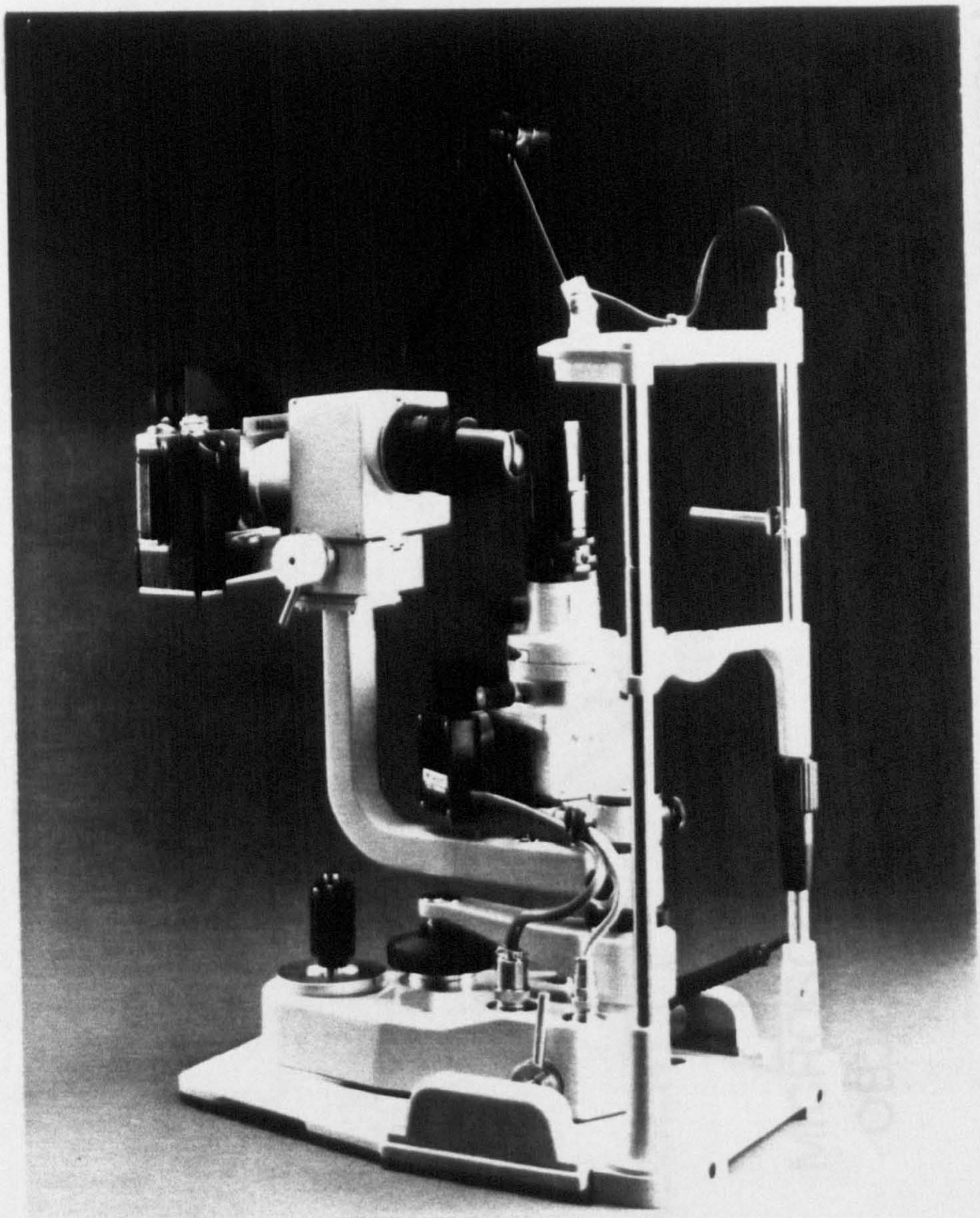

FIGURE 5.1
NIKON AS-1 NON-CONTACT ENDOTHELIAL CAMERA

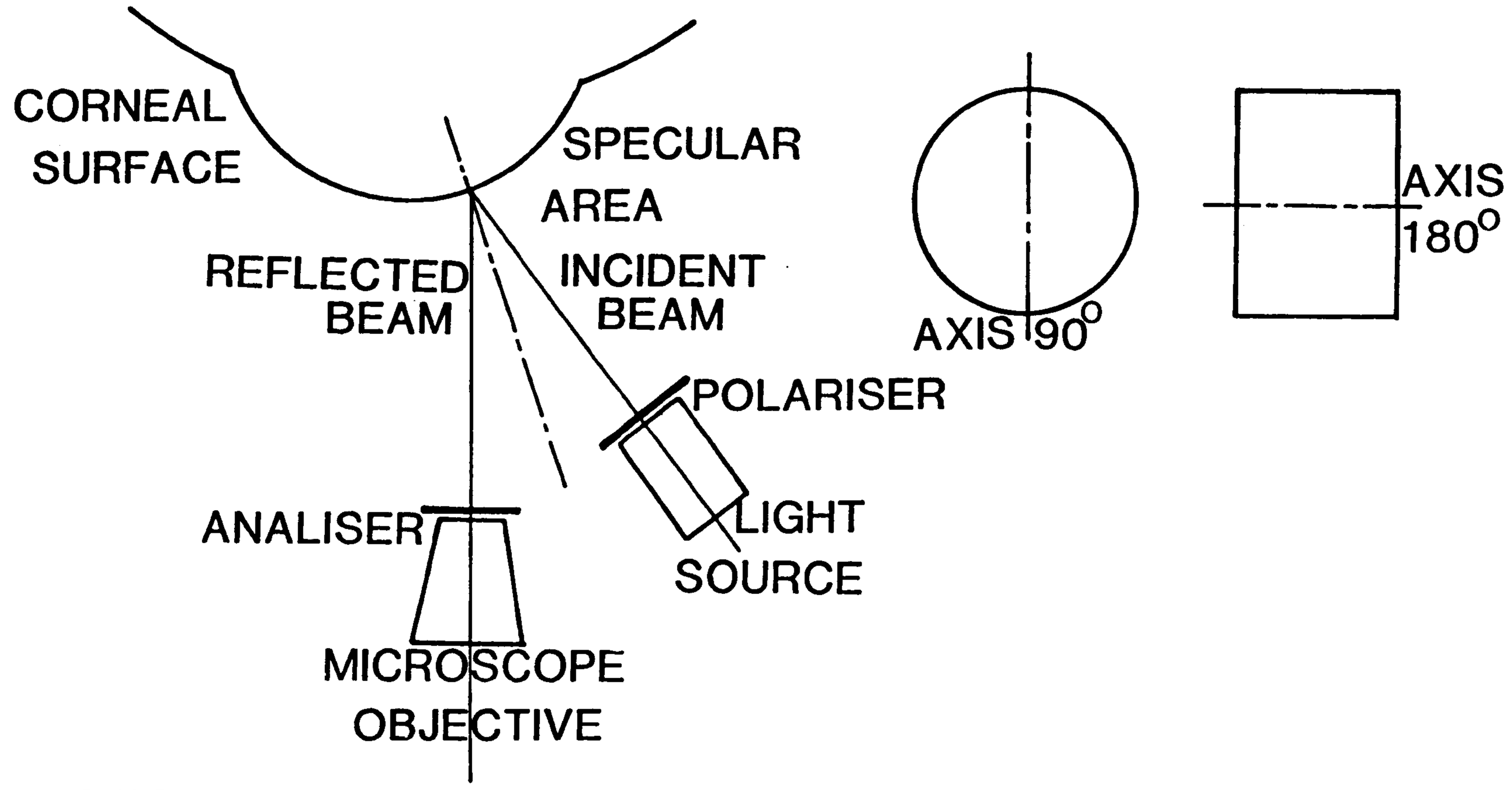

FIGURE 5.2
SCHEMATIC REPRESENTATION OF THE HIGH MAGNIFICATION ILLUMINATION AND OBSERVATION SYSTEM

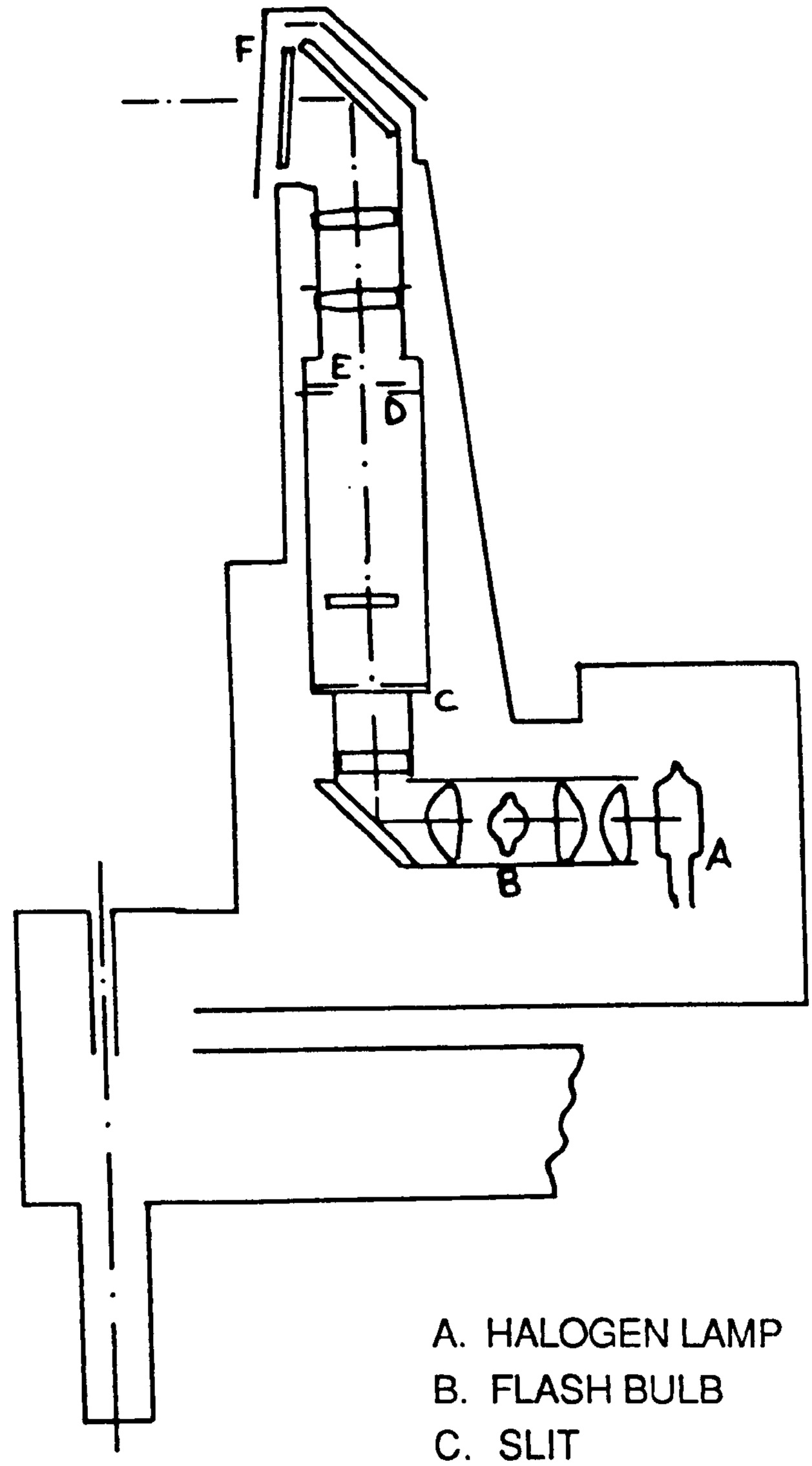

A. HALOGEN LAMP
B. FLASH BULB
C. SLIT
D. APERTURE DIAPHRAGM
E. SLIT DIAPHRAGM
F. POLARISING FILTER

FIGURE 5.3
ILLUMINATION SYSTEM FOR THE HIGH MAGNIFICATION EXPERIMENTAL SET-UP

5.2.3 OBSERVATION SYSTEM (Figure 5.4)

The instrument has a f/1.4, x10 angular magnification high resolution objective with an aperture varying in six steps from f/1.4 to f/8.

The intermediate part of the observation system contains a prism box linking the objective to a motorised Nikon F2 Camera. The obervations were made through a specially designed viewfinder with x6 magnification and incorporating a focussing screen graduated for measurements. The combination of the objective (x10) and viewfinder (x6) gave a x60 total angular magnification.

5.2.4 FIELD OF VIEW

According to the manufacturer a 10mm area can be illuminated at the object plane when the slit is fully opened.

At x60 magnification, the field of observation covered by the focussing screen is a 3.7mm x 2.2mm horizontal rectangle giving at the photographic film plane a x10 linear magnification.

The virtual image of the light source produced by specular reflection is situated beyond the plane of observation obtained in the standard position of the instrument in which the focus and rotating centres of the photographic equipment and the light source coincide.

The friction adjustment knob permits a fine longitudinal movement of the photographic equipment section towards the observer and the precise focussing at the tear film plane against the out-of-focus background of the virtual image of the light source.

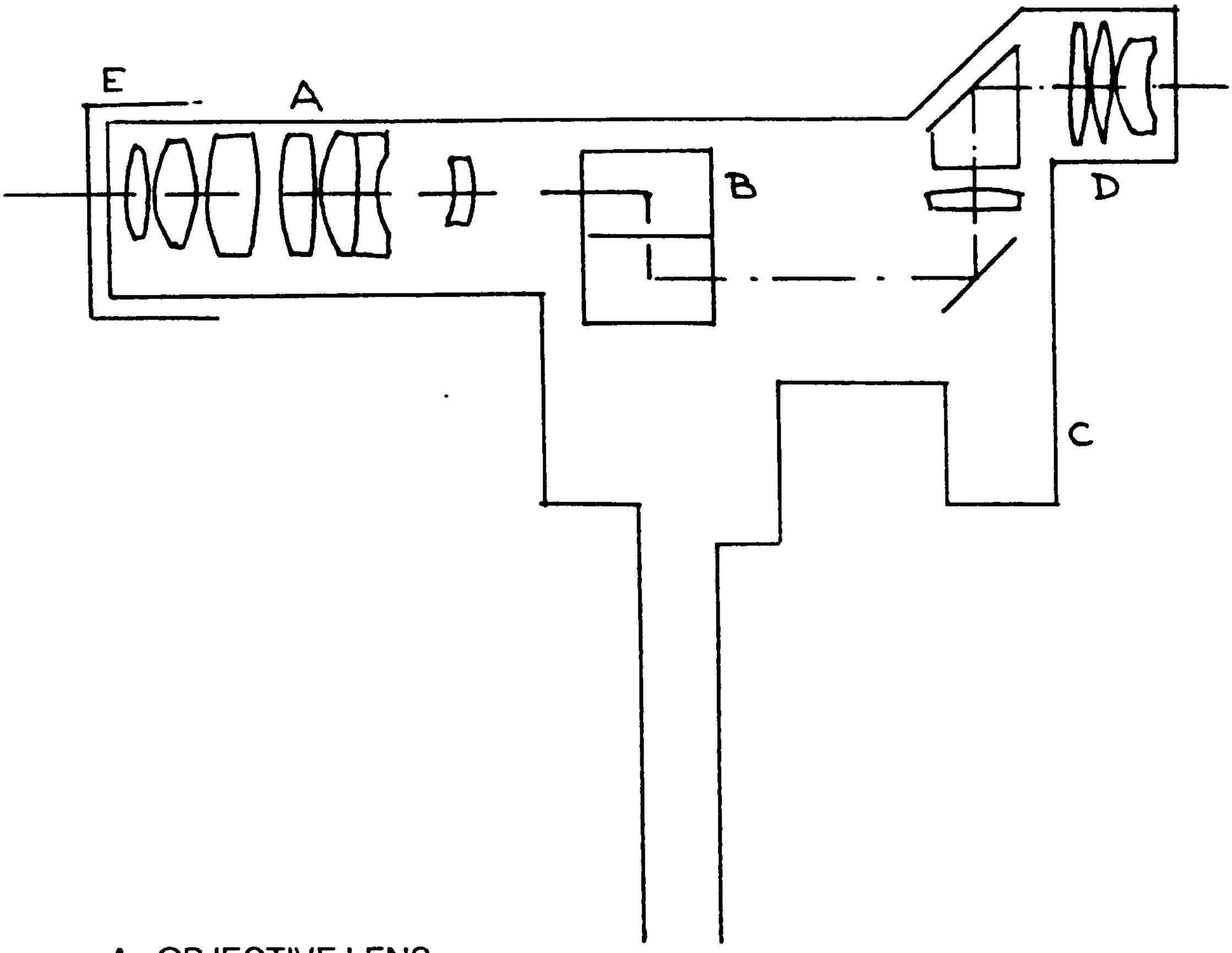

A. OBJECTIVE LENS
B. PRISM
C. NIKON CAMERA AND MOTOR DRIVE
D. VIEWFINDER
E. ROTATING ANALYSER

FIGURE 5.4
OBSERVATION SYSTEM FOR THE HIGH MAGNIFICATION EXPERIMENTAL SET-UP

The size of that virtual image varies with the aperture of the objectve lens which acts now as a field stop. The real field of view is between 0.45 and 6.5 mm^2 depending upon the lens aperture used.

The following measurements were taken directly during observation through the focussing screen:

lens aperture	specular reflection area
8.0	0.9 mm × 0.5 mm
5.6	1.1 mm × 0.5 mm
4.0	1.4 mm × 1.0 mm
2.8	1.8 mm × 1.4 mm
2.0	2.3 mm × 2.0 mm
1.4	2.7 mm × 2.4 mm

5.2.5 PHOTOGRAPHIC MATERIAL

The majority of photographs were taken using Kodak Ektachrome 64 ASA reversal film but a black and white 24 ASA negative film was also used for some of the work on the fine structure of thin lipid films. In those cases, the increase in definition allowed the production of suitably enlarged prints where a linear magnification of x60 to x100 was reached. This enables us to study very fine structural details approaching a few microns in size. That technique was mainly applied to the study of globular formation in irregularly spreading lipid layers.

i) Photographic and Projection Conditions

a) Photographic Conditions

All the photographs were taken with the polarisers in near crossed position with only the light directly reflected from the filament area of the light

source visible as described in Chapter 5.2.2. This arrangement ensures that no extraneous light affects the interference phenomena and allows the production of an increased number of coloured fringes.

The photographs were taken with Ektachrome 64 ASA transparency film, using the Nikon endothelial camera at maximal flash output (500 watt/sec).

Further, for the section dealing with abnormal tear film and in order to maintain good detail information after photographic enlargement black and white Kodak 25 ASA film was used.

b) Projection Conditions and Magnification

Two different techniques were used in those cases where on the first 4 orders of interference are present. The slides were projected on an A3 size paper (Technique 1). However for slides with larger numbers of interference fringes the slides were measured using a modified Nikon profile projector (Technique 2).

A) Technique 1

For measurement purposes, the slides were projected on A3 size paper, where the visible outline of the coloured fringes were drawn. The position of the lines on the diagram were drawn as follows:

- When a clear demarcation between coloured fringes was visible, the lines were drawn along this demarcation thus separating one colour from another.

- When the 4th order of interference was reached, if that layer was wide enough, a line was drawn on each side to follow its edges and the order of interference clearly marked within it.

- However when the layer was not wide enough, a single line was drawn in its centre and the order of interference marked at the end of the line. In that case, two successive lines represented two successive blue maxima and the distance between them corresponds to the interfringe.

When more than five orders of interference were observable, the in-vivo receding wetting angle was calculated from measurements of the distance between successive bright fringes.

In order to calculate the exact magnification a microscope measuring scale in 0.1mm graduation was photographed with the Nikon Endothelial camera and projected under the same conditions giving the following linear magnifications:

photographic system	× 10.00 ± 0.02
projection	× 9.20 ± 0.02
Total	× 92.00

For a steep wedge angle, the fringes are so close to each other (under x190 linear magnification) that their outline can only be detected for the first few orders. It is then necessary to increase the viewing to a magnification up to 960 times to detect supplementary fringes. This technique will be used later for thickness and wedge angle measurements. For illustration purposes only photographs and line drawings were included in the thesis. The photographs were produced from the slides by conventional professional commercial printing and the line drawings were reduced to A4 format by photocopying.

B) Technique 2

The slides were mounted on the travelling table of a modified Nikon profile projector. The table movements were recorded to ±0.001mm by x3 Heideman digital gauge. The slides were viewed using the highest objective available (x100). In each meridian of interest, the position of each fringe was measured x10 and the mean value taken at the best estimate of that position.

c) Analysis of the Photographs

The tracing from the photographs for 4th order of interference and above consists of a series of isobars of equal thickness (Fig 5.5). These isobars were systematically analysed as follows:

- Two meridians were chosen for analysis to represent the directions where the fringes were closest (Direction AE) and farthest apart (Direction AD). Usually these meridians were 90 degrees apart.

- The position of each interference fringe was measured in each meridian. From these measurements the thickness of the tear film was calculated at each point and from those values the wedge representing their drying angles in that region calculated.

- The best fitting curve representing the thickness changes in each meridian and was calculated by regression analysis up to the 3rd order polynomial.

5.2.6 VIDEO-FILM ARRANGEMENT

Using a video camera aligned with the optical system of the microscope, colour recording of the image

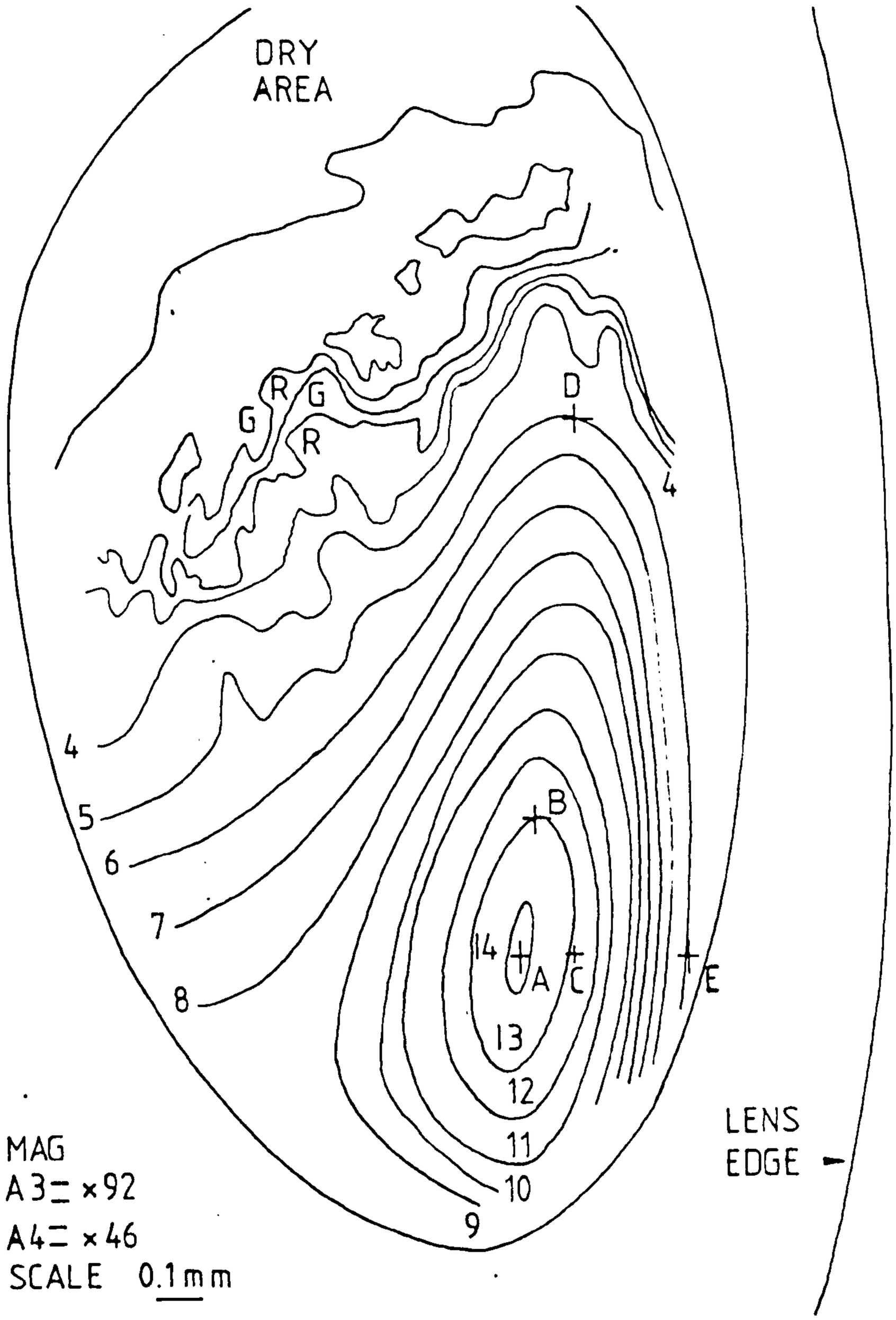

PMMA CORNEAL LENS
PRE LENS TEAR FILM 1
OUTLINES OF FRINGES 4 TO 14

FIGURE 5.5
OUTLINE OF FRINGES FOR ANALYSIS OF PHOTOGRAPHS

produced on the focussing screen of the camera were made in order to study the kinetic behaviour of the superficial lipid layer.

With this technique a linear magnification of x50 to x60 linear was obtained on the monitoring screen but the image quality did not match that obtained on reversal films.

5.3 LOW MAGNIFICATION INSTRUMENTAL ARRANGEMENT

5.3.1 INTRODUCTION

No simple modification to existing instrumentation enabled us to study under low magnification the lipid layer appearance and the colour fringes of the pre-lens tear film, hence it was necessary to design two instruments, one for routine observation, the other to obtain photographs for record and for measurement.

5.3.2 INSTRUMENTATION FOR ROUTINE OBSERVATION

i) General Description

The instrument was designed with the view to increase the area of specular reflection against which the interference phenomena can be seen. It was also necessary to obtain alignment of the centre of the illumination with the observation system.

ii) Illumination System

The illumination system consists of a light source and a reflecting surface. The light source is a 10mm thick cold cathode tube shaped as a 90mm outside

diameter ring and internally coated with white HP29 (Fig 5.6).

The reflecting surface is a 90mm diameter hemispheric cup with a brilliant white inner coating and a central 15mm observation hole (Fig 5.7). This reflecting hemispheric cup is fitted over the cathode tube and secured on the supporting handle. The dimension and shape of the cup were chosen to maximise the area of tear film coverage and allow easy observation with the naked eye or with the use of the biomicroscope observation system.

The 90mm diameter permits the instrument to be approached close to the eye with minimal interference to the subjects brow and nose. The circular shape allows the positioning for right eye and left eye observation. The observation hole situated at 45mm from the cathode edge substends only a small angle at the tear film plane and this limits the area not covered by specular reflection. When in position for biomicroscope observations, the hole is situated close to the objective and is large enough to allow monocular observation at different magnifications.

A symmetrical half-pear shaped design has also been constructed to fit more closely against the nose and brows and curve round the temporal side. The position of the hole is decentred towards the apex and the supporting handle is positioned to allow observation of each eye in turn by simple change of orientation of the instrument.

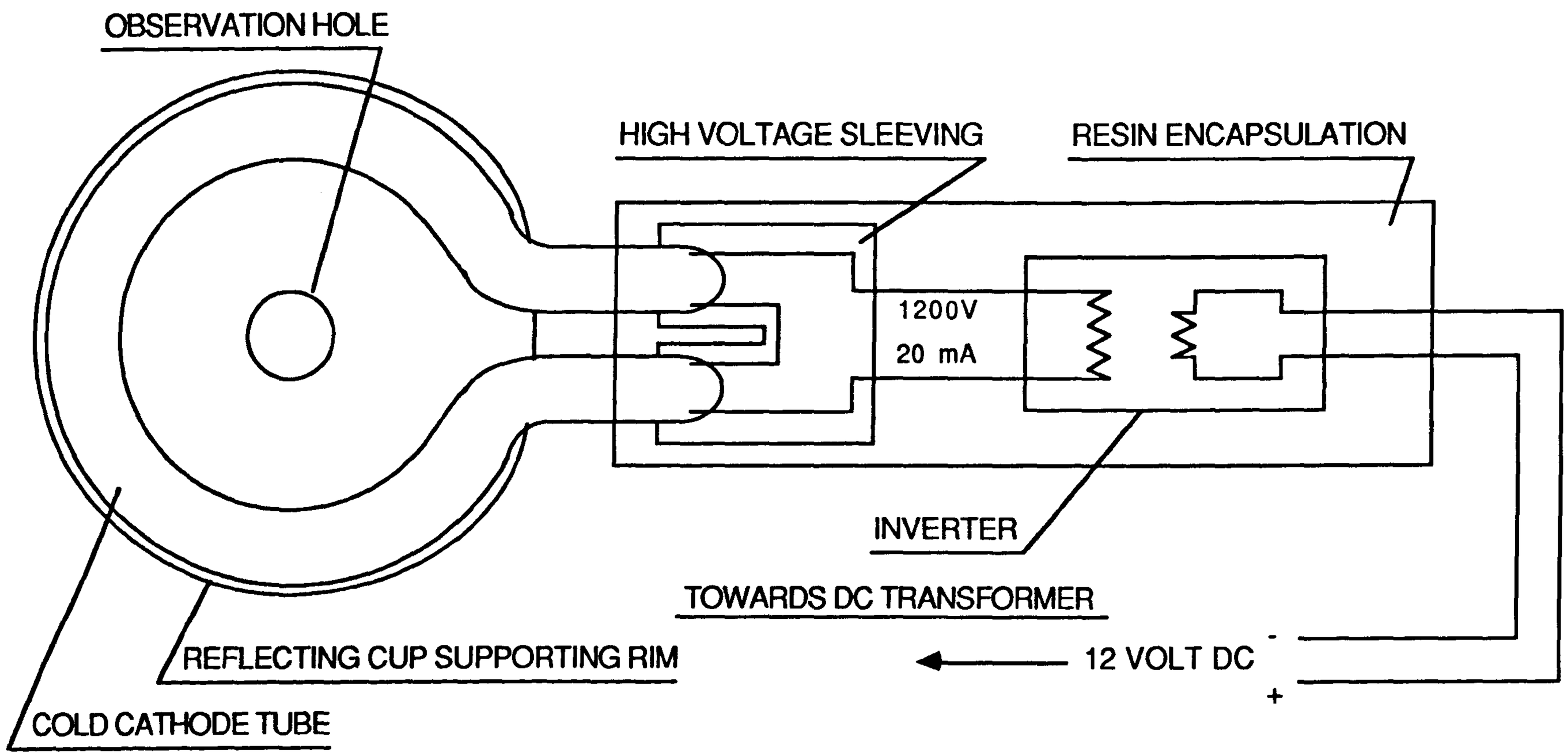

FIGURE 5.6
ILLUMINATION SYSTEM FOR THE LOW MAGNIFICATION EXPERIMENTAL SET-UP: FRONTAL VIEW

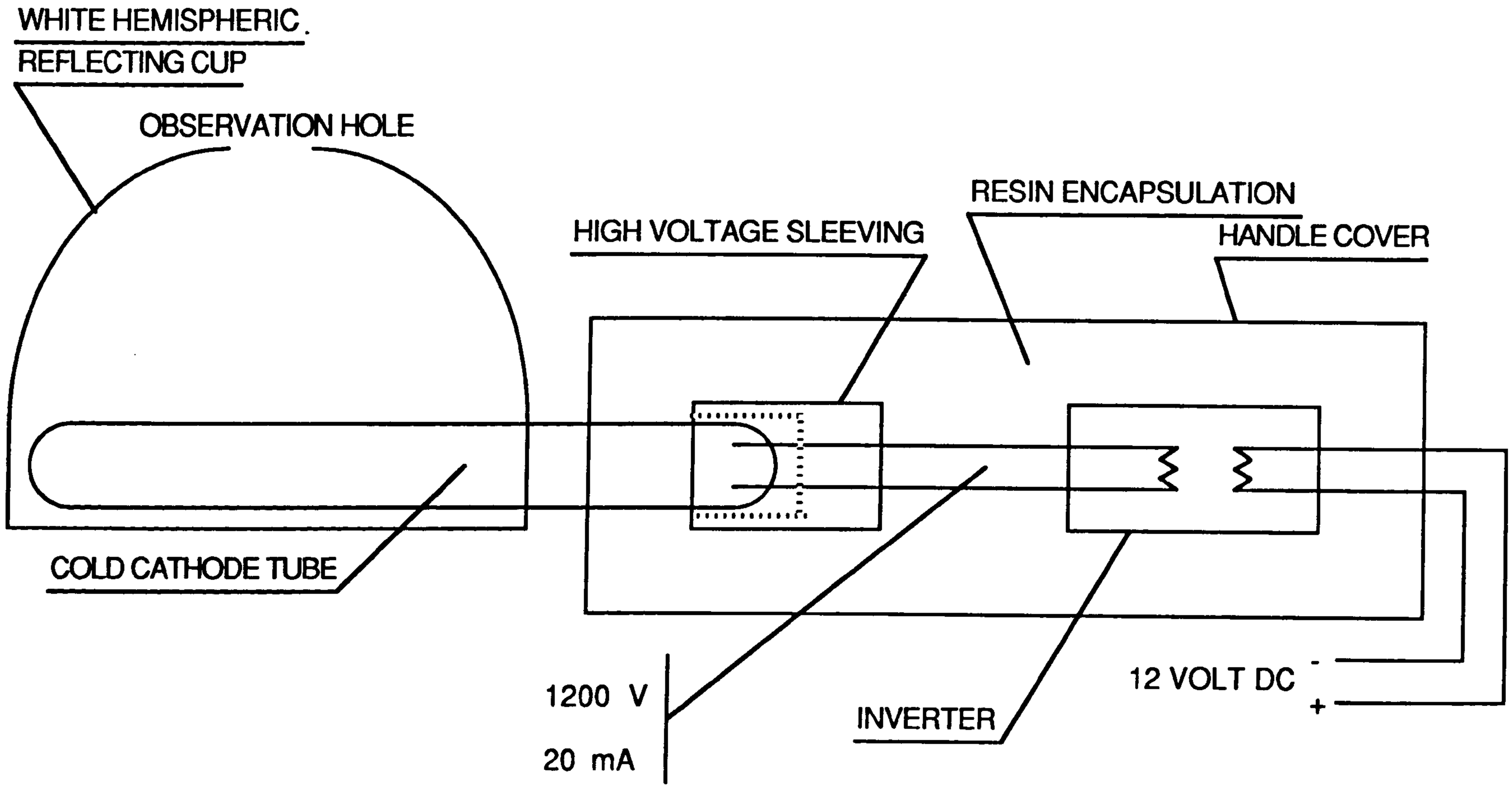

FIGURE 5.7
ILLUMINATION SYSTEM FOR THE LOW MAGNIFICATION EXPERIMENTAL SET-UP:
LATERAL VIEW

iii) Electrical Supply

The handle supporting the circular cathode tube is also encasing an inverter producing the high voltage (1200v), low amperage (20mA) necessary to activate the electric discharge through the cathode tube.

An additional 12 volt transformer permits direct connection of the system to the mains electrical supply via a flex cord. Alternatively a 12 volt D/C battery can be used to provide the necessary electrical input for the system.

A stand alone version of the instrument has been constructed and uses a 9 volt battery that can be fitted directly within the handle and provides enough output to power the instrument.

iv) Mechanical Arrangement

The last 5 cm of the cold cathode tube are curved away from the circular part to become parallel to each other and fit securely into the supporting (Fig 5.6). A one centimetre separation exists between their inner surfaces, and their extremities are encased in a thick silicone rubber high voltage sleeving.

The hollow plastic handle is filled with resin ensuring proper insulation of the electrical parts of the system and prevents the occurrence of an arc between the cathode support elements and any outside metal. Without insulation an arc could be possible with metal situated 3 or 4 mm away. The hollow handle also contains the inverter which is linked to the external transformer or the internal batteries.

The instrument can be held and positioned close to the eye under examination (Fig 5.8). The inner surface of the cup, when illuminated by the circular cathode, acts as a secondary light source which is reflected at the tear surface as a white circular area of 10 to 12mm diameter. The closer the instrument to the eye the wider the illuminated area. The tear film can be viewed against this white background. Further by lateral movement of the instrument or of the eye under examination a scan of the whole ocular surface is easily obtained.

v) Observation System

A number of alternative observation arrangements have been used. The simplest observation is made with the naked eye and a supplementary +10.00 dioptre or +12 dioptre lens placed in the observation hole to put the surface under observation in focus (Fig 5.8). The instrument can be mounted on a stand or the supporting frame of a slit-lamp biomicroscope and used with the microscope observation system. The observation hole of the reflecting cup must be aligned with the objective of the microscope.

Only monocular observation is possible and for practical purposes it is better to use the right objective for left eye examination and the left objective for the right eye examination, due to facial anatomical features.

The system can be used with most slit-lamps at low magnification (x1, x2 and x3) (Fig 5.9). Adequate rotation of the microscope observation system about its

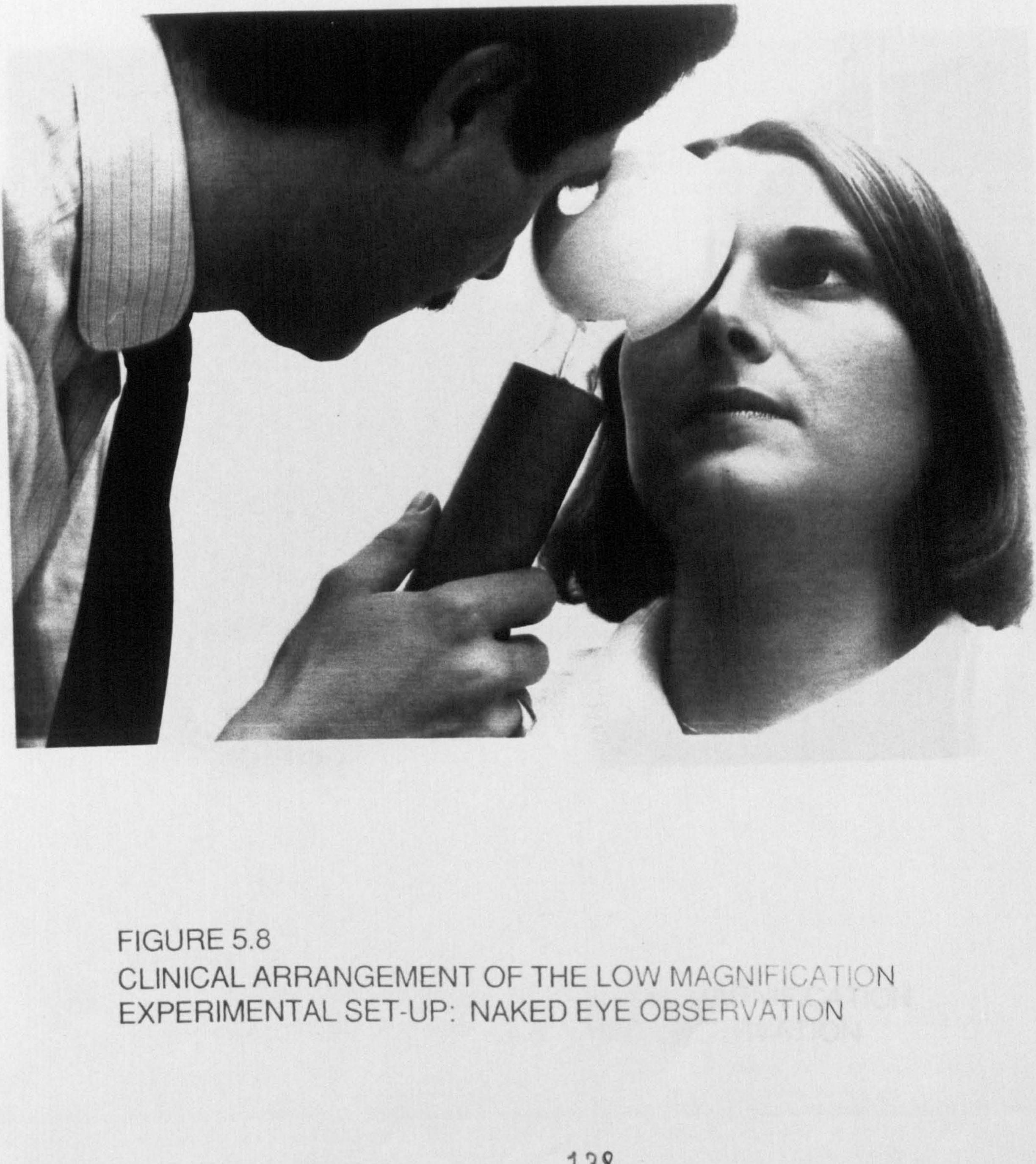

FIGURE 5.8
CLINICAL ARRANGEMENT OF THE LOW MAGNIFICATION EXPERIMENTAL SET-UP: NAKED EYE OBSERVATION

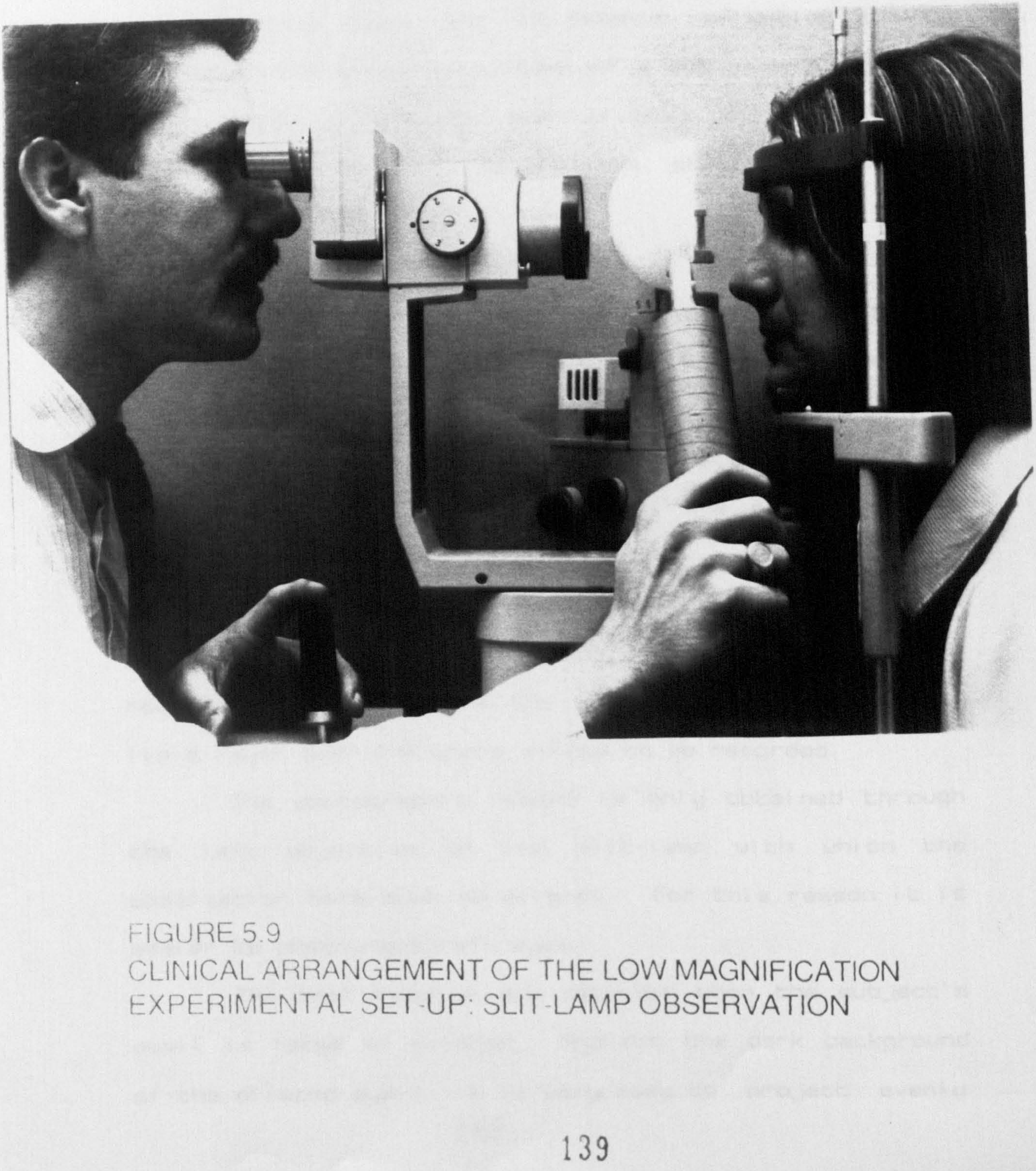

FIGURE 5.9
CLINICAL ARRANGEMENT OF THE LOW MAGNIFICATION
EXPERIMENTAL SET-UP: SLIT-LAMP OBSERVATION

axis or rotation of the eye under examination will produce a scan of the whole cornea.

5.3.3 INSTRUMENTATION FOR PERMANENT PHOTOGRAPHIC RECORD

Using a system similar to the one previously described, low magnification photography of the lipid layer over a large area can be achieved.

In this case, the hemispheric reflecting cup is mounted on the supporting frame of a sun pack 6 x8R ring flash light (Fig 5.10) and aligned with the left objective of a Carl Zeiss Jena photoslit-lamp 210 (Fig 5.11)

The ring flash hot-shoe is coupled to the photographic mechanism of the slit-lamp to ensure synchronisation during exposure. The presence of the ring flash supporting frame does not allow an illumination area as wide as our normal observation system. Only a 7 to 8mm area of the cornea can be photographed.

An adequate rotation of the microscope observation system or rotation of the eye under observation will however render possible the image of the superficial lipid layer over the whole cornea to be recorded.

The photographic record is only obtained through the left objective of the slit-lamp with which the observation hole must be aligned. For this reason it is easier to photograph left eyes.

The best results are obtained when the subject's pupil is large or dilated. Against the dark background of the dilated pupil, it is very easy to project evenly

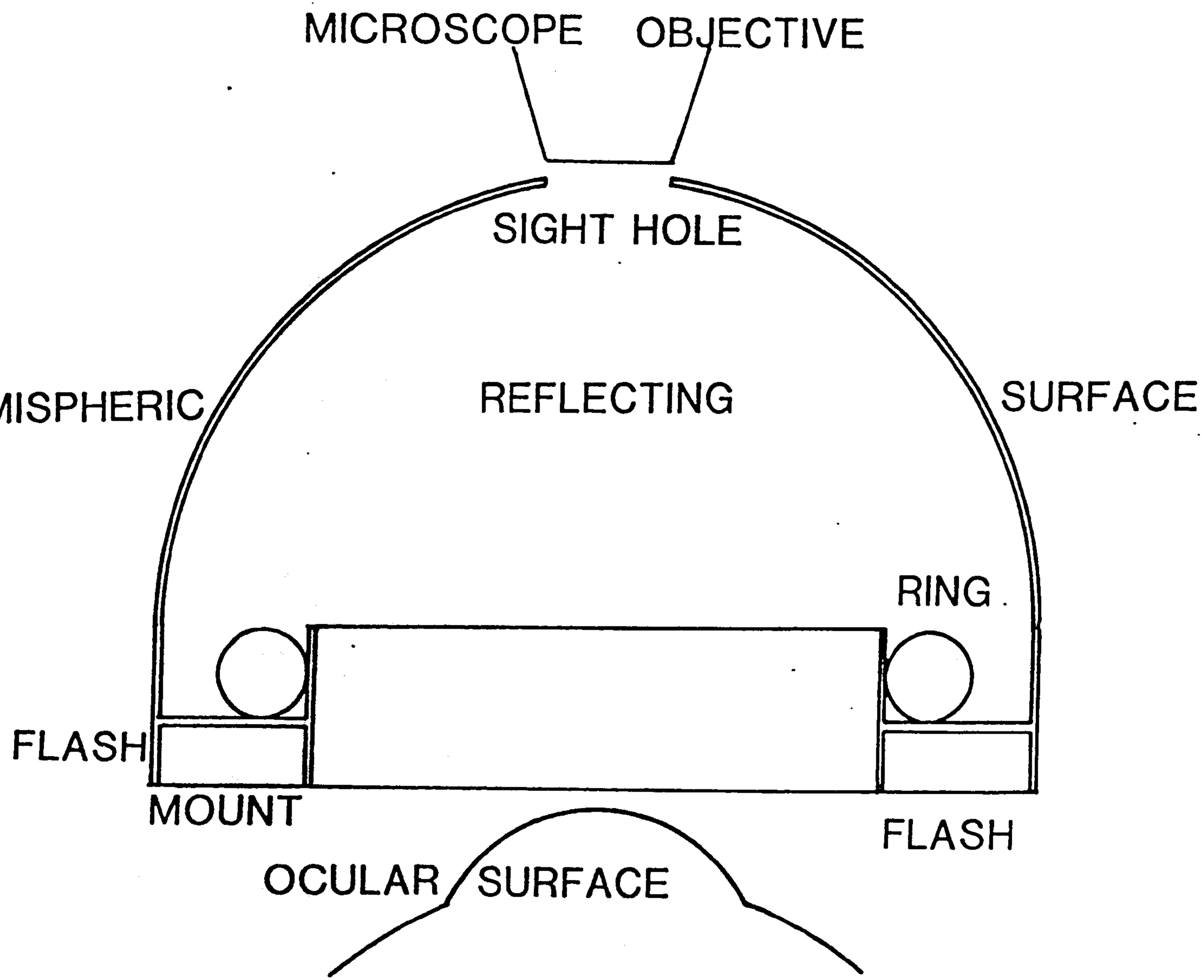

FIGURE 5.10
CROSS-SECTION ARRANGEMENT OF LOW MAGNIFICATION PHOTOGRAPHY SET-UP

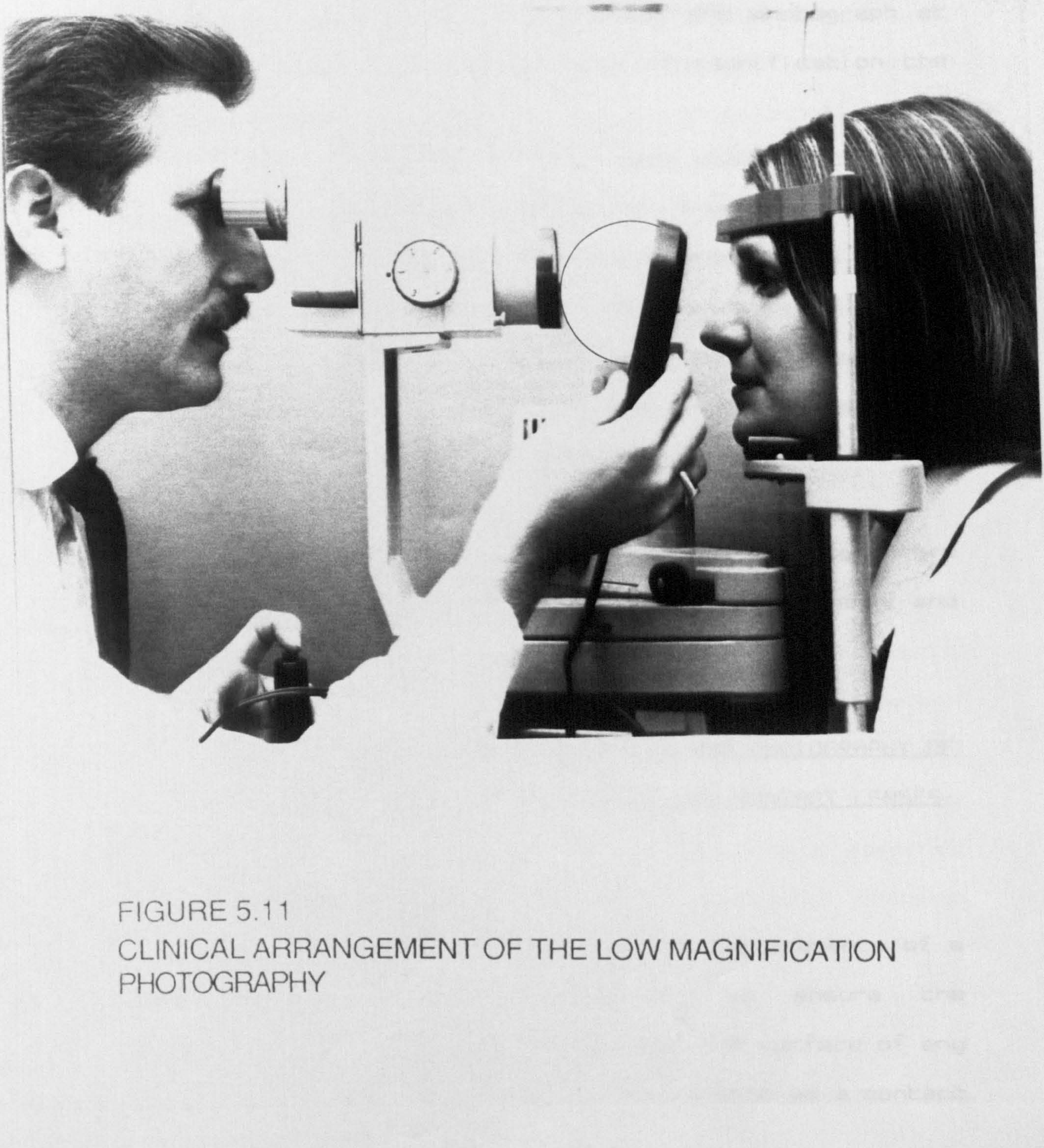

FIGURE 5.11
CLINICAL ARRANGEMENT OF THE LOW MAGNIFICATION PHOTOGRAPHY

the image of the hemispheric cup. The contrast necessary for the observation of the wavy and amorphous pattern of the thin lipid layer will be improved and focussing will be more precise.

In the presence of a small pupil, the superficial lipid layer is photographed against the colourful out-of-focus background of the iris. In that case the tear film patterns are more difficult to detect and photograph at low magnification (x1) but using a x3 magnification the focussing improved.

A combined system has also been constructed where the ring flash has been mounted in front of the cold cathode. This allows the continuous observation of the tear film, precise focussing and the possibility to photograph the patterns visible. It has been used with an Holden-Zantos attachment to the slit-lamp allowing photography through the microscope objective with a normal 35mm camera.

The observation instrument and the photographic set-up can be used very easily with most slit-lamps and photoslit-lamps.

5.4 INSTRUMENTATION FOR OBSERVATION AND PHOTOGRAPHY OF THE MUCOUS LAYER ON THE CORNEA AND CONTACT LENSES

5.4.1 GENERAL DESCRIPTION

As described in Chapter 2 and 4 the presence of a basal mucous layer is primordial to ensure the wettability of the corneal surface and the surface of any polymer introduced in the ocular environment as a contact

lens. The mucuous layer is not visible by biomicroscopical method as it is always covered by the highly reflective lipid layer and aqueous phase. Its presence has been deduced from many experiments but the layer has never been photographed in an in-vivo situation in humans. The techniques rely on the observation of an area of the cornea or contact lens from which the aqueous and lipid layer have just receded. When this occurs with the techniques previously described, the dry spot formed triggers the blink reflex and induces resurfacing of the tear film by the actions of the lids. The use of a custom designed scleral lens prevents the resurfacing of the tear film without impeding the normal blinking action. The drying area, the structure and the behaviour of the tear film surrounding it can then be observed and photographed by very high magnification photography.

5.4.2 USE OF CUSTOM DESIGNED SCLERAL LENS

A scleral lens was designed to allow the formation and photography of a dry spot of long duration over the corneal surface and any contact lens surface under test.

In the primary position of the eye, the cornea and sclera should conform to the back surface of a properly fitted scleral lens. A minimal corneal clearance is necessary and fenestration or channelling may be required to reduce negative pressure and allow fluid exchange during eye movement and to provide complete fluid coverage of the corneal surface.

One design that gives good fluid coverage and minimal negative pressure is one that is derived from the

TRODD Scleral ledge lens for use as a ptosis prop. A superior arcuate slot is cut in the area of the lens covering the corneo-scleral margin.

The lens (Fig 5.12) was based on this design but the corneal portion was elevated to provide a corneal clearance large enough to allow the formation of an air space over the whole of the pre-corneal area (Fig 5.13). A 5mm arcular fenestration was grinded at the apex of the lens.

The role of this scleral lens is manyfold. When placed in the eye, the blinking action is not impeded but the resurfacing action of the lid will only reform the tear film situated on the scleral lens surface. The pre-corneal tear film under observation is free from the lids interference and can be supplemented only from the periphery by movement of fluid under the haptic portion of the lens (Fig 5.14). Alternatively normal saline or an artificial tear solution can be added either through the superior arculate slot or by direct instillation through the central 5mm observation hole. The design of this lens creates an artificial meniscus in the area surrounding the cornea where the back surface of the lens approached the scleral surface (Fig 5.13). The morphology of this meniscus encloses the tear film under observation and its drainage effect is limited as it is supplemented by fluid situated under the scleral portion of the lens.

Such a tear film, enclosed by a fluid barrier is relatively more stable than the normal pre-ocular tear film. The scleral lens provided an open environment that

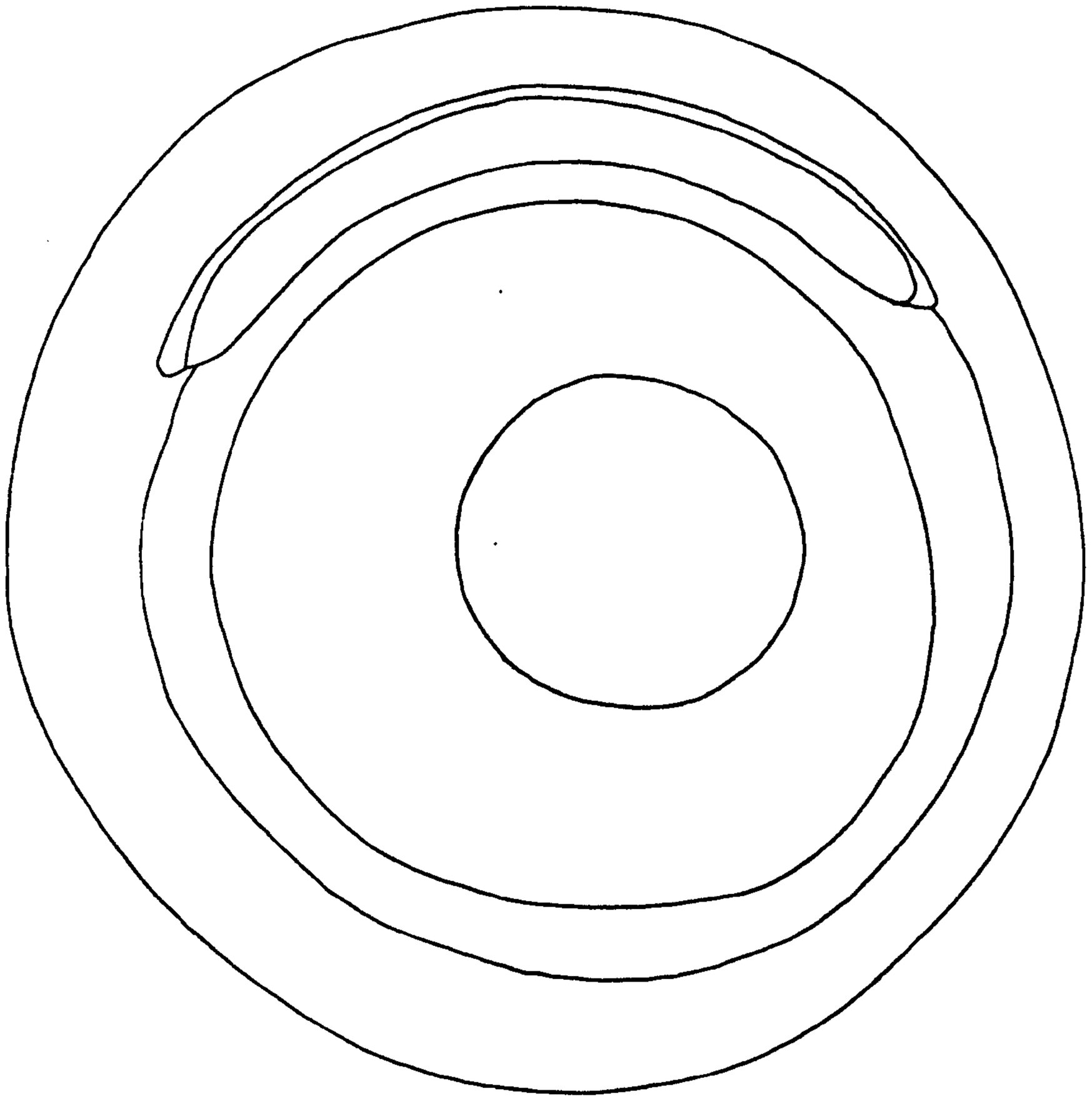

FIGURE 5.12
SCLERAL LENS FOR MUCOUS OBSERVATION:
FRONTAL VIEW

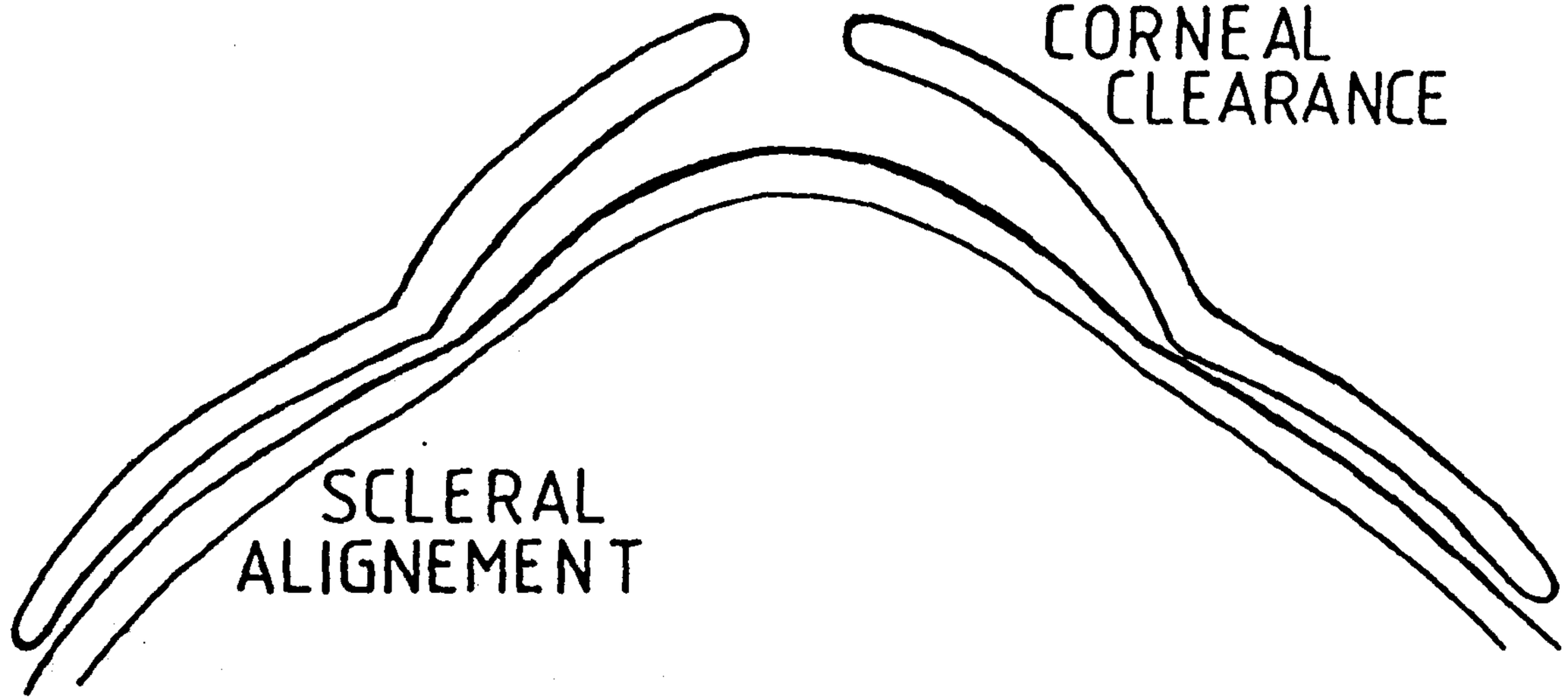

FIGURE 5.13
SCLERAL LENS FOR MUCOUS OBSERVATION: CROSS-SECTION

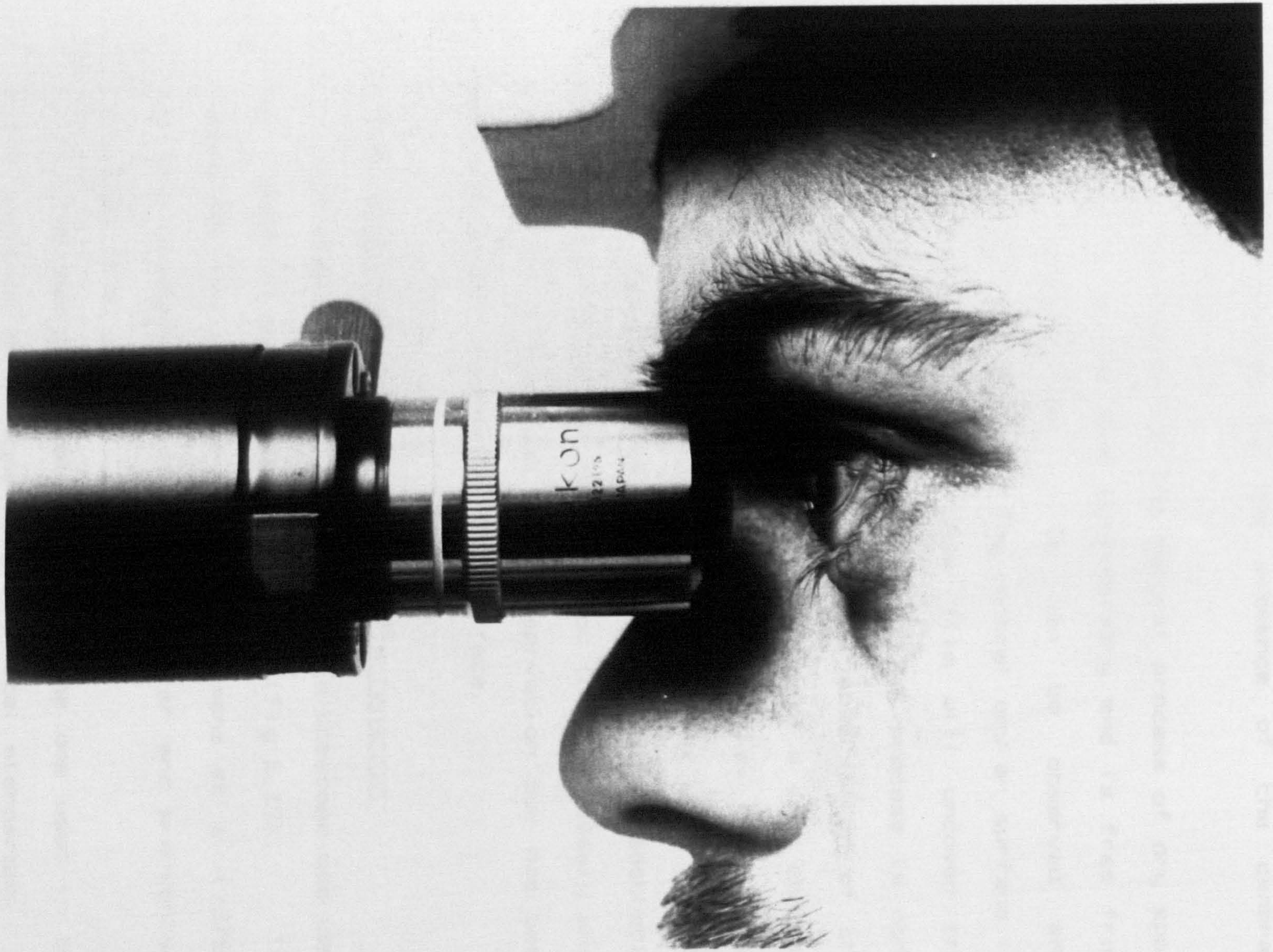

FIGURE 5.14
SCLERAL LENS FOR MUCOUS OBSERVATION: CLINICAL SET-UP

is free of draft but where steaming of the internal surface is avoided by the presence of the central observation hole.

In this condition the natural process of dry spot formation is slowed down considerably and is free from external disturbances. It can be observed and photographed very easily. The central ocular surface is scanned and the receding tear film will uncover the mucous coated epithelial surface. The process is non-invasive and can be applied to the observation of the corneal surface or that of the surface of a soft contact lens previously inserted. Excessive reflex lacrimation that may be induced by the scleral lens wear can be alleviated by the use of one drop of local anaesthetic such as amethocaine but this was not found necessary when a soft contact lens was under observation but has been used when observing the corneal surface.

5.4.3 BIODIFFERENTIAL INTERFERENCE MICROSCOPE

A biodifferential interference microscope was used for observation and photography (Fig 5.15). The instrument was originally used by Hamano et al (1979a) for their observation of the pre-ocular and pre-contact lens tear film.

The basic optical system is the one used in the Nikon Optiphot XP-NR Type Nomarski metal microscope. In order to observe the living eye it is made as a horizontal design, and mounted on the stage of a slit-lamp microscope where focussing can be done by a joystick. The illuminating source is a Tungsten lamp for

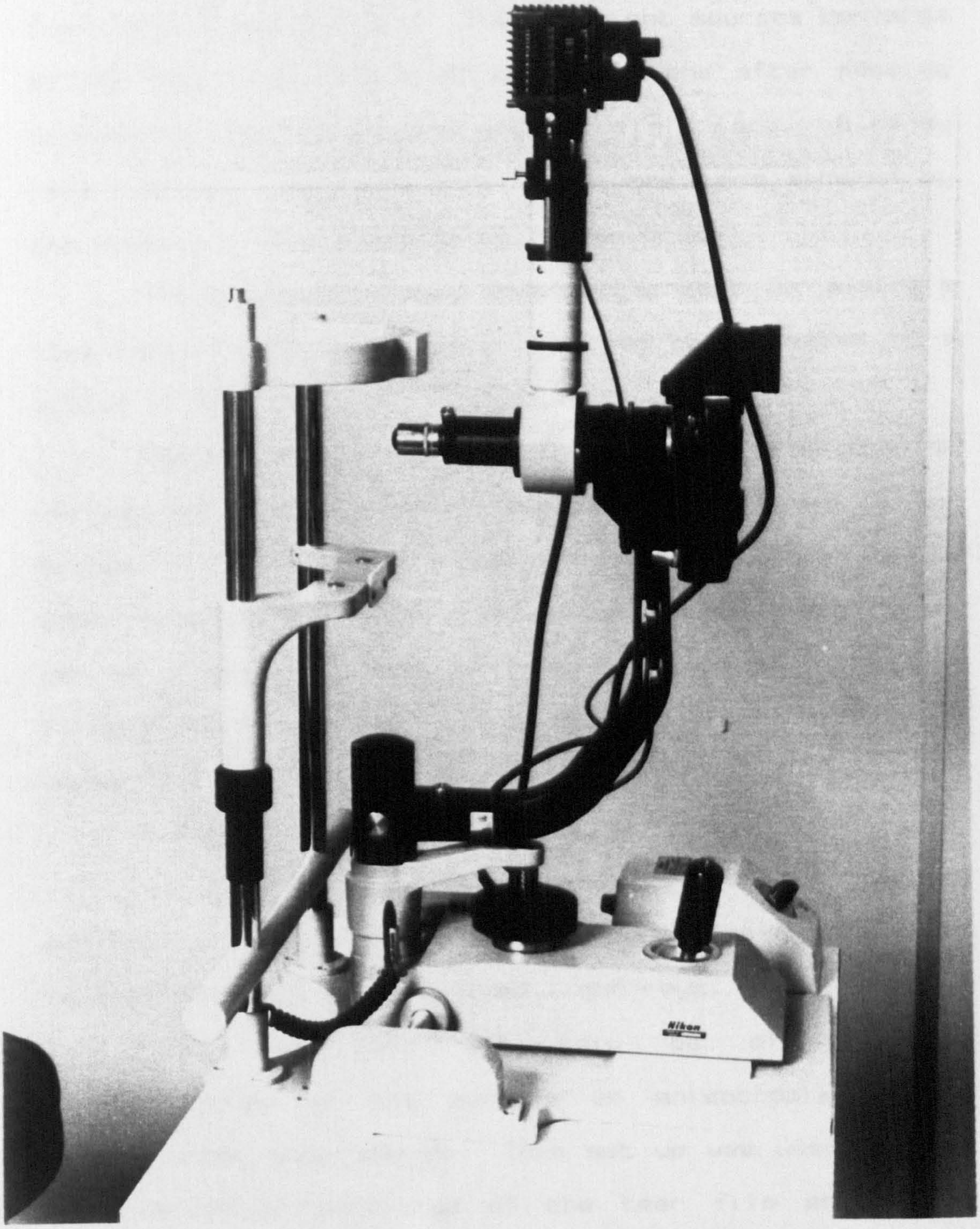

FIGURE 5.15
NIKON BIO-DIFFERENTIAL INTERFERENCE MICROSCOPE

observation and a Xenon strobe light for photography (Fig 5.16). The hue difference is compensated by a colour balancing filter (Fuji Film LBA-8 (0.5)) on the front of the Xenon light. The two light sources converge at the rear focal plane of the main lens after passing through the collector lens and the field lens. A relay lens corrects the light path which has been altered by the insertion of a modified Wollaston prism.

The eyepiece is used as an attachment for a single lens reflex motorised camera that can be activated by a button on the joystick.

As explained previously in Chapter 3 this original version of the instrument produces an oblique colour fringe in the field of view when a curved surface is under observation. The position of the Wollaston prism can be altered by means of a screen and the polarising filters can be removed. This will produce two different types of field of view;

i) <u>Dark Field Observation</u>

When the screw is turned to the maximum position of the Wollaston prism it produces a dark field by extinction of the reflected light rays.

The ray path can only be disturbed by irregularities of the surface or anisotropia of the medium under observation. This set up was used for the observation of particles of the tear film and during observation of dry spot to reveal the irregularities of the surface.

The particles appear as very bright dots in a dark field as they act as diffraction sources. This way

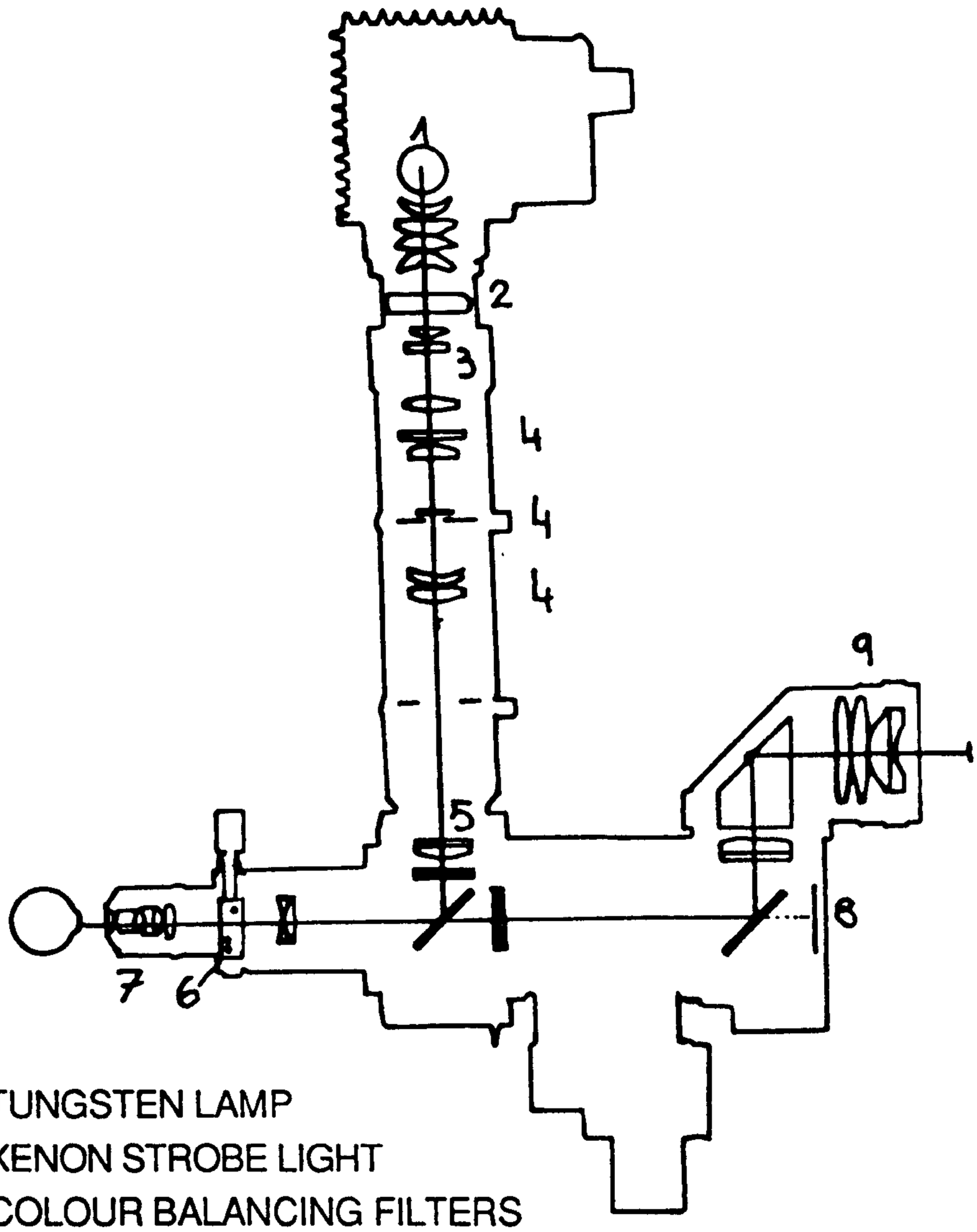

1. TUNGSTEN LAMP
2. XENON STROBE LIGHT
3. COLOUR BALANCING FILTERS
4. COLLECTOR LENS
5. FIELD LENS
6. WOLLASTON PRISM
7. OBJECTIVE
8. FILM
9. EYE-PIECE

FIGURE 5.16
SCHEMATIC OPTICAL SYSTEM OF NIKON BIO-DIFFERENTIAL INTERFERENCE MICROSCOPE

they can be very easily differentiated from the surrounding lipid layer.

ii) Normal Observation

When the screen of the Wollaston prism was not fully turned, and the polarising filter removed, the diagonal colour band was confined to the periphery of the field and full use of the microscope magnification was made in near perfect field.

iii) Photography & Measurement

The use of Ektachrome 100ASA slide reversal film was satisfactory and the recharging time of the Xenon strobe light of about one second allowed photography in rapid succession when necessary.

The analysis of the photograph of a microscope millimeter scale gave a 16.5 times linear magnification, at the film plane and a circular field of view of 1.5mm in diameter. That magnification is larger than the one obtained with the non-contact endothelial camera and allowed the observation of the different layers of the tear film in greater detail.

Lateral and vertical movement of the instrument was necessary to cover the 5mm of the field of observation created by the central observation hole of the scleral contact lens. Accurate focussing on the surface was necessary but surprisingly easy for such a high magnification.

A series of photographs was taken every time a dry spot was forming on the corneal or contact lens surface to assess its dynamic behaviour.

iv) Use of Micrometer Latex Spheres

Micrometer latex spheres (1.099µm diameter) in aqueous solution were used in an attempt to measure the thicknesses of the various tear film layers under observation. A two microlitre drop was instilled in the tear film before the insertion of any contact lens and the behaviour of the spheres was observed in the pre-ocular and pre-lens tear film.

5.5 METHODS OF EXAMINATION

5.5.1 METHOD FOR HIGH MAGNIFICATION PHOTOGRAPHY

The method for observation and photography of the tear film layers under high magnification is as follows:

i) Use of Nikon non-contact Endothelial Camera

The x10 objective should be used at maximum aperture f/1.4 to ensure the widest specular reflection. The polariser is placed in position in front of the prism of the illumination system. The slit and the aperture diaphragm should be fully opened.

The instrument focussing can then be adjusted on the target surface provided with the instrument. The target can be viewed through the viewfinder of the attached camera and a cross-line can be seen by reflected light. The dioptre adjustment ring of the camera can be altered to suit the examiners correction.

The slit width is reduced and the photographic system is adjusted backward or forward until the slit illumination is brought in the centre of the viewfinder. The illumination system and the photographic system have

the same focal point when the cross-line and the target surface are seen sharply at the centre of the thin reflected slit. The slit is opened fully and the analyser is placed in position in front of the objective lens and rotated at 90 degrees from the polariser until the rough target surface is void of reflection.

The brightness of the illuminating light can be adjusted to the medium setting (M) or low setting (L) to limit the heat produced on the surface under observation.

The flash setting of 4 or 5 is used for photography as the effect of the polariser in near crossed position will cut down by nearly 95 percent the light entering the photographic system.

The system is ready for tear film observation.

ii) <u>Routine for Clinical Observation</u>

The patient is set comfortably at the slit-lamp and looks straight ahead:

- the specular reflection is centred in the field of view and focussing is achieved on the image of the lamp filament.

- the analyser rotation can be adjusted between 85 and 90 degrees to a level avoiding complete extinction of the reflection of the lamp filament. This position will ensure cut-off of all extraneous light, it will narrow the spectrum of light received at the film plane after interference within the tear layers under observation.

- by use of the joystick, the slit-lamp is moved a few millimetres away from the ocular surface to obtain a clear focus of the tear film. The photographs are taken by pushing the shutter release situated on the top of the

joystick. The Nikon F2 camera is provided with a motor drive for advancing the film automatically after each exposure.

5.5.2 METHOD FOR LOW MAGNIFICATION OBSERVATION

The instrument for wide-field examination of the tear film can be used for naked eye observation or in conjunction with a biomicroscope.

i) Naked Eye Observation

Clinically the simplest method to use, it only requires the use of a high powered positive lens (+10.00 to +12.00 dioptres) in the observation hole. This will put the tear film in focus for an emetropic observer. The patient is sitting in the examination chair, in an upright position or leaning back against the head rest.

It is advisable when the instrument is used for the first time on a subject to demonstrate that the cold cathode light does not produce heat. It is best shown by placing it in front of one's eye and looking through the hole from the subjects position. Alternatively, hand contact with the cathode surface can be used.

The instrument is switched on and placed in line with the subjects eye and rests against the brows and nose. The patient looks in the direction of the observation hole to limit the possible reflex lacrimation that could be induced by looking straight at the light source or the reflecting surface.

The tear film can be observed against the background formed by the white reflecting surface. Similarly to ophthalmoscopy examination, the subjects

left eye is best examined when holding the instrument in the left hand and observing with the left eye. The opposite can be done for contralateral examination.

The naked eye observation is used for observation of the tear film movement, general behaviour, and non-invasive break-up time measurement on the pre-ocular tear film and pre-lens tear film.

ii) Observation with a Biomicroscope

The observation system of any biomicroscope can be used in conjunction with the wide illumination hand held instrument. It permits the observation of the tear film in low and medium magnification.

The subject is seated at the microscope, in position against the head rest. For the observation of the subjects left eye. the instrument is held in the right hand and the observation hole is aligned with the microscope right objective. The illumination system of the slit-lamp is not used and is positioned on the left not to interfere with the hand held instrument.

If the subjects nose impedes full corneal coverage, the system can be rotated 20 degrees to the right while the subject maintains fixation towards the observation hole. This alignment and initial focussing is most effective under low magnification (x1). When full corneal coverage is achieved, the magnification of the system can be increased to two times (x2). The whole of the cornea and contact lens can be observed at one time. The localised break-up can be easily seen and the measurement of non-invasive break-up time is best done at this magnification. Observation at three times

magnification is useful when a particular zone needs to be studied. That is the case when the tear film breaks up repeatedly in the same area, when the observer wants to ascertain the presence and appearance of this very thin lipid layer at the surface of the pre-lens tear film, or when the tear film behaviour is studied at the edge of contact lenses.

With higher magnification, x5, the intensity of the reflected light is too low, observation is difficult and the alternative system of specular reflection is better suited.

5.5.3 METHOD FOR LOW MAGNIFICATION PHOTOGRAPHY

The Zeiss Jena 210 photoslit-lamp was used for our photographic examples in Chapter 4.

The patient is positioned as described previously. The ring flash can be mounted directly on the hemispheric cup or preferably on the hand held instrument. In the latter case, the examination is done in a darkened room and the alignment and focussing is done as described previously with the illumination of the cold cathode. The light is turned off and the photograph taken about three seconds later. During those three seconds, the subjects pupil dilates enough in the dark room condition to provide a larger dark pupil area, thus increase the zone where a clear photograph of the tear film can be taken.

The same routine can be used for photography with the Zeiss Jena 210 slit-lamp with the Holden-Zantos attachment.

5.5.4 METHOD FOR THE OBSERVATION OF THE MUCOUS LAYER

i) Observation on the Cornea

The subject is seated at the Nikon biodifferential microscope and all adjustments are made during the observation of the pre-ocular tear film.

At this very high magnification (x16.5) and because of the very limited field of view (1.5mm diameter) over which the instrument operates, the centration, the head position and stability of the subject during the observation is primordial.

The scleral contact lens is then inserted with the help of a wetting solution to coat its surface and limit the effect of steaming during wear. The observations start immediately following the scleral lens insertion for a maximum duration of 5 minutes. As the technique had not been used before the 5 minute duration was imposed as a precautionary measure.

The central area was scanned until a thinning area and the ensuing dry spot was seen. Photographs were taken during all stages of break-up and observation continued for about one minute after dry spot formation. The scleral lens was then removed and fluorescein was instilled and the cornea checked for superficial staining.

When necessary the micrometric latex spheres in aqueous solution were instilled with a micropipette two to three minutes before the scleral lens insertion.

ii) Observation on Contact Lens

The lenses were inserted and allowed to settle for 20 to 30 minutes before scleral lens insertion

to allow for the normalisation of the pre-lens tear film and the formation of a stable mucuous layer.

Following observation the scleral lens was removed and a drop of Clerz in-eye wetting solution was instilled to refurbish the water lost through evaporation. The soft lens was checked for movement and removed. Fluorescein was instilled and the cornea checked for staining.

CHAPTER 6

METHOD FOR THE MEASUREMENT OF TEAR FILM THICKNESS AND ITS CONSTITUENT PHASES

6.1 WAVE THEORY OF LIGHT

6.1.1 INTRODUCTION

The purpose of the photographic techniques previously described is to record for analysis the coloured interference fringes produced in the different layers of the pre-corneal and pre-contact lens tear films. This analysis will enable presentation of precise data measured in-vivo of those layers' thicknesses, their structures and their interactions.

To appreciate the precision of those measurements and the sensitivity of the technique and its limitations, it is necessary to consider the optics and to review the theory of interference and their use in the measurement of optical thicknesses.

6.1.2 OPTICAL INTERFERENCES

The phenomenon of interference arises directly out of the wave theory of light. Light can be regarded as an electromagnetic wave motion travelling with a velocity V. When a light wavefront is propagated in a given direction, it can be represented as a sinusoidal function characterised by its wavelength λ and its amplitude A. The wavelength λ is a function of the wavefront speed in

a vacuum or in air and the amplitude A varies between a maximum and a minimum as a function of time (Fig 6.1).

When two light wavefronts travel in the same direction, they interfere with one another and their superposition produces a new wavefront whose characteristics will depend on the wavelengths of the original wavefronts and their phase difference.

There is a special case that warrants particular attention. It is when two identical monochromatic waves (same single wavelength) combine. If they are said to be 'in phase' their maxima and minima coincide in time. The wavelength of the resulting wavefront will be unchanged and the amplitude will be the sum of the amplitudes. This situation is known as 'constructive interference'.

If their maxima and minima differ by half a wavelength the two vibrations are in opposition of phase. The resulting amplitude is 'zero'. This situation is known as 'destructive interference' (Fig 6.2).

In all other cases, the characteristics of the resulting vibration will be a function of the number of wavefronts involved, their wavelength, amplitudes, degree of monochromaticity, and phase difference. For most combinations, interference fringes cannot be observed.

6.2 CONDITIONS OF INTERFERENCE

A laser produces a powerful, highly directional monochromatic and coherent beam of light. When lasers are used, the phase of the radiations they generate remains constant during a long period of time (up to

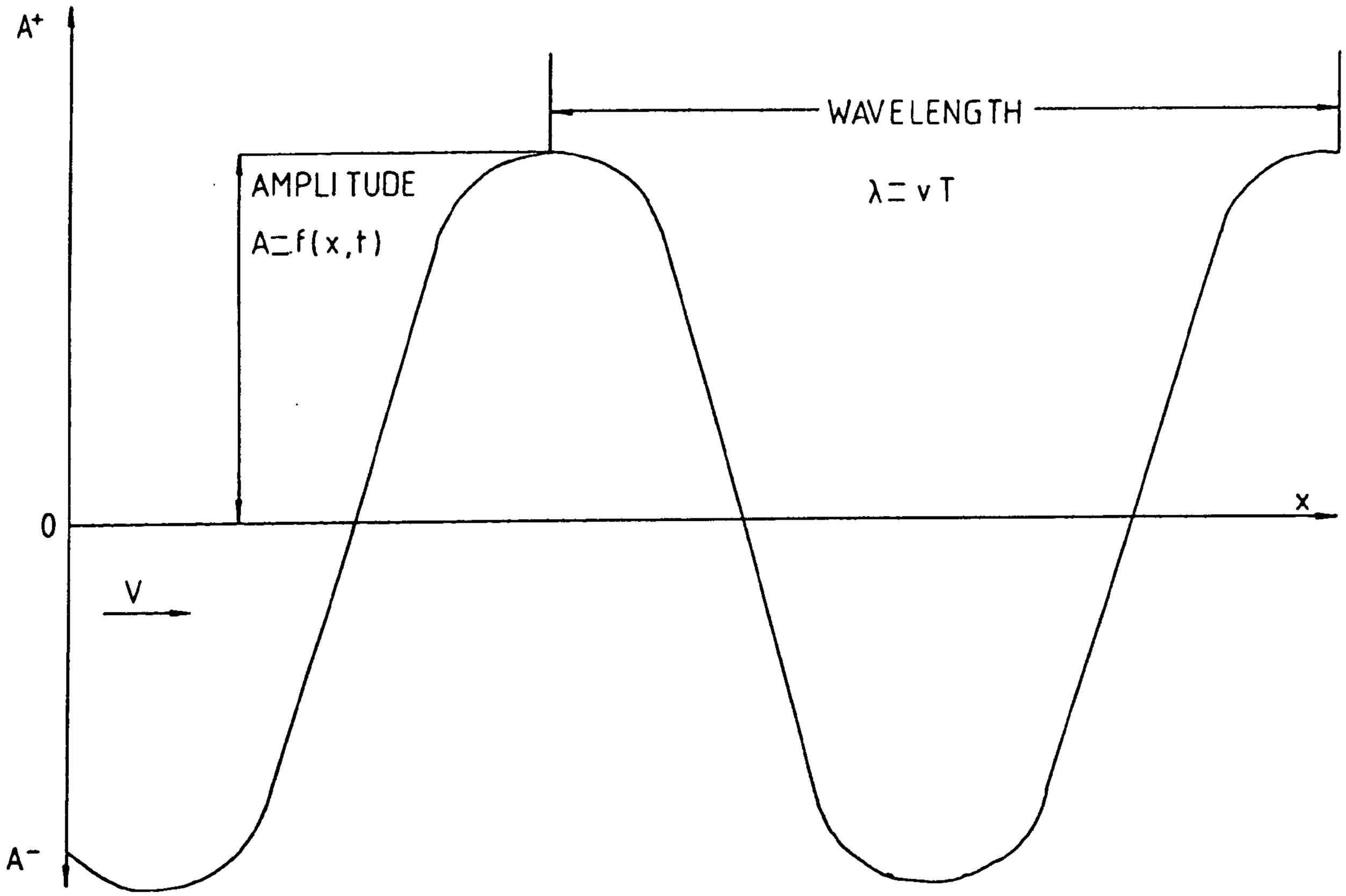

FIGURE 6.1
PROPOGATION OF WAVE MOTION

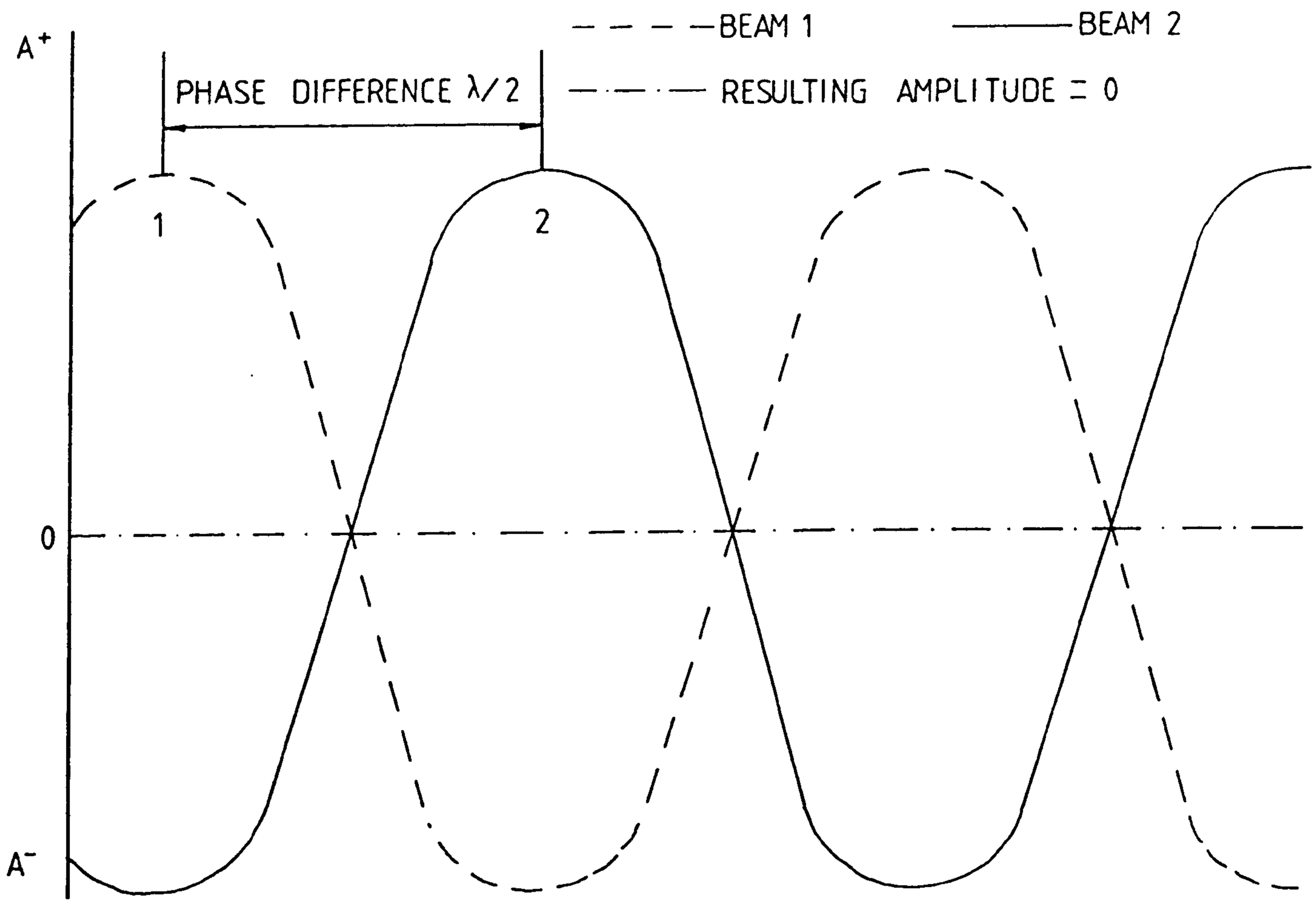

FIGURE 6.2
DESTRUCTIVE INTERFERENCE OF TWO IDENTICAL BEAMS IN OPPOSITION OF PHASE

1/10th sec) and the interferences between the emission of two lasers may be observed even by means of very simple devices. The light from two non-laser sources remain in phases for much shorter periods of time so that no interference can be observed. In the general case, interference fringes can only be observed when some very specific physical and geometrical conditions are satisfied.

6.2.1 PHYSICAL CONDITIONS

The production of a system of interference fringes requires that the light sources must be coherent and their spectral width must be limited.

i) Coherence

With two conventional sources of light, it is not possible to obtain any reinforcement or weakening of light intensity in the illuminated space. In order to make the interference visible, coherent sources of light must be used. Two sources of light are said to be coherent if they emit coherent wavefronts whose phase difference is constant in time.

There are two basic methods to obtain partial coherence experimentally by dividing an initial single light wavefront into two coherent wavefronts.

The first method uses a 'wavefront splitting' technique as in Young's experiment where the secondary waves interfere with each other according to the principle of superposition (Fig 6.3). This principle was used to produce interferences by Fresnel by means of a biprism and a double mirror and by Lloyd using a single

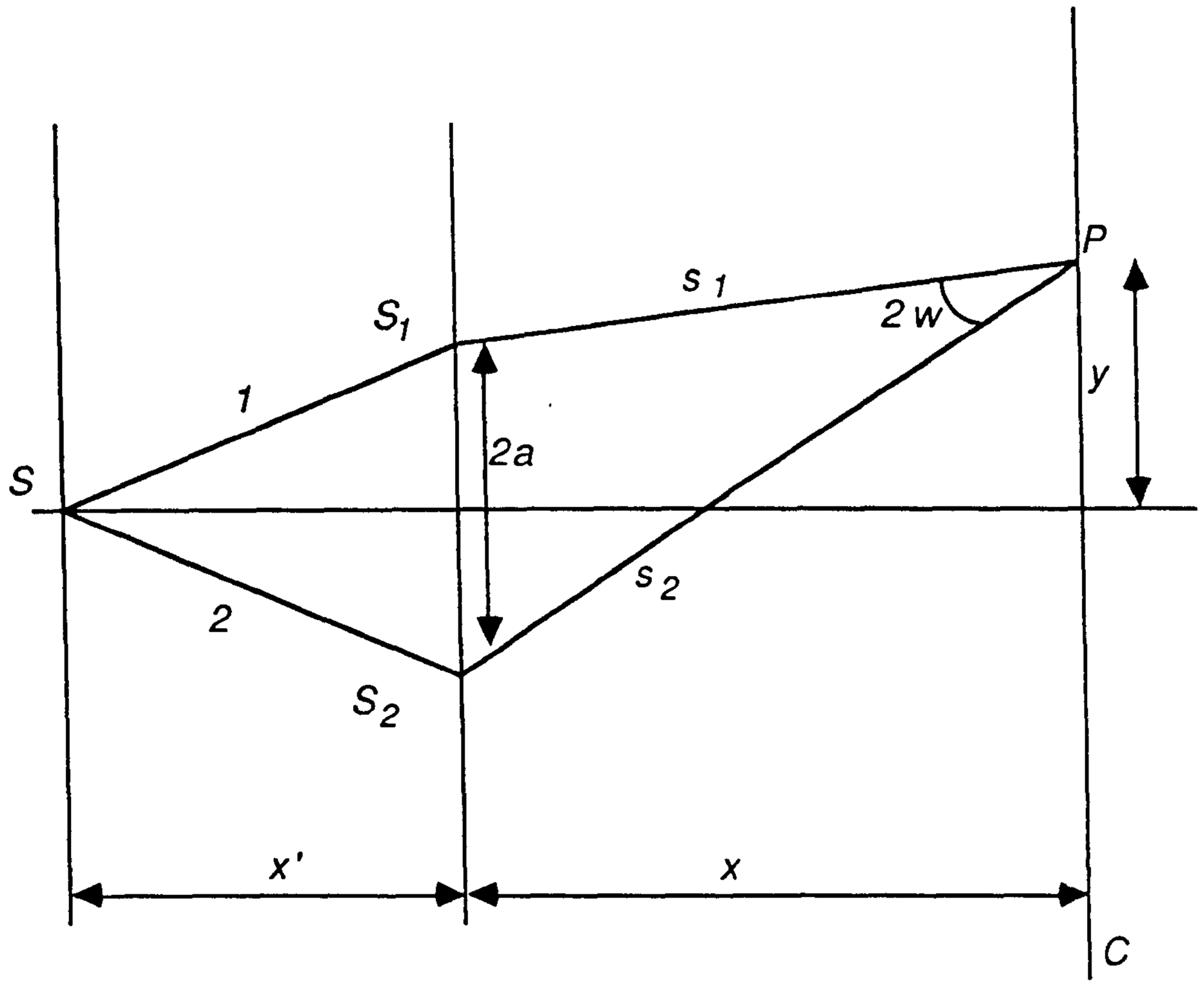

FIGURE 6.3
OPTICAL ARRANGEMENTS TO PRODUCE YOUNG'S 'WAVEFRONT SPLITTING' INTERFERENCE

mirror at grazing incidence which could be coupled to a grating or a prism to improve the separation and the visibility of the fringes. This principle does not apply to the system used in our work and will not be discussed further.

The second method uses an 'amplitude splitting' technique as is the case in Newton's original observations (Fig 6.8). It is that principle which applies to the production of reflected and transmitted interference fringes in parallel sided plates in very thin films and in narrow wedge films. This type of interference is the basis for the development of anti-reflection coatings and many types of measuring interferometers following such as those designed by Michelson, Twyman and Green, Jamin, and Mach-Zehnder.

ii) Spectral Width

A complete coherence is obtained only when using laser light emitted within an extremely narrow band width. In all other cases only partial condition of coherence is present because when the light source is spread over a wide or continuous spectral band $\Delta\lambda$, a progressive disappearance of the fringes will occur with increasing path difference.

This will occur when the order of interference reaches the following value

$$P = \frac{\text{Phase difference } \delta}{\text{Wavelength } \lambda}$$

$$P = \frac{\delta}{\lambda} = \frac{\lambda}{\Delta\lambda} \qquad [1]$$

P = order of interference
δ = phase difference
λ = main wavelength of light
$\Delta\lambda$ = spectral band

When P is known, the spectral width of the source can be calculated. A narrow spectral width, however, is favoured as it ensures a stronger coherence and sharper definition of the interference fringes.

6.2.2 GEOMETRICAL CONDITIONS

i) Localisation of Fringes using a Point Source

If a point source is used, interferences will be present wherever the two interfering beams meet in space and the fringes will not be localised. This is the case in Young's experiment (Fig 6.3), where the fringes are present in a large area of space and their form will depend on the relative position of the coherent sources and the screen (Fig 6.4). Fringes of this type are called non-localised. The interference field is formed by a system of hyperboloids of revolution whose foci are at the point source S_1 and S_2. Different sections through the hyperboloids may be observed by moving the screen in the interference field illustrated in Figure 6.4.

ii) Localisation of Fringes using a Wide Source

If a wide source is used, the interference fringes produced by different points of the source must coincide.

That is the case in a thin parallel film and in a thin wedge where thickness and related phase differences are relatively constant.

When the interfering rays are obtained by splitting an original single source, this source can be wide.

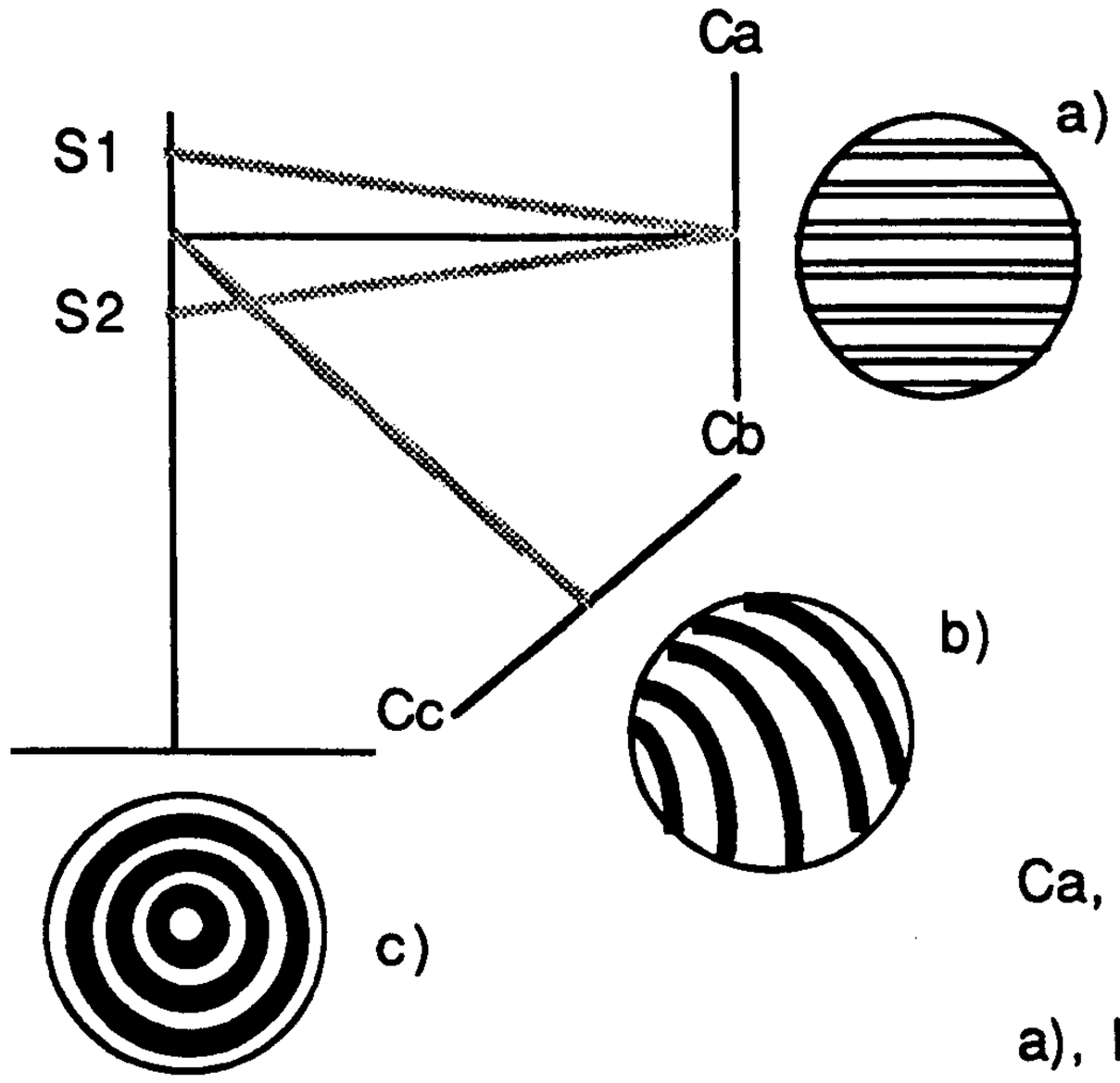

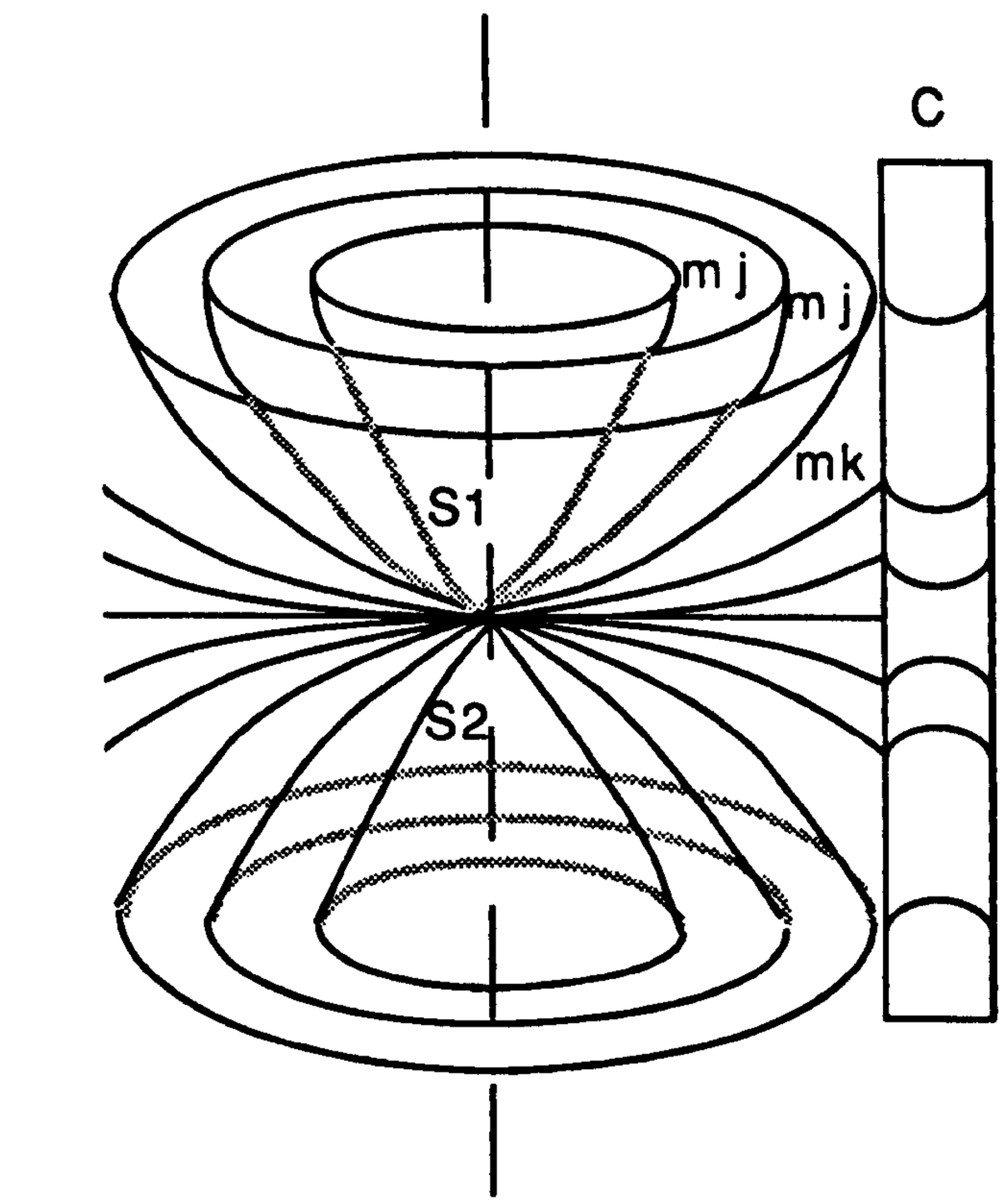

FIGURE 6.4
EFFECT OF THE POSITION OF THE SCREEN ON THE SHAPE OF THE INTERFERENCE PATTERN

In the case of a thin film and a wide source (Fig 5.10), the fringes will be formed in the reflected image space where the rays intersect. The fringes are said to be 'localised' on the film.

In our present experimental technique, the localised coloured fringes observed are a special case relying on the division of amplitude to produce interference of two beams.

6.2.3 APPLICATIONS OF DIVISION OF AMPLITUDE TECHNIQUE

The visible interference phenomena result from the recombination of the two parts of a beam of light after a partial reflection and refraction. These interference phenomena are of two main types, those seen in parallel sided plates and those seen in very thin films of varying thickness.

i) Interference in Parallel Sided Plates

To explain the phenomena we will consider first the case of a single incident ray on a parallel sided plate and the reflected rays paths at the front and back surface and their recombination (Fig 6.5).

The ray from a monochromatic source S is partly reflected and partly refracted at A. At each point, A, B, C, D, E etc a small proportion of the incident light is refracted and the rest is reflected. When we consider the first couple of rays emerging from A and C, their intensity will be very similar and they will recombine at P after refraction by lens L. At that point P they will be out of phase by an amount determined by their optical path difference (Fig 6.6).

AIR = n = 1
S = SOURCE
SA = INCIDENT RAY
AL = PARTIAL REFLECTION
AB = PARTIAL REFRACTION
BC = PARTIAL REFLECTION
CL = PARTIAL REFRACTION

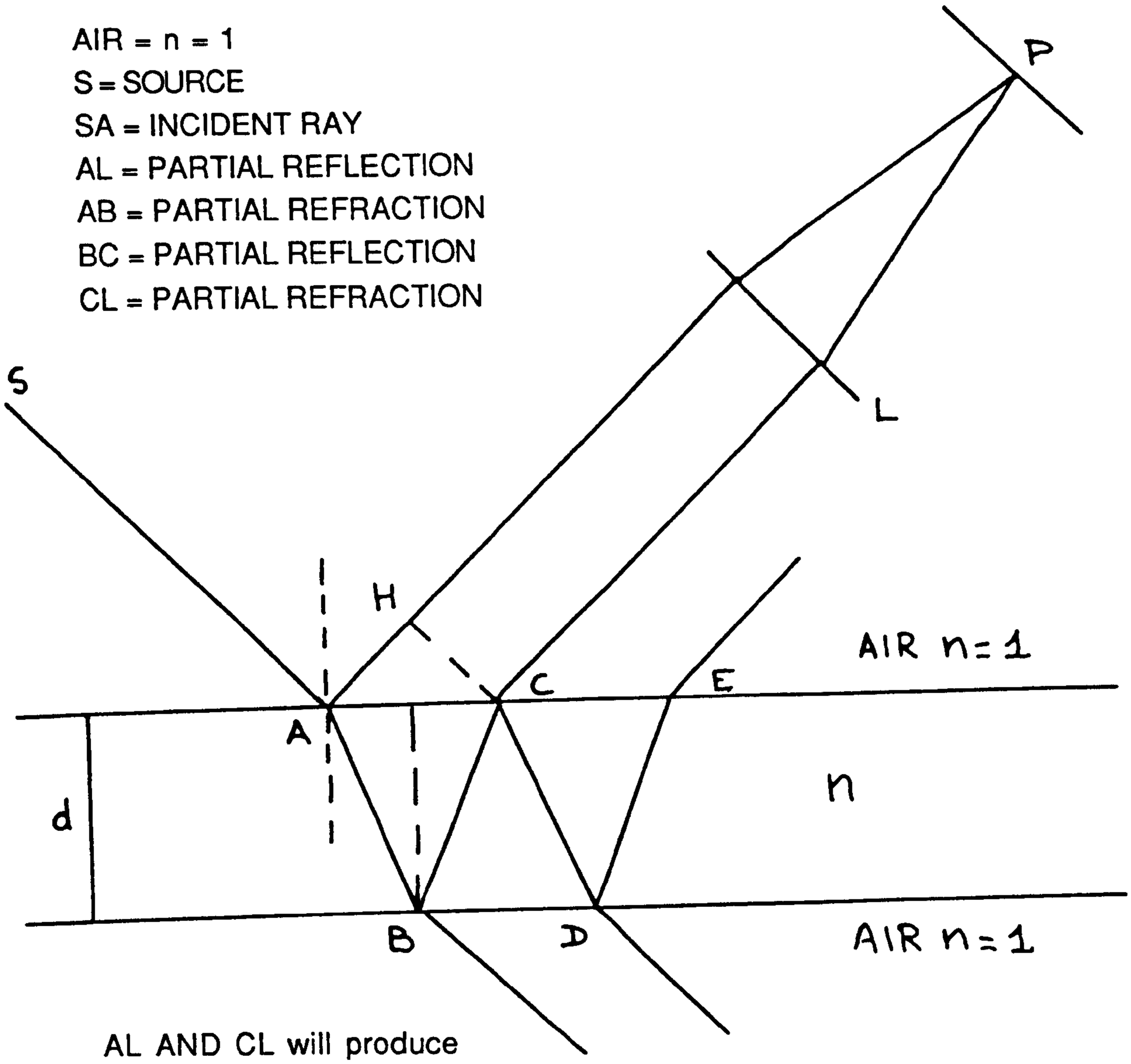

AL AND CL will produce interference fringes on plate P after recombination by lens L

At A: there is a change of phase due to reflection at a denser medium

(n) plate refractive index
(d) plate thickness

FIGURE 6.5
INTERFERENCE FRINGE FORMATION BY A PARALLEL SIDED PLATE IN AIR

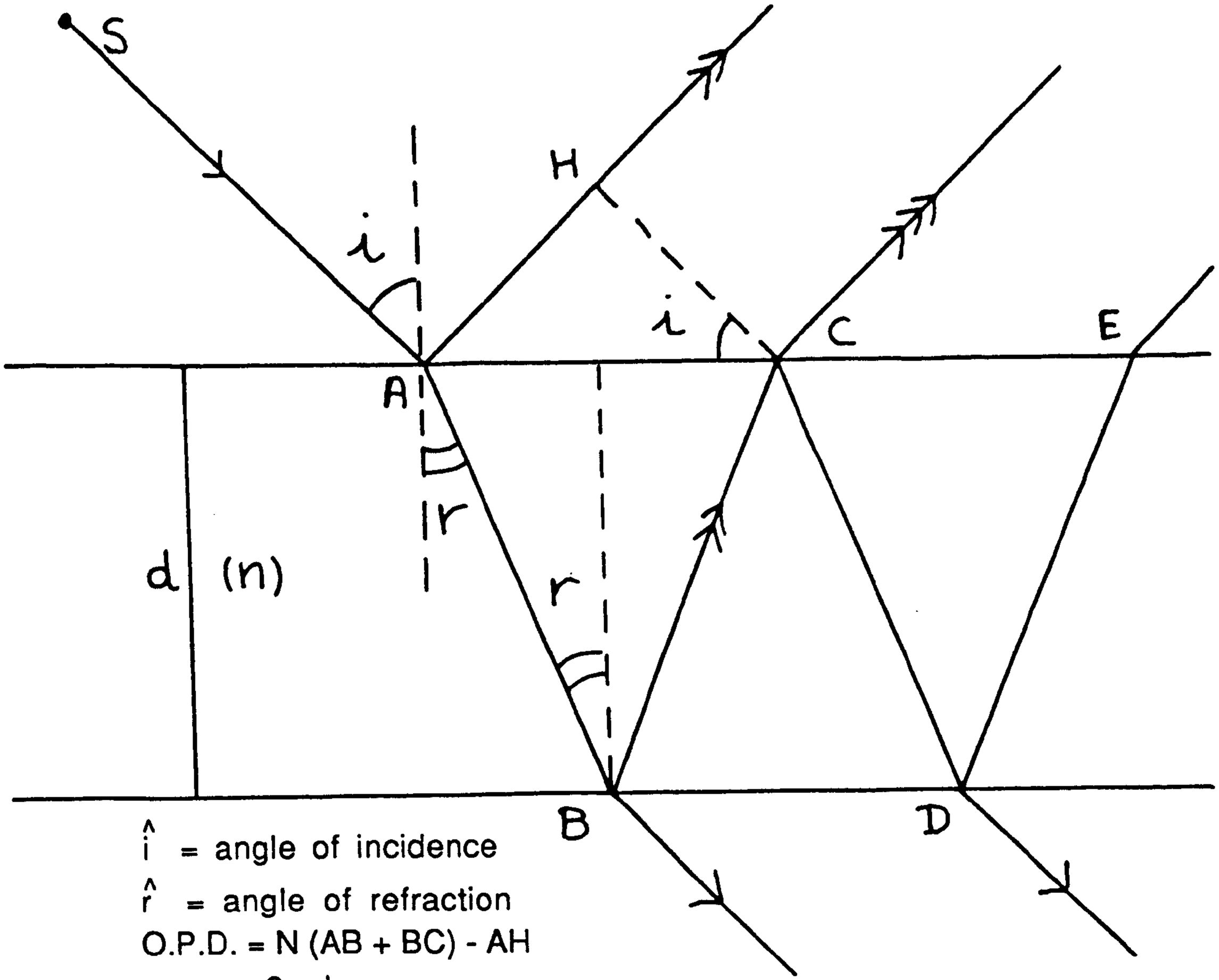

$\hat{i}$ = angle of incidence

$\hat{r}$ = angle of refraction

O.P.D. = N (AB + BC) - AH

$$= \frac{2\,nd}{\cos r} - AC \sin i$$

$$\sin i = n \sin r$$

$$AC = 2\,d \tan r$$

$$OPD = \frac{2\,dn}{\cos r} - \frac{2\,dn \sin^2 r}{\cos r}$$

At A: phase change of π due to reflection at a denser medium

MAXIMUM = constructive interference $2\,nd \cos r = (p + 1/2)\,\lambda$

MINIMUM - destructive interference $2\,nd \cos r = p\,\lambda$

FIGURE 6.6
MEASUREMENT OF PATH DIFFERENCE IN A PARALLEL SIDED PLATE

$$OPD = (ADB) - (AH) \qquad [2]$$

From the calculation we can see that constructive interference will be present in the following condition

$$2nd\cos r = (p + \tfrac{1}{2})\lambda \qquad [3]$$

and destructive interference when

$$2nd\cos r = p\lambda \qquad [4]$$

where n = plate refractive index

r = angle of refraction

λ = illuminating wavelength

p = integer = order of interference

In the experimental set up shown in Figures 6.5 and 6.6, a monochromatic light will create a succession of bright and dark circles corresponding to the constructive and destructive areas in the fields of observation. A white light source for the same arrangement will produce instead a succession of coloured circles.

ii) <u>Interference in Very Thin Films</u>

When d is very small, the variation induced by cos r can be disregarded in the calculations because (1 - cos r) is less than 2 percent for up to 10 degrees of incidence and the distance AC so small that we can consider that the interference is issued from a single point of reflection whose intensity will be the superposition of the internally and externally reflected rays. Constructive interference will be present in the following condition:

$$2nd = (p + \tfrac{1}{2})\lambda \qquad [5]$$

and destructive interference when:

$$2nd = p\lambda \qquad [6]$$

When d varies across the film, the OPD will depend on the thickness of the film at the point of reflection and will be independent of the point of emergence.

The resulting interferences will be a characteristic of the local thickness of the film. They can be observed using a wide source with a low powered microscope. These localised interference fringes occur for thin films whose thickness undergoes abrupt changes as if it consisted of a number of adjacent parallel sided films. Such film may consist of the air gap between an optical flat and the surface of a sheet of mica which exhibits abrupt changes of level. It is also the case, as we will see later, in the superficial lipid layer. When using white light illumination the interference pattern produced is seen as bright coloured fringes, whereas when using monochromatic light it appears as a succession of dark and bright fringes.

iii) <u>Interference in a Wedge Film</u>

The fringes can also be observed in a wedge shaped film. The fringes of equal thickness will be equally spaced in straight lines parallel to the edge of the wedge and will represent the increase in wedge thickness. Using these fringes one can measure the angle of very thin wedge-shaped sheets of any transparent material (Fig 6.7).

When the wedge angle is vanishingly small, a maximum occupies a relatively large area and variations in colour appearance will allow measurable observations.

When using a large source, a number of internally reflected rays are associated with it. As the

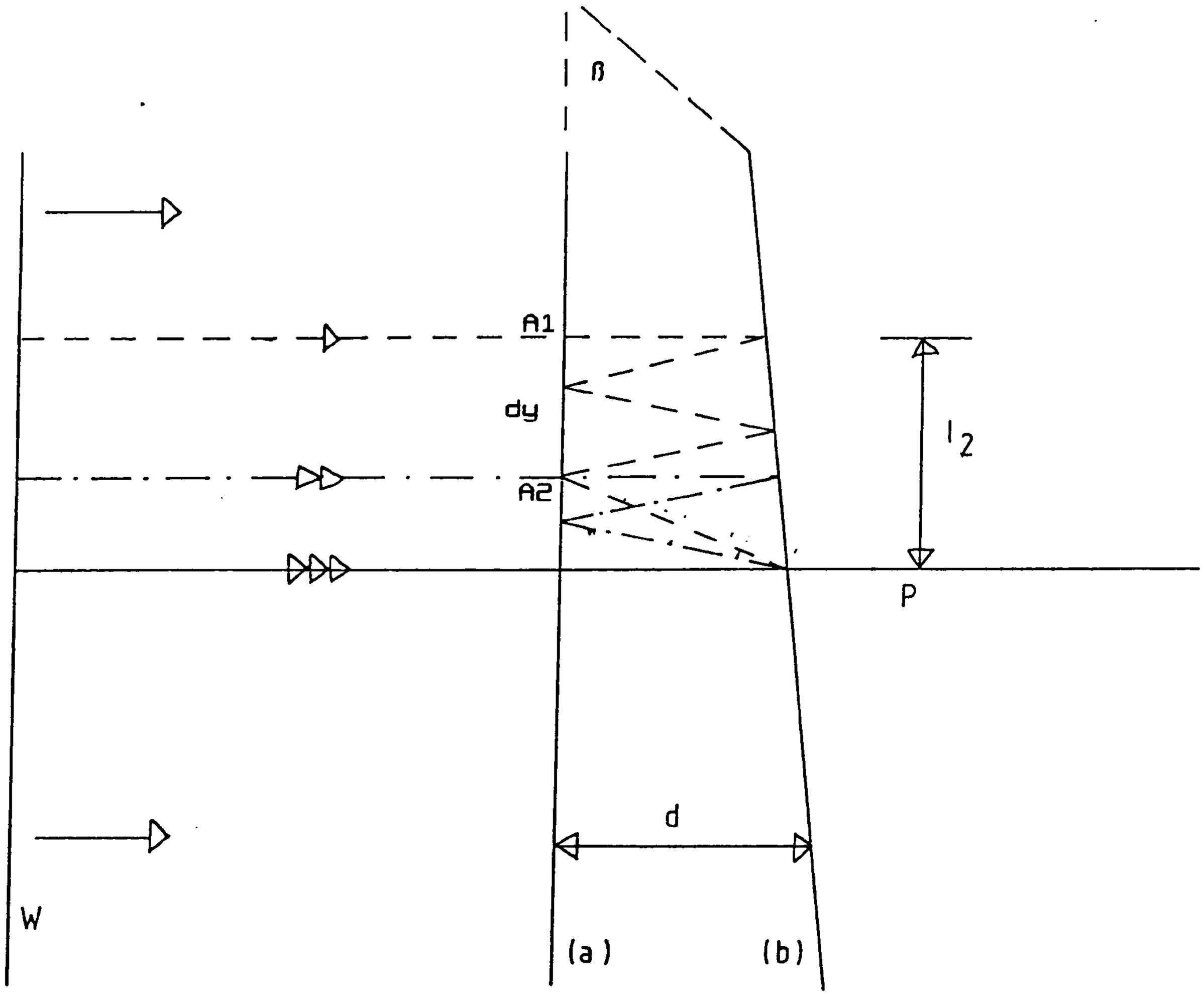

FIGURE 6.7
INTERFERENCE FRINGE FORMATION BY REFLECTION IN A THIN WEDGE

disturbance undergoes repeated internal reflections between the surfaces, they move across the wedge towards the thicker side (Fig 6.7). Thus the phase difference between the beams undergoing a successive number of reflections is not constant. This causes the high order beams to begin to interfere destructively with those of low order thereby reducing the sharpness of the fringes. Since the beams will get out of phase more rapidly with thicker wedges, this effect places an upper limit on the value which can be used when a given number of multiple reflected beams are to be superposed.

The higher the reflectivity of the surfaces, the less rapidly does the intensity of the beam decrease and the larger is the number of reflections before the intensity is reduced to a negligible value.

As we will see later the drying of the tear film on a corneal lens surface reproduces approximately the conditions just described.

6.3 THICKNESS MEASUREMENT BY INTERFEROMETRY

The information given by an interferometric thickness measuring system is contained within the interference effects produced by the element measured. Both position and shape of the fringes are determined by the path-difference introduced between two or more interference beams by the element measured and the information relating to its thickness can be extracted by measuring this path-difference.

6.3.1 NEWTON'S EXPERIMENT

In his original experiment, Newton produced interference fringes of equal thickness in the air film situated between a flat surface and a plano-convex lens of large radius (Fig 6.8).

The fringes of equal thickness have the form of concentric circles with the centre lying at the point of contact of the lens and the plate. The central spot, when viewed by reflection is dark, because a phase change of $\frac{\lambda}{2}$, associated with the reflection at a denser medium is present for all wavelengths.

Table 6.1 shows the Newton's 'Scale of Colour' and their order of interference and their corresponding path difference in air. The associated interference colours and their thicknesses have also been calculated from a medium of refractive index n = 1.5 (lipid layer) and n = 1.337 (aqueous phase).

The order of interference increases from the centre of the pattern outward. The direct visual observation of those 'Newton's rings' using white light is only possible for the first 5 or 6 orders of interference. This sets to about 3 microns the maximum thickness of air measurable in these conditions.

6.3.2 INTERFERENCE IN WHITE LIGHT

When a large number of wavelengths are present in the illuminating source; each wavelength produces its own fringe system. The fringes produced by the shorter wavelengths will occur at a shorter distance from the centre than those produced by the longer wavelengths.

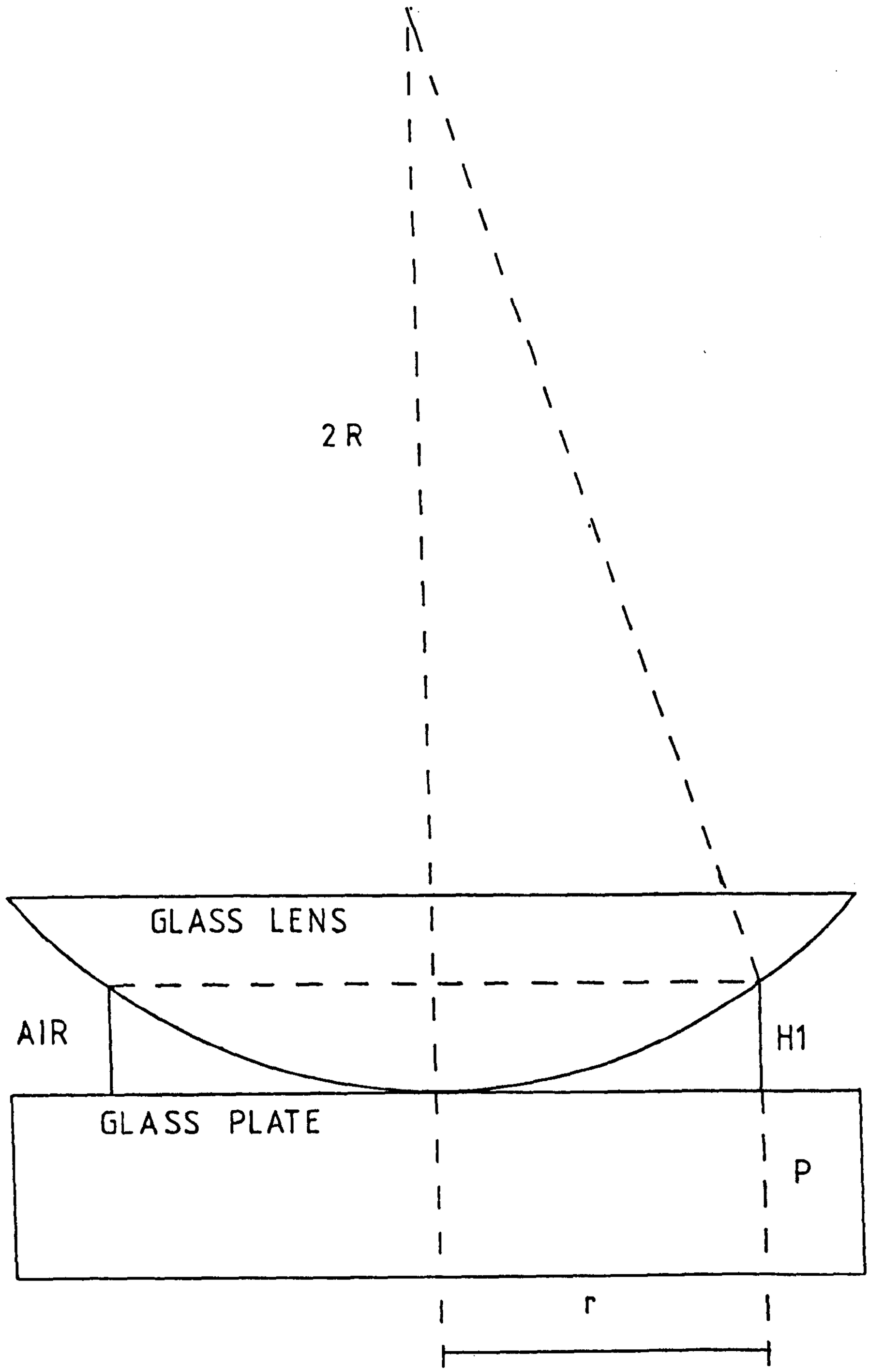

FIGURE 6.8
OPTICAL LAYOUT OF NEWTON'S RING IN AIR

REFLECTED INTERFERENCE IN WHITE LIGHT IN A LIPID LAYER

Order of Interference	Phase Difference In Air (in microns)	Lipid Layer	Thickness (in microns)	Interference Colour
0	n = 1		n = 1.5	
	0.040		0.013	Iron Grey
	0.097	Grey	0.032	Lavender Grey
¼	0.158		0.053	Grey Blue
	0.218		0.073	Lighter Grey
	0.234	White	0.078	White, Greenish-White
	0.259		0.086	White
	0.267		0.089	Yellowish White
	0.275		0.092	Pale Straw Yellow
		Yellow		
	0.281		0.094	Yellow, Straw-Yellow
½	0.306		0.102	Light Yellow
	0.332		0.111	Strong Yellow
	0.430	Brown	0.143	Brown, Brownish-Yellow
¾	0.505		0.168	Reddish Orange
	0.536		0.179	Hot Red
	0.551		0.183	Dark Red
	0.565	Purple	0.188	Purple
	0.575		0.192	Violet
1	0.589		0.196	Indigo
	0.664		0.221	Blue Sky Blue
	0.728	Blue	0.243	Greenish Blue
	0.747		0.249	Green
	0.826	Green	0.279	Green, Lighter-Green
	0.843	Green	0.281	Yellowish Green
	0.866		0.288	Greenish Yellow
1½	0.910	Yellow	0.303	Pure Yellow
	0.948		0.316	Orange
	0.998	Orange	0.333	Orange Red
	1.101	Violet	0.367	Violet Dark Red
	1.128	Blue	0.376	Light Blueish-Violet
	1.151		0.384	Indigo
	1.258	Green	0.419	Blue Green Tint
	1.334		0.445	Sea Green
	1.376	Green	0.459	Bright Green
2½	1.428		0.476	Greenish Yellow
	1.497	Pink	0.499	Flesh Colour
	1.534		0.511	Carmine
	1.652	Grey	0.550	Violet Grey
	1.682		0.560	Greyish Blue
	1.711	Green	0.570	Dull Sea Green
3	1.744		0.581	Blueish Green

TABLE 6.1A
NEWTON'S SCALE OF COLOURS AND ASSOCIATED PHASE DIFFERENCES AND CORRESPONDING LAYER THICKNESSES

REFLECTED INTERFERENCE IN WHITE LIGHT IN AN AQUEOUS LAYER

Order of Interference	Phase Difference In Air (in microns)	Aqueous Layer	Thickness (in microns)	Interference Colour
0	n = 1		n = 1.337	
	0.040		0.015	Iron Grey
	0.097	Grey	0.036	Lavender Grey
¼	0.158		0.044	Grey Blue
	0.218		0.081	Lighter Grey
	0.234	White	0.087	White, Greenish-White
	0.259		0.097	White
	0.267		0.100	Yellowish White
	0.275		0.206	Pale Straw Yellow
		Yellow		
	0.281		0.105	Yellow, Straw-Yellow
½	0.306		0.114	Light Yellow
	0.332		0.124	Strong Yellow
	0.430	Brown	0.161	Brown, Brownish-Yellow
¾	0.505		0.189	Reddish Orange
	0.536		0.200	Hot Red
	0.551		0.206	Dark Red
	0.565	Purple	0.211	Purple
	0.575		0.215	Violet
1	0.589		0.220	Indigo
	0.664		0.248	Blue Sky Blue
	0.728	Blue	0.272	Greenish Blue
	0.747		0.280	Green
	0.826	Green	0.309	Green, Lighter-Green
	0.843	Green	0.315	Yellowish Green
	0.866		0.324	Greenish Yellow
1½	0.910	Yellow	0.340	Pure Yellow
	0.948		0.354	Orange
	0.998	Orange	0.373	Orange Red
	1.101	Violet	0.412	Violet Dark Red
	1.128	Blue	0.422	Light Blueish-Violet
	1.151		0.430	Indigo
	1.258	Green	0.470	Blue Green Tint
	1.334		0.500	Sea Green
	1.376	Green	0.515	Bright Green
2½	1.428		0.533	Greenish Yellow
	1.497	Pink	0.560	Flesh Colour
	1.534		0.574	Carmine
	1.652	Grey	0.618	Violet Grey
	1.682		0.629	Greyish Blue
	1.711	Green	0.640	Dull Sea Green
3	1.744		0.652	Blueish Green

TABLE 6.1B
NEWTON'S SCALE OF COLOURS AND ASSOCIATED PHASE DIFFERENCES AND CORRESPONDING LAYER THICKNESSES

Thus the first order of interference will be seen as a thin sharp ring with coloured edges.

The following orders of interference will spread over a greater width and will appear drawn out into spectra. Eventually, the maxima for various orders and different wavelengths will overlap and produce a sensation of white continuum where no fringes are observable with the naked eye (Fig 6.9). This white continuum has a spectral composition different from that of white light but this can only be detected by a spectrometric measurement.

6.3.3 SPECTRAL COMPOSITION OF INTERFERENCE PATTERN

It is possible to show graphically the spectral composition of the reflected light obtained along the series of visible coloured fringes and the ensuing white continuum produced in a given experimental situation (Fig 6.10). The x-axis represents the thickness in microns of the film under observation. The y-axis represents the wavelength of the visible spectrum, from 400 nm to 700 nm.

As seen, the condition of destructive interference or extinction is satisfied when:

$$2\,nd = P\lambda \qquad [6]$$

where: n = refractive index of the layer

d = thickness of the layer

λ = wavelength

P = order of interference

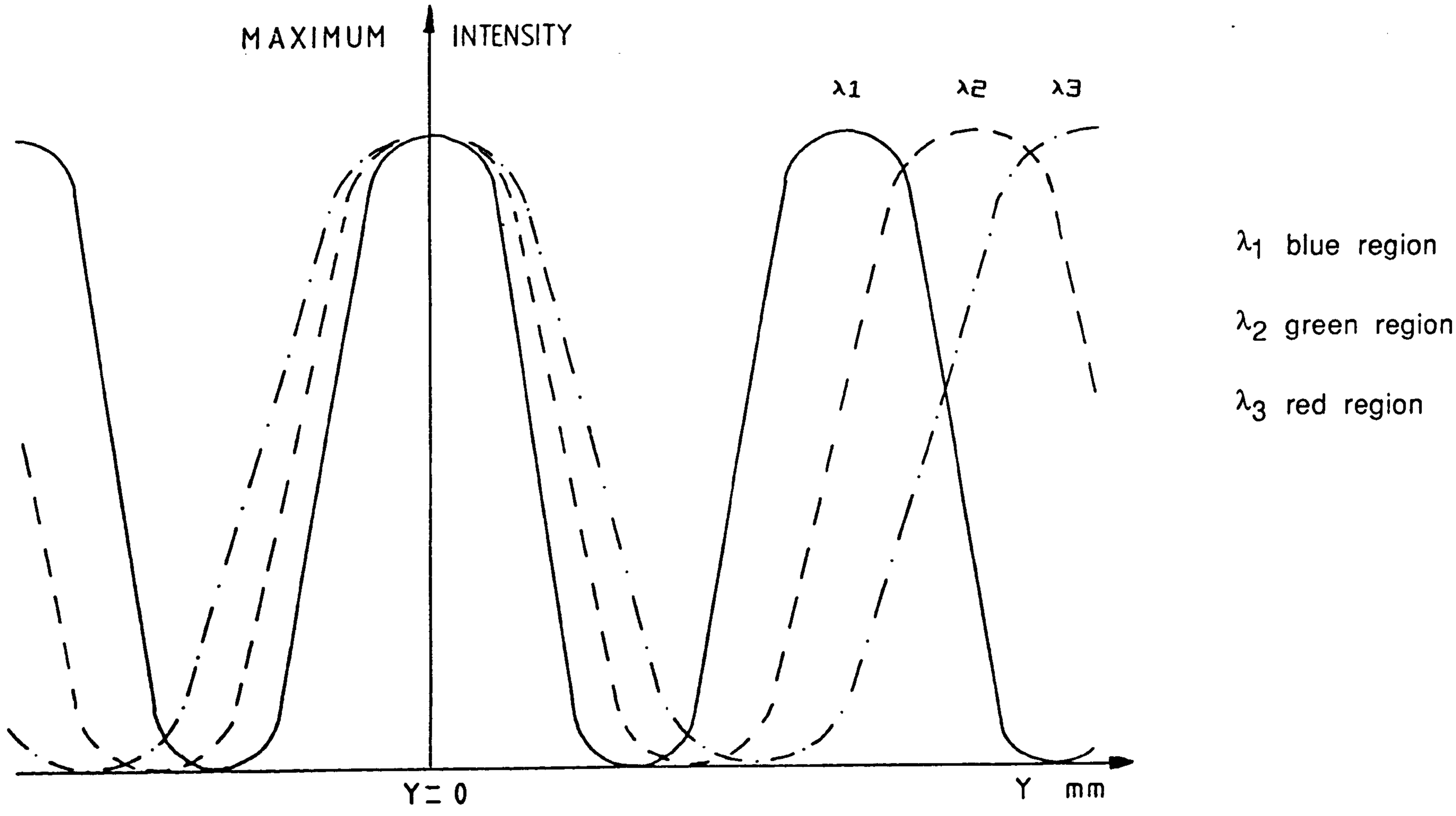

FIGURE 6.9
INTERFERENCE FRINGES IN WHITE LIGHT: PRODUCTION OF WHITE CONTINUUM

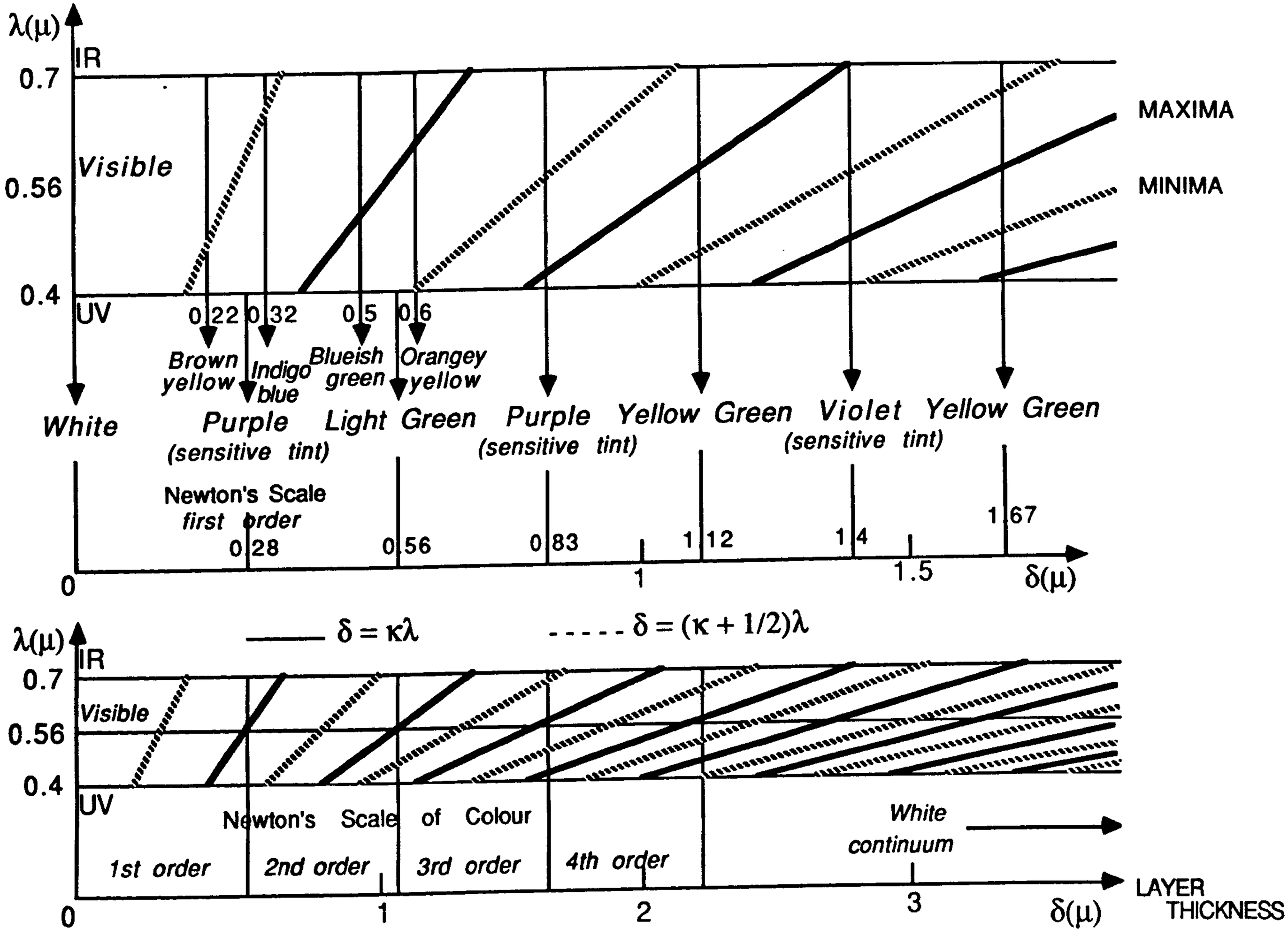

FIGURE 6.10 SPECTRAL COMPOSITION OF WHITE CONTINUUM FOR AQUEOUS LAYER

It becomes possible to calculate the thickness of layer d at which this situation occurs for a given wavelength λ and a given order of interference P.

$$d_{min} = \frac{P\lambda}{2n} \qquad [7]$$

d_{min} has been calculated in aqueous tears

for n = 1,337

for λ = 400 nm (Table 6.2) colour purple

for λ = 550 nm (Table 6.3) colour yellow

for λ = 700 nm (Table 6.4) colour red

From these values we can determine the range of layer thickness over which each order of destructive interference will be spread (Table 6.5).

Hence for P = 0, d = 0 for all wavelengths, this explains the dark spot at the centre of the picture of Newton's experiment.

The condition of constructive interference or maximum is satisfied when:

$$2nd = (P + \tfrac{1}{2})\lambda \qquad [5]$$

The layer thickness d at which this situation occurs for a given wavelength λ and a given order of interference P is:

$$d_{max} = \frac{(P + \tfrac{1}{2})\lambda}{2n} \qquad [8]$$

d_{max} has been calculated in aqueous tears

for n = 1.337

for λ = 400 nm (Table 6.6)

for λ = 550 nm (Table 6.7)

for λ = 700 nm (Table 6.8)

AQUEOUS TEARS

Index $n = 1.337$

Wavelength $\lambda \simeq 400nm \simeq 0.4\ \mu m$

Destructive Interference

Minimal Visible

When $2nd = P\lambda$

$$d = \frac{P\lambda}{2n} = \frac{400\ P}{2 \times 1.337} = \frac{200\ P}{1.337}$$

P = Order of Interference

d = Thickness of Film

P = 0	d0 = 0				
P = 1	d1 = 0.149 μm		P = 23	d23 = 3.441 μm	
P = 2	d2 = 0.299 μm		P = 24	d24 = 3.590 μm	
P = 3	d3 = 0.449 μm		P = 25	d25 = 3.740 μm	
P = 4	d4 = 0.598 μm		P = 26	d26 = 3.889 μm	
P = 5	d5 = 0.748 μm		P = 27	d27 = 4.039 μm	
P = 6	d6 = 0.898 μm		P = 28	d28 = 4.188 μm	
P = 7	d7 = 1.047 μm		P = 29	d29 = 4.338 μm	
P = 8	d8 = 1.197 μm		P = 30	d30 = 4.487 μm	
P = 9	d9 = 1.346 μm		P = 31	d31 = 4.637 μm	
P = 10	d10 = 1.496 μm		P = 32	d32 = 4.787 μm	
P = 11	d11 = 1.645 μm		P = 33	d33 = 4.936 μm	
P = 12	d12 = 1.795 μm		P = 34	d34 = 5.086 μm	
P = 13	d13 = 1.945 μm		P = 35	d35 = 5.237 μm	
P = 14	d14 = 2.094 μm		P = 36	d36 = 5.385 μm	
P = 15	d15 = 2.244 μm		P = 37	d37 = 5.535 μm	
P = 16	d16 = 2.393 μm		P = 38	d38 = 5.684 μm	
P = 17	d17 = 2.543 μm		P = 39	d39 = 5.834 μm	
P = 18	d18 = 2.963 μm		P = 40	d40 = 5.984 μm	
P = 19	d19 = 2.842 μm		P = 41	d41 = 6.133 μm	
P = 20	d20 = 2.991 μm		P = 42	d42 = 6.283 μm	
P = 21	d21 = 3.141 μm		P = 43	d43 = 6.432 μm	
P = 22	d22 = 3.291 μm		P = 44	d44 = 6.582 μm	

TABLE 6.2
DESTRUCTIVE INTERFERENCE IN AQUEOUS TEARS: CALCULATED LAYER THICKNESS FOR SUCCESSIVE ORDERS OF DESTRUCTIVE INTERFERENCE IN THE 400nm REGION OF THE SPECTRUM

AQUEOUS TEARS

Index $n = 1.337$

Colour Yellow $\simeq$ 555 nm $\simeq$ 0.555 µm

Destructive Interference

Minimal Visible

When $d = \frac{P\lambda}{2n} = \frac{0.555\ P}{2 \times 1.337}$

P = Order of Interference

d = Thickness of Film

P = 0	d0 = 0		
P = 1	d1 = 0.207 µm	P = 17	d17 = 3.528 µm
P = 2	d2 = 0.415 µm	P = 18	d18 = 3.736 µm
P = 3	d3 = 0.623 µm	P = 19	d19 = 3.944 µm
P = 4	d4 = 0.830 µm	P = 20	d20 = 4.151 µm
P = 5	d5 = 1.038 µm	P = 21	d21 = 4.359 µm
P = 6	d6 = 1.245 µm	P = 22	d22 = 4.566 µm
P = 7	d7 = 1.452 µm	P = 23	d23 = 4.774 µm
P = 8	d8 = 1.660 µm	P = 24	d24 = 4.981 µm
P = 9	d9 = 1.868 µm	P = 25	d25 = 5.188 µm
P = 10	d10 = 2.075 µm	P = 26	d26 = 5.396 µm
P = 11	d11 = 2.283 µm	P = 27	d27 = 5.604 µm
P = 12	d12 = 2.490 µm	P = 28	d28 = 5.812 µm
P = 13	d13 = 2.698 µm	P = 29	d29 = 6.019 µm
P = 14	d14 = 2.905 µm	P = 30	d30 = 6.227 µm
P = 15	d15 = 3.113 µm	P = 31	d31 = 6.434 µm
P = 16	d16 = 3.320 µm	P = 32	d32 = 6.642 µm

TABLE 6.3
DESTRUCTIVE INTERFERENCE IN AQUEOUS TEARS
FOR λ = 550 nm (YELLOW)

AQUEOUS TEARS

Index $n = 1.337$

Colour Red $\approx$ 700 nm $\approx$ 0.7 µm

Destructive Interference

Minimal Visible

When $2 n d = P \lambda$

$$d = \frac{P \lambda}{2n} = \frac{700 P}{2 \times 1.337}$$

P = Order of Interference

d = Thickness of Film

P = 0	d0 = 0		
P = 1	d1 = 0.262 µm	P = 14	d14 = 3.665 µm
P = 2	d2 = 0.526 µm	P = 15	d15 = 3.927 µm
P = 3	d3 = 0.785 µm	P = 16	d16 = 4.188 µm
P = 4	d4 = 1.047 µm	P = 17	d17 = 4.450 µm
P = 5	d5 = 1.309 µm	P = 18	d18 = 4.712 µm
P = 6	d6 = 1.571 µm	P = 19	d19 = 4.974 µm
P = 7	d7 = 1.832 µm	P = 20	d20 = 5.236 µm
P = 8	d8 = 2.094 µm	P = 21	d21 = 5.497 µm
P = 9	d9 = 2.356 µm	P = 22	d22 = 5.759 µm
P = 10	d10 = 2.618 µm	P = 23	d23 = 6.021 µm
P = 11	d11 = 2.880 µm	P = 24	d24 = 6.283 µm
P = 12	d12 = 3.141 µm	P = 25	d25 = 6.545 µm
P = 13	d13 = 3.403 µm		

TABLE 6.4
DESTRUCTIVE INTERFERENCE IN AQUEOUS TEARS
FOR λ = 700 nm (RED)

AQUEOUS TEARS

R0 = Range for P = 0

R0 :	From	d0	= 0	To	0	µm
R1 :		d1	= 0.149 µm		0.262	µm
R2 :		d2	= 0.299 µm		0.526	µm
R3 :		d3	= 0.449 µm		0.785	µm
R4 :		d4	= 0.598 µm		1.047	µm
R5 :		d5	= 0.748 µm		1.309	µm
R6 :		d6	= 0.898 µm		1.571	µm
R7 :		d7	= 1.047 µm		1.832	µm
R8 :		d8	= 1.197 µm		2.094	µm
R9 :		d9	= 1.346 µm		2.356	µm
R10:		d10	= 1.496 µm		2.618	µm
R11:		d11	= 1.645 µm		2.880	µm
R12:		d12	= 1.795 µm		3.141	µm
R13:		d13	= 1.945 µm		3.403	µm
R14:		d14	= 2.094 µm		3.665	µm

TABLE 6.5
RANGE OF SUCCESSIVE ORDERS OF DESTRUCTIVE INTERFERENCE
FOR A SOURCE DISTRIBUTION $\Delta\lambda$ (400 to 700 nm)

AQUEOUS TEARS

Index $n = 1.337$

Wavelength $\lambda \simeq 400$ nm $\simeq 0.4$ μm

Constructive Interference

Maximum Visible

When $$d = \frac{(P + \frac{1}{2})\lambda}{2n} = \frac{(P + \frac{1}{2})\,400}{2 \times 1.337}$$

$$d = \frac{(P + \frac{1}{2})\,200}{1.337}$$

P = Order of Interference

d = Thickness of Film

$$d0 = \frac{200}{2.674} = 74.8 = 0.074\ \mu m$$

P = 0	d0 = 0.074 μm				
P = 1	d1 = 0.224 μm		P = 23	d23 = 3.515 μm	
P = 2	d2 = 0.378 μm		P = 24	d24 = 3.665 μm	
P = 3	d3 = 0.524 μm		P = 25	d25 = 3.815 μm	
P = 4	d4 = 0.673 μm		P = 26	d26 = 3.964 μm	
P = 5	d5 = 0.823 μm		P = 27	d27 = 4.114 μm	
P = 6	d6 = 0.987 μm		P = 28	d28 = 4.263 μm	
P = 7	d7 = 1.122 μm		P = 29	d29 = 4.413 μm	
P = 8	d8 = 1.272 μm		P = 30	d30 = 4.562 μm	
P = 9	d9 = 1.421 μm		P = 31	d31 = 4.712 μm	
P = 10	d10 = 1.571 μm		P = 32	d32 = 4.862 μm	
P = 11	d11 = 1.720 μm		P = 33	d33 = 5.011 μm	
P = 12	d12 = 1.870 μm		P = 34	d34 = 5.161 μm	
P = 13	d13 = 2.019 μm		P = 35	d35 = 5.310 μm	
P = 14	d14 = 2.169 μm		P = 36	d36 = 5.460 μm	
P = 15	d15 = 2.319 μm		P = 37	d37 = 5.610 μm	
P = 16	d16 = 2.468 μm		P = 38	d38 = 5.759 μm	
P = 17	d17 = 2.618 μm		P = 39	d39 = 5.909 μm	
P = 18	d18 = 2.767 μm		P = 40	d40 = 6.058 μm	
P = 19	d19 = 2.917 μm		P = 41	d41 = 6.208 μm	
P = 20	d20 = 3.067 μm		P = 42	d42 = 6.358 μm	
P = 21	d21 = 3.216 μm		P = 43	d43 = 6.507 μm	
P = 22	d22 = 3.366 μm		P = 44	d44 = 6.656 μm	

TABLE 6.6
CONSTRUCTIVE INTERFERENCE IN AQUEOUS TEARS
FOR $\lambda = 400$ nm

AQUEOUS TEARS

Index $n = 1.337$

Colour Yellow $\approx$ 555 nm $\approx$ 0.555 μm

Constructive Interference

Maximum Visible

When $d = \frac{(P + \frac{1}{2})\lambda}{2n} = \frac{(P + \frac{1}{2})\ 0.555}{2 \times 1.337}$

P = Order of Interference

d = Thickness of Film

P = 0	d0 = 0.104 μm		
P = 1	d1 = 0.311 μm	P = 17	d17 = 3.632 μm
P = 2	d2 = 0.519 μm	P = 18	d18 = 3.840 μm
P = 3	d3 = 0.726 μm	P = 19	d19 = 4.047 μm
P = 4	d4 = 0.934 μm	P = 20	d20 = 4.255 μm
P = 5	d5 = 1.141 μm	P = 21	d21 = 4.462 μm
P = 6	d6 = 1.349 μm	P = 22	d22 = 4.670 μm
P = 7	d7 = 1.556 μm	P = 23	d23 = 4.878 μm
P = 8	d8 = 1.764 μm	P = 24	d24 = 5.085 μm
P = 9	d9 = 1.971 μm	P = 25	d25 = 5.293 μm
P = 10	d10 = 2.179 μm	P = 26	d26 = 5.500 μm
P = 11	d11 = 2.387 μm	P = 27	d27 = 5.707 μm
P = 12	d12 = 2.594 μm	P = 28	d28 = 5.915 μm
P = 13	d13 = 2.802 μm	P = 29	d29 = 6.123 μm
P = 14	d14 = 3.009 μm	P = 30	d30 = 6.330 μm
P = 15	d15 = 3.217 μm	P = 31	d31 = 6.538 μm
P = 16	d16 = 3.424 μm		

TABLE 6.7
CONSTRUCTIVE INTERFERENCE IN AQUEOUS TEARS
FOR λ = 555 nm (YELLOW)

AQUEOUS TEARS

Index $n = 1.337$

Colour Red $\approx$ 700 nm $\approx$ 0.7 µm

Constructive Interference

Maximum Visible

When $d = \frac{(P + \frac{1}{2})\lambda}{2n}$

$= \frac{(P + \frac{1}{2})\ 0.7}{2 \times 1.337}$

P = Order of Interference

d = Thickness of Film

P = 0	d0	= 0.131 µm			
P = 1	d1	= 0.393 µm	P = 14	d14	= 3.796 µm
P = 2	d2	= 0.654 µm	P = 15	d15	= 4.058 µm
P = 3	d3	= 0.916 µm	P = 16	d16	= 4.319 µm
P = 4	d4	= 1.178 µm	P = 17	d17	= 4.581 µm
P = 5	d5	= 1.440 µm	P = 18	d18	= 4.843 µm
P = 6	d6	= 1.702 µm	P = 19	d19	= 5.105 µm
P = 7	d7	= 1.963 µm	P = 20	d20	= 5.366 µm
P = 8	d8	= 2.225 µm	P = 21	d21	= 5.628 µm
P = 9	d9	= 2.487 µm	P = 22	d22	= 5.890 µm
P = 10	d10	= 2.749 µm	P = 23	d23	= 6.152 µm
P = 11	d11	= 3.010 µm	P = 24	d24	= 6.414 µm
P = 12	d12	= 3.273 µm	P = 25	d25	= 6.675 µm
P = 13	d13	= 3.534 µm			

TABLE 6.8
CONSTRUCTIVE INTERFERENCE IN AQUEOUS TEARS
FOR λ = 700 nm (RED)

i) Orders of Interference Overlap for Wide Spectral Distribution Sources

From these values we can determine the range of layer thickness over which each order of constructive interference will be spread (Table 6.9). Figure 6.10 shows the position of the successive constructive interference ranges with increasing layer thickness for an illuminating light source covering the whole visible spectrum (400 nm to 700 nm).

From Figure 6.11 it can be seen that the minima and maxima occur at shorter intervals for the blue end of the spectrum than they do for the red end of the spectrum.

For the first orders of interference, the resulting interference colours will have a high contrast and high intensity; sharp delimitation between colours can be noted. As the layer thickness and order of interference increase, two or more maxima corresponding to different wavelengths, occur at the same point. The resulting interference colours produce fringes of increasingly blurred edges, lower contrast and purity. The total disappearance of the fringes and a change to a continuous white field occur after 5 or 6 fringes. Still the spectral composition of this white continuum does not correspond to that of white light. It only appears so to the naked eye, which compensates as it becomes unable to discern individual colours and intensity changes.

To be able to measure accurately greater layer thickness with an interferometric technique, the spectral domain of the light source must be limited.

R0 = Range for P = 0

R0 :	From	d0	= 0.074 µm	To	0.131 µm
R1 :		d1	= 0.224 µm		0.393 µm
R2 :		d2	= 0.378 µm		0.654 µm
R3 :		d3	= 0.524 µm		0.916 µm
R4 :		d4	= 0.673 µm		1.178 µm
R5 :		d5	= 0.823 µm		1.440 µm
R6 :		d6	= 0.987 µm		1.702 µm
R7 :		d7	= 1.122 µm		1.963 µm
R8 :		d8	= 1.272 µm		2.225 µm
R9 :		d9	= 1.421 µm		2.487 µm
R10:		d10	= 1.571 µm		2.749 µm
R11:		d11	= 1.720 µm		3.010 µm
R12:		d12	= 1.870 µm		3.273 µm
R13:		d13	= 2.019 µm		3.534 µm
R14:		d14	= 2.169 µm		3.796 µm

TABLE 6.9
RANGE OF SUCCESSIVE ORDERS OF CONSTRUCTIVE INTERFERENCE
FOR A SOURCE DISTRIBUTION $\Delta\lambda$ (400 to 700 nm)

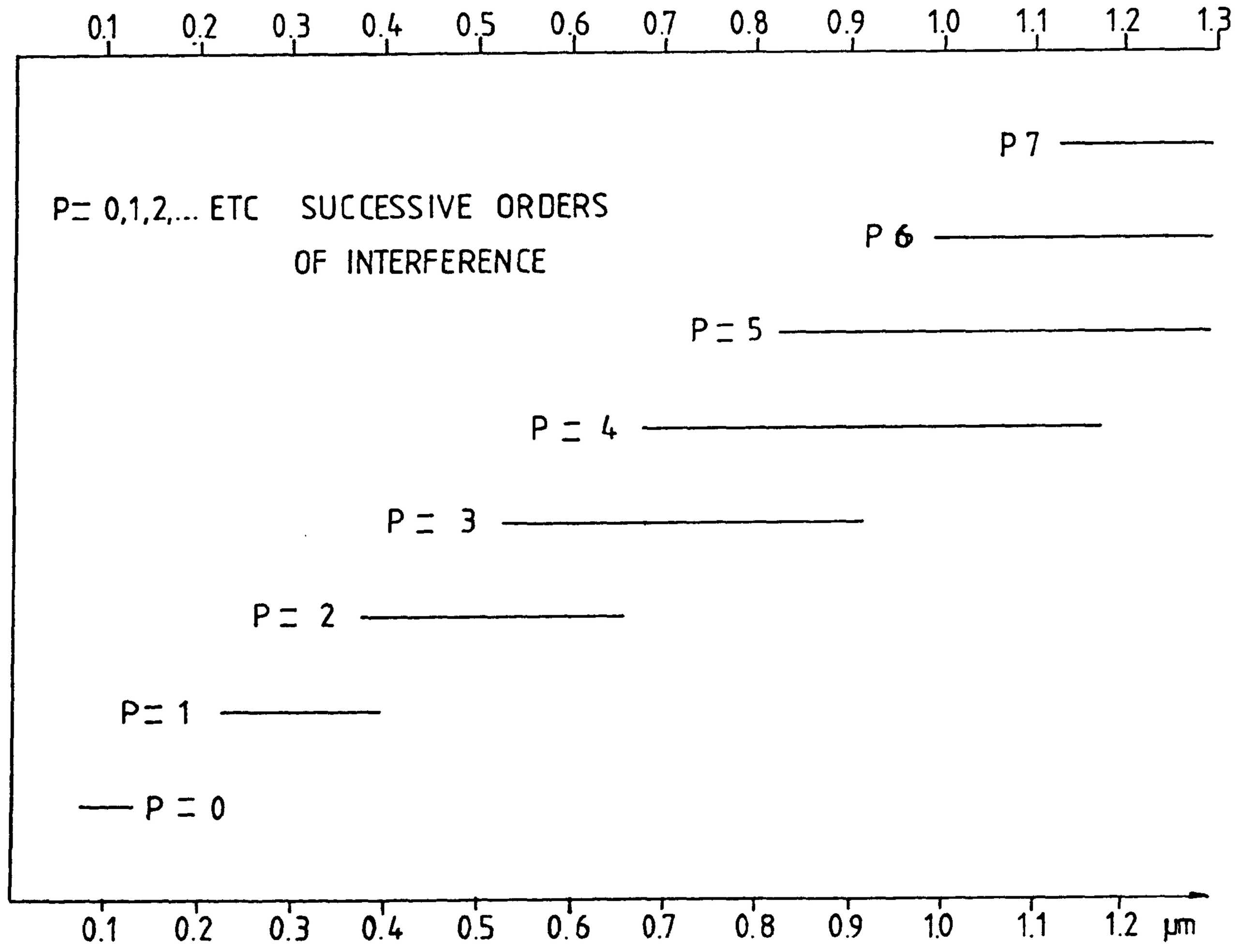

FIGURE 6.11
DIAGRAMMATIC REPRESENTATION OF INTERFERENCE ORDER OVERLAP IN WHITE LIGHT

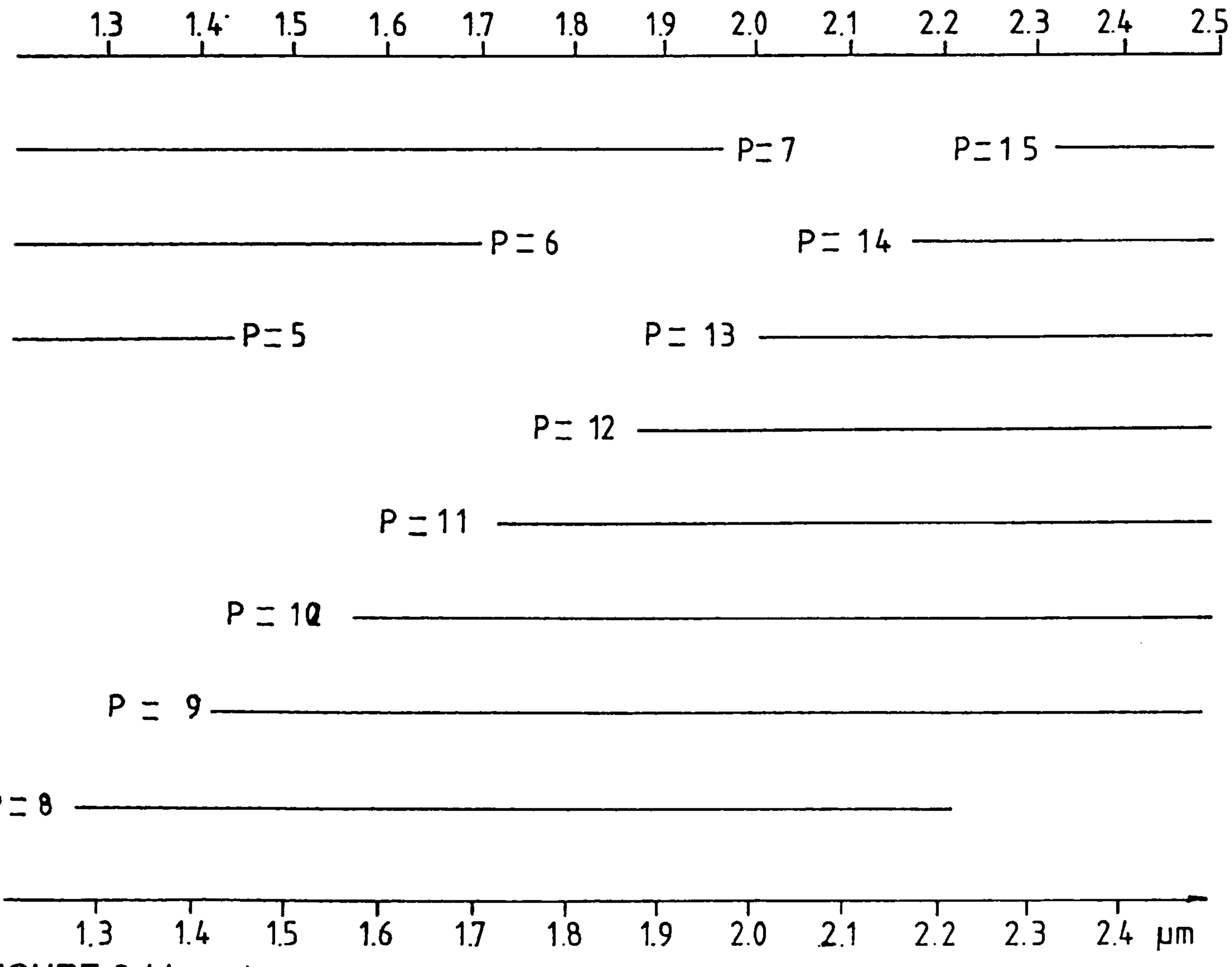

FIGURE 6.11 cont.
DIAGRAMMATIC REPRESENTATION OF INTERFERENCE ORDER OVERLAP IN WHITE LIGHT

ii) Influence of the Light Source Spectral Characteristics on the Interference Pattern

We have seen (6.3.2) that when the source is not perfectly monochromatic, the resulting interference pattern will be composed of the individual patterns produced by each wavelength. The composition of that pattern will depend on the length of coherence of the main spectral line of emission and that of the remaining part of the emitted spectrum.

a) Width of the spectral line

The width of the main spectral line λo of the light source is characterised by its half width: the length of the interval $\Delta\lambda o$ measured at the half height of the spectral line (Fig 6.12). In practice, the illuminating source is composed of a great number of different wavelengths lying in the interval:

$$(\lambda o \pm \frac{1}{2} \Delta \lambda o) \qquad [9]$$

Let's consider two slightly different wavelengths $\lambda 1$ and $\lambda 2$. Each wavelength has its own fringe system that coincide at the centre of the interference pattern ($Y = 0$). But since the width of the band is proportional to the wavelength, as the distance Y from the centre increases, the fringes corresponding to the shorter wavelength will lag behind the fringes corresponding to the longer wavelength (Fig 6.13). It can be seen that at a given order of interference, the delay will be equal to the half width of the band, the maximum of the first wavefront will then correspond to the minimum of the second wave and the fringes brightness will be minimal at that point (point A). Further away from the centre, the

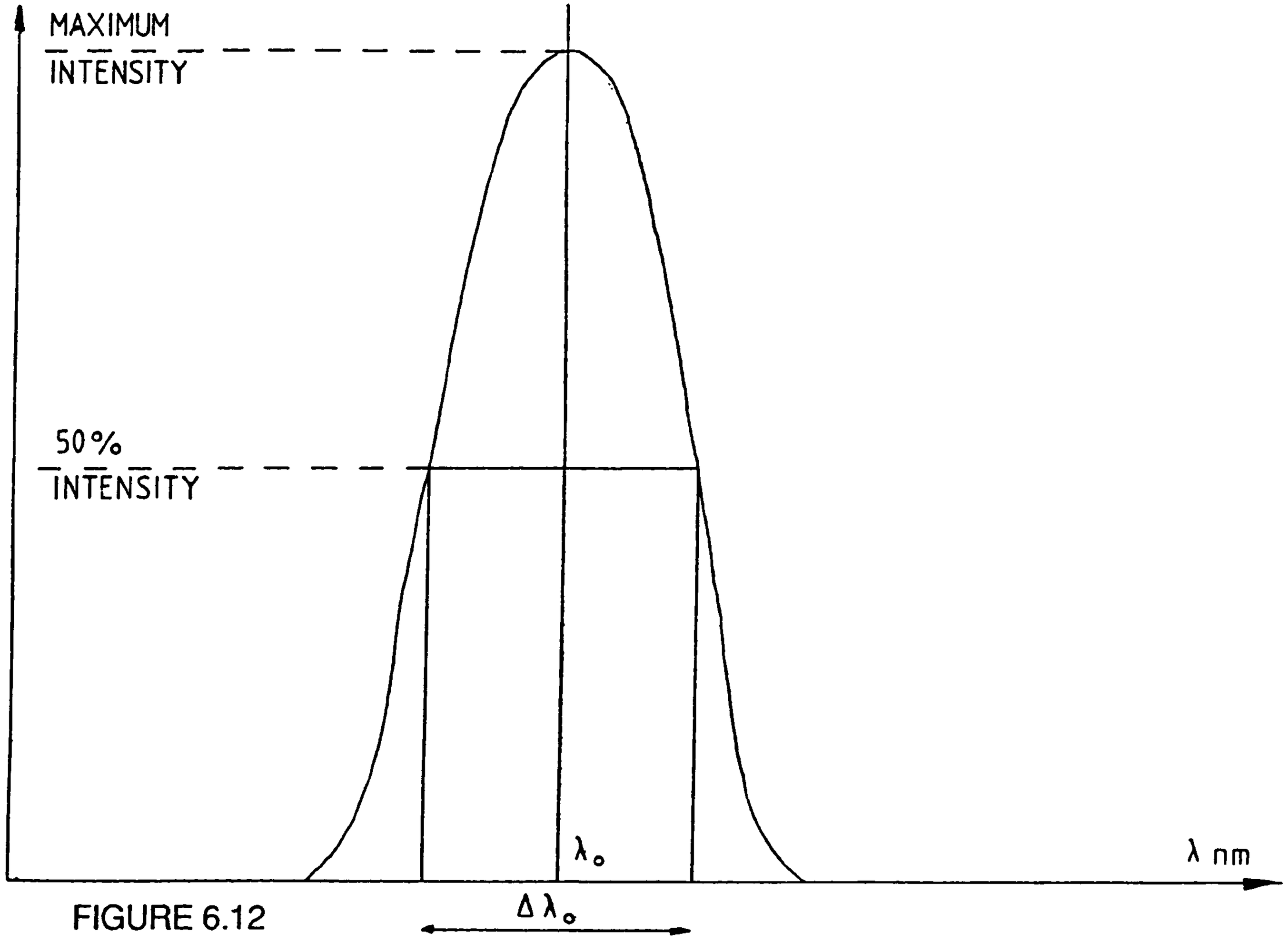

FIGURE 6.12
WIDTH OF A SPECTRAL LINE

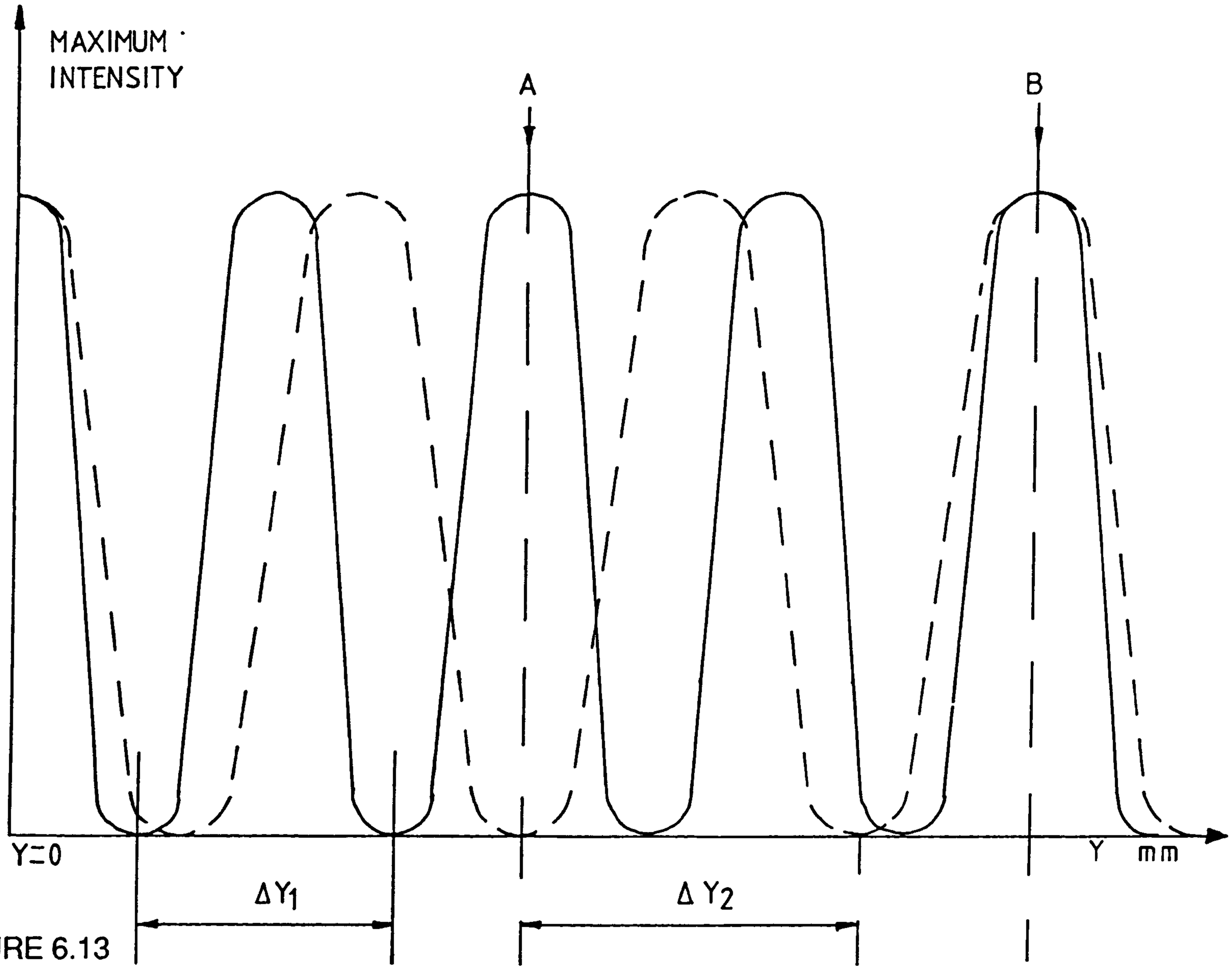

FIGURE 6.13
THE EFFECT OF IMPERFECT MONOCHROMATISM OF LIGHT ON THE INTERFERENCE PATTERN

two maxima will coincide and the observed phenomena will be of maximal brightness (point B).

b) Length of coherence

If we call

$$k = P_1 - P_2 \qquad [10]$$

the difference between the orders of interference, the path difference δ will be:

$$\delta = P_1\lambda_1 = (P_1 - k) \lambda_2 \qquad [11]$$

$$\text{and} \quad P_1 = \frac{k \lambda_2}{\lambda_2 - \lambda_1} \qquad [12]$$

For k values = 0, 1, 2, in [12], the equation gives the values P, of the order of interference for which the maxima of the two systems overlap.

For k values = 0.5, 1.5, 2.5, etc. equation [12] will give the values for which the minima of the two systems overlap.

The superposition of maxima will repeat after a certain number of maxima denoted N calculated from [12].

$$N = \frac{(k + 1) \lambda_2}{\lambda_2 - \lambda_1} - \frac{k \lambda_2}{\lambda_2 - \lambda_1} \qquad [13]$$

$$N = \frac{\lambda_2}{\lambda_2 - \lambda_1} \qquad [14]$$

Interference fringes disappear for the first time . for N/2.

The correspondent path difference is:

$$\delta = (N/2)\lambda_1 \qquad [15]$$

As we assumed that the two wavelengths were very similar, we can write:

$$\lambda_1 \lambda_2 = \lambda o^2 \quad \text{and} \quad \lambda_2 - \lambda_1 = \Delta \lambda o$$

By substitution in [14] and [15], we get the relation for the first disappearance of the interference fringes:

$$\delta_{coh} = \frac{\lambda_0^2}{2\Delta\lambda_0} \qquad [16]$$

This path difference [16] is called the length of coherence. As soon as the path difference is equal to the length of coherence of the source used, the interference pattern disappears.

After exceeding the length of coherence, the fringes reappear but with lower contrast and visibility.

c) Coherence of white light

In the case of a white light source between 400 nm and 700 nm.

$$\Delta\lambda_0 = 300 \text{ nm}$$

with $\lambda_0 = 550$ nm at the centre of the range.

Thus the length of coherence of visible light is equal to:

$$\delta_{coh} = 5.10^{-4}\text{mm} = 0.5 \text{ nm} \qquad [17]$$

But with a continuous distribution of wavelength, the fringes never become in step again, so that a continued increase in layer thickness causes a steady decrease of visibility of the fringes.

6.3.4 VISIBILITY OF FRINGES IN A THIN FILM IN AIR

If we consider a thin soap film or a thin glass plate in the air, the illuminating light falls on the film with an intensity I^i. The reflected intensity I^r is proportional to I^i.

The constant of proportionality R is called the Reflectivity of the given film.

$$R = \frac{I^r}{I^i} \text{ X. } 100\% \qquad [18]$$

Similarly, the transmitted intensity I^t is proportional to I^i. And the constant T or Transmissivity is given by

$$T = \frac{I^t}{I^i} X.\ 100\% \qquad [19]$$

The reflectivity R and the transmissitivity T depend mainnly upon the refractive indices of the film (n1) and the surrounding media (n0) and the angle of incidence of light.

At normal incidence the reflectivity is given by the relation $R = \left(\frac{n1 - n0}{n1 + n0}\right)^2$ [20]

The intensity of rays reflected from the film increases with the reflectivity of the film. The higher the reflectivity of the surfaces, the less rapidly does the intensity of the beam decrease and the larger the number of reflections before the intensity is reduced to a negligible value. It can be shown that the maximum intensity of the interference fringes observed in the focal plane of a photographic system is given by

$$I^r \text{ max} = \frac{4R}{(I + R)^2} X.\ I^i \qquad [21]$$

The coefficient of visibility of the fringes is determined by the relation:

$$V = \frac{I \text{ max} - I \text{ min}}{I \text{ max} + I \text{ min}} \qquad [22]$$

The absolute values of I max and I min depend upon the reflection at each surface:

$$\frac{I \text{ max}}{I \text{ min}} = \left(\frac{1 + R}{1 - R}\right)^2 \qquad [23]$$

And the visibility of the fringes is given by:

$$V = \frac{2R}{I + R^2} \qquad [24]$$

6.3.5. REFLECTED INTENSITY IN A DIELECTRIC THIN FILM

In the case of a dielectric thin film where the incident light encounters an increase of refractive index n1, n2, n3, with the consequent change of phase at both surfaces the reflection factor is given as follows:

Air

n1

---

n2

---

n3

---

n1 < n2 < n3

$$R = \frac{(r_1^2 + 2r_1r_2 \cos\delta + r_2^2)}{(1 + 2r_1r_2 \cos\delta + r_1^2r_2^2)} \qquad [25]$$

with: reflectivity at the 1st interface;

$$r1 = \frac{n1 - n2}{n1 + n2} \qquad [26]$$

reflectivity at the 2nd interface;

$$r2 = \frac{n2 - n3}{n2 + n3} \qquad [27]$$

For $\delta = m\lambda$ where a minimum of fringe visibility occurs the relative reflected intensity for a normal incident light is:

$$\text{Relative Intensity} = \frac{r_1 - r_2}{1 - r_1r_2}^2 \qquad [28]$$

$$\text{Relative Intensity} = \frac{n_2^2 - n_1n_3}{n_2^2 + n_1n_3}^2 \qquad [29]$$

6.3.6 INTERFERENCE FRINGES OF EQUAL THICKNESS FORMED BY A WEDGE SHAPED FILM

Let us consider a monochromatic light (λ) falling on to a surface of a wedge-shaped film (Fig 6.7).

The angle ß formed by the side of the wedge is very small.

For a normal illumination, the path difference of the reflected interfering rays when a bright band is present is given by:

$$S = 2\, n_1 d_1 \pm \lambda/2 \qquad [32]$$

For two adjacent bright bands A1 and A2, the path difference S1 and S2 will be:

$$S_1 = 2\, n_1 d_1 \pm \lambda/2 = p\, \lambda \qquad [33]$$

$$S_2 = 2\, n_1 d_2 \pm \lambda/2 = (\, p + 1\,)\, \lambda \qquad [34]$$

The path difference between two bright bands is equal to λ:

$$d_m = S_2 - S_1 = 2\, n_1 (\, d_2 - d_1\,) = \lambda \qquad [35]$$

From the diagram, the linear distance between the bands or interfringe dy is approximately:

$$dy = \frac{d_2 - d_1}{\beta} \qquad [36]$$

From [35]: $$d_2 - d_1 = \frac{\lambda}{2n} \qquad [37]$$

Included above, we obtain:

$$dy = \frac{\lambda}{2n\beta} \qquad [38]$$

When the interfringe distance dy is known, the . wedge angle ß can be calculated:

$$\beta = \frac{\lambda}{dy\ 2\ n} \qquad [39]$$

When given a number of fringes (P) are present over a known distance X = P . dy. [40]

The precision of the measurement of the interfringe dy can be increased as it is the ratio of:

$$dy = \frac{X}{P} \qquad [41]$$

6.4 APPLICATION TO THE EXPERIMENTAL TECHNIQUE

The photographic techniques previously described make use of a combination of the basic optic principles presented above.

In the experimental photographic technique, the interference colours are localised in the different layers of the pre-corneal and pre-contact lens tear films and can be analysed very precisely by assessing the following:

- the spectral distribution of the light source.
- the effect on the light source of the polarising filters in crossed position.
- the structure of the thin films where the interference fringes are localised.
- the spectral sensitivity of the photographic film.

6.4.1 SPECTRAL DISTRIBUTION OF THE LIGHT SOURCE

Figure 6.14 shows the schematic spectral distribution of the strobe light source over the visible spectrum with its corresponding luminous efficiency values Eλ expressed in percentage.

It presents 1) a flat area between 500 and 730 nm at 20% efficency; 2) a peak appears in the blue region centred around 465 nm; 3) another peak in the red region centred around 755 nm.

The spectral width of the two peaks can be calculated from Fig 6.15. The width of the blue peak is shown to be of $\Delta\lambda$ = 480 nm - 445 nm = 35 nm. The difference between the luminous efficiency level of the

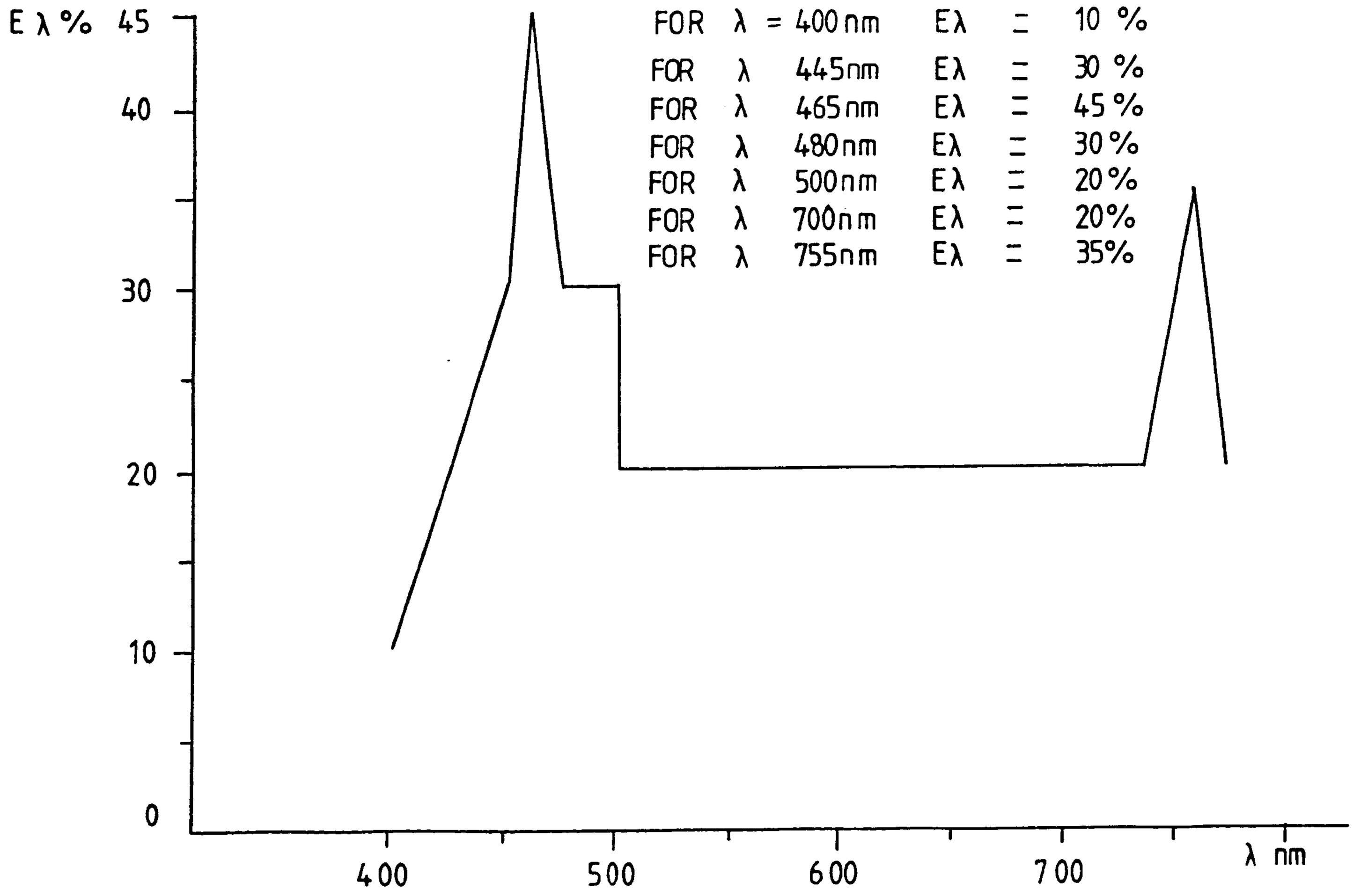

FIGURE 6.14
SPECTRAL DISTRIBUTION OF THE STROBE LIGHT SOURCE
after data from NIKON

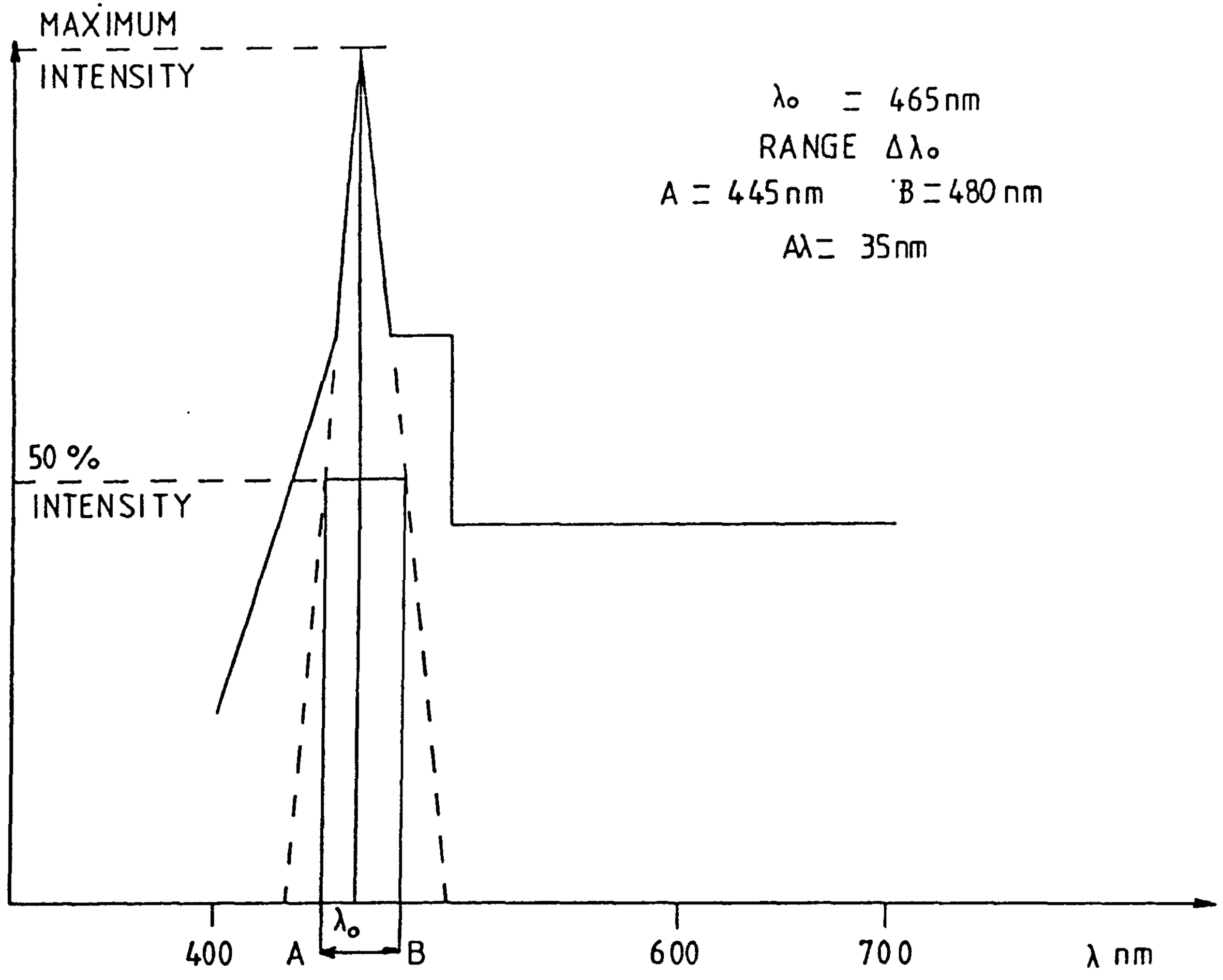

λ_o = 465nm

RANGE $\Delta\lambda_o$

A = 445nm B = 480nm

$\Delta\lambda$ = 35nm

FIGURE 6.15
WIDTH OF PRINCIPAL PEAK $\Delta\lambda o$ OF STROBE LIGHT SOURCE

main peak at 45 percent and the rest of the light source at 20 percent is quite large.

6.4.2 COHERENCE OF THE LIGHT SOURCE

The light source can be divided for calculation purposes into two parts:

1. The favoured peak of emission of high luminous efficiency

$$\Delta\lambda = 445 \text{ nm to } 480 \text{ nm}$$

$$\text{maxi } \lambda = 465 \text{ nm}$$

2. The rest of the spectral distribution of low luminous efficiency, mainly from 480 nm to 700 nm.

To find out the spectral composition of the interference pattern photographed and the length of coherence of the light source, the maxima of interference have been calculated for the following values:

$\lambda_1 = 445$ nm (Table 6.10)

$\lambda_2 = 465$ nm (Table 6.11)

$\lambda_3 = 480$ nm (Table 6.12).

From this we can deduct the ranges of layer thickness over which each individual order spreads (Table 6.13 & Fig 6.16).

It can be seen that for the values of the peak of emission of the light that the range start overlapping at the 15th to 17th orders of interference. Thus limiting the visibility of the fringes to an aqueous layer thickness of 2.5 μm to 2.8 μm.

The ranges overlap by more than 50 percent for the 24th and 25th orders of interference where the fringes

AQUEOUS TEARS

Index $n = 1.337$

Colour Blue $\lambda = 0.445\ \mu m$

Constructive Interference

Maximum Visible

When $d = \frac{(P + 0.5)\lambda}{2n} = \frac{(P + \frac{1}{2})\ 0.445}{2.674}$

P = Order of Interference

d = Thickness of Film

P = 0	d0 = 0.083 μm	P = 2	d2 = 0.416 μm
P = 1	d1 = 0.249 μm	P = 4	d4 = 0.749 μm
P = 3	d3 = 0.582 μm	P = 6	d6 = 1.082 μm
P = 5	d5 = 0.915 μm	P = 8	d8 = 1.415 μm
P = 7	d7 = 1.248 μm	P = 10	d10 = 1.747 μm
P = 9	d9 = 1.581 μm	P = 12	d12 = 2.080 μm
P = 11	d11 = 1.914 μm	P = 14	d14 = 2.413 μm
P = 13	d13 = 2.247 μm	P = 16	d16 = 2.746 μm
P = 15	d15 = 2.579 μm	P = 18	d18 = 3.079 μm
P = 17	d17 = 2.912 μm	P = 20	d20 = 3.412 μm
P = 19	d19 = 3.245 μm	P = 22	d22 = 3.744 μm
P = 21	d21 = 3.578 μm	P = 24	d24 = 4.077 μm
P = 23	d23 = 3.911 μm	P = 26	d26 = 4.410 μm
P = 25	d25 = 4.244 μm		

TABLE 6.10
CONSTRUCTIVE INTERFERENCE IN AQUEOUS TEARS
FOR $\lambda = 445$ nm

AQUEOUS TEARS

Index n = 1.337

Colour Blue λ = 0.465 µm

Constructive Interference

Maximum Visible

When $d = \frac{(P + 0.5)\lambda}{2n} = \frac{(P + \frac{1}{2})\,0.465}{2.674}$

P = Order of Interference

d = Thickness of Film

P = 0	d0 = 0.086 µm		
P = 1	d1 = 0.261 µm	P = 2	d2 = 0.435 µm
P = 3	d3 = 0.609 µm	P = 4	d4 = 0.783 µm
P = 5	d5 = 0.956 µm	P = 6	d6 = 1.130 µm
P = 7	d7 = 1.304 µm	P = 8	d8 = 1.478 µm
P = 9	d9 = 1.652 µm	P = 10	d10 = 1.826 µm
P = 11	d11 = 2.000 µm	P = 12	d12 = 2.174 µm
P = 13	d13 = 2.348 µm	P = 14	d14 = 2.522 µm
P = 15	d15 = 2.696 µm	P = 16	d16 = 2.870 µm
P = 17	d17 = 3.044 µm	P = 18	d18 = 3.218 µm
P = 19	d19 = 3.392 µm	P = 20	d20 = 3.566 µm
P = 21	d21 = 3.740 µm	P = 22	d22 = 3.914 µm
P = 23	d23 = 4.088 µm	P = 24	d24 = 4.262 µm
P = 25	d25 = 4.436 µm	P = 26	d26 = 4.610 µm
P = 27	d27 = 4.784 µm	P = 28	d28 = 4.958 µm
P = 29	d29 = 5.132 µm	P = 30	d30 = 5.306 µm
P = 31	d31 = 5.480 µm	P = 32	d32 = 5.654 µm
P = 33	d33 = 5.828 µm	P = 34	d34 = 6.000 µm

TABLE 6.11
CONSTRUCTIVE INTERFERENCE IN AQUEOUS TEARS
FOR λ = 465 nm

AQUEOUS TEARS

Index n = 1.337

Colour Blue-Green λ = 0.480 μm

Constructive Interference

Maximum Visible

When $d = \frac{(P + \frac{1}{2})\lambda}{2n} = \frac{(P + \frac{1}{2})\ 0.480}{2.674}$

P = Order of Interference

d = Thickness of Film

P = 0	d0	= 0.090 μm	P = 2	d2	= 0.449 μm
P = 1	d1	= 0.269 μm	P = 4	d4	= 0.808 μm
P = 3	d3	= 0.628 μm	P = 6	d6	= 1.167 μm
P = 5	d5	= 0.987 μm	P = 8	d8	= 1.526 μm
P = 7	d7	= 1.346 μm	P = 10	d10	= 1.885 μm
P = 9	d9	= 1.705 μm	P = 12	d12	= 2.249 μm
P = 11	d11	= 2.064 μm	P = 14	d14	= 2.603 μm
P = 13	d13	= 2.423 μm	P = 16	d16	= 2.962 μm
P = 15	d15	= 2.782 μm	P = 18	d18	= 3.321 μm
P = 17	d17	= 3.141 μm	P = 20	d20	= 3.680 μm
P = 19	d19	= 3.500 μm	P = 22	d22	= 4.039 μm
P = 21	d21	= 3.860 μm	P = 24	d24	= 4.398 μm
P = 23	d23	= 4.218 μm	P = 26	d26	= 4.757 μm
P = 25	d25	= 4.577 μm			

TABLE 6.12
CONSTRUCTIVE INTERFERENCE IN AQUEOUS TEARS
FOR λ = 480 nm

R0 = Range for Order of Interference P = 0

R0	= From	0.083	To	0.090 μm
R1	=	0.249		0.269 μm
R2	=	0.416		0.449 μm
R3	=	0.582		0.628 μm
R4	=	0.749		0.808 μm
R5	=	0.915		0.987 μm
R6	=	1.082		1.167 μm
R7	=	1.248		1.346 μm
R8	=	1.415		1.526 μm
R9	=	1.581		1.705 μm
R10	=	1.747		1.885 μm
R11	=	1.914		2.064 μm
R12	=	2.080		2.249 μm
R13	=	2.247		2.423 μm
R14	=	2.412		2.603 μm
R15	=	2.579		2.782 μm
R16	=	2.746		2.962 μm
R17	=	2.912		3.141 μm
R18	=	3.079		3.321 μm
R19	=	3.245		3.500 μm
R20	=	3.412		3.680 μm
R21	=	3.578		3.860 μm
R22	=	3.744		4.039 μm
R23	=	3.911		4.218 μm
R24	=	4.077		4.398 μm
R25	=	4.244		4.577 μm
R26	=	4.410		4.757 μm

TABLE 6.13
RANGE OF SUCCESSIVE ORDERS OF CONSTRUCTIVE INTERFERENCE
FOR A SOURCE DISTRIBUTION ∴λ (445 to 480 nm)

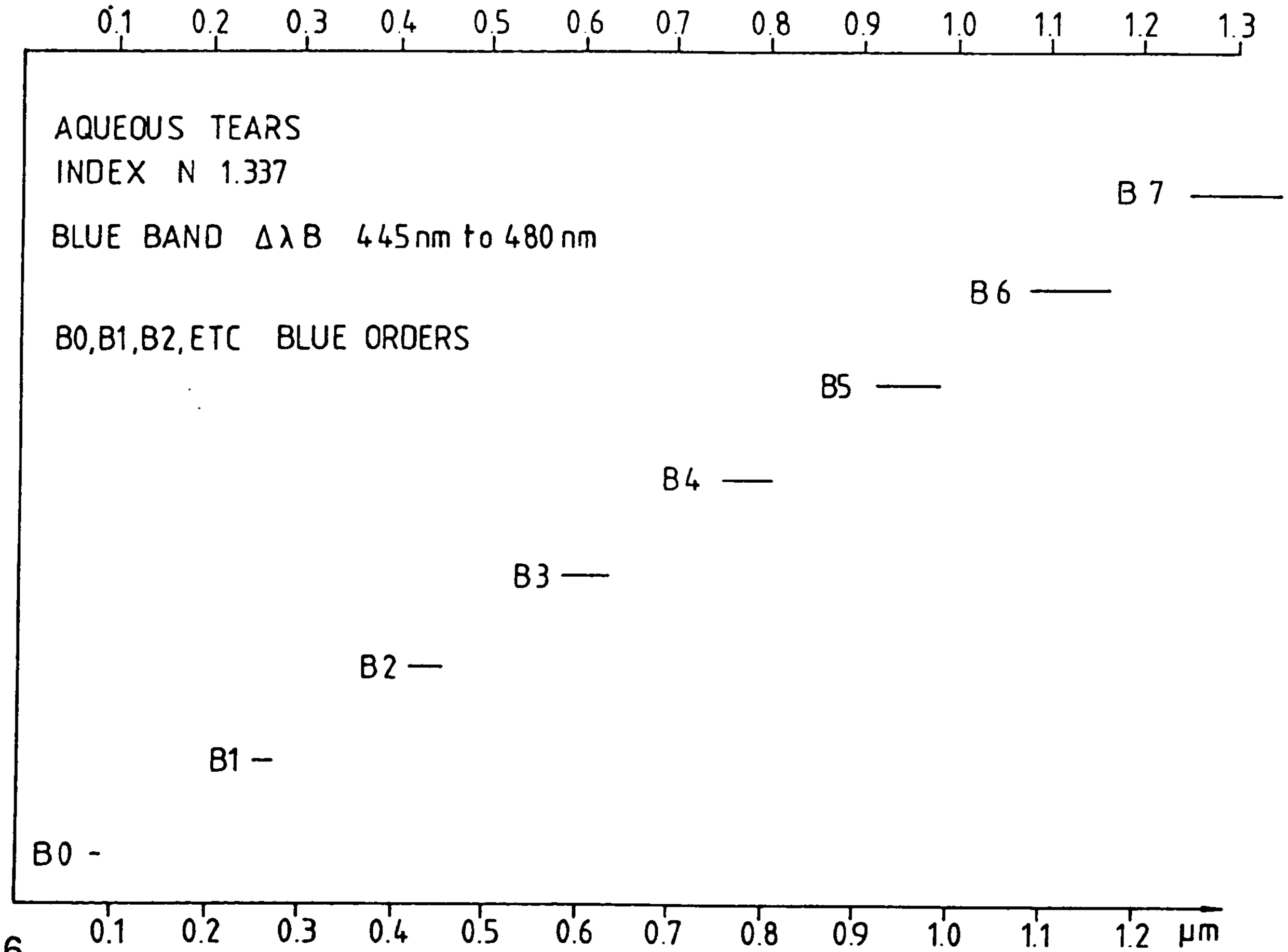

FIGURE 6.16
DISTRIBUTION AND SPREAD OF INTERFERENCE FRINGES OVERLAP WITH INCREASING LAYER THICKNESS

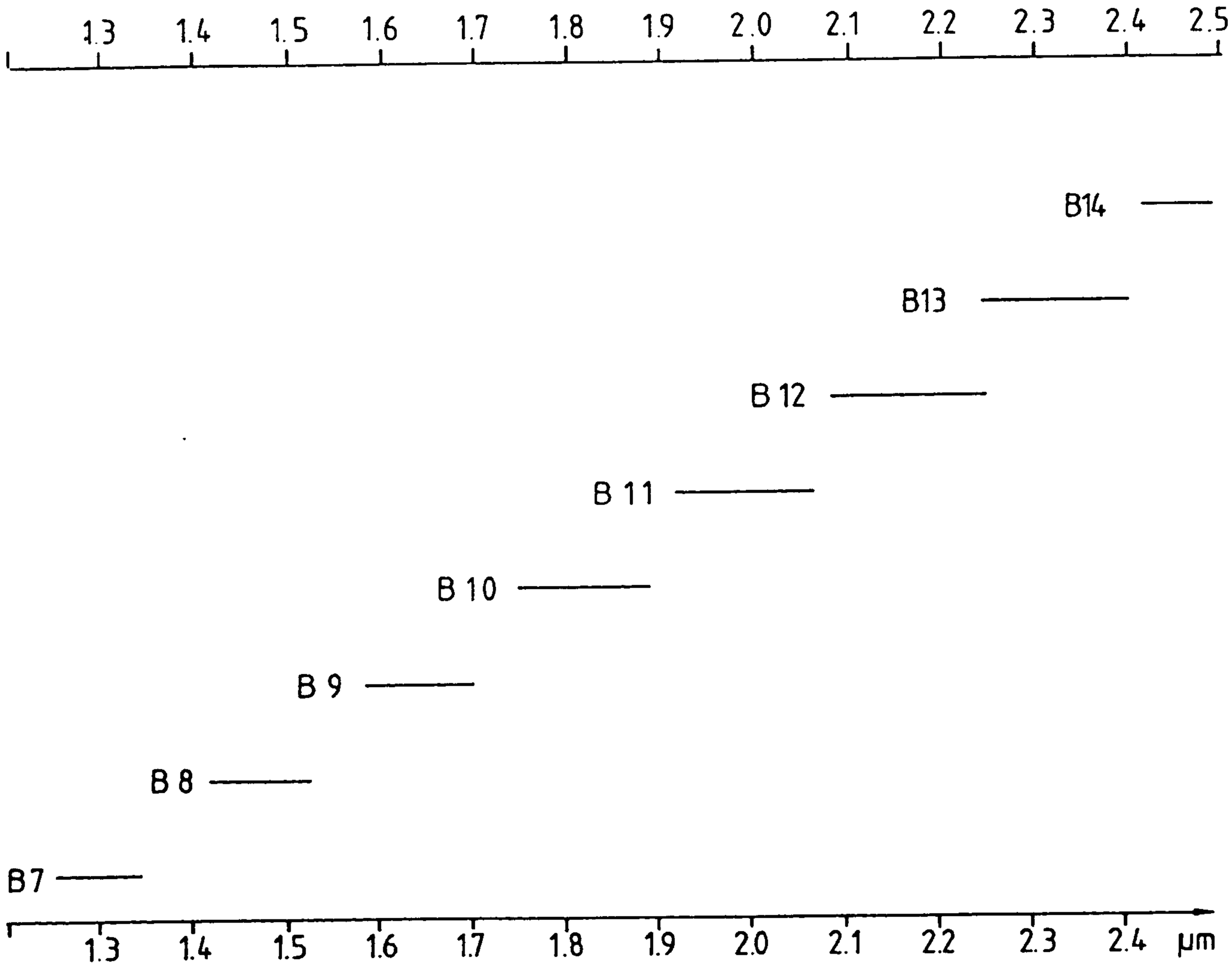

FIGURE 6.16 cont 1
DISTRIBUTION AND SPREAD OF INTERFERENCE FRINGES OVERLAP WITH INCREASING LAYER THICKNESS

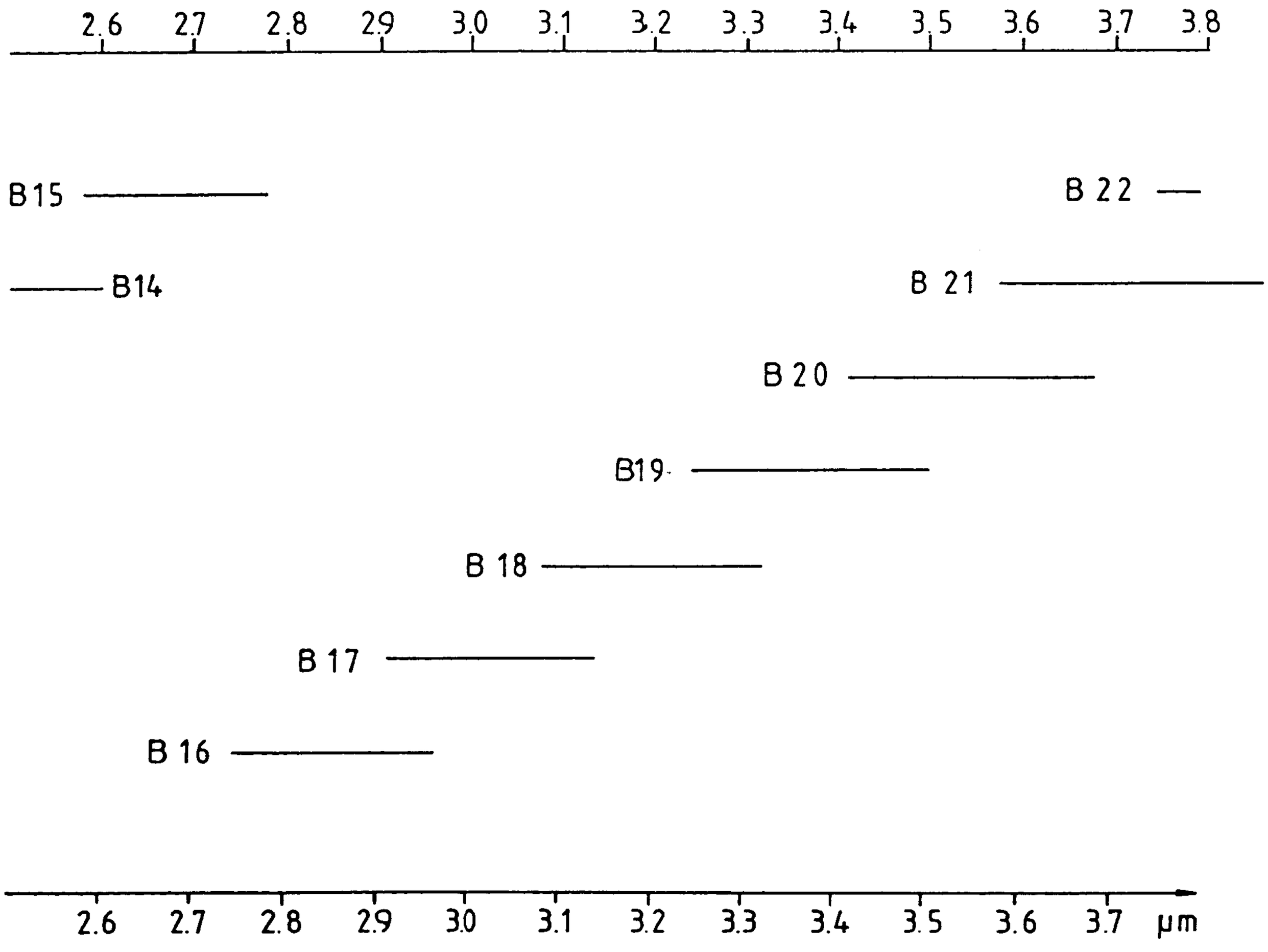

FIGURE 6.16 cont 2
DISTRIBUTION AND SPREAD OF INTERFERENCE FRINGES OVERLAP WITH INCREASING LAYER THICKNESS

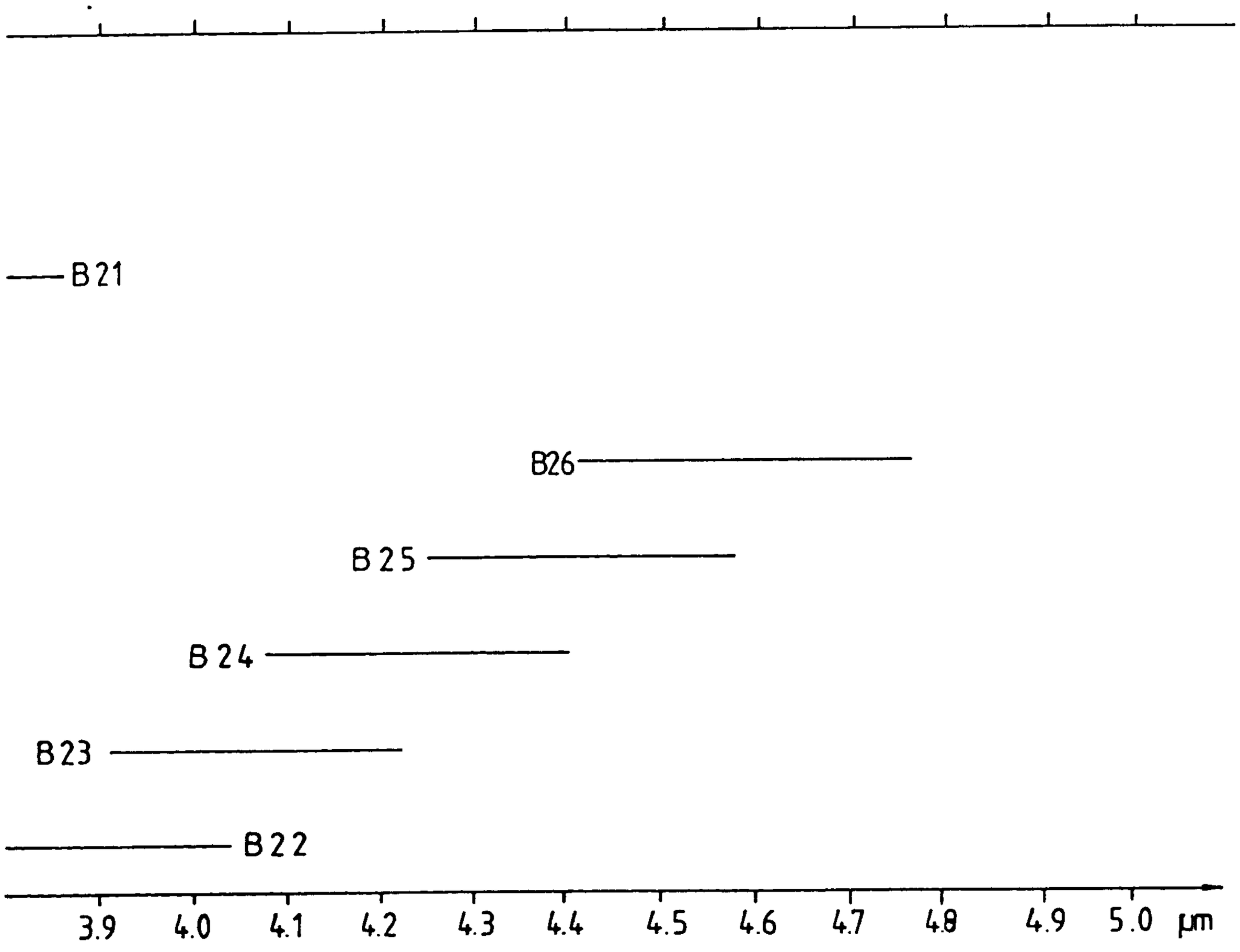

FIGURE 6.16 cont 3
DISTRIBUTION AND SPREAD OF INTERFERENCE FRINGES OVERLAP WITH INCREASING LAYER THICKNESS

are not visible any more and a white continuum is present.

The calculations shown in Fig 6.16 for a layer of refractive index 1.337 corresponding to that of the aqueous phase of the tears will allow us to measure a layer thickness of approximately 4 µm by counting the visible blue fringes in our photographs.

The values of the maxima for the main band have been calculated for its extremities:

$$\lambda = 480 \text{ nm and } \lambda = 700 \text{ nm.}$$

The range over which the successive orders of interference spreads demonstrate that for the third order of interference an overlap is present, thus inducing the production of a white continuum (Table 6.14) (Fig 6.17).

i) Length of Coherence of the Strobe Light Source

The knowledge of the spectral distribution of the strobe light source allows us to analyse its effect on the interference colours and fringes photographed in the superficial lipid layer of the pre-corneal tear film and in the aqueous layer of the pre-contact lens tear film.

The length of coherence of a light source determines the number of interference fringes which can be produced in an experimental set up. It does so by governing the visibility of the fringes.

The longer the length of coherence, the higher the number of fringes visible and the sharper their definition. The shorter the length of coherence the lower the number of fringes, the poorer their definition.

R0 = Range for Order of Interference P = 0

R0 :	From	d0	= 0.090 µm	To	0.131 µm
R1 :		d1	= 0.269 µm		0.393 µm
R2 :		d2	= 0.499 µm		0.654 µm
R3 :		d3	= 0.628 µm		0.916 µm
R4 :		d4	= 0.808 µm		1.178 µm
R5 :		d5	= 0.987 µm		1.440 µm
R6 :		d6	= 1.167 µm		1.702 µm
R7 :		d7	= 1.346 µm		1.963 µm
R8 :		d8	= 1.526 µm		2.225 µm
R9 :		d9	= 1.705 µm		2.487 µm
R10:		d10	= 1.885 µm		2.749 µm

TABLE 6.14
RANGE OF SUCCESSIVE ORDERS OF CONSTRUCTIVE INTERFERENCE
FOR A SOURCE DISTRIBUTION $\Delta\lambda$ (480 to 700 nm)

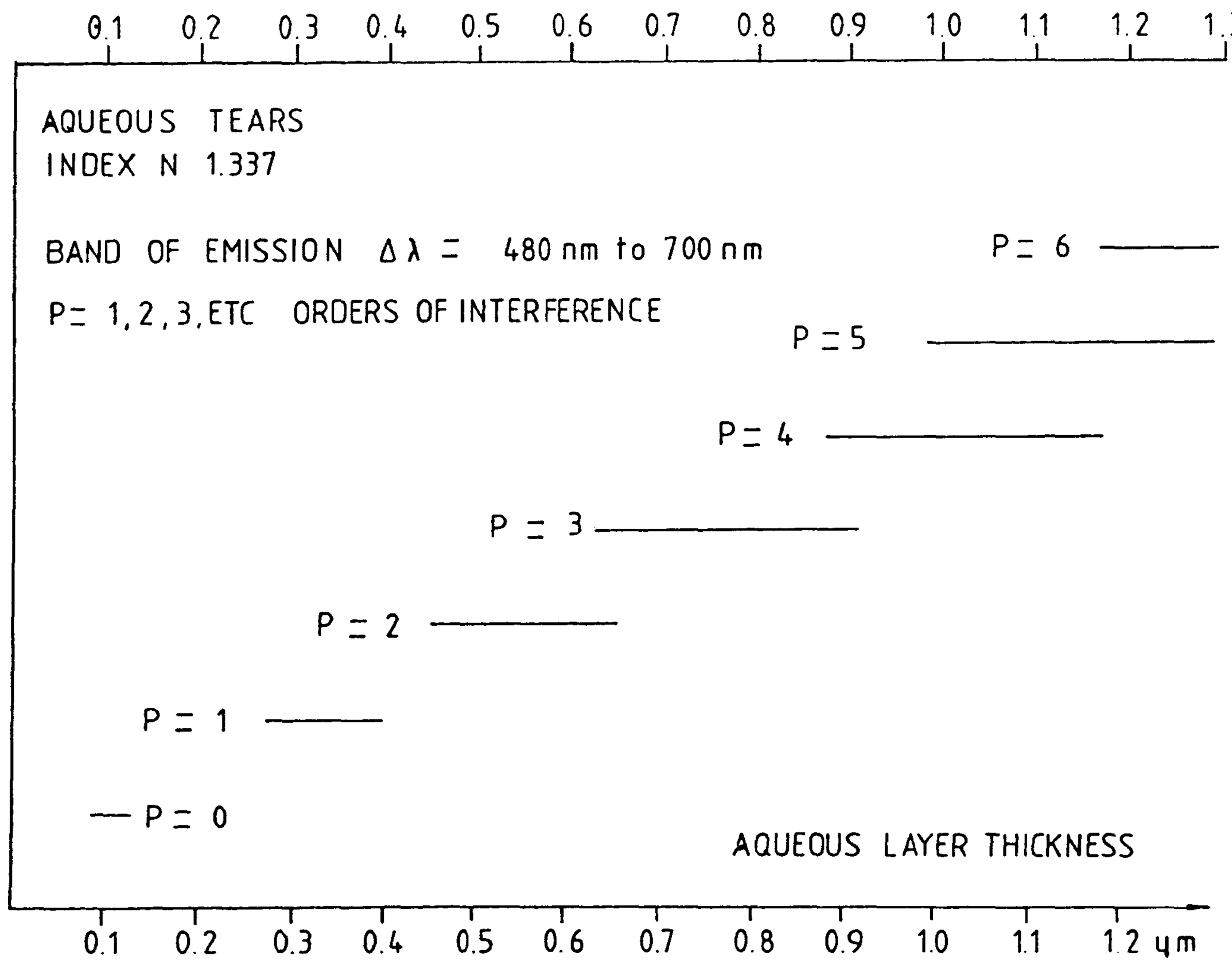

FIGURE 6.17
PRODUCTION OF WHITE CONTINUOUS BACKGROUND BY MAIN BAND OF EMISSION OF LIGHT SOURCE

As seen previously, the main factor regulating the length of coherence of the light source is the 'half width' of peak or emission.

a) Length of coherence of the peak of emission

For the experimental set up the length of coherence of the peak of emission it is situated between 445 nm and 480 nm with its maximum at 465 nm.

The length of coherence of that light source is given by:

$$Sk = \frac{\lambda_0^2}{2\Delta\lambda_0} = \frac{\lambda_0\lambda_1}{2\Delta\lambda_0} \qquad [16]$$

$$Sk = \frac{(445)\ (480)}{2\ (35)} = \frac{3.051\ nm}{} = 3.051\ \mu m$$

$$Sk = 3.051 \text{ microns} \qquad [42]$$

When the path difference between two interfering rays is equal to this 'length of coherence' ($\delta = Sk$) the interference pattern will be at its minimum of intensity.

The phase difference at that point is:

$$\delta = 2\ n\ d \qquad [43]$$

n = index of film

d = film layer thickness

δ = phase difference

The layer thickness at which this happens is:

$$d = \frac{\delta}{2\ n} \qquad [44]$$

$$d = \frac{3.051}{2 \times 1.337} = 1.141 \text{ microns} \qquad [45]$$

It can be concluded that for an aqueous layer of index n = 1.337, when the thickness of the film reaches 1.141 microns the interference fringe due to the main

peak of emission will, in our case, be at its minimum of visibility.

As it will be seen later, this minimum of visibility depends on the reflection coefficients of the layer surfaces. From Figure 6.16 it can be seen that this happens for the sixth order of interference P = 6.

The fringe system due to the main peak of emission will reappear further away but with a lower contrast and visibility.

b) Length of coherence of the main band of emission

The main band of emission situated between 480 mm and 700 mm has a low level of luminous efficiency (20 percent) and a large spread 220 nm.

When calculated in the same manner, the length of coherence due to that part of the spectrum emitted and recorded is found to be:

$$5k = \frac{700 - 480}{2\,(220)} = \frac{3.360}{440} \qquad [46]$$

$$= 766.63 \text{ nm}$$

$$5k = 0.763 \text{ microns}$$

The layer of thickness at which this happens is:

$$d = \frac{\ell}{2n} = \frac{0.763}{2(1.337)} = 0.285\ \mu m \qquad [47]$$

For such a layer thickness the system of interference fringes produced by that part of the spectrum starts losing some visibility.

From Figure 6.17 it can be seen that this occurs for an order of interference P = 1 in a layer of index n = 1.337.

The fringes due to that part of the spectrum will reappear for an increased layer thickness but the emission being at such a low luminous efficiency, it will soon coalesce in a white continuum and will only be recorded on the photographic film as a whitish background, against which the fringes produced by the main peak of emission will be discernible.

ii) Visibility of Interference Fringes

As we have seen previously, 6.3.5, the visibility of interference fringes depends also on the structure and thickness of the thin film where the fringes are localised.

We have just seen that the thickness of the layer and the coherence of the light source are important factors of fringe visibility.

The other important factor is the reflectivity of the film under observation which depends on its refractive index and that of the surrounding media.

For the observation of the tear film two cases will be considered:

1) The case of a lipid layer (index n_2 = 1.482) (Tiffany, 1986) found on the aqueous phase of the tear film (index n_3 = 1.337) and bounded by air (n_1 = 1) on one side. This corresponds to the accepted structure of the pre-corneal tear film (Fig 2.10).

2) The case of the dielectrical film formed by the aqueous phase (index n_2 = 1.337) bounded by air on one side (n_1 = 1) and spread over PMMA (n_3 = 1.49).

It will be seen in Chapter 7 that it corresponds to our proposed structure of the tear film situated in front of a corneal PMMA contact lens.

a) CASE ONE: Visibility of the lipid layer of the pre-ocular tear film normal incidence

Lipid Layer

n1	1	(1)	AIR
n2	1.482		LIPID
n3	1.337	(2)	AQUEOUS

$$R = \frac{(r_1^2 + 2 r_1 r_2 \cos\delta + r_2^2)}{(1 + 2 r_1 r_2 \cos\delta + r_1^2 r_2^2)} \qquad [27]$$

Reflectivity at First Interface

$$r_1 = \frac{n_2 - n_1}{n_2 + n_1} \qquad [28]$$

$$= \frac{1.482 - 1}{1.482 + 1}$$

$$= \frac{0.482}{2.482}$$

$$r_1 = 0.1942 \qquad [48]$$

Reflectivity at Second Interface

$$r_2 = \frac{n_2 - n_3}{n_2 + n_3} \qquad [29]$$

$$r_2 = \frac{1.482 - 1.337}{1.482 + 1.337}$$

$$= \frac{0.145}{2.819}$$

$$r_2 = 0.0514 \qquad [49]$$

Maximum Reflection factor

The maximum reflected intensity is reached for a path difference = p λ when cos δ = 1.

$$R_{max} = \left(\frac{r_1 + r_2}{1 + r_1 r_2} \right)^2 \qquad [50]$$

$r_1 = 0.1942$

$r_2 = 0.0514$

$$R_{max} = \left(\frac{0.2456}{1.0100} \right)^2$$

For Cos $\delta = 1$

$R_{max} = 0.0591$

$R_{max} = 5.91\%$ [51]

Minimum Reflection Factor

The minimum of reflected intensity is reached when the path difference = p λ and cos $\delta = -1$.

$$R_{min} = \left(\frac{r_1 - r_2}{1 - r_1 r_2} \right)^2 \qquad [52]$$

$$R_{min} = \left(\frac{0.1428}{0.99} \right)^2$$

$R_{min} = 0.0208$

$R_{min} = 2.08\%$ [53]

For Cos $\delta = -1$

The above results are compiled in Figure 6.18.

b) CASE TWO: Visibility of the aqueous phase on rigid contact lenses

Aqueous Layer

n1 1 (1) AIR

n2 1.337 AQUEOUS LAYER

n3 1.49 (2) PMMA SURFACE

Reflectivity at First Interface

$$r_1 = \frac{n_2 - n_1}{n_2 + n_1} \qquad [28]$$

$r_1 = 0.1442$ [54]

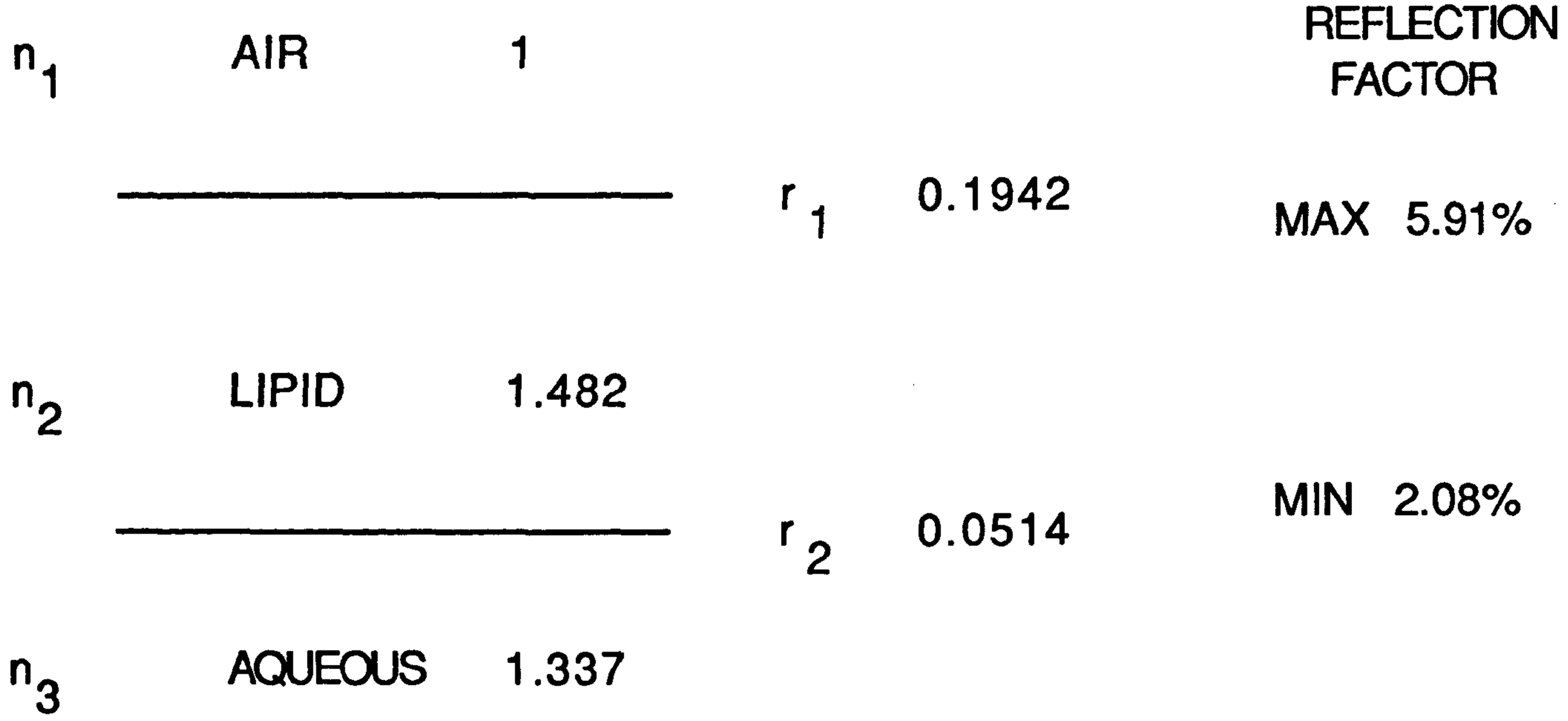

FIGURE 6.18
VARIATION OF REFLECTIVITY WITH THIN FILM STRUCTURES: LIPID LAYER

Reflectivity at Second Interface

$$r_2 = \frac{n_a - n_2}{n_a + n_2} \qquad [29]$$

$$r_2 = 0.0541 \qquad [55]$$

Maximumum Reflection Factor

The maximum reflected intensity is reached for a path difference = p λ when cos δ = 1.

$$R_{max} = \left(\frac{r_1 + r_2}{1 + r_1 r_2}\right)^2 \qquad [50]$$

$$R_{max} = \left(\frac{0.1983}{1.0078}\right)^2$$

$$R_{max} = 0.0387$$

$$R_{max} = 3.87\% \qquad [56]$$

Minimum Reflection Factor

The minimum of reflected intensity is reached when the path difference δ = p λ and cos δ = -1.

$$R_{min} = \left(\frac{r_1 - r_2}{1 - r_1 r_2}\right)^2 \qquad [52]$$

$$R_{min} = \left(\frac{0.0901}{0.9922}\right)^2$$

$$R_{min} = 0.0083$$

$$R_{min} = 0.83\% \qquad [53]$$

The above results are compiled in Figure 6.19. These results will be used in the qualitative evaluation of the photographs in Chapter 7.

In the case of the normal pre-ocular tear film where a lipid layer is always present and the aqueous phase nears 7μm on average, only the fringes of the lipid layer will be visible because the aqueous phase thickness is much greater than the length of coherence of our light source and the presence of a thick mucous phase of decreased reflectivity will not produce any visible fringes.

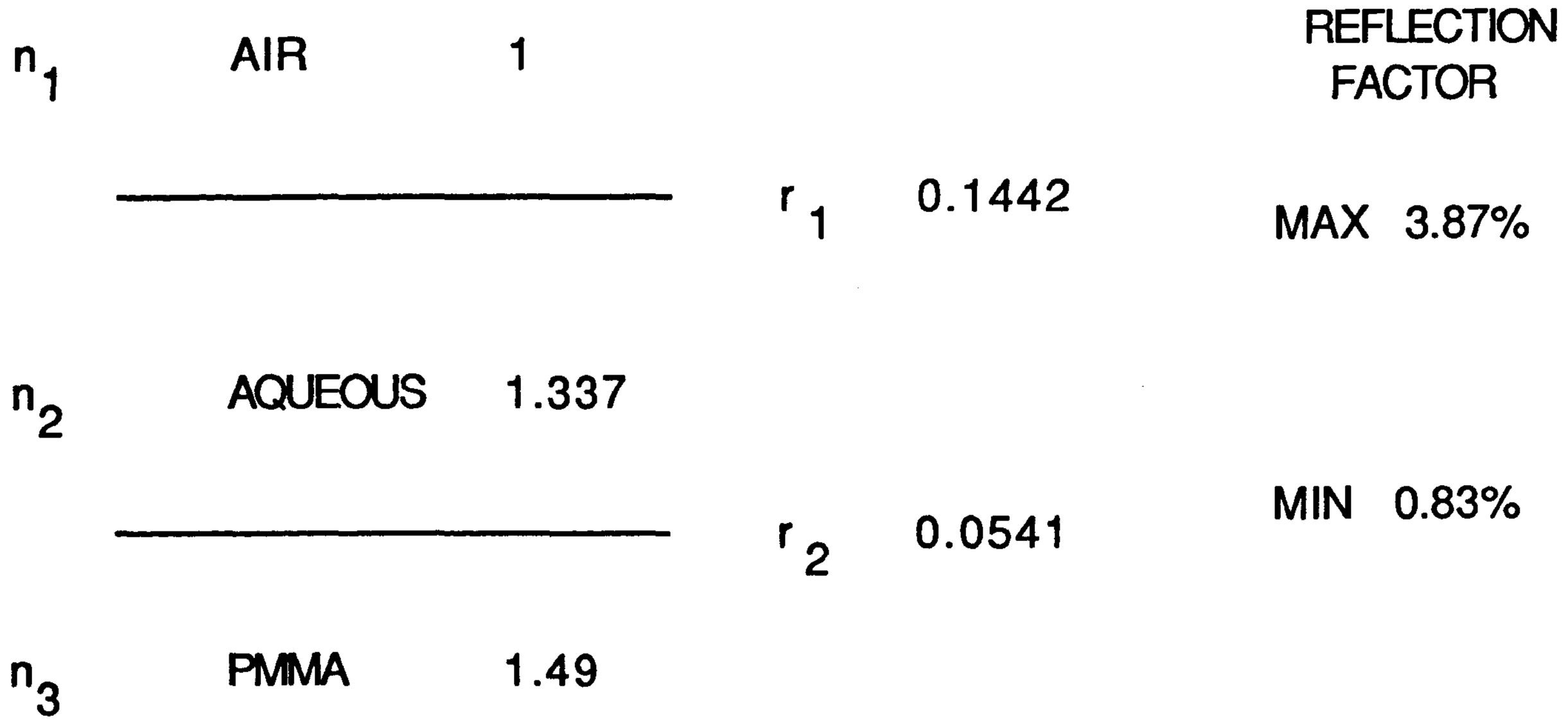

FIGURE 6.19
VARIATION OF REFLECTIVITY WITH THIN FILM STRUCTURES: AQUEOUS PHASE

In the case of the pre-soft contact lens tear film, the visibility of the aqueous fringes will be decreased with increased aqueous phase thickness and with increased thickness of the mucous layer adsorbed at the lens surface.

These aqueous fringes may be completely hidden when a thick lipid layer is present and the intensity of its colour fringes too high.

When the mucous layer is thin or sparse, the aqueous phase thin, the lipid layer minimal, the fringes of the aqueous phase will have high visibility.

In the case of the pre-rigid contact lens tear film the visibility of the aqueous fringes is governed by the same rules but a higher reflectivity level is expected from the well polished surface of the lens, increasing their visibility.

As it will be shown in Chapter 7, the absence or limited thickness of the lipid layer in front of rigid contact lenses will limit the reflection occurring at that level. The increased transmission will enhance the intensity of the interference fringes in the aqueous phase.

In the rigid lens tear film, where the lipid layer is not visible, and the mucous layer is thin or sparse the interference fringes formed within the aqueous phase will have the highest visibility of all the tear film structures studied.

6.4.3 EFFECT OF THE POLARISERS ON THE LIGHT SOURCE

The main effect of the polarisers is to cut down the incident light level by 50 percent. When used in conjunction with an analyser at a 90 degree angle, it should produce extinction of all wavelength of the light source. But the polarisers used are not neutral polarisers as they selectively transmit the blue end of the spectrum even in crossed polarised position. It can be readily seen when held in front of the light source. The filament is seen possessing a blue colouration and all other extraneous light is cancelled.

This selective blue bias decreases further the width of the principal peak of emission. It also cuts down the secondary peak in the red end of the spectrum (Fig 6.14).

In Chapter 7 we will show that up to 31 interference fringes can be seen in the aqueous phase formed over a rigid contact lens. This corresponds to a layer thickness d = 5.48 μm (Figs 7.41 and 7.42). This thickness allows us to assess the lengths of coherence and the width of the spectral band created by our cross-polarised system at the photographic plane.

The length of coherence is given by:

$$Sk = \frac{\lambda o^2}{2\Delta\lambda o} \qquad [16]$$

Sk = length of coherence

λo = main peak of emission

Δλo = width of spectral line

This occurs for a phase difference:

$$\delta = 2\,n\,d \qquad [3]$$

δ = phase difference

n = index of film

d = thickness of the film

For a loss of fringe visibility occurring at the 31st fringe. It corresponds to a layer thickness:

$$d = 5.48\ \mu m = \frac{\delta}{2n}$$

The path difference at that point is equal to:

$$\delta = 2\,n\,d = 2 \times 1.337 \times 5.48 = 14.65\ \mu m \qquad [54]$$

This is the length of coherence Sk of the system produced in our experiment:

$$\text{From [16]}\ Sk = 14.65\ \mu m = \frac{\lambda o^2}{2\Delta\lambda o} \qquad [55]$$

We can deduce the width of the spectral band created in our system:

$$2\Delta\lambda o = \frac{\lambda o^2}{14.65}$$

$$\Delta\lambda o = \frac{\lambda o^2}{2 \times 14.65}$$

$$= \frac{0.465^2}{2 \times 14.65} = \frac{0.216}{29.31} = 0.00737\ \mu m$$

$$= 7.4\ nm.$$

The width of the spectral line created by the use of the polarising filter in near crossed position is $\Delta\lambda o = 7.4nm$. This is a large improvement over the amount (35nm) calculated from Figure 6.12.

6.4.4 CONCLUSION

It can be concluded that our system does not make equal use of the whole spectrum of colours, but it favours the selection of a broad band of high luminous

efficiency in the blue end of the spectrum against the remainder of the spectrum present at a low luminous efficiency. For our purpose, it combines the benefit of having all the spectral colours present and at the same time or posessing a narrower reference peak.

The reduction from 35nm to 7.4nm creates a photographic system superior to those using other means to decrease the intensity of the light specularly reflected (Josephson, 1983; Kilp, 1985; Knoll & Walters 1985).

The system used in our experiment permits a greater image sharpness, and renders visible a larger number of interference fringes and still keeps the appearance of white light interference fringes. It is an improvement on the use of monochromatic sources as it allows the thinner parts of the tear film to produce colour interferences which differentiate much more precisely the layer thicknesses.

CHAPTER 7

RESULTS AND ANALYSIS

7.1 EXPERIMENTAL STUDY 1: PRE-OCULAR TEAR FILM LIPID LAYER

7.1.1 INTRODUCTION

Both photographic and observation techniques described in Chapter 5 are used in this study to investigate the nature and thickness of the lipid layer of the pre-ocular tear film (POTF). The high magnification technique gives precise information on localised lipid patterns whereas the low magnification method depicts the overall pattern, which usually is a combination of two or more individual patterns.

7.1.2 MATERIAL AND METHOD

i) Material

The observations made in this section were carried out on normal patients free of any ocular abnormality with the exception of low refractive errors. None were contact lens wearers, however, some were subsequently fitted with lenses.

ii) Method

The nature of the lipid layer of the pre-ocular tear film was analysed as described in Chapter 6.

In each case, photographs were taken two seconds after eye opening following a normal blink. At that time all tear film movements are completed and the patients'

normal tear film is present (Brown and Dervichian, 1969; Holly, 1973a; Benedetto et al, 1984).

Several aspects of the pre-ocular lipid layer are reported depicting both normal and abnormal conditions:

- description of the different lipid patterns normally encountered in a normal asymptomatic population.

- description of the lipid layer appearance in cases of Meibomian gland over secretion.

- sequential analysis of lipid spreading following Meibomian gland expression.

- study of the lipid layer structural changes with reduced palpebral aperture.

- analysis of the disruptive effect on the lipid layer of a single eye drop instillation.

iii) Photographic and Observation Conditions

a) Photographic conditions

The high magnification photographs were taken with the polarisers in near crossed position (80 to 90 degrees) and concentrated on the specular reflection produced by the lipid layer. Ektachrome 64 transparencies were used, with a Nikon Endothelial camera at maximal flash output (500 watt/sec). Also, in two instances, where higher final magnification was required, a black and white 25 ASA Kodak film was utilised.

The low magnification photographs were taken using the attachment described in Chapter 5, Section 3. Photographs were also taken with Ektachrome ASA 64 transparency film.

b) Qualitative analysis

Analysis of the different patterns were made directly from the projected slides in a dark room using a Kodak carousel slide projector. Further, for this thesis A4 size prints were produced for illustration purposes only.

7.1.3 RESULTS

i) Introduction

The results reported with regard to the pre-ocular lipid layer are solely examples of the most commonly encountered patterns present in a normal population and some of their variations.

ii) Common Lipid Patterns

Each individual pattern is first described from high magnification photographs, whereas, the usual pattern combinations are observed using the low magnification method that covers the whole cornea at once.

a) Normal individual patterns

A) Normal marmoreal pattern

The normal marmoreal pattern (Fig 7.1) as its name indicates, resembles marble veining with darker grey (Area A) - lines over a lighter slightly indistinct grey background (Area B). The blueish tint of the photograph is mainly due to the effect of the polarising filter tint. The superficial darker lipids appear linked together to form a meshwork. The more intricate the meshwork, the darker the layer. Some minute particles are seen floating at the surface. A

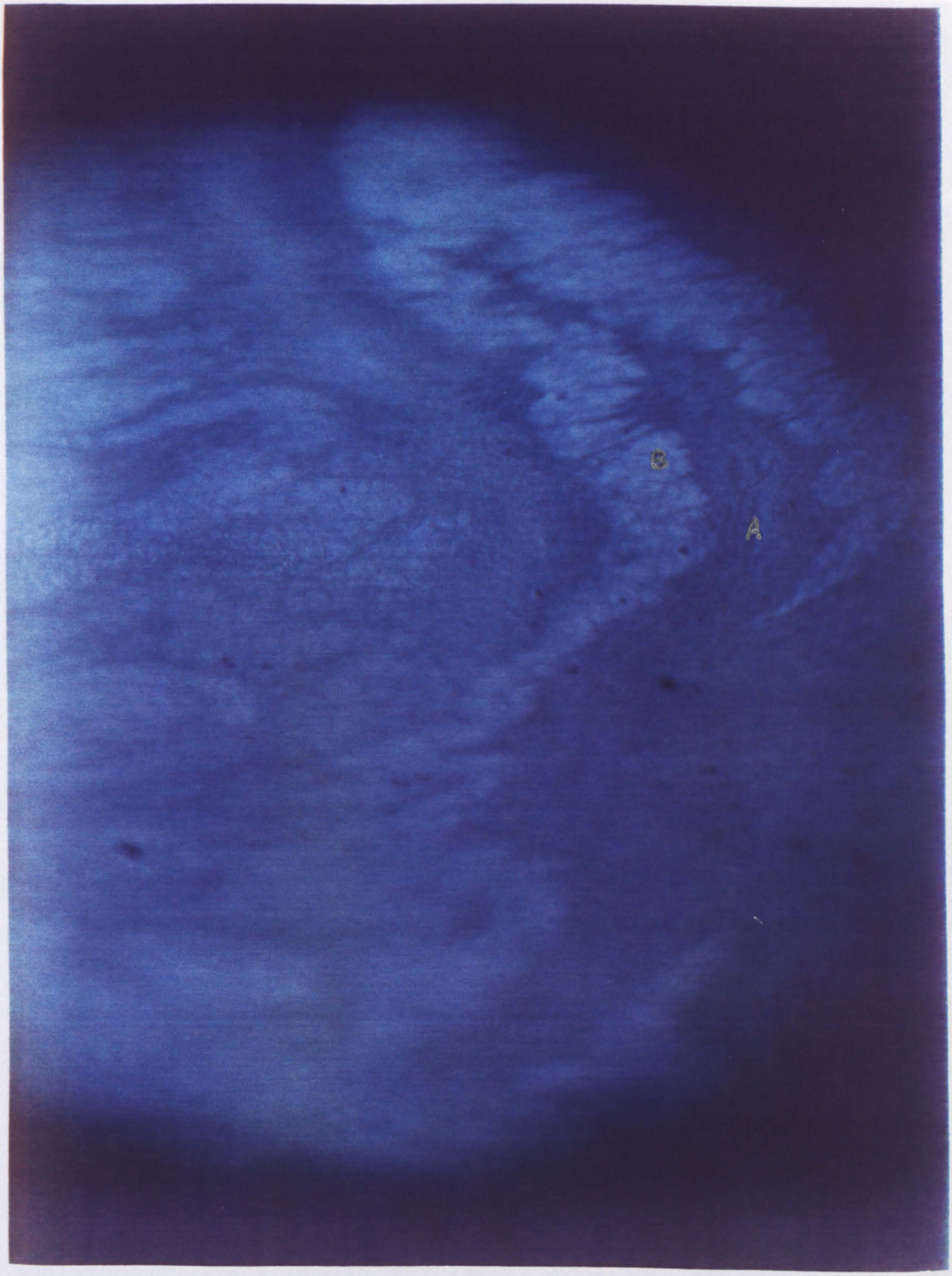

FIGURE 7.1
PRE-OCULAR TEAR FILM MARMOREAL LIPID PATTERN
ORIGINAL MAGNIFICATION (X9.6)
PHOTOGRAPH MAGNIFICATION (APPROX 95)

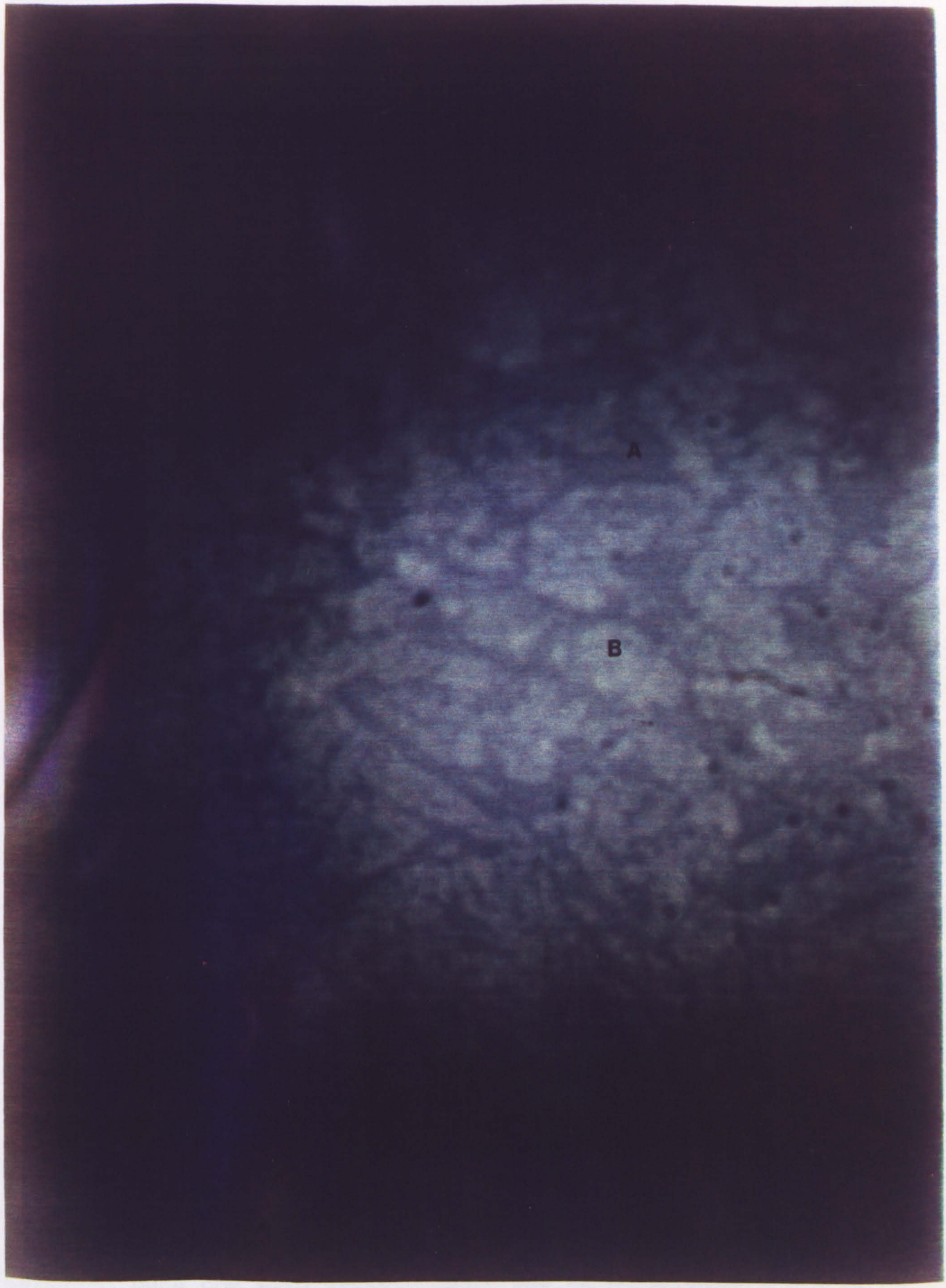

FIGURE 7.2
PRE-OCULAR TEAR FILM MARMOREAL LIPID PATTERN
ORIGINAL MAGNIFICATION (X32)
PHOTOGRAPH MAGNIFICATION (APPROX 300)

higher magnification photograph (Fig 7.2) shows the marble-like pattern in greater detail.

The intricacies of the superficial meshwork can readily be seen. The darker patches are not isolated but linked by stretched connecting lines giving it the fragile appearance of a very thin lipid layer.

B) Contaminated marmoreal pattern

The contaminated marmoreal pattern (Fig 7.3) has an appearance similar to the normal pattern described above, with darker grey lines over a lighter background. The much tighter meshwork appearance is produced by a thicker lipid layer which achieved coverage without stretching. In addition, a number of particles are seen in focus and are floating within the lipid layer. These particles are of various origins: atmospheric debris (Arrow A), epithelial cells (Arrow B) and most commonly mucous dots or strands (Arrow C) that are migrating from the basal mucin layers towards the canthi. At the bottom of the picture a small depression of the tear film is visible.

Contamination of the lipid layer by mucous strands is commonly observed after localised disruption of the mucous layer and interruption of the normal secretion process following contact lens removal or eye rubbing.

C) Flow pattern

The flow pattern (Fig 7.4) has an almost smooth streak-like structure of bright appearance. Here the wavy pattern described is continuously migrating even several seconds after a blink. Only in a small area, at the right of the picture, is a meshwork-like

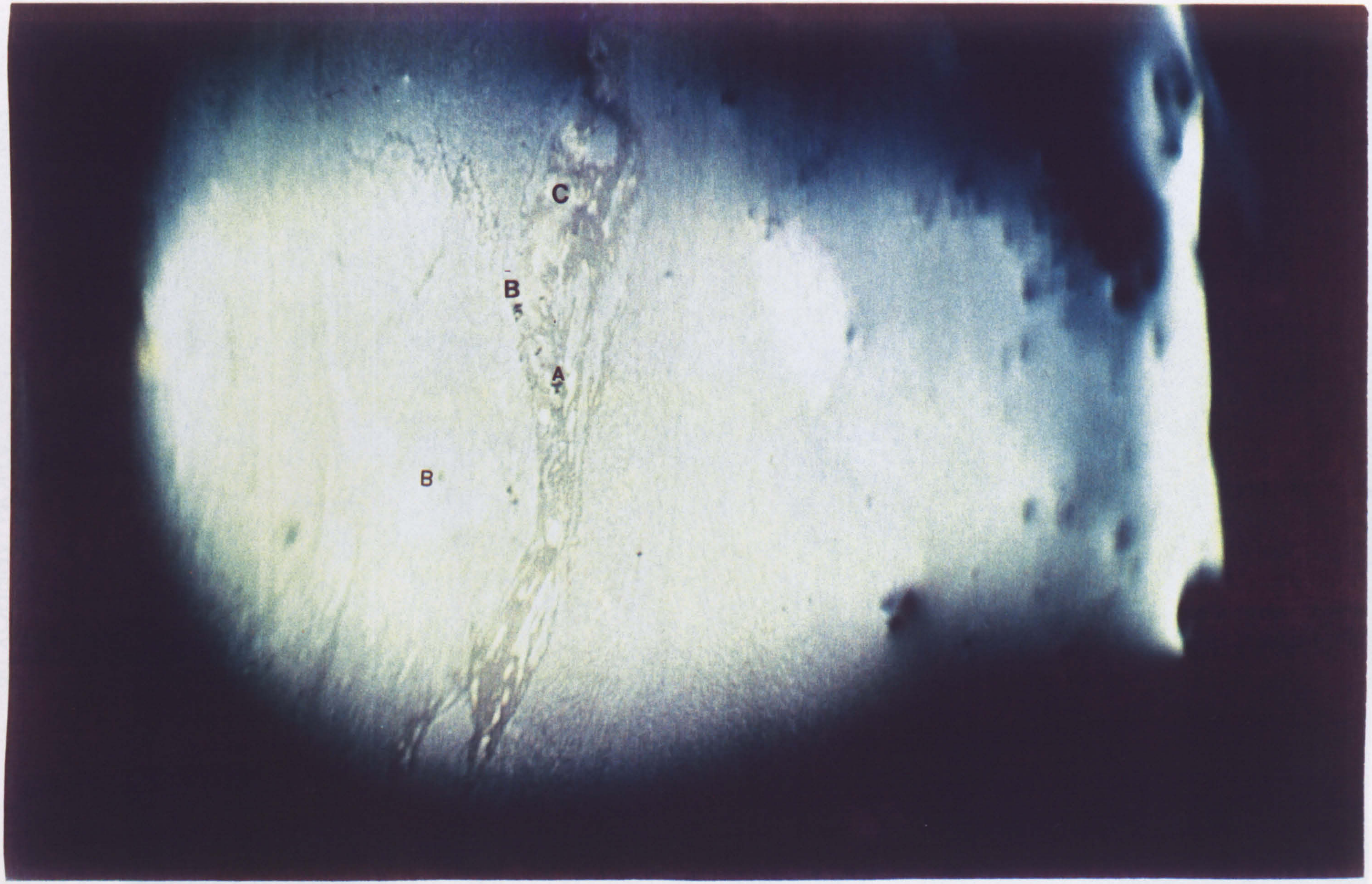

FIGURE 7.3
PRE-OCULAR TEAR FILM CONTAMINATED LIPID PATTERN
ORIGINAL MAGNIFICATION (X9.6) PHOTOGRAPH MAGNIFICATION (APPROX 95)

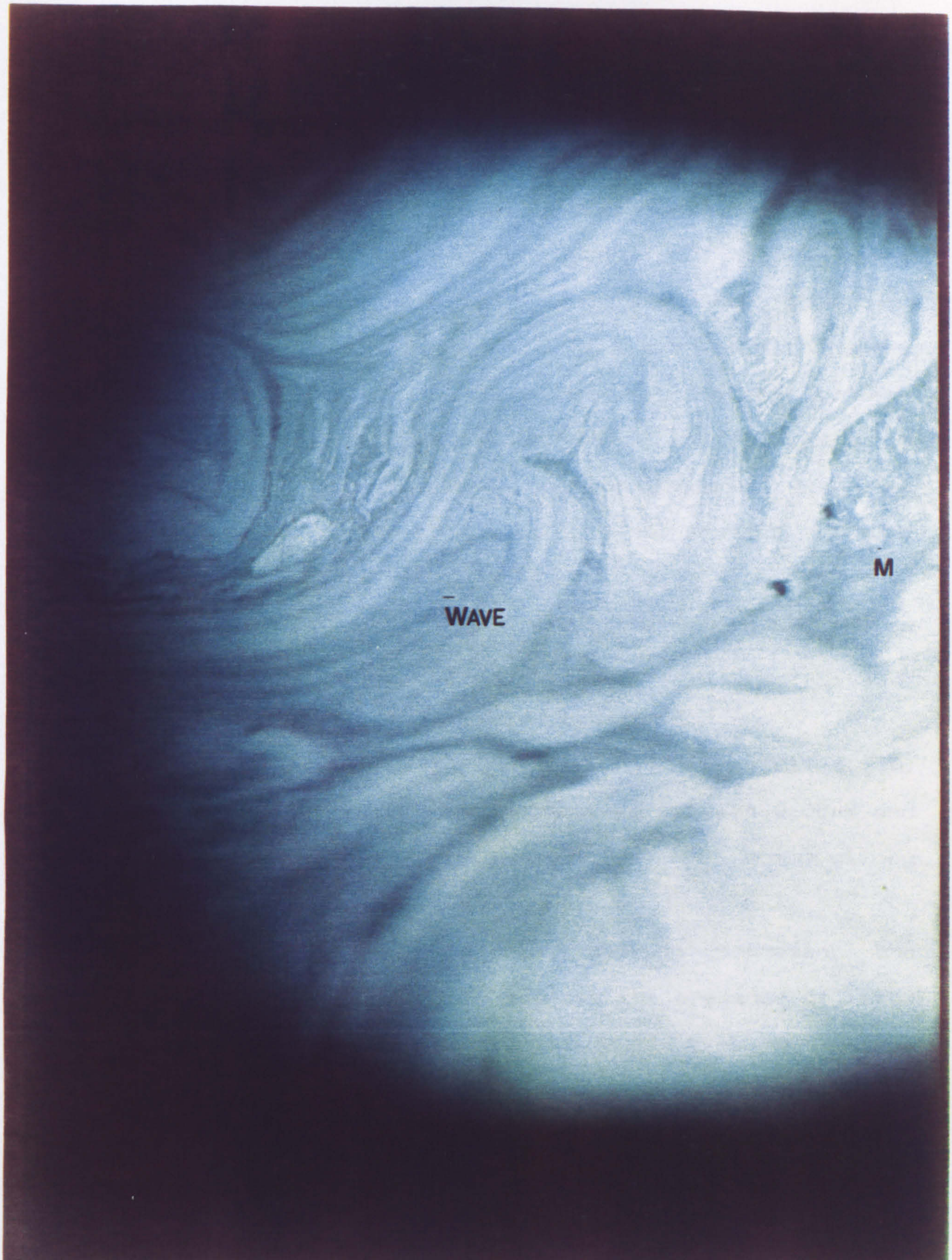

FIGURE 7.4
PRE-OCULAR TEAR FILM FLOW LIPID PATTERN
ORIGINAL MAGNIFICATION (X9.6)
PHOTOGRAPH MAGNIFICATION (APPROX 95)

appearance present (M). The intricate convolutions represent a flow occurring freely at the surface as opposed to the linked structure of the marbled pattern.

D) Amorphous pattern

The amorphous pattern (Fig 7.5) has a grey-bluish appearance with no discernible structure whatsoever. As the volume of lipid available increases it produces a full and even coverage of the tear surface and looses its meshwork appearance. This occurs at a greater layer thickness than in the marmoreal and wave pattern but as no interface colours are present, it must be below 0.086μm.

On the right of the picture the minute depression is the start of a dry formation.

E) Coloured fringe pattern

The coloured fringe pattern (Fig 7.6) is visible with tear film thicknesses between 0.08μm and 0.37μm. The coloured appearance is produced by destructive interference.

When this coloured fringe pattern is present, the eye being fully opened, it denotes the presence of large amounts of lipids. The whitish even background corresponds to a thickness of around 0.08μm (Table 6.1A). The light brown haze is for a thickness between 0.09μm and 0.14μm. It coalesces with the purple at 0.19μm and the sky blue at 0.22μm at the top of the picture. The yellow and purple are interference colours of the second order with thicknesses of 0.30μm and 0.37μm respectively. It is necessary to differentiate between the case of a

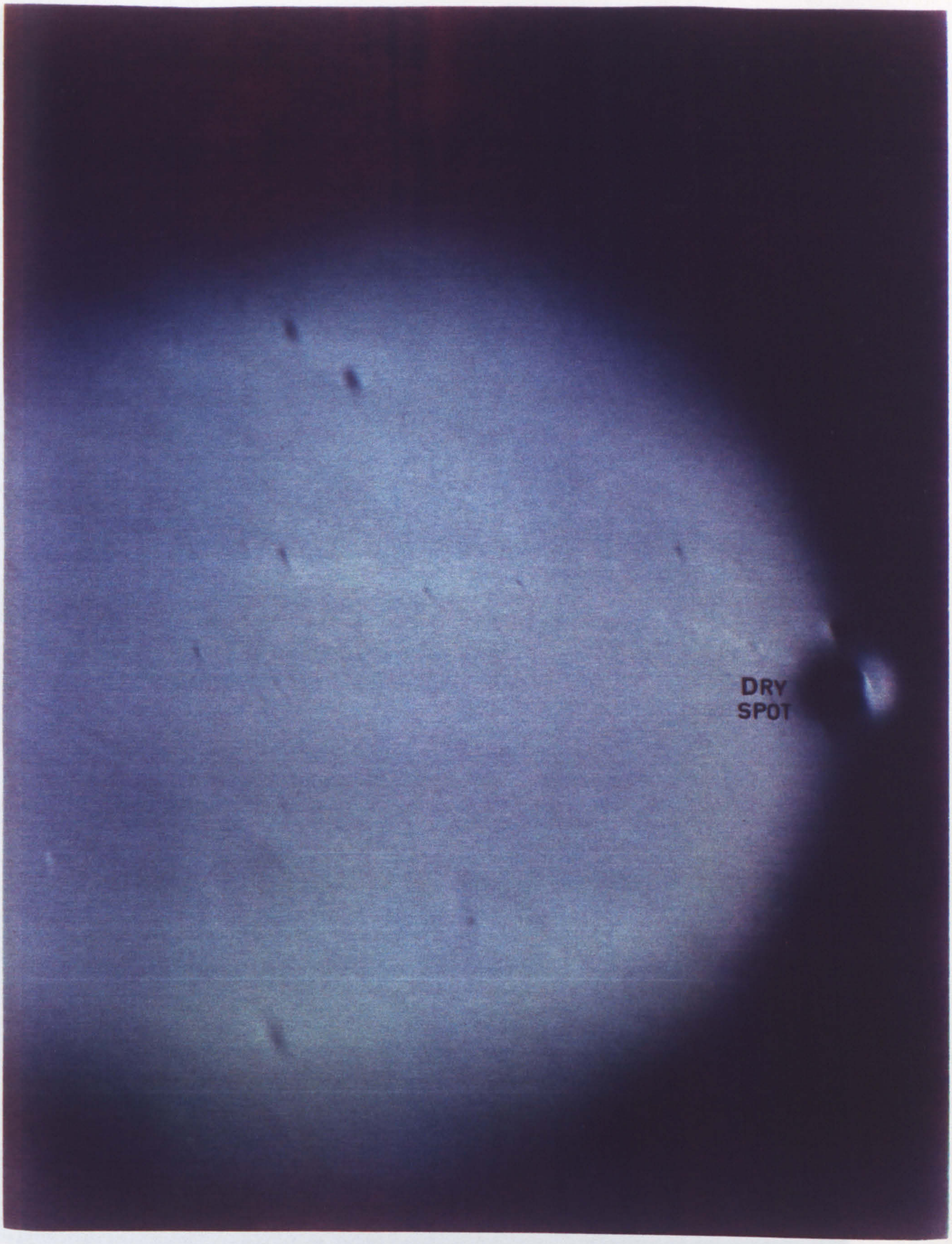

FIGURE 7.5
PRE-OCULAR TEAR FILM AMORPHOUS LIPID PATTERN
ORIGINAL MAGNIFICATION (X9.6)
PHOTOGRAPH MAGNIFICATION (APPROX 95)

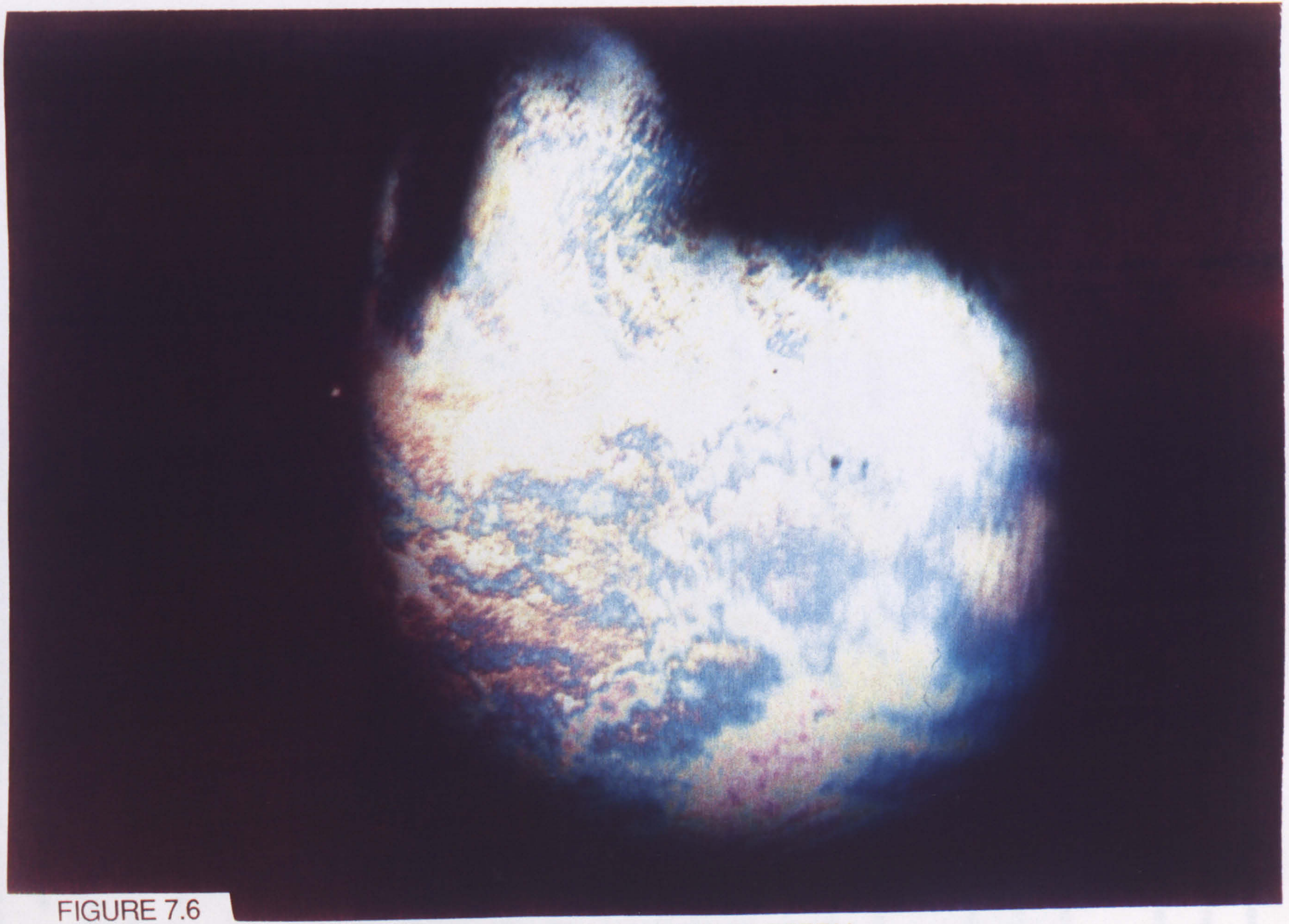

FIGURE 7.6
PRE-OCULAR TEAR FILM COLOURED FRINGE LIPID PATTERN
ORIGINAL MAGNIFICATION (X9.6) PHOTOGRAPH MAGNIFICATION (APPROX 95)

normal, very stable thick and trouble free lipid layer and an abnormal, unstable and problematic layer resulting from Meibomian gland over-secretion and present in cases of chronic blepharitis.

In the former case (Fig 7.6) the interference colours are spread evenly over large areas and are confined mainly to the first few colours; yellow, brown and blue.

In the latter case the appearance is characterised by a multitude of clumps of lipids, unevenly distributed with a large lipid thickness variation occurring around each clump - where interference colours of 2nd and 3rd order (up to 0.6µm) may be visible within an extremely small area.

b) Overall pre-corneal lipid pattern

Very often more than one lipid pattern is observable over the whole cornea when the low magnification system is used. In theory, any two or more individual patterns could be found to cover the cornea. However, clinically two combinations are mainly found, the tendency being for layers of similar thickness to combine.

A) Combination 1 (Figure 7.7)

Quite commonly patients are seen with a main marmoreal pattern, (here the upper part of the photograph Area A) in combination with a flow pattern (main part of the photograph Area B). The lipid layer is seen in detail against the even white background produced by the illuminated hemispheric cup. The black area at

FIGURE 7.7
PRE-OCULAR TEAR FILM LIPID PATTERN COMBINATION 1
ORIGINAL MAGNIFICATION (X2)
PHOTOGRAPH MAGNIFICATION (APPROX 20)

the centre represents the observation hole where lipid coverage cannot be visualised.

B) Combination 2 (Figure 7.8)

The second combination often found is an amorphous pattern (Area A) and a coloured fringe pattern (Area B). Here the interference colours are of the first order yellow and brown and occasionally blue which corresponds to lipid layer thicknesses of 0.09µm, 0.14µm and 0.22µm. The coloured areas are scattered and isolated and most of the layer has a thickness just below 0.09µm (white).

iii) Abnormal Lipid Patterns

Two abnormal lipid layers are described and were photographed with 25 ASA black and white film to obtain a higher magnification by photographic enlargement without loss of details.

a) Lipid clumping (Figure 7.9)

In some instances newly secreted lipids fail to spread after blink, and mix with the underlying lipid film but take the form of numerous clumps that migrate towards the upper part of the cornea. The clumps appear as discrete dark spots (Area A) over a lighter background. The lipid clumping effect occurs in areas where the meshwork appearance is absent and is never present over the whole of the surface. When the lipid layer is stretched with increased palpebral aperture, the clumps move independently from the lighter grey background.

This abnormal lipid pattern is often initially encountered after the instillation of benzalchromium

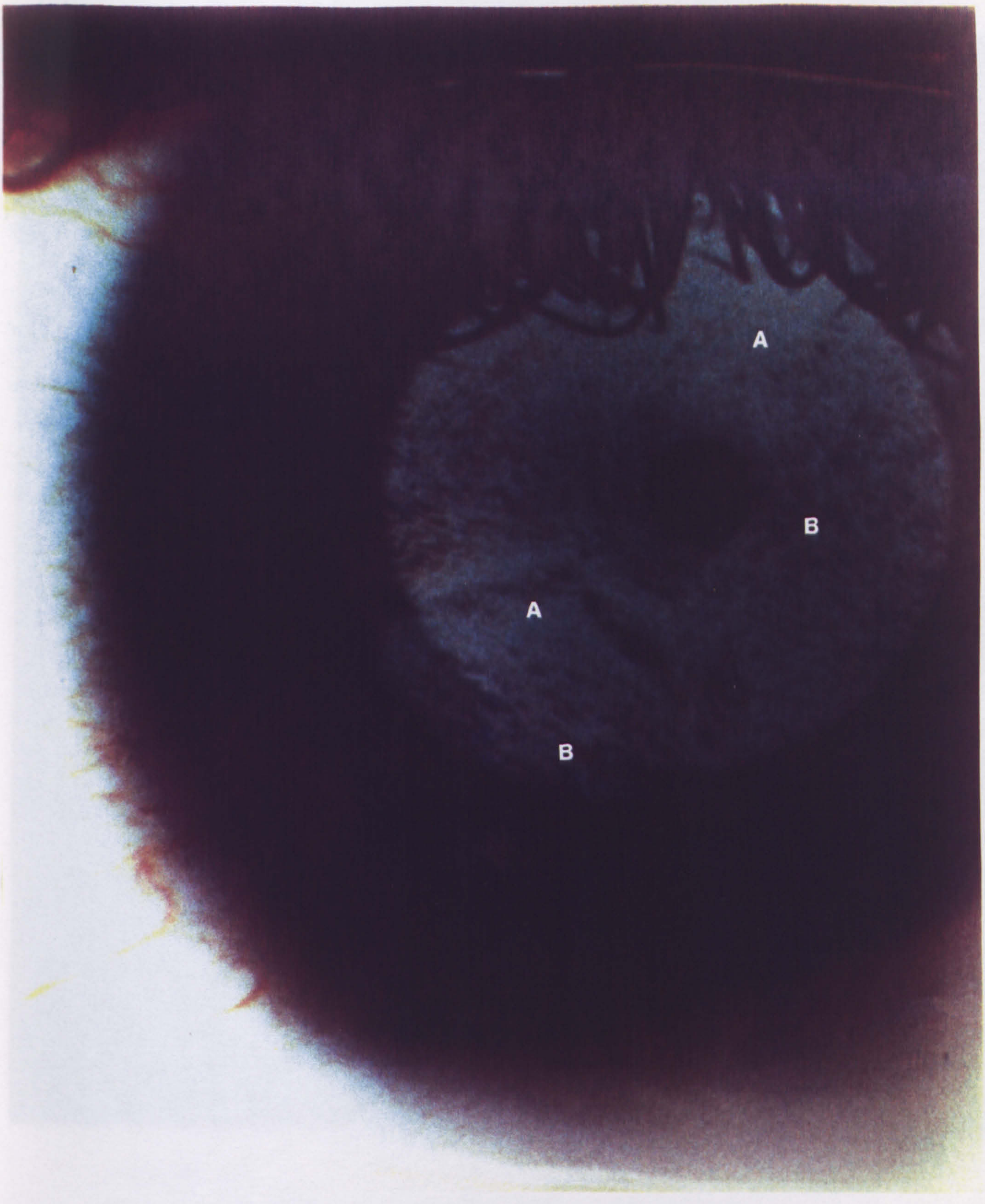

FIGURE 7.8
PRE-OCULAR TEAR FILM LIPID PATTERN COMBINATION 2:
ORIGINAL MAGNIFICATION (X2)
PHOTOGRAPH MAGNIFICATION (APPROX 20)

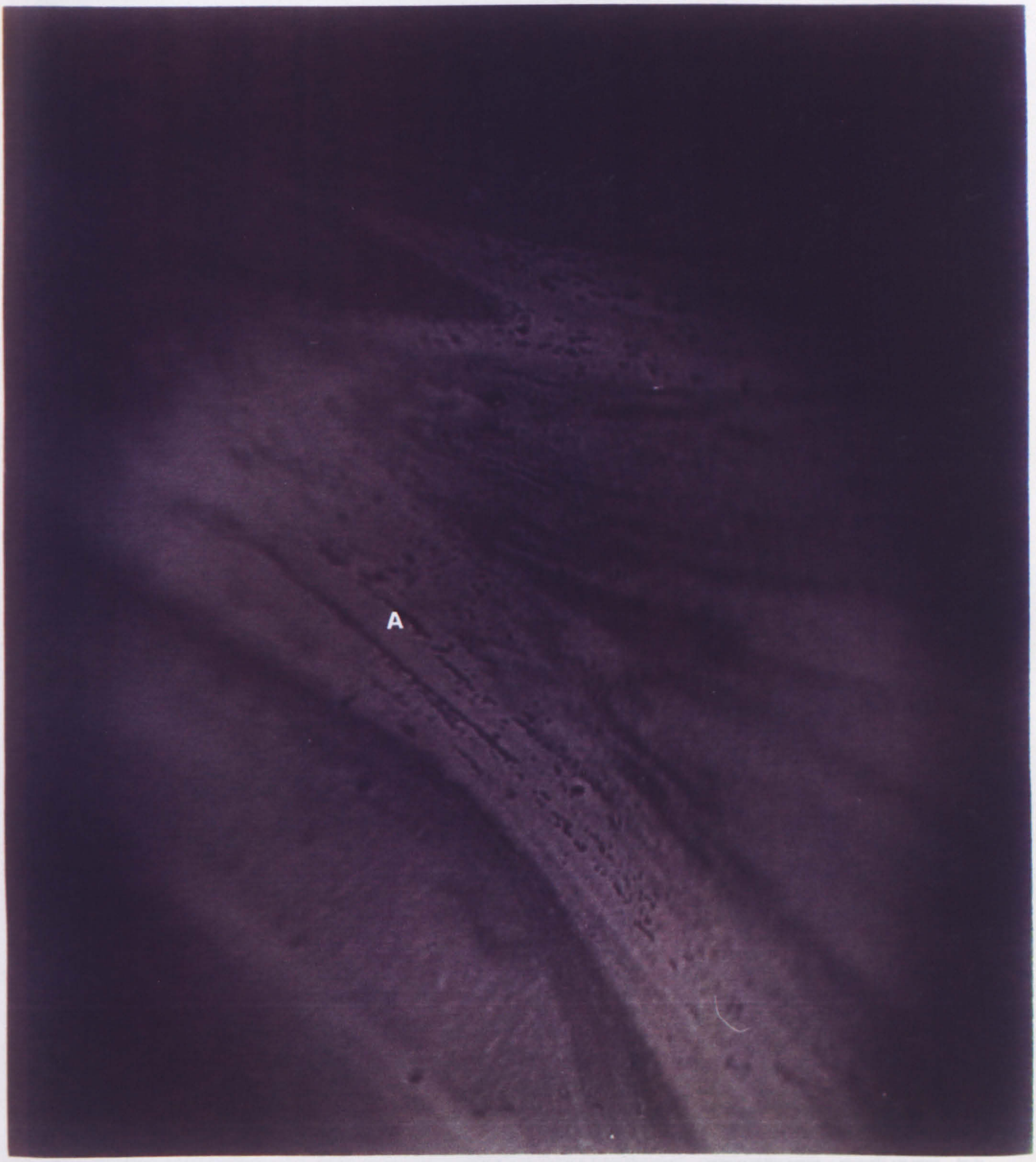

FIGURE 7.9
PRE-OCULAR TEAR FILM ABNORMAL LIPID CLUMPING
ORIGINAL MAGNIFICATION (X9.6)
PHOTOGRAPH MAGNIFICATION (APPROX 200)

chloride containing eyedrops. But with eyedrops the situation returns to normal after a few blinks. At the opposite, in the case of the unaltered pre-ocular tear film mixing does not take place with time.

b) Localised lipid layer break-up

In the normal case the tear film break up involves both the lipid and aqueous layer following the instability created at the lower mucin layer. In the case illustrated here (Fig 7.10) the break-up is initiated at the level of the lipid layer and is localised (Areas A and B).

iv) Lipid Layer Pattern with Reduced Palpebral Aperture (Figures 7.11, 7.12 and 7.13)

The photographs show the changes in lipid layer appearance when the eye lids are slowly shut in a controlled manner.

The picture in Fig 7.11 was taken with the eyes half closed. The mainly brownish background indicates a thickness of 0.14μm at the centre. The nature of the numerous dark spots floating at the surface is difficult to ascertain but their number increased with eye closure. The lower tear meniscus is visible at the bottom of the picture.

The picture in Fig 7.12 contains the upper and lower tear meniscus with a palpebral aperture reduced to around 3mm. A full lipid coverage is present even over the area of the 'black line' at the base of the meniscus. Near the top of the photograph the compression of the

FIGURE 7.10
PRE-OCULAR TEAR FILM LOCALISED LIPID BREAK-UP
ORIGINAL MAGNIFICATION (X9.6)
PHOTOGRAPH MAGNIFICATION (APPROX 200)

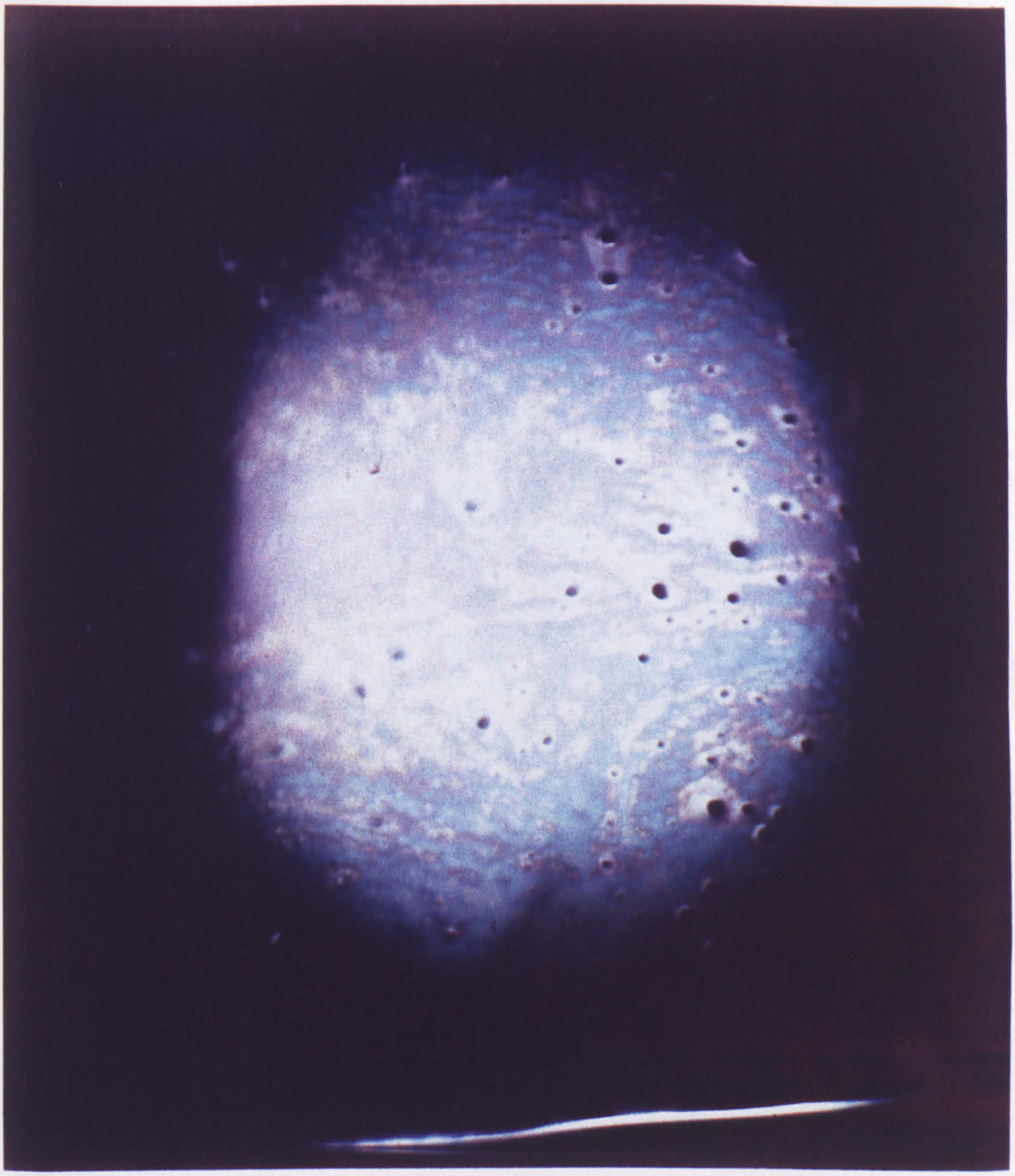

FIGURE 7.11
PRE-OCULAR TEAR FILM LIPID PATTERN CHANGE
WITH REDUCED LID APERTURE: OPEN EYE
ORIGINAL MAGNIFICATION (X9.6)
PHOTOGRAPH MAGNIFICATION (APPROX 95)

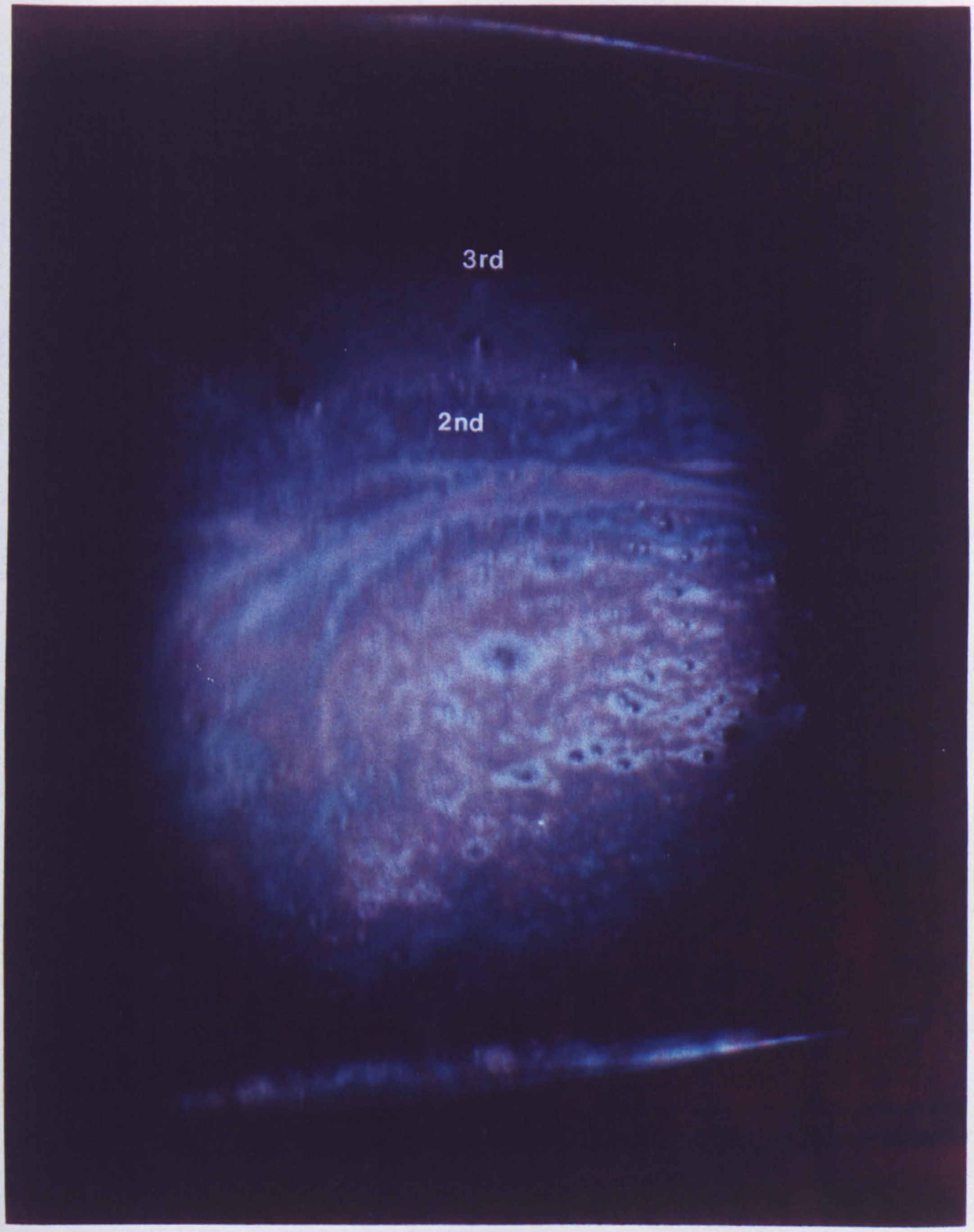

FIGURE 7.12
PRE-OCULAR TEAR FILM LIPID PATTERN CHANGE :
WITH REDUCED LID APERTURE
PARTIAL LID CLOSURE PHASE 1

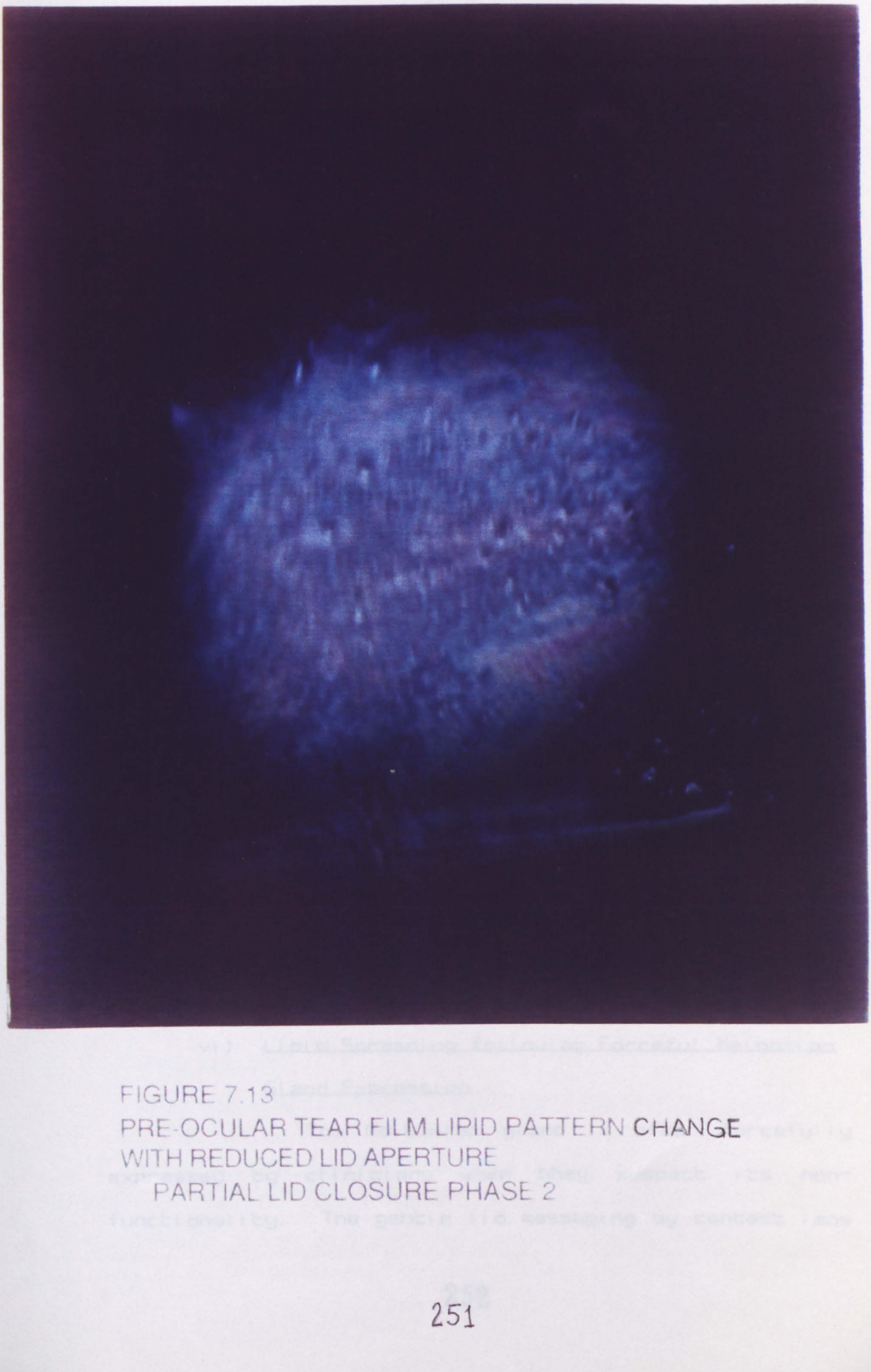

FIGURE 7.13
PRE-OCULAR TEAR FILM LIPID PATTERN CHANGE
WITH REDUCED LID APERTURE
PARTIAL LID CLOSURE PHASE 2

lipid layer produces interference colours of the 2nd order of interference (green - 0.42µm) and 3rd order (pink - 0.5µn).

The order of interference increases as the lids are shutting. With the palpebral aperture down to around 1.5mm the increase in lipid layer thickness is seen as blueish background. This thickening continues until the lids are closed. The group of photographs showed the presence of a lipid film with a constantly increasing thickness and its corresponding interference colours.

v) Sequential Analysis of Lipid Spreading

A series of three photographs depicts the spreading sequence following normal Meibomian gland secretion from a singie gland orifice. The photographs were taken immediately after secretion (Fig 7.14) after one (Fig 7.15) and two blinks (Fig 7.16). The main lipid layer thickness is around 0.09µm. The secretion is restricted to the blue area (near the lid margin) but this colour corresponds to the combined thickness of the background lipid and the new secretion. The extra thickness is approximately 0.19µm and is limited to a very small area. The consecutive blink produces a thinning of that zone and disappearance of the interface colours.

vi) Lipid Spreading following Forceful Meibomian Gland Expression

The Meibomian gland is often forcefully expressed by clinicians when they suspect its non-functionality. The gentle lid massaging by contact lens

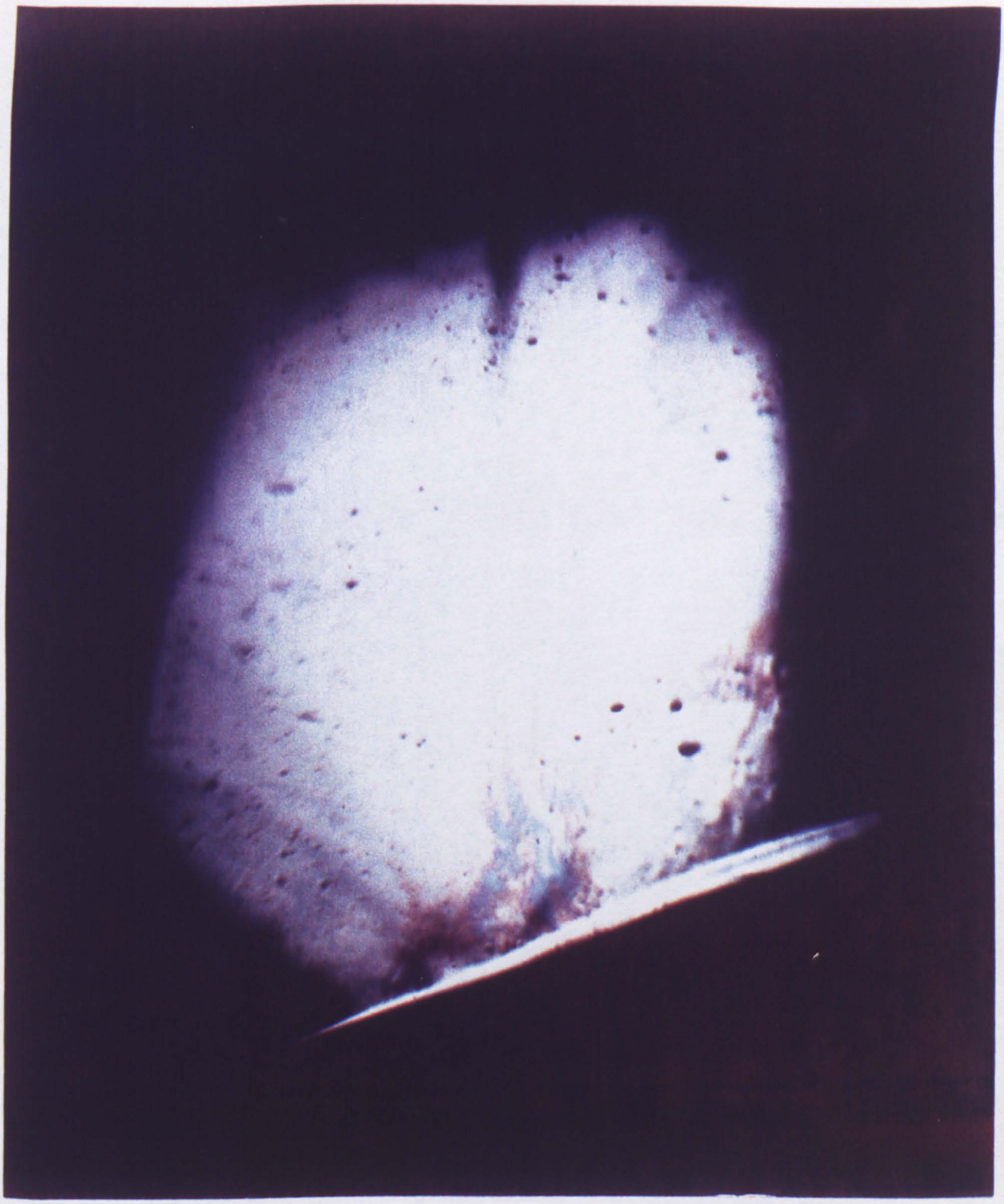

FIGURE 7.14
PRE-OCULAR TEAR FILM LIPID SPREADING SEQUENCE
IMMEDIATELY AFTER SECRETION
ORIGINAL MAGNIFICATION (X9.6)
PHOTOGRAPH MAGNIFICATION (APPROX 95)

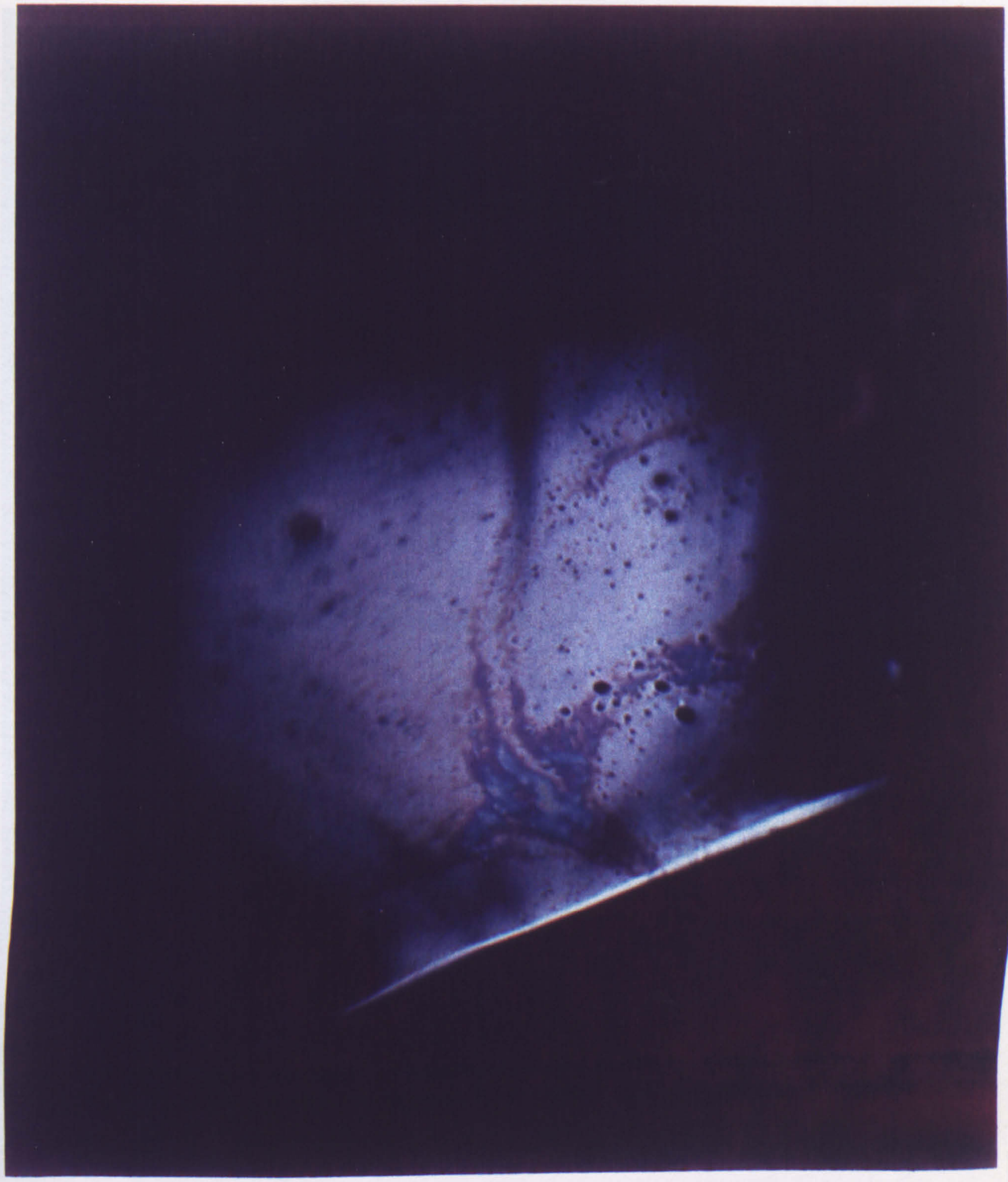

FIGURE 7.15
PRE-OCULAR TEAR FILM LIPID SPREADING SEQUENCE
1 BLINK AFTER SECRETION
ORIGINAL MAGNIFICATION (X9.6)
PHOTOGRAPH MAGNIFICATION (APPROX 95)

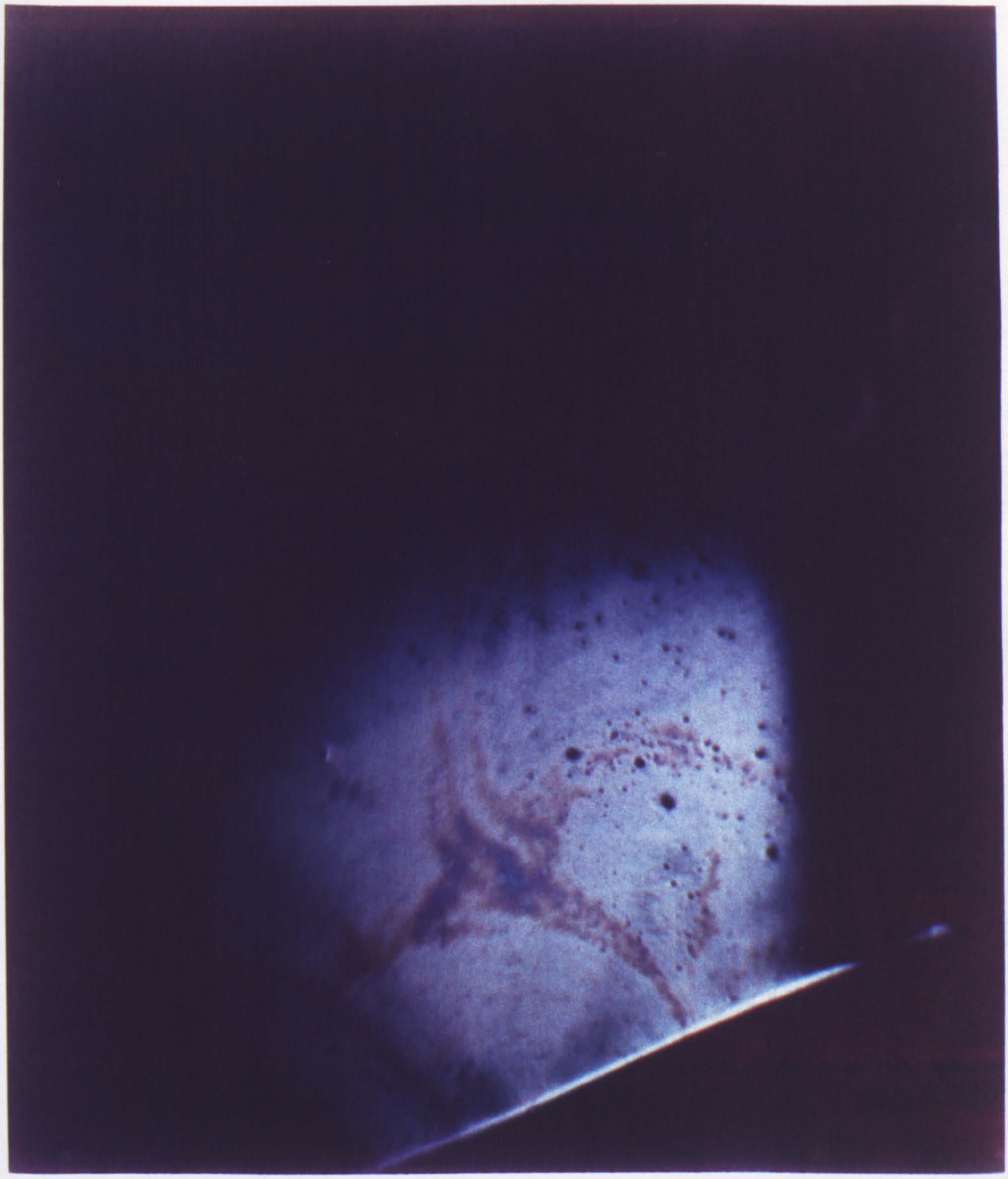

FIGURE 7.16
PRE-OCULAR TEAR FILM LIPID SPREADING SEQUENCE
2 BLINKS AFTER SECRETION
ORIGINAL MAGNIFICATION (X9.6)
PHOTOGRAPH MAGNIFICATION (APPROX 95)

wearers or the action of the eye rubbing will also express certain amount of Meibomian secretion.

In such a case, a phenomenon similar to the normal tear spreading takes place. However, the pattern observed (Fig 7.17) differs on several points. The volume expressed is greater than with a normal secretion, hence the expressed lipid layer is thicker; here the lower lid was pressed three times producing the three distinctive waves of lipid visible on the photograph. Colour density thicknesses of up to 0.4µm and numerous black spots are present in the area where the secretion is spreading. Few blinks will be necessary to distribute this new quantity of lipid over the whole of the POTF as it mixes with the remainder of the lipid layer, its distinctive interface colours will dissipate and merge with the background lipid.

vii) Eye Drop Instillation

Artificial tears have been used extensively to relieve dry eye symptoms, whatever the origin of the underlying conditions.

However, in all cases initially the lipid layer breaks up (Fig 7.18 grey area) and it takes 2 to 3 blinks for that layer to reform. The metallic grey at the top of the photograph represents the area where the lipid layer is absent and where the light reaching the aqueous surface is not reflected but undergoes a phase change of $\lambda/2$. It is only when the artificial tears have mixed to the normal tear film that the beneficial effects of these eye drops take place.

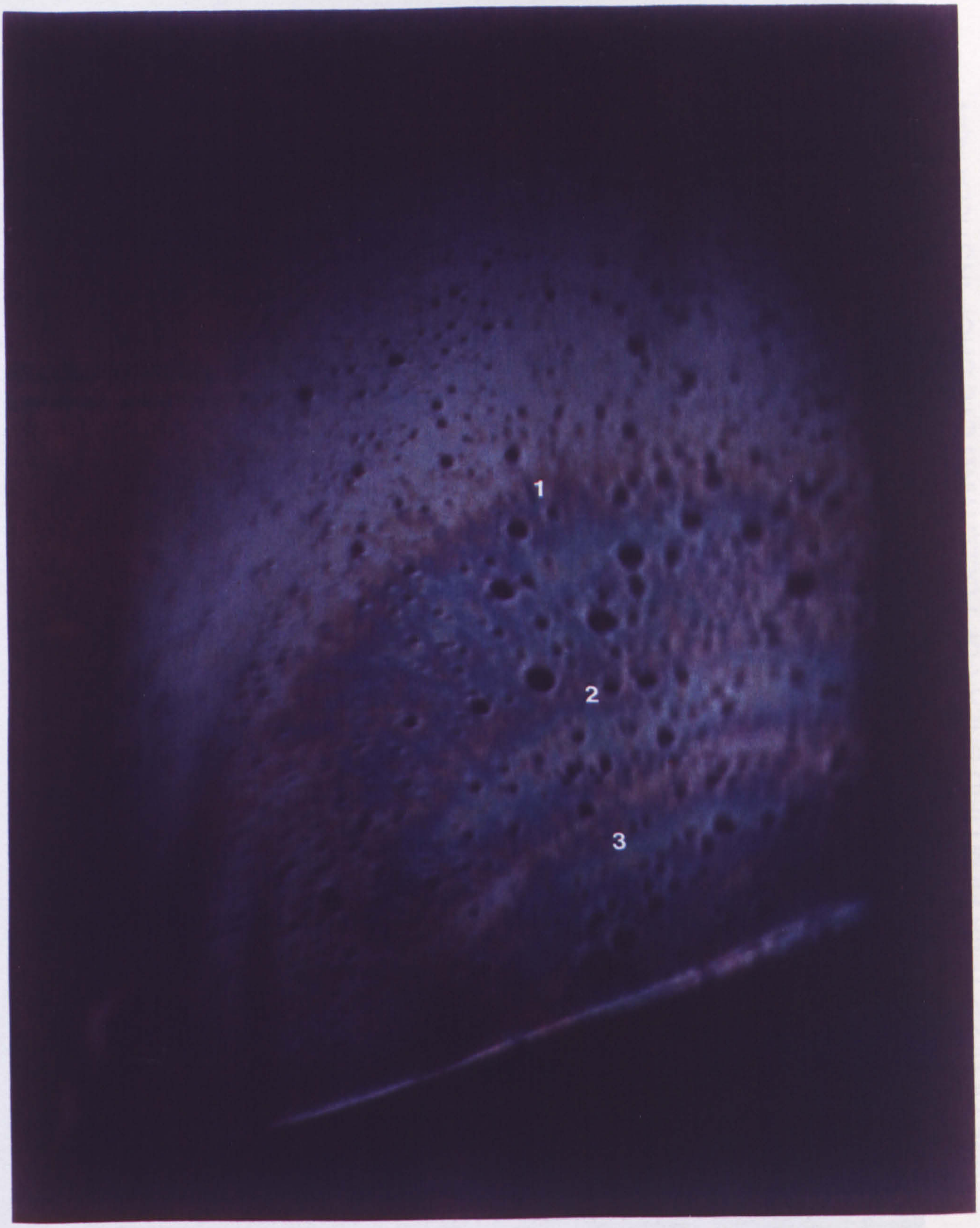

FIGURE 7.17
PRE-OCULAR TEAR FILM LIPID SPREADING FOLLOWING FORCEFUL MEIBOMIAN GLAND EXPRESSION
ORIGINAL MAGNIFICATION (X9.6)
PHOTOGRAPH MAGNIFICATION (APPROX 95)

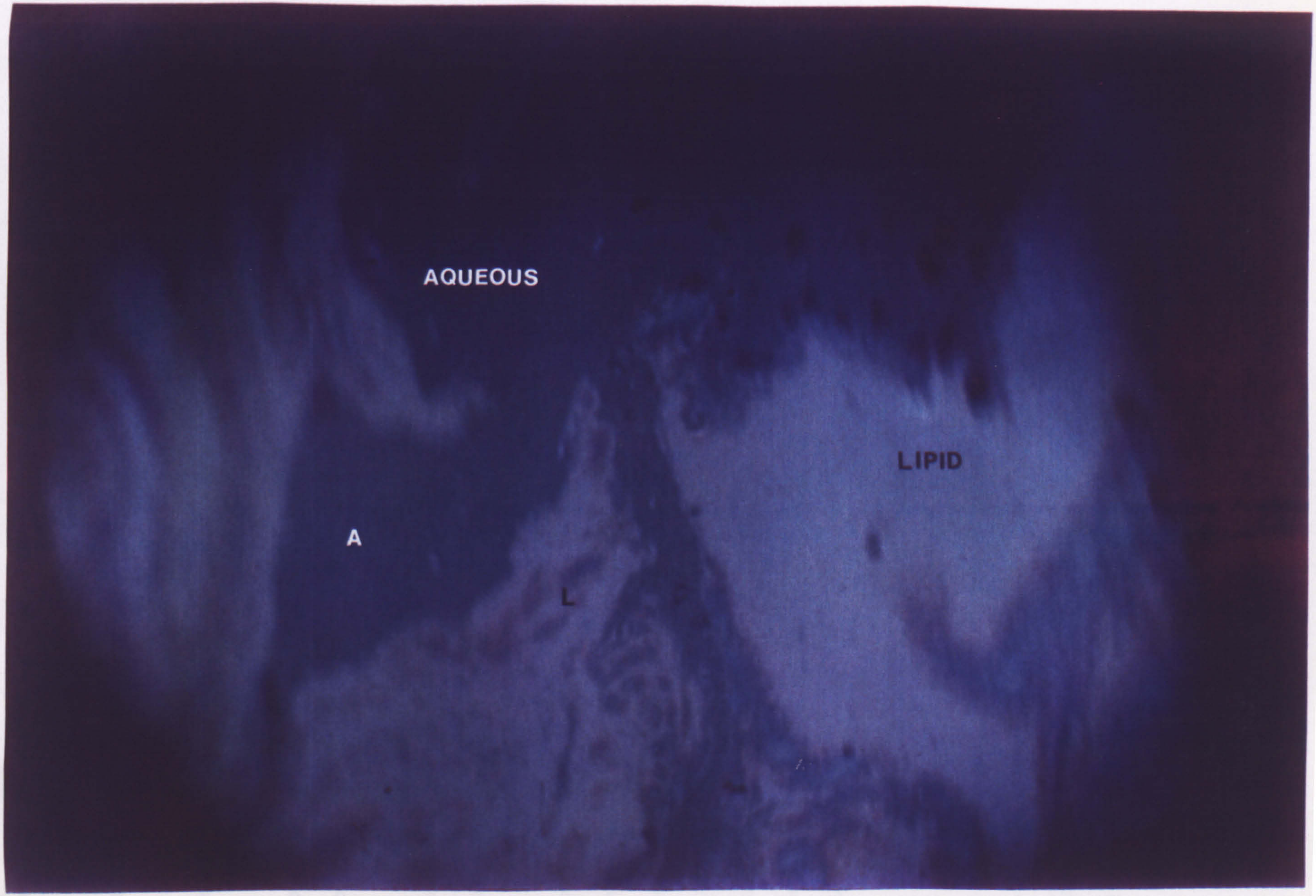

FIGURE 7.18
PRE-OCULAR TEAR FILM LIPID BREAK-UP FOLLOWING EYE DROP INSTILLATION
ORIGINAL MAGNIFICATION (X9.6) PHOTOGRAPH MAGNIFICATION (APPROX 95)

7.2 EXPERIMENTAL STUDY 2: PRE-SOFT LENS TEAR FILM

7.2.1 INTRODUCTION

The techniques used to study the pre-ocular tear film are also employed to study the pre-soft lens tear film. However, under certain conditions both the lipid and aqueous layers are sometimes visible.

7.2.2 MATERIAL AND METHOD

All reported observations of the pre-soft lens tear film have been carried out on established, asymptomatic soft contact lens patients. In some cases, photographs were taken while in others the observations were just recorded during a routine contact lens aftercare. These observations were a part of our evaluation of the application of the techniques described to the normal clinic environment.

As for the pre-ocular tear film, the photographs and observations were made approximately two seconds after eye opening, following a normal blink.

The photographic conditions for both high and low magnifications were described in Section 7.1.2. iii), for the pre-ocular tear film.

Several aspects were considered and are reported as follows:-

- description of the lipid patterns normally present at the front surface of soft lens.

- spreading sequence of the pre-soft lens lipid layer and its influence on the visibility of the aqueous layer.

7.2.3 RESULTS

i) Normal Pre-Soft Lens Lipid and Aqueous Layers

A thin lipid layer is usually present at the front of soft lenses. Similarly to the pre-ocular tear film, the low magnification photographic method reveals a combination of patterns. The individual patterns most commonly encountered are a thin marmoreal or flow pattern (Fig 7.19). In Fig 7.19 the edge of the well centred soft contact lens is noted by its translucent appearance. The pre-lens tear film is seen against the black background of the pupil. When the iris is present in the background, it becomes difficult to view the tear film.

The lashes at the top of the pupil are a virtual image created by the tear surface acting as a spherical mirror - they appear to be directed downward and inward in opposite direction to the real lashes which are not in the picture.

This pre-lens tear film possesses a superficial lipid layer similar to that described in 7.1.3 ii) (Fig 7.7), a combination of marmoreal and wave appearance. The lack of interference colour signifies a lipid layer thickness in the region of 0.02μm to 0.09μm and that no visible interference coloured fringes are produced within the underlying aqueous phase.

These fringes only appear when the lipid layer is very thin.

A typical case is illustrated (Fig 7.20) and under high magnification; a marmoreal main lipid pattern (Arrow A), nearly invisible under low magnification, and beneath it a succession of blue and red coloured waves of

FIGURE 7.19
PRE-SOFT LENS TEAR FILM LOW MAGNIFICATION
COMBINATION *LIPID PATTERN*
ORIGINAL MAGNIFICATION (X2)
PHOTOGRAPH MAGNIFICATION (APPROX 20)

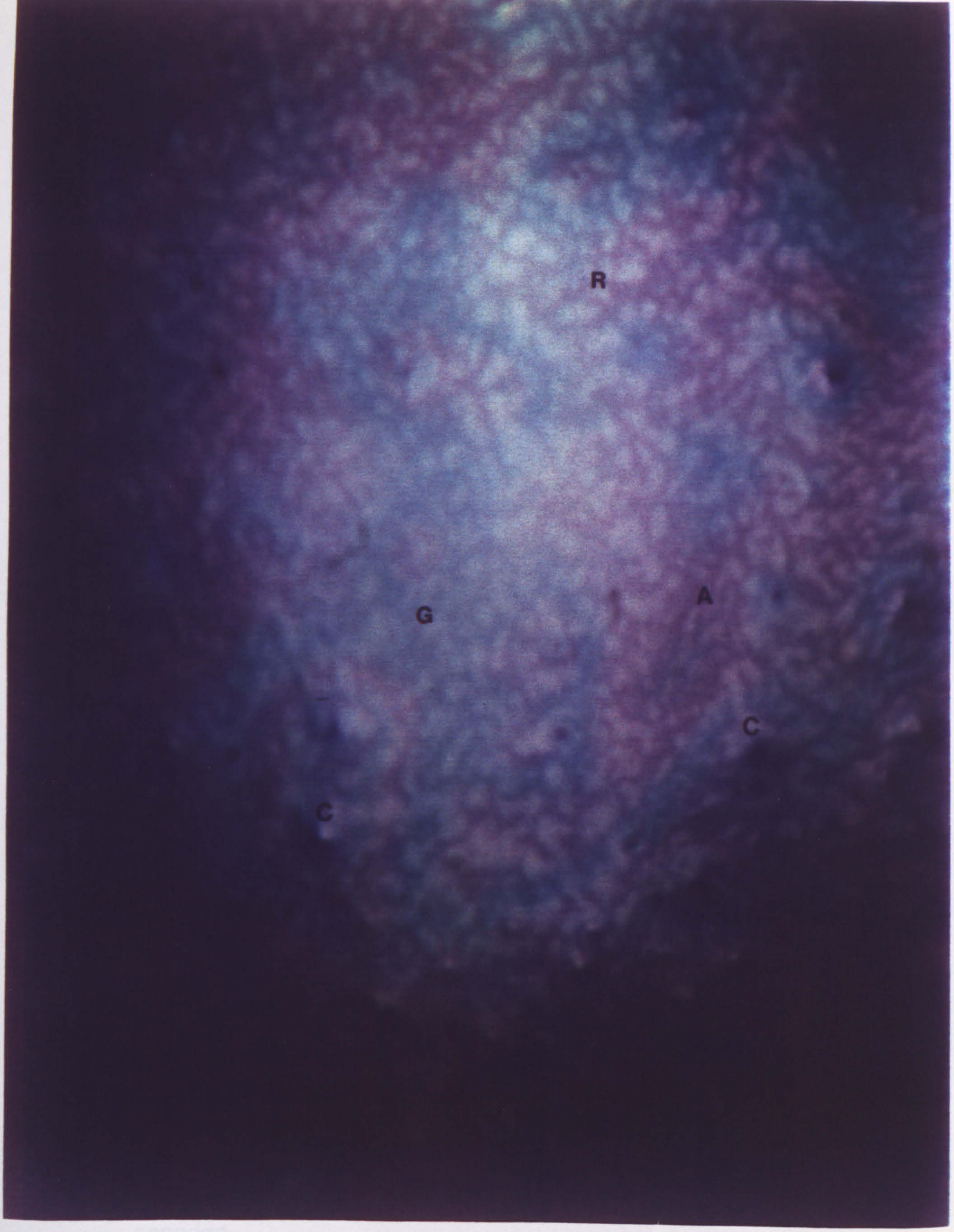

FIGURE 7.20
PRE-SOFT LENS TEAR FILM
ORIGINAL MAGNIFICATION (X32)
PHOTOGRAPH MAGNIFICATION (APPROX 300)

weak intensity. The reflectivity of that lipid layer is minimal and occurs when the layer itself is very thin, in the lower end of the range; 0.01µm to 0.02µm. These interference colours are produced by the aqueous phase, they show no precise organisation and their spread is produced by the evenness of the layer. This makes the measurement of the aqueous phase thickness difficult as it is not possible to ascertain their order of interference.

- black dots (Arrow C), which are tear film contaminants or minute surface deposits visible through the abnormally thin pre-lens tear film or mucous lumps loosely attached to the surface. A large presence of such dots is always associated with soft contact lens front surface deposit problems.

ii) <u>Localised Dry Spot Formation</u>

The photograph in Fig 7.21A and its diagrammatic outline (Fig 7.21B) depicts most of the features of a pre-soft lens tear film that can be analysed.

- the shiny narrow zone at the centre (Area A of Fig 7.21B) represents the surface of the contact lens and the centre of the dry spot.

- this is surrounded by an oblong black area (Area B of Fig 7.21B) with curved edge not covered by the tear film interference. This area represents the basal mucous coating of the contact lens from which the tear film has receded.

- Area C (of Fig 7.21B) covers the succession of interference fringes produced within the aqueous phase increasing in thickness away from the dry spot.

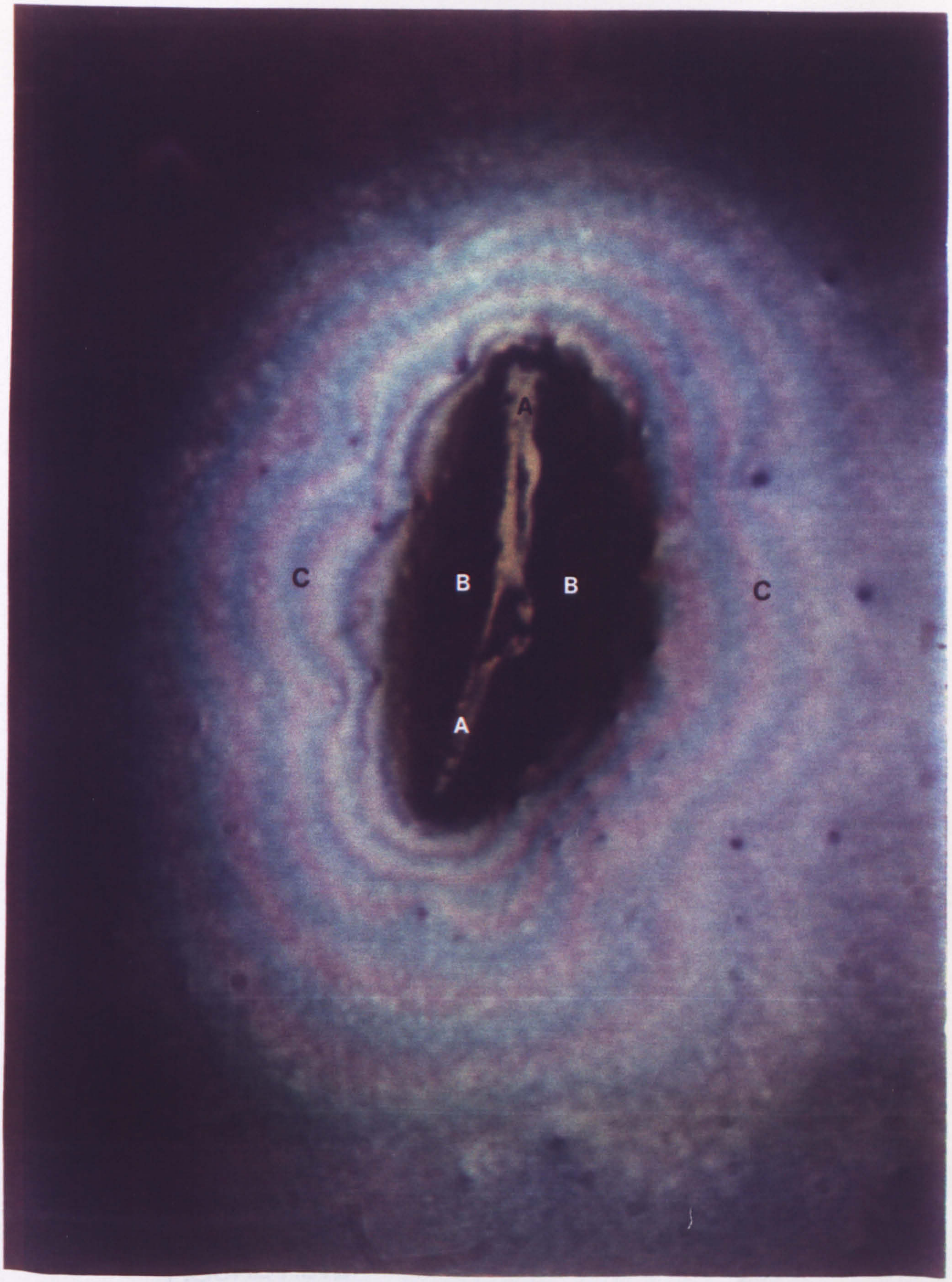

FIGURE 7.21A
PRE-SOFT LENS TEAR FILM LOCALISED DRY SPOT FORMATION
ORIGINAL MAGNIFICATION (X32)
PHOTOGRAPH MAGNIFICATION (APPROX 300)

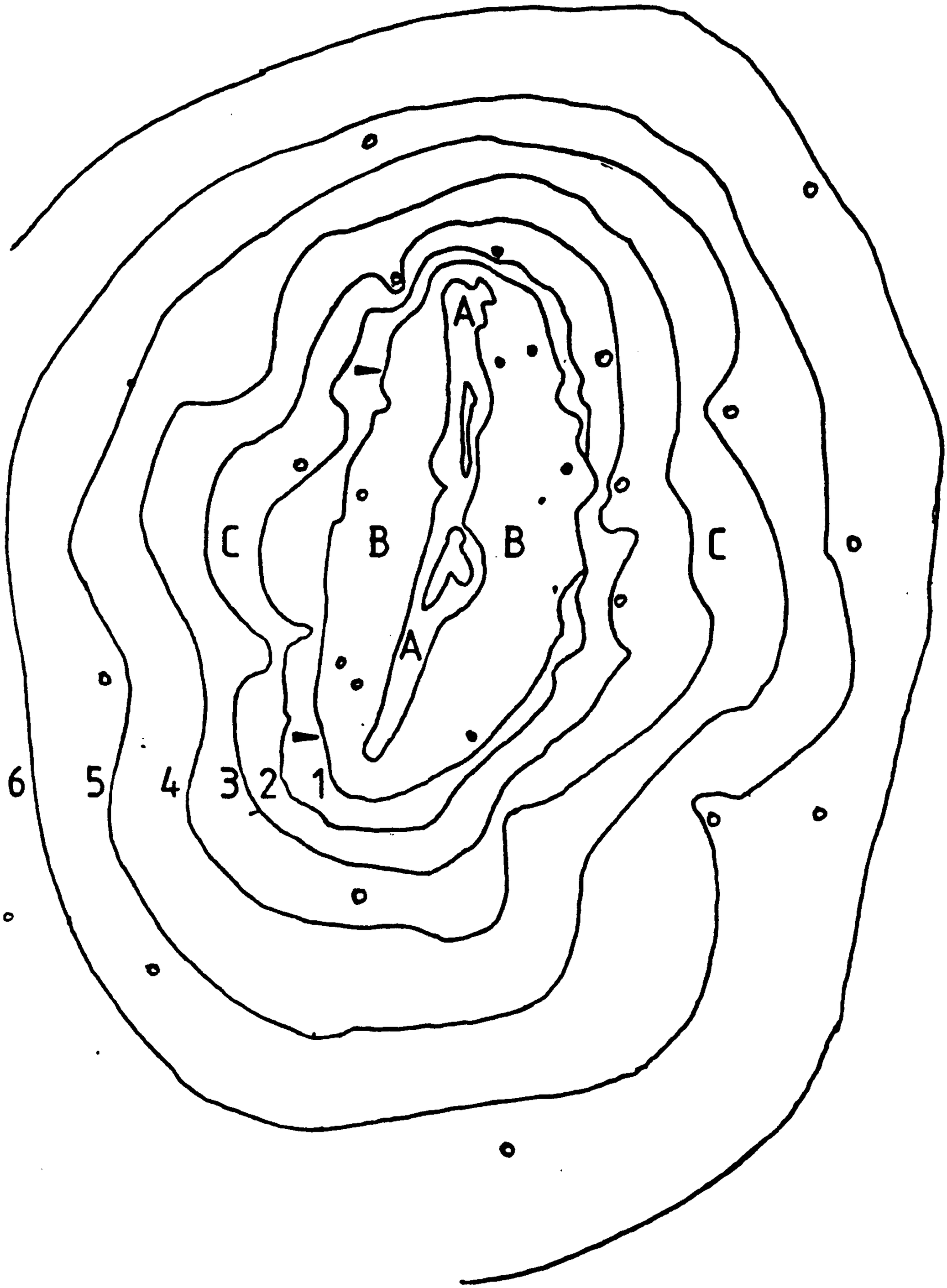

FIGURE 7.21B
DIAGRAMMATIC OUTLINE OF PRE-SOFT LENS TEAR FILM
LOCALISED DRY SPOT FORMATION
ORIGINAL MAGNIFICATION (X32)
PHOTOGRAPH MAGNIFICATION (APPROX 300)

Six orders of interference have been outlined, this corresponds to an aqueous phase range of up to 1μm in thickness. In Table 6.11, p = 5 corresponds to d5 = 0.96μm, and p = 6 gives d6 = 1.13μm.

The intensity of the fringes is much weaker than those found in the lipid layer of the pre-ocular tear film (Fig 7.6, 7.12 and 7.17) and their visibility decreases very rapidly. At the bottom and right side of the picture, a thin marmoreal superficial lipid layer is visible. Its presence diminished further the visibility of the underlying aqueous interference fringes.

The presence of dark particles is confined to the thinner part of the tear film; second order fringe = 0.26μm and third order fringe = 0.44μm. If when they are linked to the surface their diameter must be inferior to 0.5μm. Their presence in large numbers as in Fig 7.20 where they protrude at the surface suggest an aqueous phase thickness of that order. In thicker films they will be fully covered by the tear film.

7.3 EXPERIMENTAL STUDY 3. PRE-RIGID CONTACT LENS TEAR FILM

7.3.1 INTRODUCTION

The high magnification photographic technique described in Chapter 5 is applied in this study to investigate the nature and drying characteristics of the tear film formed at the front of a rigid contact lens of an established PMMA wearer. This tear film is referred

to, in the rest of this chapter as pre-lens tear film abbreviated to PLTF.

7.3.2 MATERIAL & METHOD

i) Material

The study was carried out on well adapted long term PMMA and gas permeable lens wearers free of any contact lens induced symptoms.

ii) Method

The nature of the pre-contact lens tear film was analysed as described fully in Chapter 5. For that purpose a photographic record was made two seconds after eye opening following a normal blink.

An analysis was undertaken for three different clinical situations:

- a PMMA contact lens after several hours (approximatley 4 hours) of wear to depict the normal lens in-vivo wetting characteristics.

- the same PMMA contact lens immediately upon lens insertion and after soaking in a conventional wetting solution to assess the short term in-vivo influence of a conventional (P.V.P. 0.5 percent) wetting agent.

- an identical contact lens made from a low wetting angle material to investigate whether or not a material with improved in-vitro wetting characteristics demonstrates an improved in-eye wetting properties.

In addition, in this study a series of photographs was taken at four second intervals to study the PLTF drying characteristics while the patient kept her eyes

open. Twenty seconds follow up was considered sufficient as it represents a longer time scale than the normal interblink period for contact lens wearers (Brown et al, 1973; Bier & Lowther, 1977; Hill & Carney, 1984).

iii) Photographic and Observation Conditions

The technique used to photograph the pre-rigid lens tear film is described fully in Chapter 5.

The technique used to analyse and measure the photographs is also described in Chapter 6.

7.3.3 RESULTS

i) PMMA Corneal Lens: Pre-Lens Tear Film Drying Sequence

The sequence of five photographs (Figures 7.22, 7.27, 7.30 7.32 and 7.34) illustrates the tear film drying sequence on PMMA corneal lenses. The first photograph was taken two seconds after a blink, and the series spans the following 16 seconds. In order to facilitate interpretation and measurement of these photographs, a diagram representing the different orders of interference was traced from each photograph as described in Section Chapter 5.

The following is a description of the successive photographs.

a) Drying Sequence Phase I

The PMMA lens tear film drying pattern, 2 seconds post blink, is illustrated on Figure 7.22 and on the fringes observed outlined in Figure 7.23.

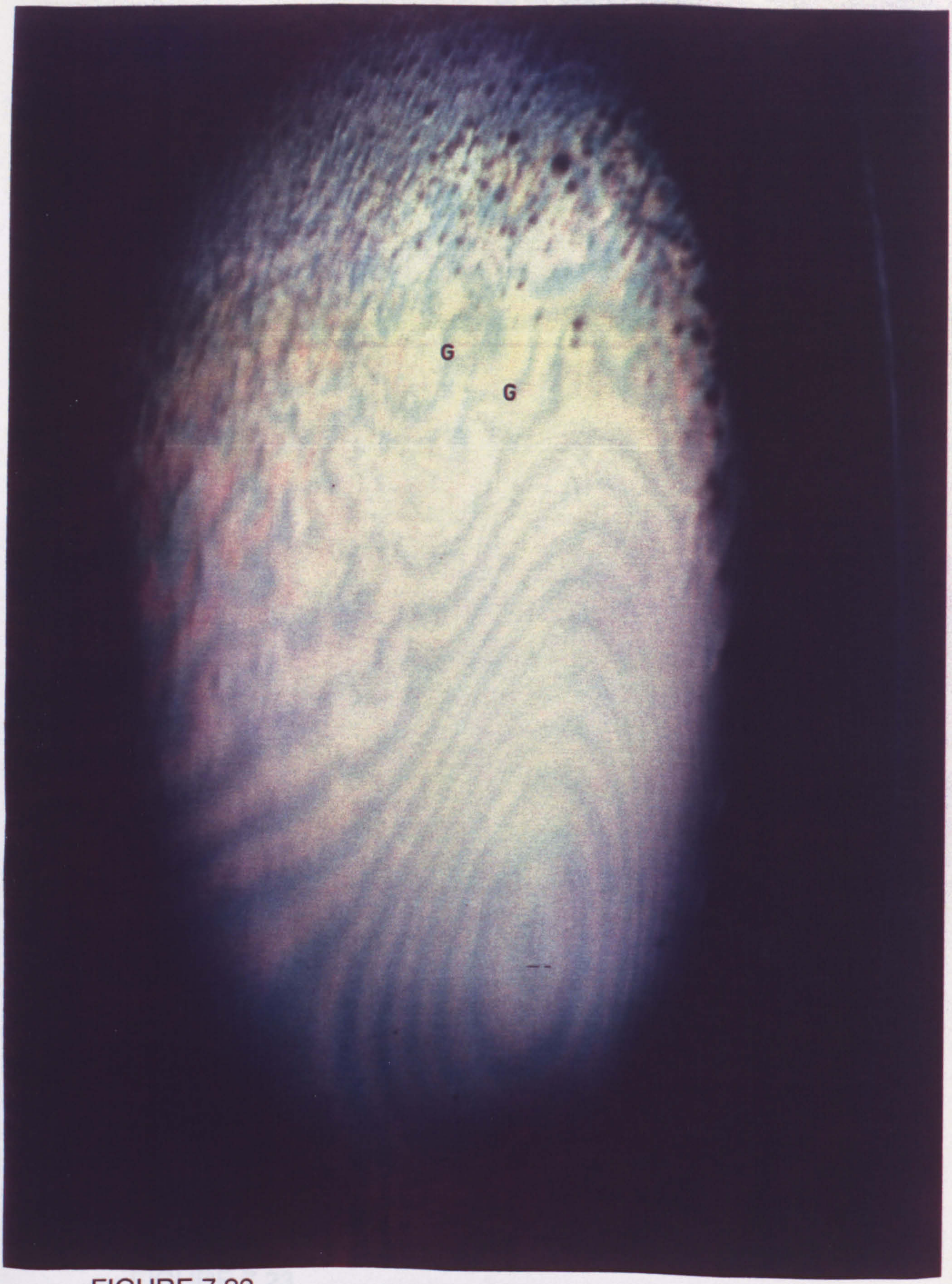

FIGURE 7.22
PRE-PMMA LENS TEAR FILM DRYING SEQUENCE PHASE 1:
2 SECOND POST BLINK
ORIGINAL MAGNIFICATION (X9.6)
PHOTOGRAPH MAGNIFICATION (APPROX 95)

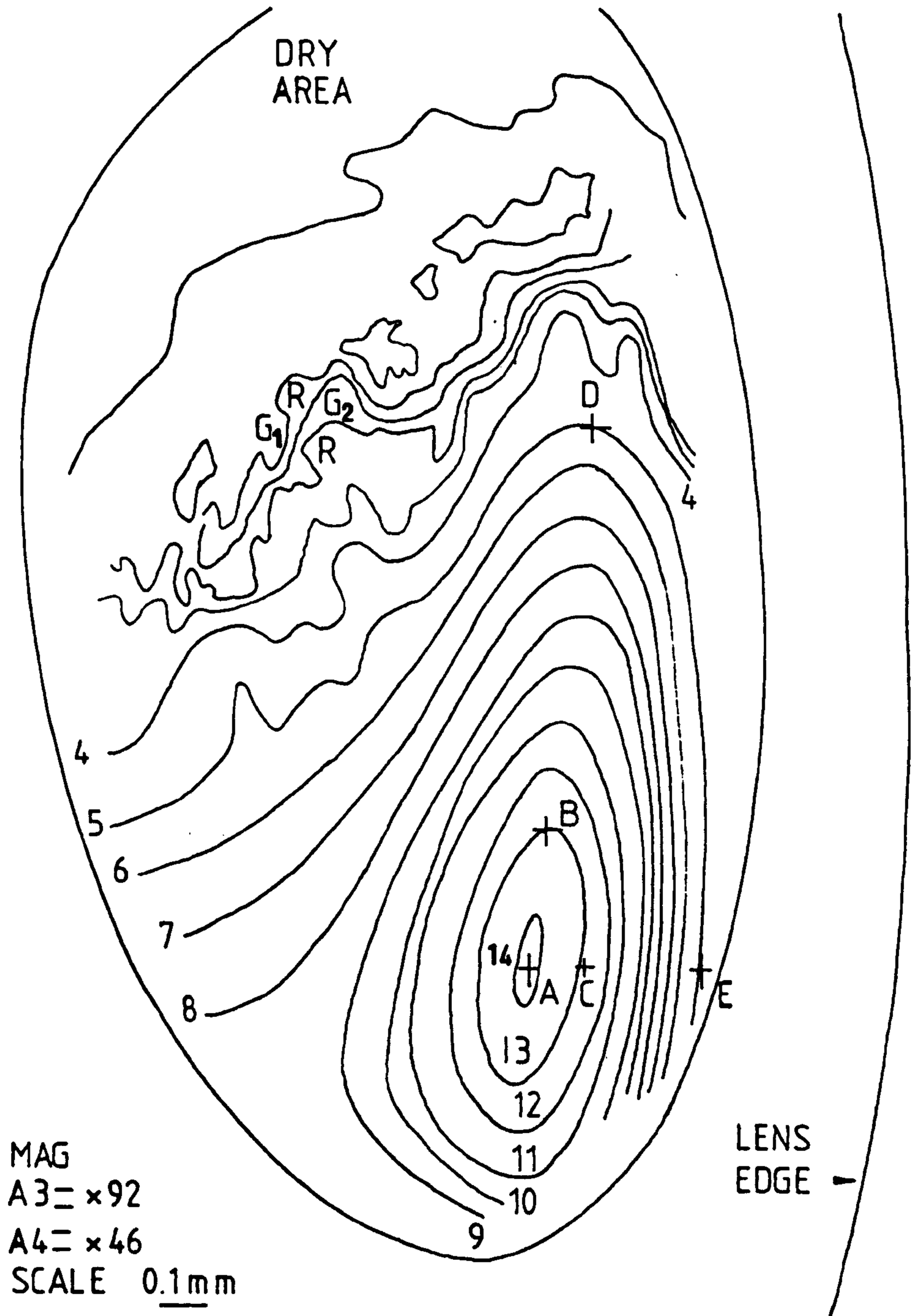

FIGURE 7.23
PRE-PMMA LENS TEAR FILM DRYING SEQUENCE PHASE 1:
OUTLINE OF FRINGES 4 TO 14

A) PLTF qualitative evaluation

The edge of the contact lens visible to the right as a thin reflection from the tear prism surrounding it.

The illuminated oval area approximately 1.5mm x 2.6mm, at the centre represents the interference pattern produced by the PLTF.

This area can be divided in the different zones from the appearances observed (Fig 7.26):

Zone 1 - a dry area (Area 1)

Zone 2 - an area of varying interference colours corresponding to a tear layer of increasing thickness (Area 2)

Zone 3 - an area presenting a succession of blue interference fringes where the tear layer shape approximate that of a wedge (Area 3).

Zone 1 Dry Area (Area 1)

The drying grey area is visible at the top. As seen previously, for a layer thickness d = 0, a phase change $\lambda/2$ is present, creating a situation of total destructive interference and an ensuing black colour if the light source is monochromatic. However in our case, because of the extended range of emission of the light source, a portion of the output is reflected by the contact lens surface which takes this grey appearance.

Zone 2 Coloured Fringed Tear Layer of Increasing Thickness (Area 2)

From a layer thickness d = 0 to approximately d = 0.7µm, the various visible colours are

produced by interferences originating from the whole of the spectrum of the light source.

This range of thickness corresponds to the first two or three orders of interference, after that due to the loss of contrast, a whitish continuous background appears. The colours observed follow approximately the Newton's scale for white light illumination (Table 6.1).

Zone 2 can be used as an area of reference recognisable on all the photographs by the colour sequence of green, red, green-red preceding the first of the blue fringes, that correspond to the 5th order of interference (p = 4).

Zone 3 Blue Fringed Wedge Shape Tear Layer (Area 3)

From the 5th order of interference (p = 4) the reflections produced by interference are becoming very faint and only blue fringes are visible. They correspond to the wavelength of peak emission for the flash used (λ = 465nm). Each blue fringe corresponds to one order of interference and is produced by the PLTF due to its thickness. These increasing orders of interference are easily traceable and can be counted until the blue fringes are no longer discernible from the background.

Each interference fringe is represented by a line on Figure 7.23 which is an isobar representing a region of equal tear film thickness. The distance between successive fringes indicates the rate at which the tear film thickness changes in any meridian. By calculations

the nature of this film can be established. This film most commonly appears as a thinning wedge.

From theory, it is known that the visibility of the fringes decreases regularly with increased tear layer thickness. The whitish background over which these blue fringes are seen is formed by a mixture of colours emitted at low luminous efficiency and on close examination, it can be seen that this background is not white. Faint colours with poorly defined edges can be identified.

B) Quantitative evaluation

α) PLTF thickness

Zone 1

It corresponds to an area of dry appearance, where the PLTF is absent or extremely thin and beyond the range of the measuring techniques and possibly formed by dehydrated remnants of a very thin adsorbed mucous layer.

Zone 2

In zone 2, the local thickness is calculated with regard to the wave length corresponding to bright colour fringe for the green interference and for the red interference.

Two reference points have been chosen as examples:

Green G1:	3rd Fringe order	P = 2
	Thickness	0.500μm
Green G2:	4th Fringe order	P = 3
	Thickness	0.652μm

In that zone some colours described by Newton are missing from the photographs. This is possibly due to

the slightly irregular nature of the contact lens surface.

Zone 3

Corresponds to zones with interference fringes. The thickness of the tear film at points where brightness is maximal is deducted from the following formula already described in Chapter 6.

$$d = \frac{(P + \frac{1}{2})}{2n} \qquad [8]$$

d = layer thickness in microns

λ = wavelength in microns

P = successive order of interference

n = refractive index of the film (1.5 for the lipid layer).

Zone 3 starts when the first blue fringes for 5th order (P = 4) has been recognised and extends up to the 14th order. The relative position of those fringes is recorded on Table 7.1 for the two principal axes of the configuration: short axis CE and long axis BD (Fig 7.23). Fringe P = 12 was taken as the origin for all measurements and for each fringe the corresponding tear film thickness was calculated using the above formula [8]. For these calculations, λ was taken as 465nm corresponding to the instrument peak emission and the value for n = 1.337.

For illustration purposes the drying profile in that region of the contact lens is produced on Figure 7.24. From this diagram it is obvious that the change in tear film thicknesses along each principal meridian is linear. For this particular case the best fitting least square regression have the following values:

	Order of Interference	P value	Tear Film Thickness (μm)	Position on slide (mm)	Drying Angle (mrad)
C	13	12	2.174	0.00	1.58
	12	11	2.070	0.437	1.80
	11	10	1.826	0.701	2.12
	10	9	1.652	0.896	1.78
	9	8	1.478	1.192	2.11
	8	7	1.304	1.398	2.09
	7	6	1.130	1.567	2.03
	6	5	0.956	1.738	2.11
E	5	4	0.783	1.905	
				average =	1.93mrad
B	13	12	2.174	0.00	3.56
	12	11	2.600	1.013	5.13
	11	10	1.826	1.948	6.24
	10	9	1.652	2.786	11.22
	9	8	1.478	3.697	7.85
	8	7	1.304	4.491	9.39
	7	6	1.130	5.284	10.13
	6	5	0.956	6.107	12.76
D	5	4	0.783	6.887	
				average =	7.04mrad

TABLE 7.1
PRE-LENS TEAR FILM DRYING SEQUENCE PHASE 1:
RELATIVE POSITION OF FRINGES ALONG CE AND BD

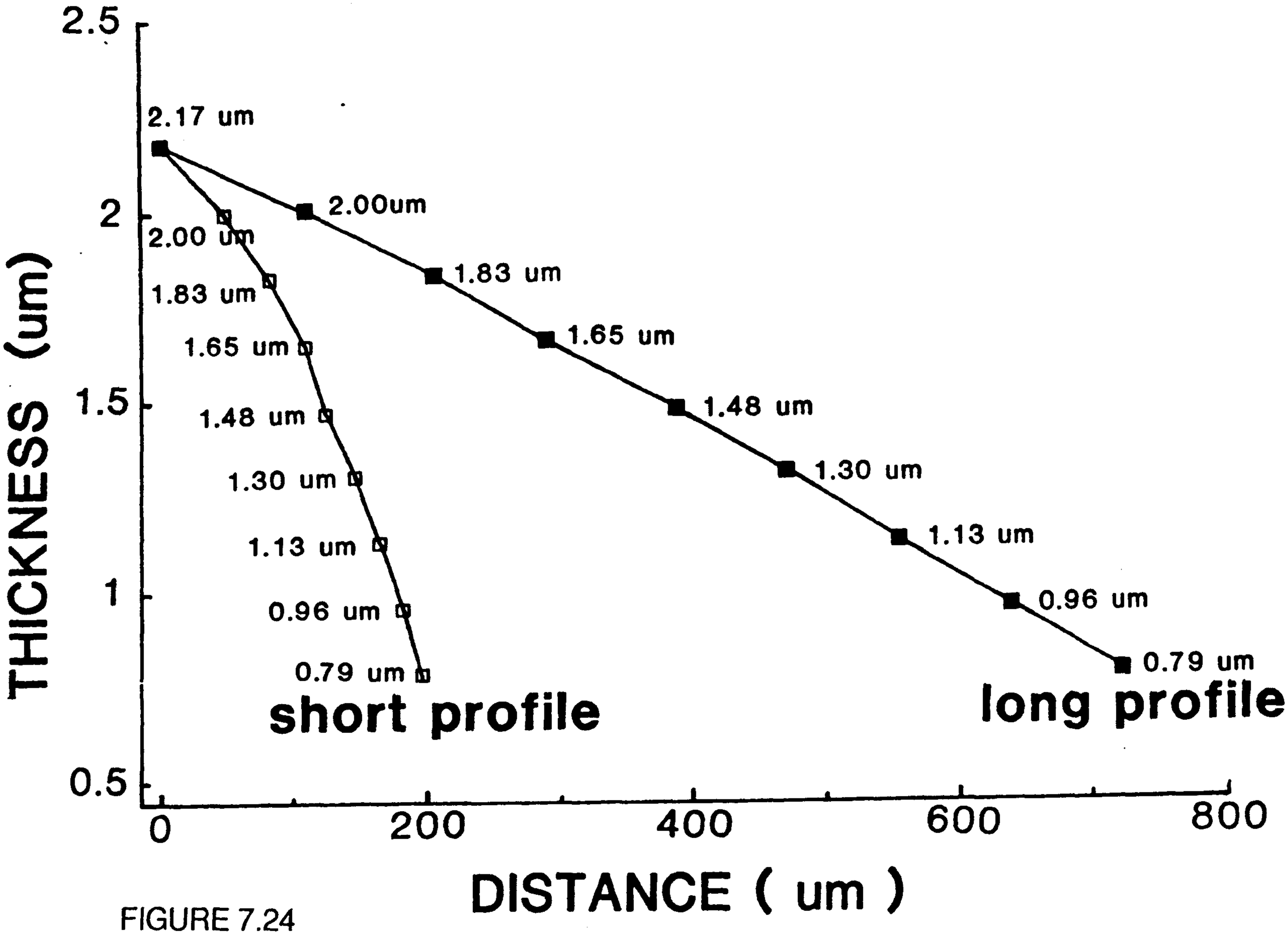

FIGURE 7.24
PRE-LENS TEAR FILM DRYING SEQUENCE PHASE 1:
SECTIONAL ANALYSIS THICKNESS PROFILE

long axis: $t_1 = 2.0 \times 10^{-3} \chi + 2.4$

$r = -0.999$

$S/E = 0.0195$

t = tear film thickness in microns

χ = distance from origin in mm

(14th fringe)

β) <u>2LIF drying angle</u>

As seen previously, the drying tear film in front of a rigid contact lens is a dielectric layer whose shape resembles that of a wedge. When the interfringe (the linear distance between maxima) is known, the wedge angle can be calculated.

From the knowledge of the fringe positions and corresponding film thicknesses the drying angle was calculated using the following formula:

$$\beta = \frac{dt}{d}$$

$$\beta = \frac{\text{d thickness (in } \mu m)}{\text{d distance (in } \mu m)}$$

dt = tear film thickness difference for any pair of fringes.

d = distance between corresponding pair of fringes.

The results are also recorded on Table 7.1 and illustrated in Figures 7.25 and 7.26. The recorded drying angle confirms the qualitative impression of a difference in drying angle along these meridians. The short axis dries approximately 4 times faster than the long axis. This difference along the vertical and horizontal meridian may be accentuated by the drainage effect from the lens meniscus which is very close.

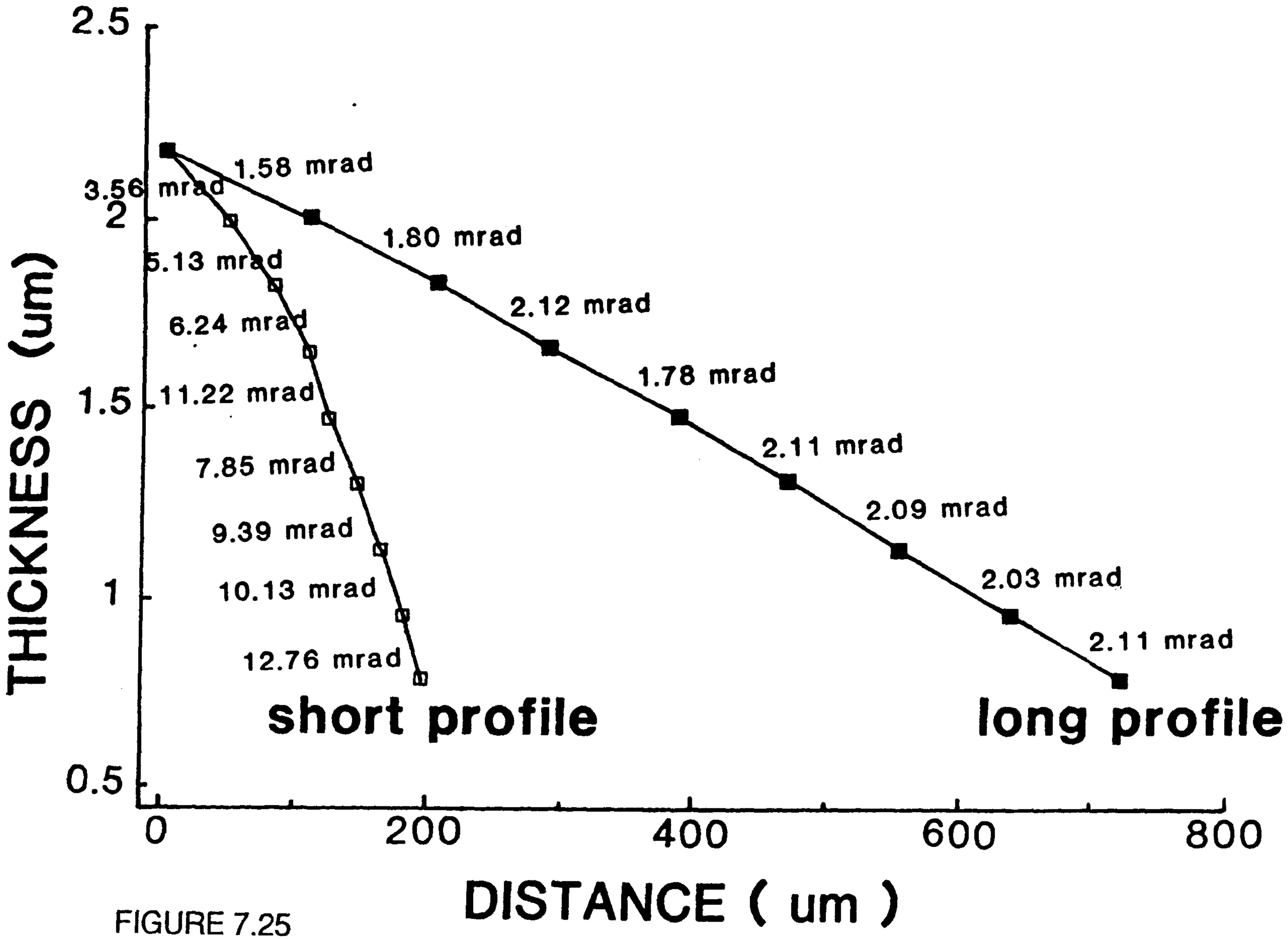

FIGURE 7.25
PRE-LENS TEAR FILM DRYING SEQUENCE PHASE 1: SECTIONAL ANALYSIS DRYING ANGLE

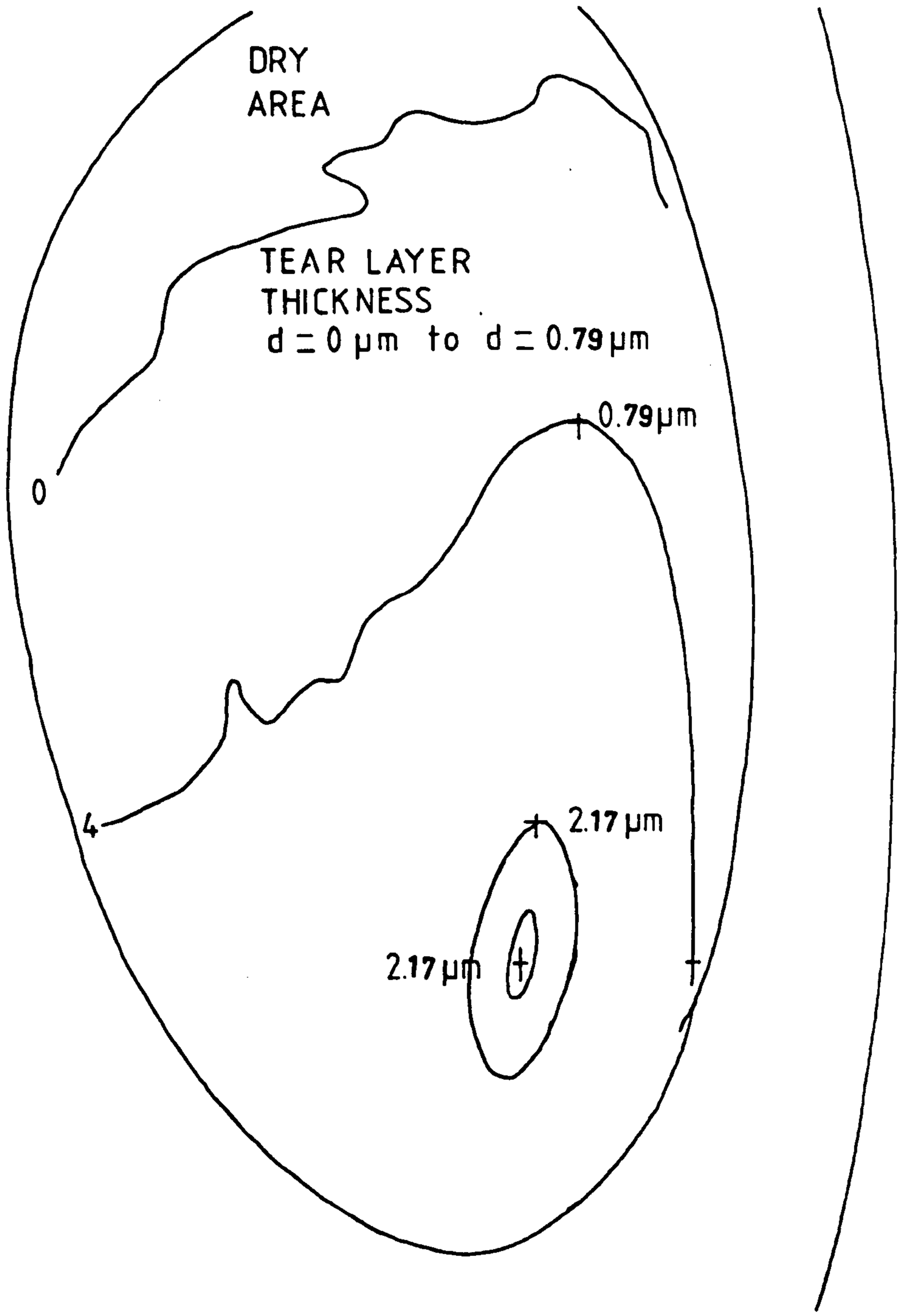

FIGURE 7.26
PRE-PMMA LENS TEAR FILM DRYING SEQUENCE PHASE 1:
SUMMARY OF RESULTS

b) Drying sequence Phase II

The drying pattern, six seconds past blink, is recorded in Figures 7.27 and 7.28. The second photograph in the sequence is always taken 4 seconds after the first due to time necessary to recharge the strobe light.

A) Qualitative evaluation

The PLTF qualitative evaluation, 6 seconds after blink, demonstrates clearly the difference between the appearance and the nature of the pre-corneal tear film and the pre-lens tear film. On the right, the grey area is due to the reflection from superficial lipid layer of the pre-corneal tear film. Its regular appearance denotes its amorphous nature. From our previous calculation (Chapter 7.1.3 ii 8 d) we know that its thickness is around 90nm (0.09µm) and it is associated with a stable tear film. As we move to the left, the increased reflection from the curved tear prism at the edge of the lens can be seen with a thinning at its base. Next to it, the dark area is produced by the periphery of the lens whose reflection at a wider angle is not contained within the entrance window of the observation system.

The main part of the photograph (measuring 1.3mm horizontally and 2.4mm vertically) shows very sharply the succession of interference colours produced within the aqueous phase of the pre-lens tear film.

In this area a superficial lipid layer cannot be detected and the intensity of the aqueous phase fringes is at its maximum.

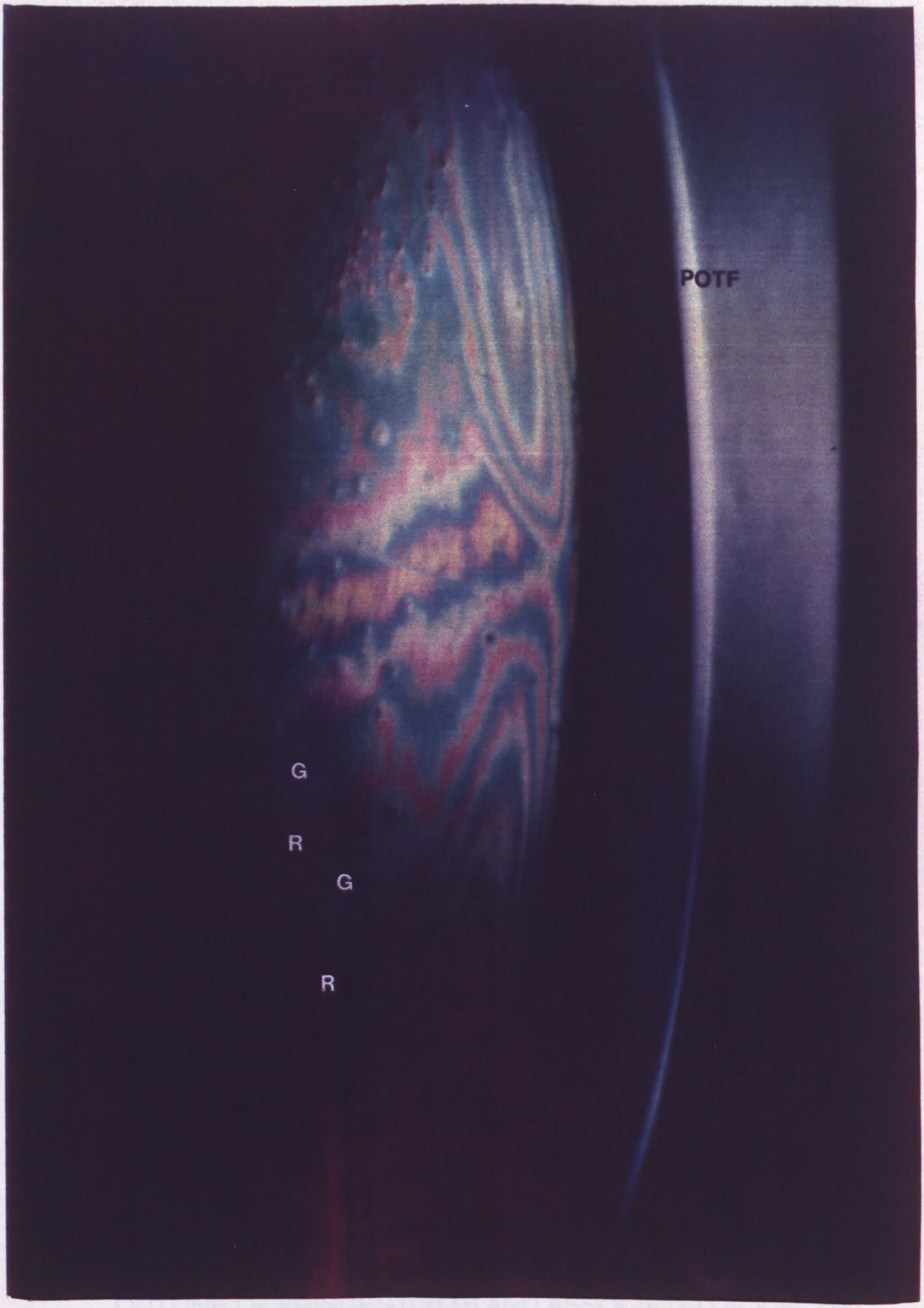

FIGURE 7.27
PRE-PMMA LENS TEAR FILM DRYING SEQUENCE PHASE 2
ORIGINAL MAGNIFICATION (X9.6)
PHOTOGRAPH MAGNIFICATION (APPROX 95)

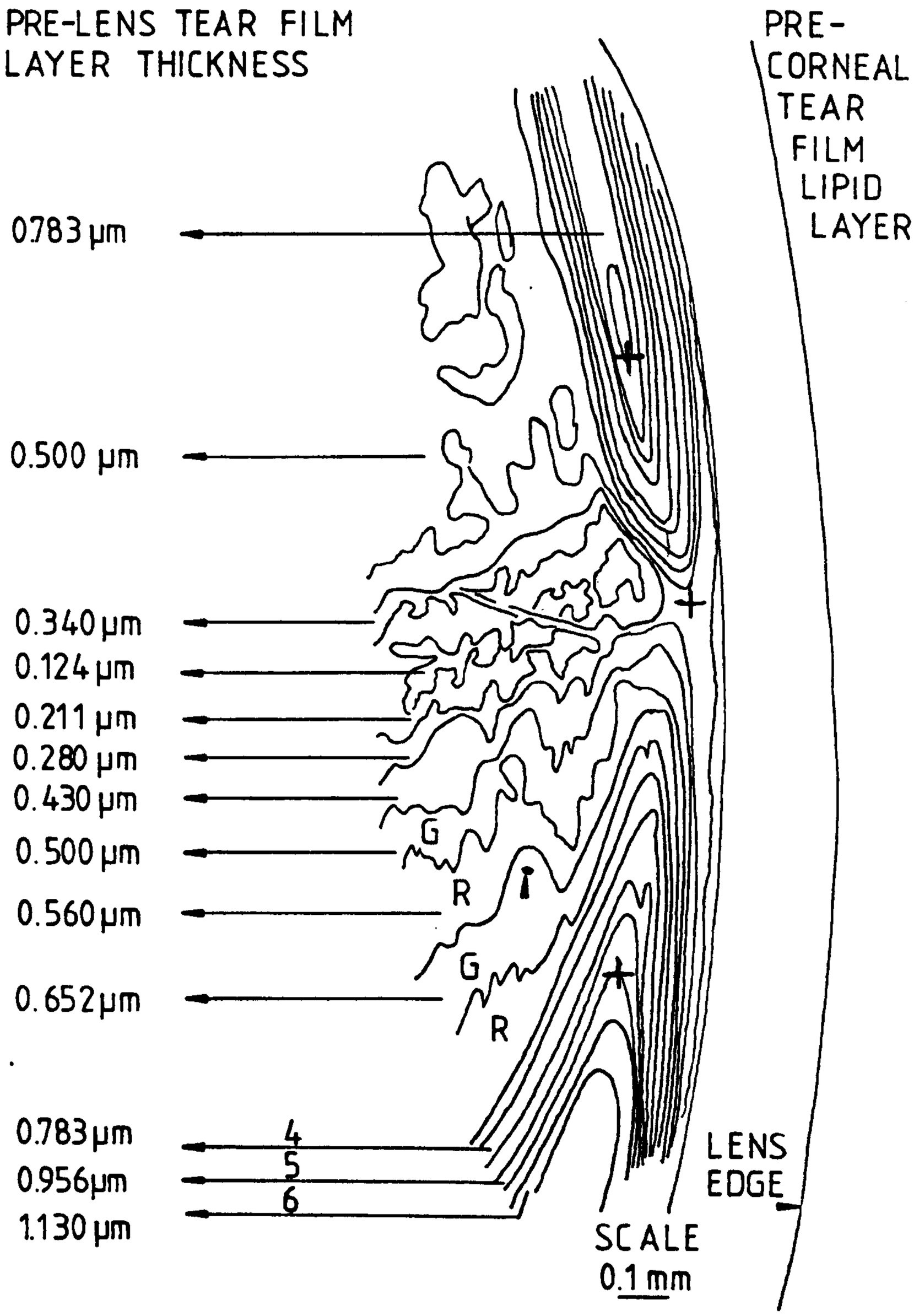

FIGURE 7.28

PRE-PMMA LENS TEAR FILM DRYING SEQUENCE PHASE 2: OUTLINE OF FRINGES 0 TO 6 AND ASSOCIATED AQUEOUS THICKNESSES

B) Quantitative evaluation

α) PLIF thickness

The aqueous phase thickness increases from 0.124μm at the centre to 0.783μm at the top and 1.130μm at the bottom (Fig 7.28). All the intermediate values are also presented on the accompanying diagram. The sequence green-red-green-red has also been noted along with the next three visible blue fringes (p = 4,5,6 equivalent to 5th, 6th and 7th order). The position of the 5th and 6th fringes in the lower part of the slides were easily measurable and are illustrated on Fig 7.29. They reveal a drying angle of 8.72 mrad in that region.

The thickness of the scratch at the centre of the picture can be determined with the help of the tables. The light blue streak across the yellow background denoted a layer thickness and thus a scratch depth of approximately 0.24 microns.

In the same way the size of the dust particle arrowed in the diagram has been calculated to be 0.78 microns as it culminated at the level of the first blue fringe (P = 4).

A large number of particles are seen at the top of the photograph. They are situated in the area covered by an aqueous phase of 0.5μm thickness.

c) Drying sequence Phase III

Pre-lens tear film drying sequence Phase III, corresponding to approximately 10 seconds post blink, is recorded on Figures 7.30 and 7.31.

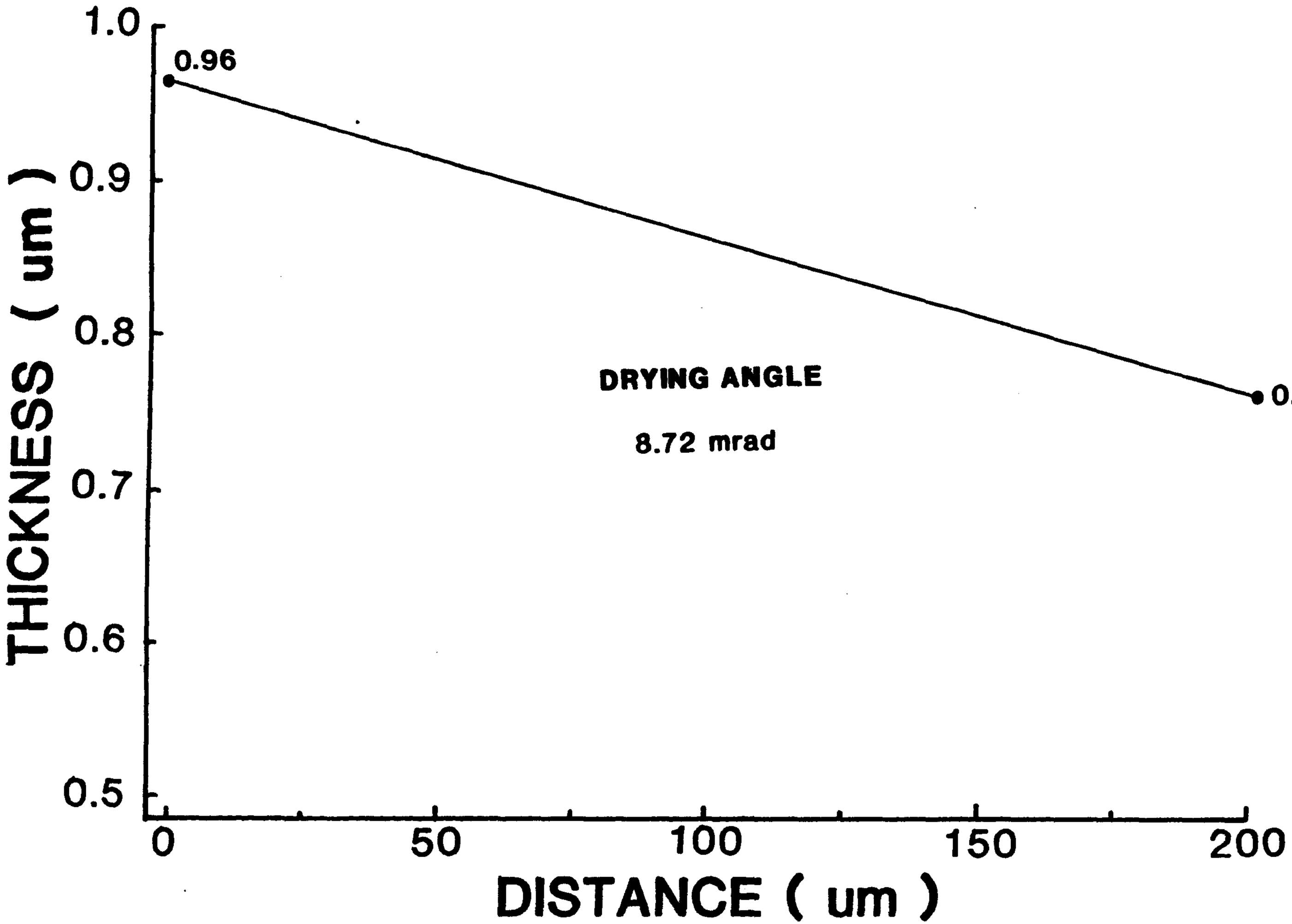

FIGURE 7.29
PRE-PMMA LENS TEAR FILM THICKNESS PROFILE

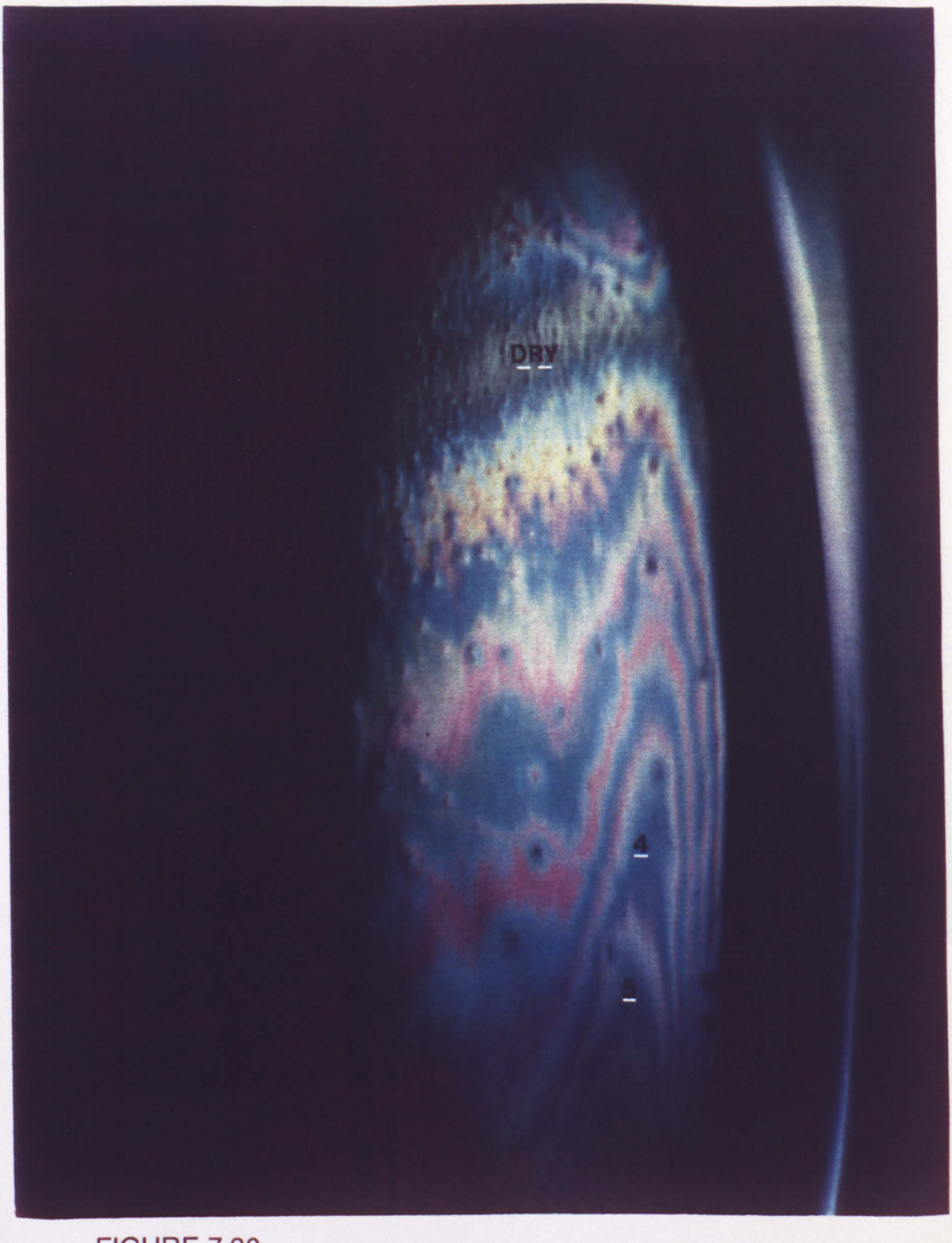

FIGURE 7.30
PRE-PMMA LENS TEAR FILM DRYING SEQUENCE PHASE 3:
ORIGINAL MAGNIFICATION (X9.6)
PHOTOGRAPH MAGNIFICATION (APPROX 95)

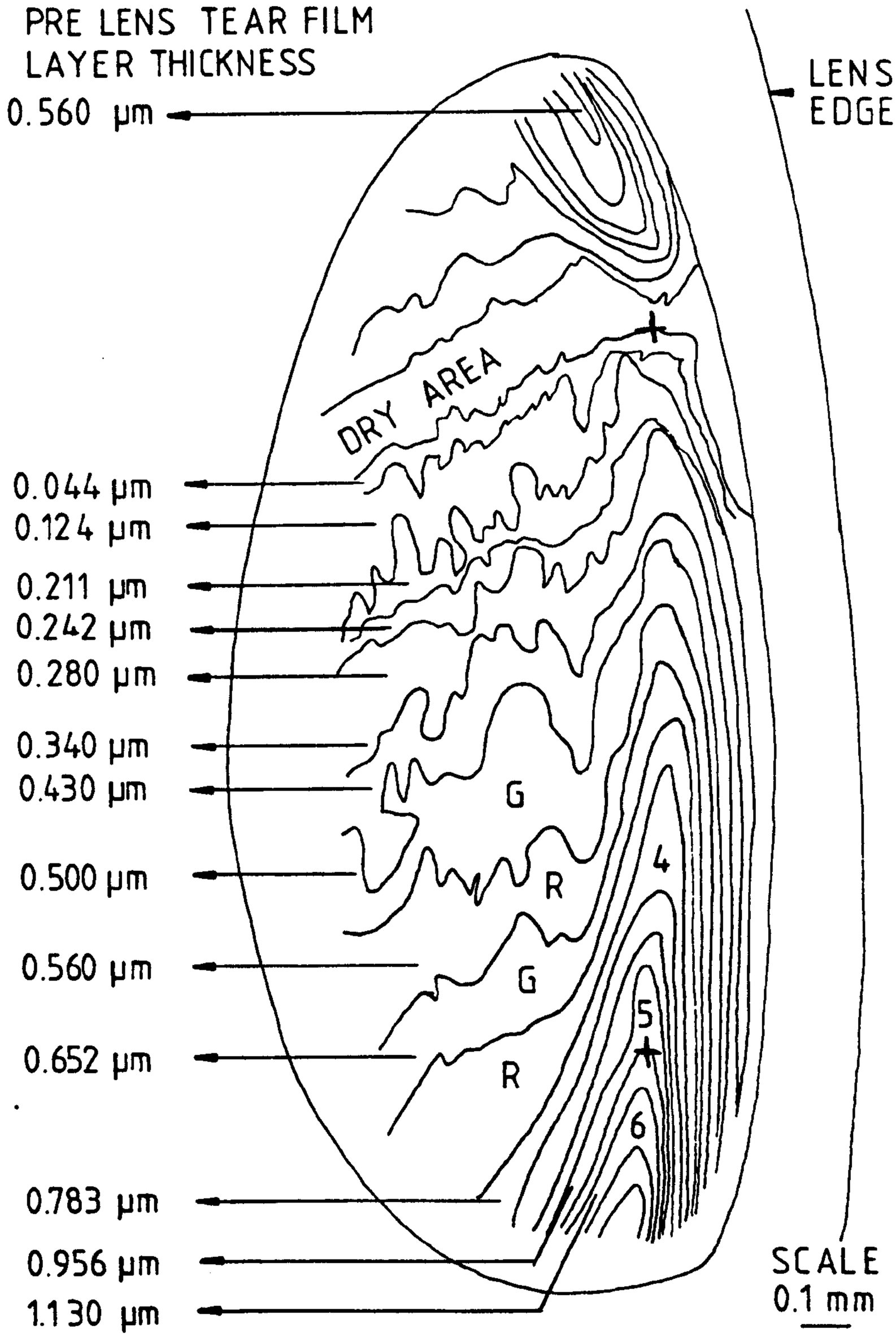

FIGURE 7.31
PRE-PMMA LENS TEAR FILM DRYING SEQUENCE PHASE 3:
OUTLINE OF FRINGES 0 TO 6

Its analysis has been limited to a qualitative evaluation only.

At 10 seconds post blink, a dry grey area has appeared at the top of the picture. The grey drying surface and the adjacent thin tear film are clustered by particles whose origin is not clear. Their numbers increase at the thinner end of the film and only very few appear in the layers about 0.50µm in thickness.

d) Drying sequence Phase IV

Pre-lens tear film drying sequence Phase IV is recorded on Figures 7.32 and 7.33.

This corresponds to 14 seconds post blink in an area situated below the central drying to analyse the difference in the appearance of the fringes produced in areas of the tear film characterised by two different drying angles.

PLTF Qualitative evaluation. From the top to the bottom, three quarters of the photograph consist of a very thin tear film where the 1st micron of the colour sequence is well spread between A and B.

On the right hand side the tear film appears as narrow fringes in a reduced area between D and C and A and C. It progresses from 0.78µm to 1.30µm.

Quantitative evaluation shows two distinct areas. The first is an area of well defined colours going from A corresponding to the 5th order of interference (p = 4; thickness = 0.78µm) to B corresponding to the dry border (p = 0; thickness = 0). These two points are separated by 1.96mm giving a drying angle in that region of 0.398 mrad.

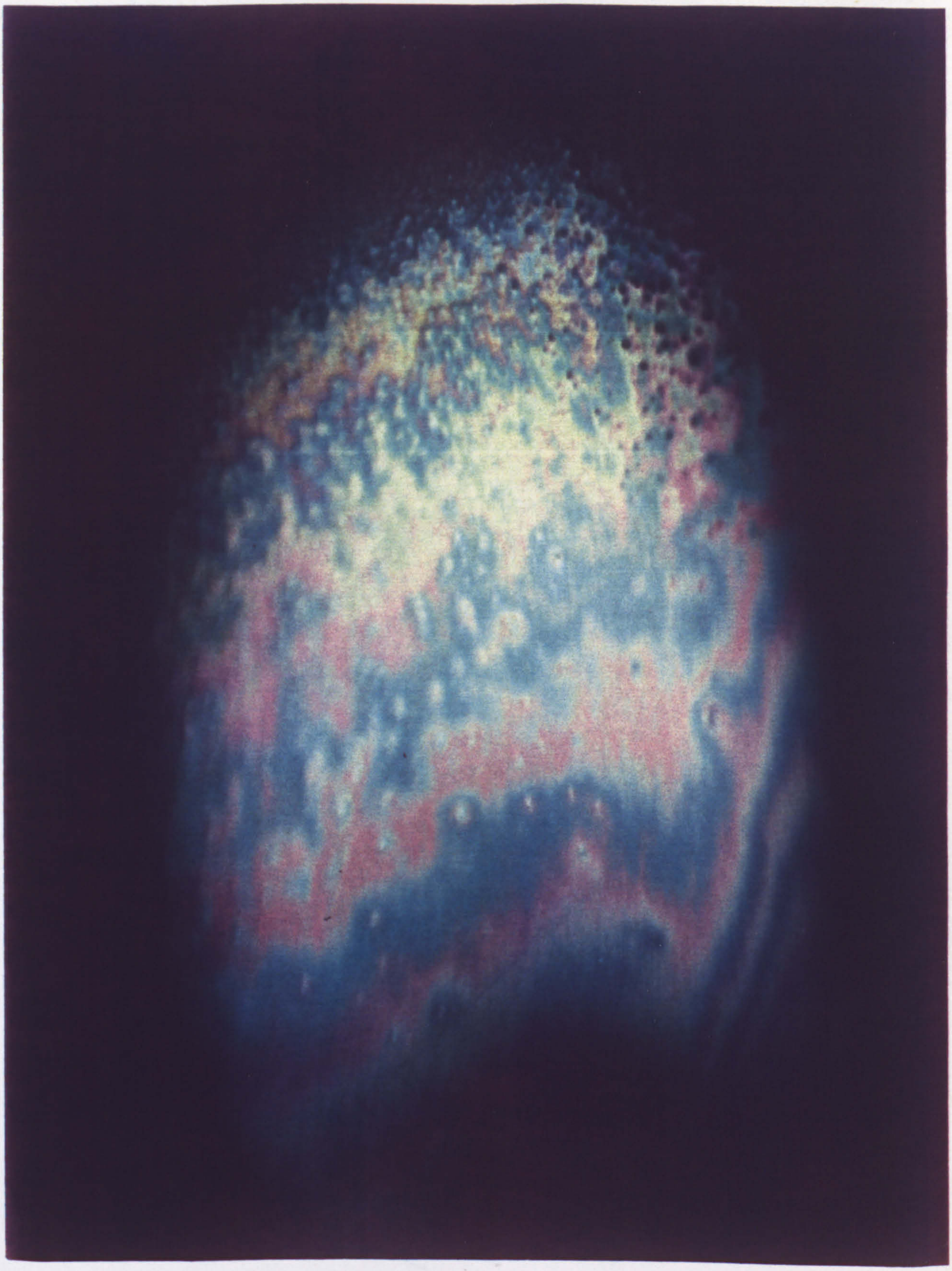

FIGURE 7.32
PRE-PMMA LENS TEAR FILM DRYING SEQUENCE PHASE 4
ORIGINAL MAGNIFICATION (X9.6)
PHOTOGRAPH MAGNIFICATION (APPROX 95)

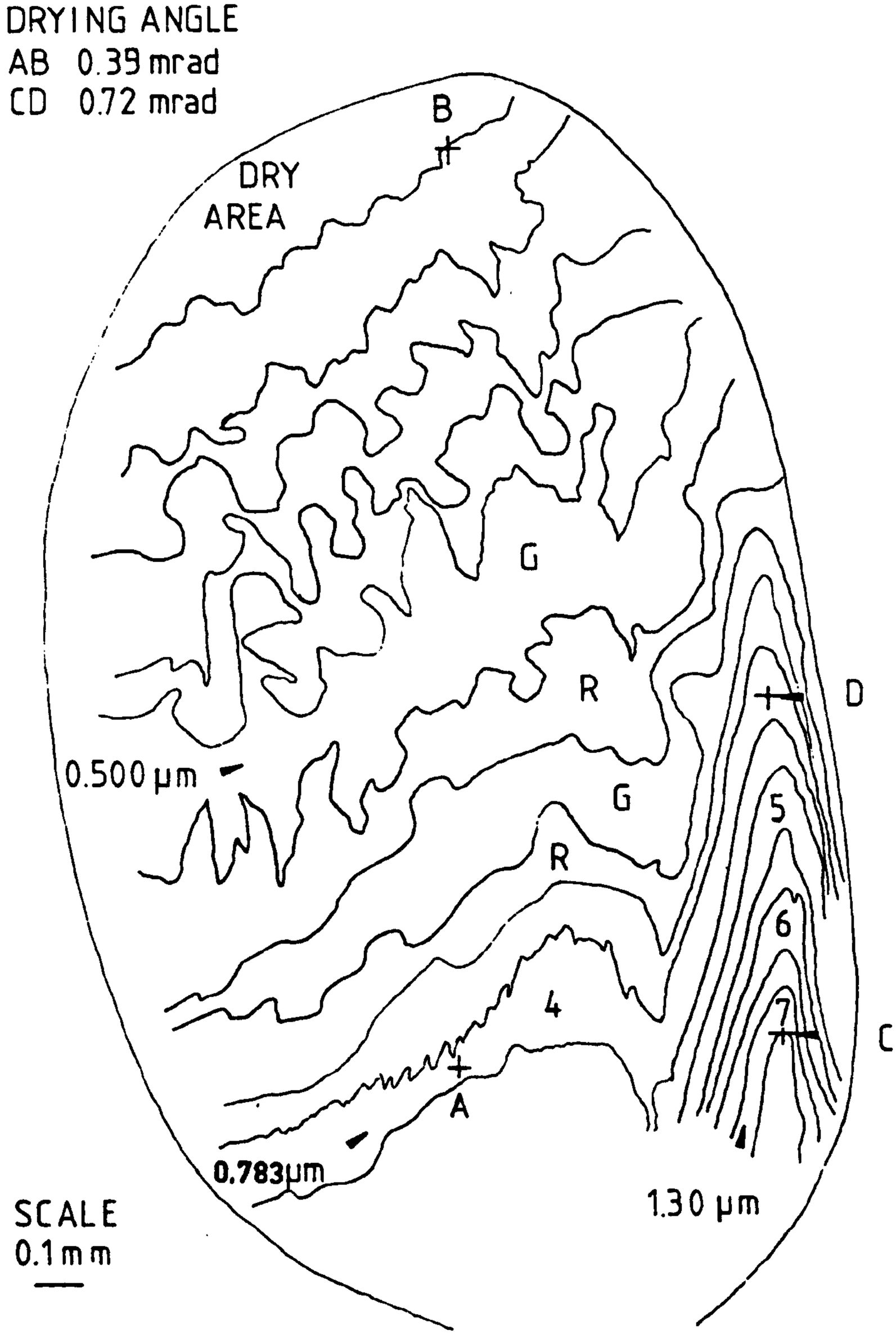

FIGURE 7.33
PRE-PMMA LENS TEAR FILM DRYING SEQUENCE PHASE 4:
OUTLINE OF FRINGES 0 TO 7

In the second region, corresponding to an area of closely packed fringes, between point C of the 8th order of interference (p = 7; thickness = 1.30μm) and D of the 5th order of interference (p = 4; thickness = 0.78μm), separated by 0.72mm, thus a greater drying angle of 0.72 mrad.

This again shows that the variable appearance of the fringes at the surface of the contact lens, their proximity and visibility is a good representation of pre-lens tear film topography at any point.

e) Drying sequence Phase V

The PLTF drying sequence Phase 5 is recorded on Figures 7.34 and 7.35. These illustrations correspond to 18 seconds post blink.

Qualitative evaluation reveals a thinner part of the PLTF that has dried up due to the effect of evaporation. The dry area at the centre is still clustered by the remnants of the 'particles' noted previously (Figs 7.30 and 7.32). They appear much smaller and may have undergone a partial and slower process of drying which would be consistent with an hydrated mucous-lipid complex.

The remaining PLTF in the lower part of the photograph has thinned down from 1.30μm to 0.78μm. This area will subsequently evaporate and the PLTF drying sequence will be complete.

Quantitative evaluation is concerned with three points A, B and C. A corresponds to the area with the thickest tear thickness of the 5th order of interference

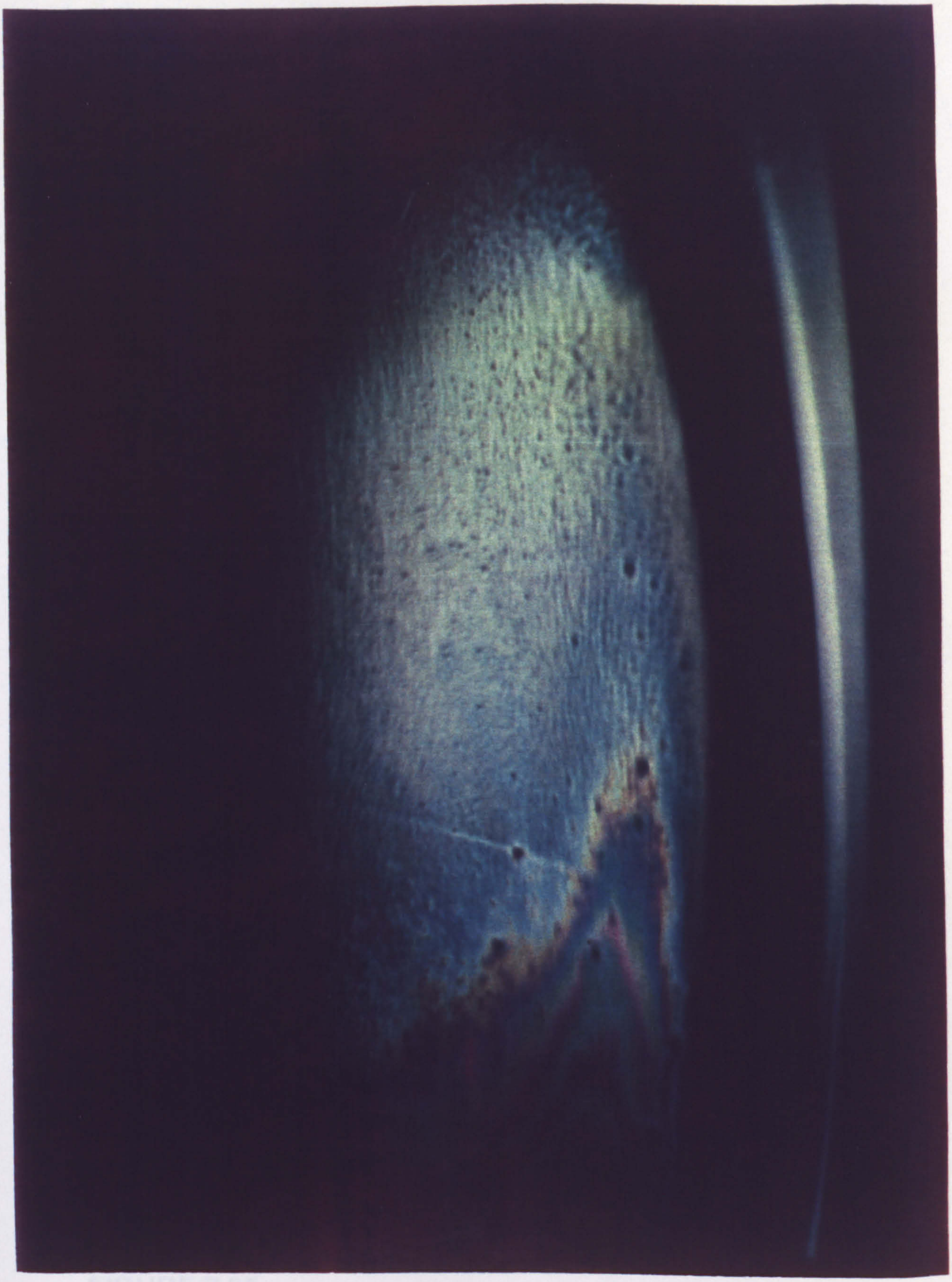

FIGURE 7.34
PRE-PMMA LENS TEAR FILM DRYING SEQUENCE PHASE 5
ORIGINAL MAGNIFICATION (X9.6)
PHOTOGRAPH MAGNIFICATION (APPROX 95)

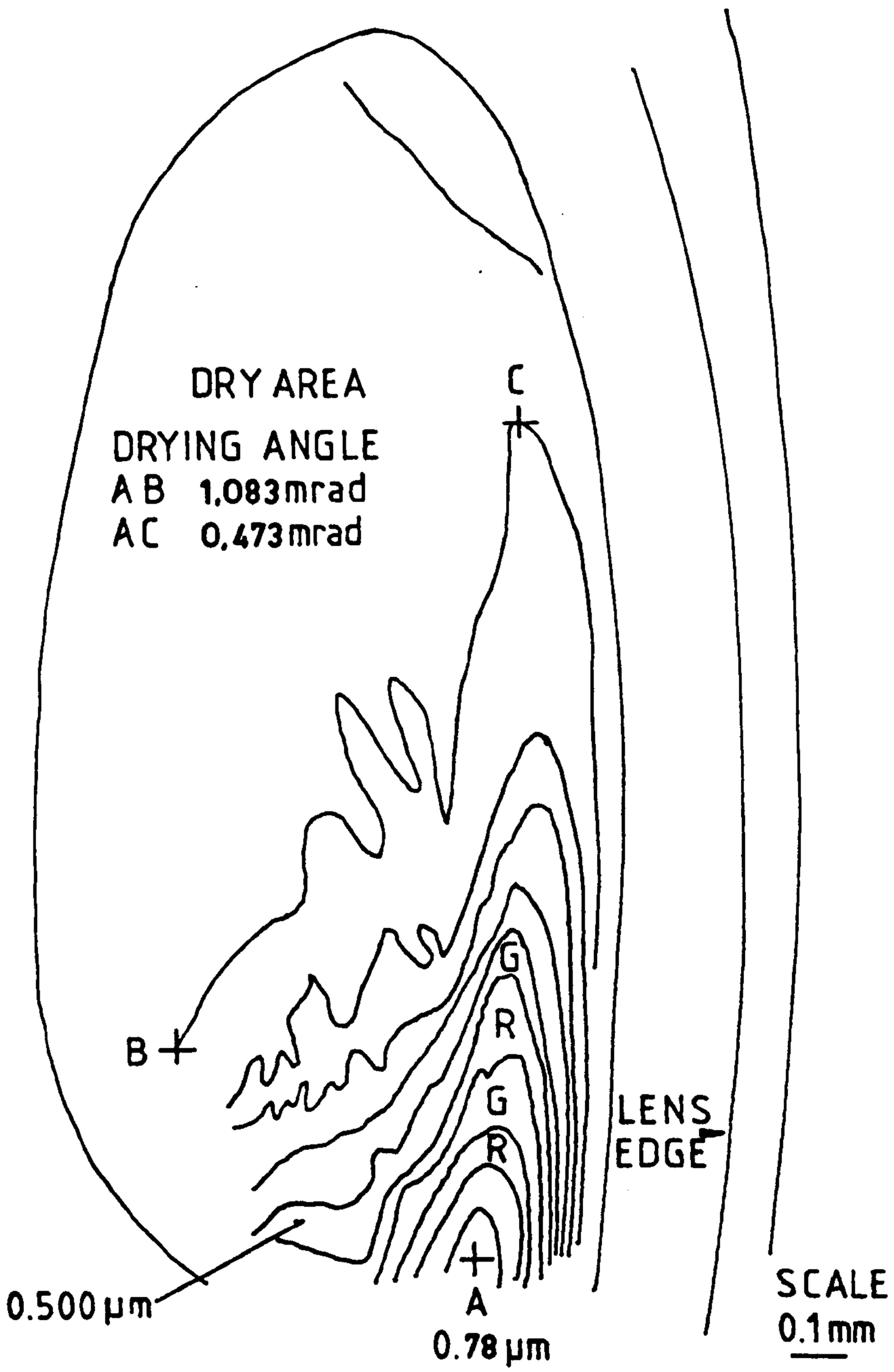

FIGURE 7.35
PRE-PMMA LENS TEAR FILM DRYING SEQUENCE PHASE 5
OUTLINE OF FRINGES 0 TO 4

(p = 4; thickness = 0.78μm) with B and C to the edge of the dry area in two different directions.

They are separated from A respectively, by 0.72mm and 1.65mm. These correspond to drying angles of 1.083 mrad and 0.473 mrad.

f) Use of wetting solution

Figures 7.36, 7.37 and 7.38 represent the PLTF after the instillation of a wetting solution. For that the lens was removed, a wetting solution, Polyvinylpyrrolidone 0.5 percent (PVP 0.5 percent), applied to its surface and the lens reinserted and the photograph (Fig 7.36) was taken immediately after re-insertion to show the effect of the wetting solution on pre-lens tear film thickness and on the drying angle.

The illuminated area (approx. 1.8 mm horizontally by 2.5mm vertically) has now taken a very different appearance. A dry area is visible in the lower part, a sharp border present, and the sequence green-red-green-red is easily visible allowing us to detect the blue fringe corresponding to the 5th (p = 4) and the higher orders of interference. Only a few particles are floating at the surface of the film - a lot more are present on the dry surface and in the thinner parts of the film there is no obvious evidence of a visible superficial lipid film.

The quantitative evaluation of the PLTF was carried out for seven points (A, B, C, D, E, F and G). These calculations are summarised on Table 7.2 and Figure 7.38 and give a topographical representation of the variations in the PLTF thickness and drying angle.

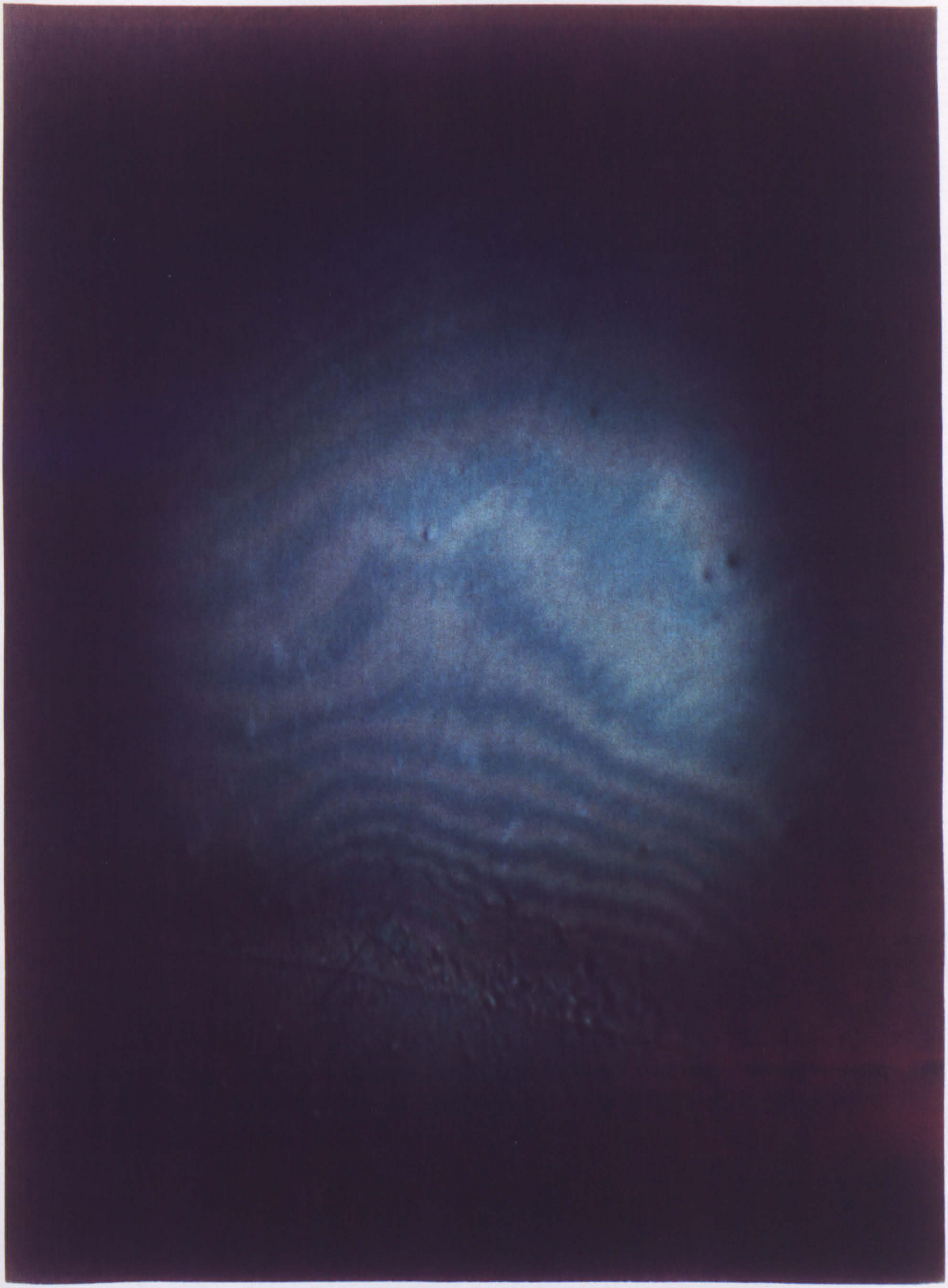

FIGURE 7.36
PRE-PMMA LENS TEAR FILM USE OF WETTING SOLUTION
ORIGINAL MAGNIFICATION (X9.6)
PHOTOGRAPH MAGNIFICATION (APPROX 95)

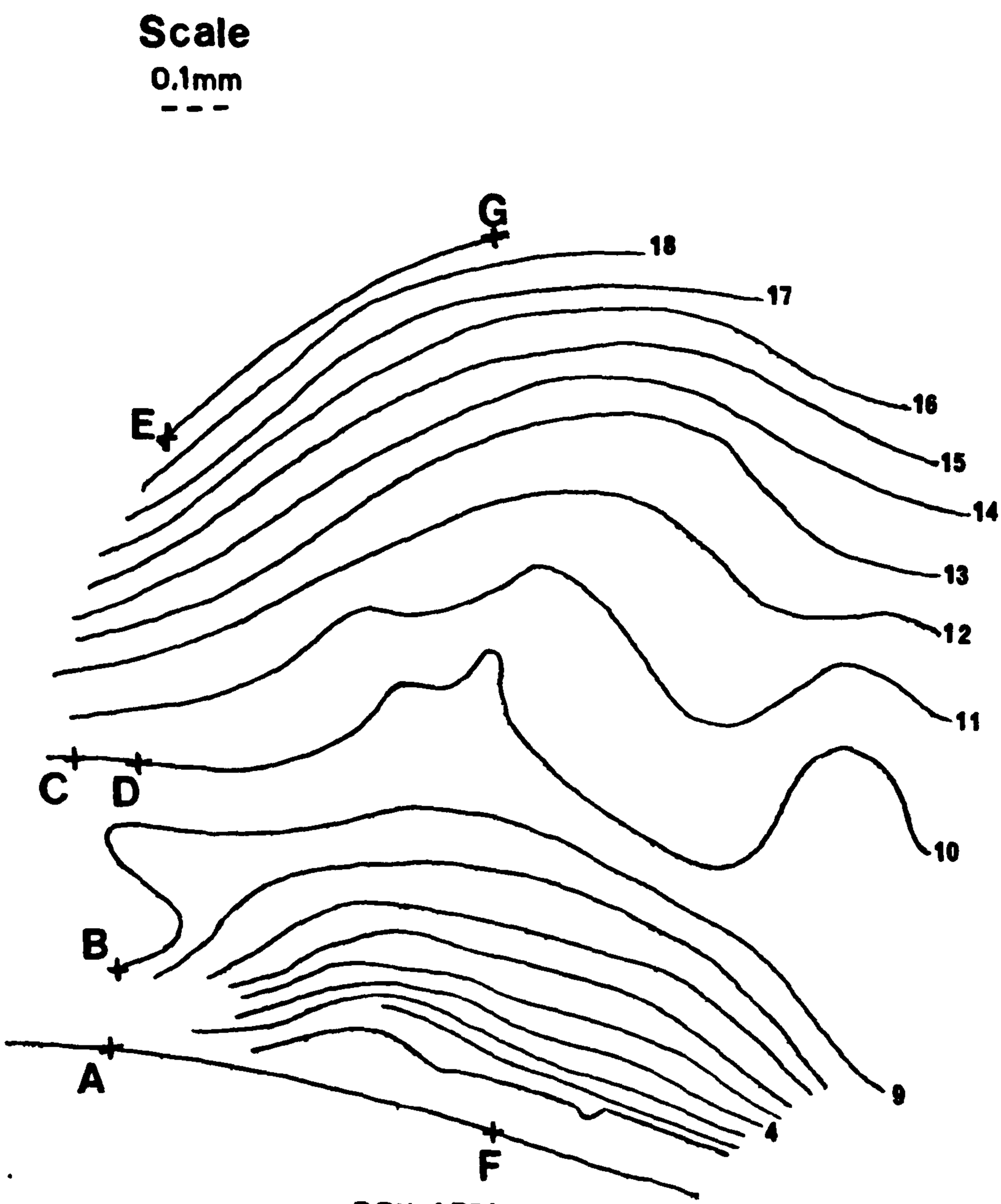

FIGURE 7.37
PRE-PMMA LENS TEAR FILM USE OF WETTING SOLUTION:
OUTLINE OF FRINGES 0 TO 19

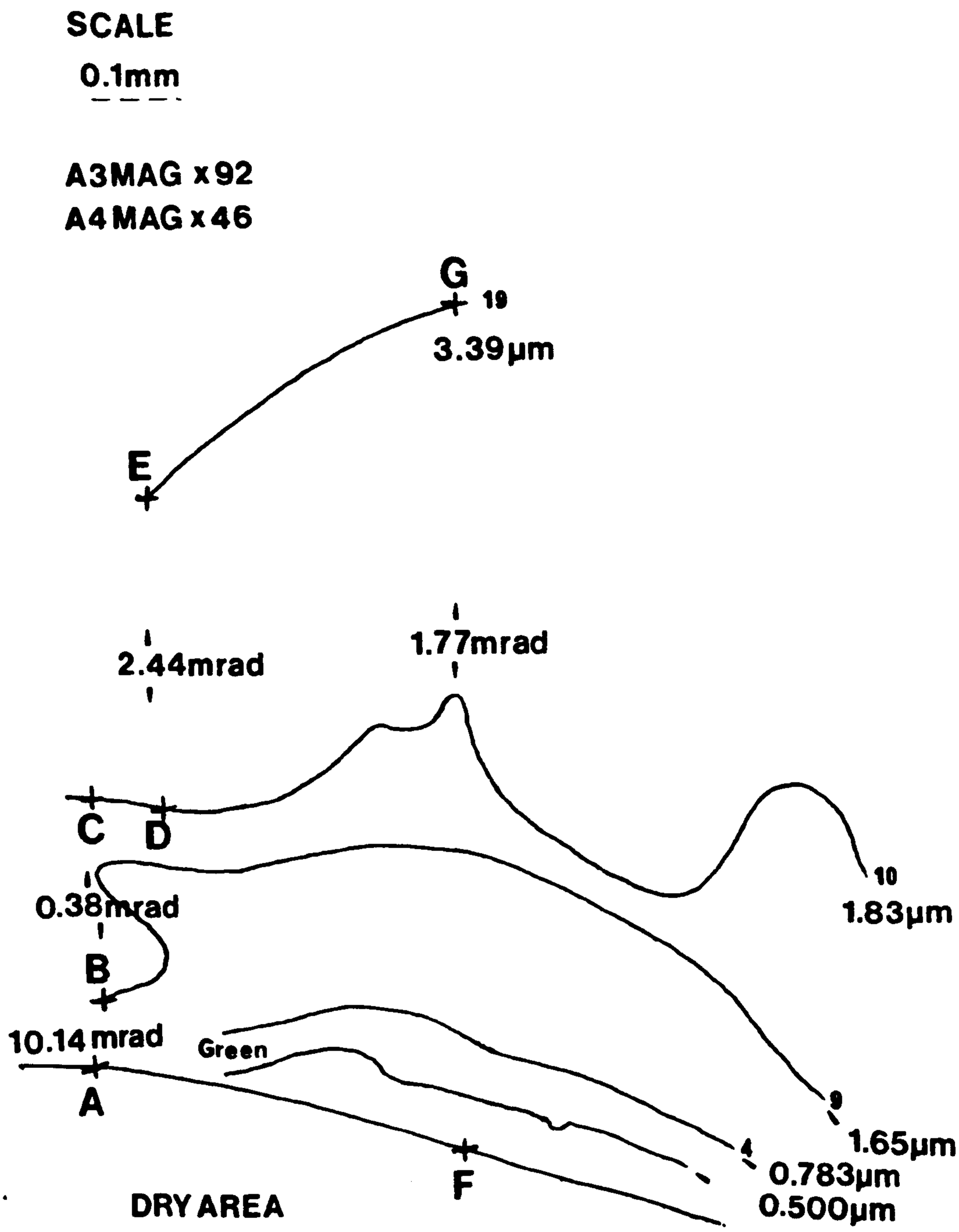

FIGURE 7.38
PRE-PMMA LENS TEAR FILM USE OF WETTING SOLUTION:
SUMMARY OF RESULTS: THICKNESS AND DRYING ANGLE

Reference on slide and Nature of Interference		Tear Film Thickness (μm)	Drying Direction (Distance mm)	Drying Angle (mrad)
A	Dry border	0.000		
B	(p = 9)	1.652	AB = 0.163	10.135
C	(p = 10)	1.826	BC = 0.619	0.382
D	(p = 10)	1.826	-	
E	(p = 19)	3.390	DE = 0.641	02.440
F	Dry border	0.000		
G	(p = 19)	3.390	FG = 1.913	01.772

TABLE 7.2
USE OF WETTING SOLUTION: FILM THICKNESS AND DRYING ANGLE

ii) Low Wetting Angle Material: Pre-Lens Tear Film Drying Sequence

To study the influence of the contact lens material on the thickness and the structure of the pre-contact lens tear film. A series of photographs was taken on subjects wearing low wetting angle material corneal lenses (Paragon 18). They have taken part in a study conducted by Don Lydon at Moorfields Eye Hospital.

When the photographs were taken the patient was fully adapted to their contact lenses, all day wearers with at least 6 months wear after the issue of lenses.

The series of photographs chosen was taken in succession on the same contact lens area, although blinking was allowed between photographs resulting in lens movement; it is nevertheless possible in this series of pictures to match closely enough the contact lens area under observation.

This series of photographs is presented as an example of improved wetting conditions on a rigid corneal lens.

a) Drying Sequence Phase I

This photograph (Fig 7.39) and its diagrammatic tracing (Fig 7.40) shows a combination of the features of the pre-lens tear film commonly found when a corneal lens made of low wetting material is used.

From right to left, the grey superficial lipid layer of the pre-corneal tear film outside the lens is visible on the right. A slight brownish colour is apparent in traces corresponding to lipid layer of the combination type II (Chapter 7.1.3), its thickness

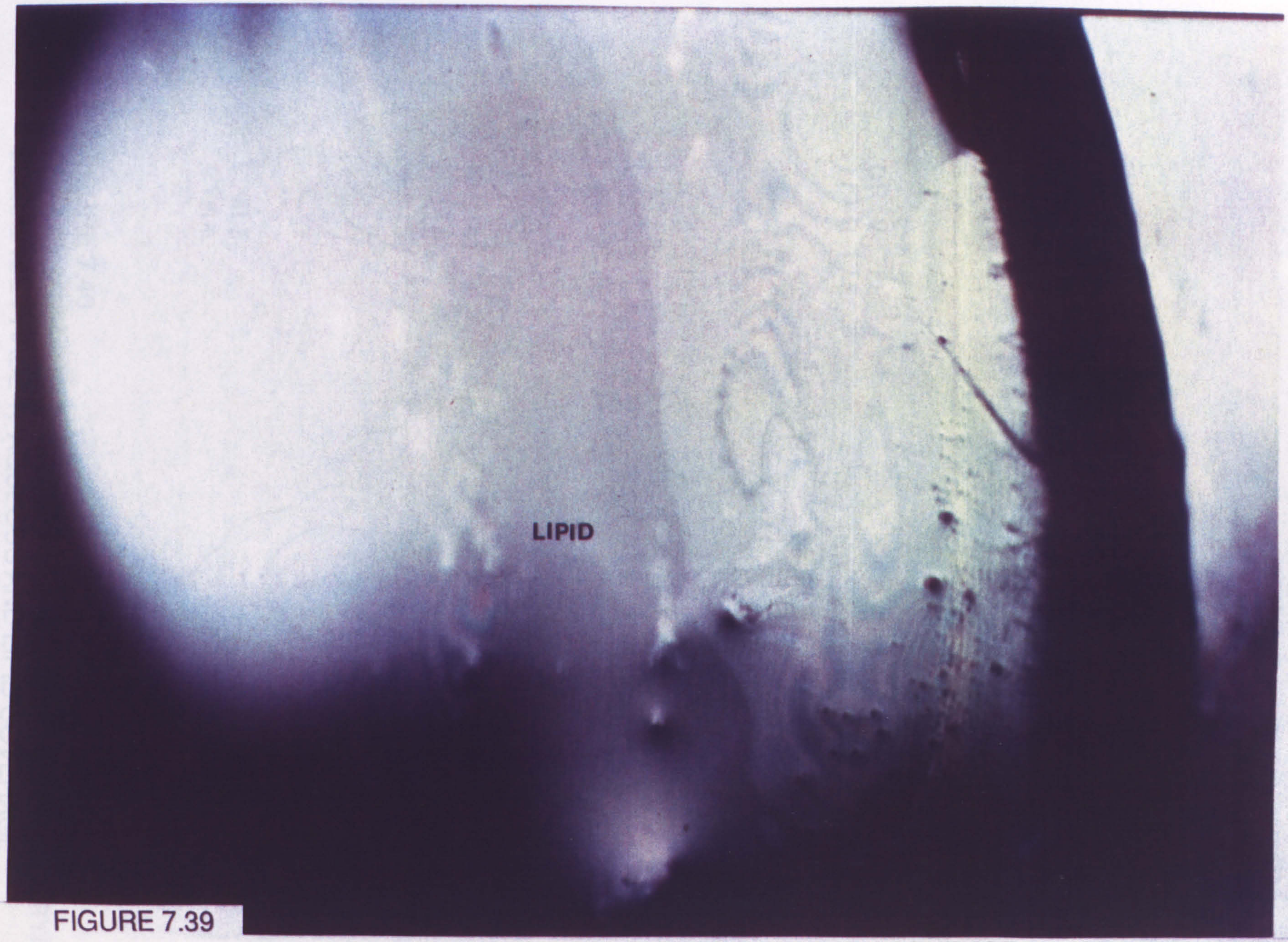

FIGURE 7.39
PRE-LENS TEAR FILM LOW WETTING ANGLE MATERIAL DRYING SEQUENCE PHASE 1
ORIGINAL MAGNIFICATION (X9.6) PHOTOGRAPH MAGNIFICATION (APPROX 95)

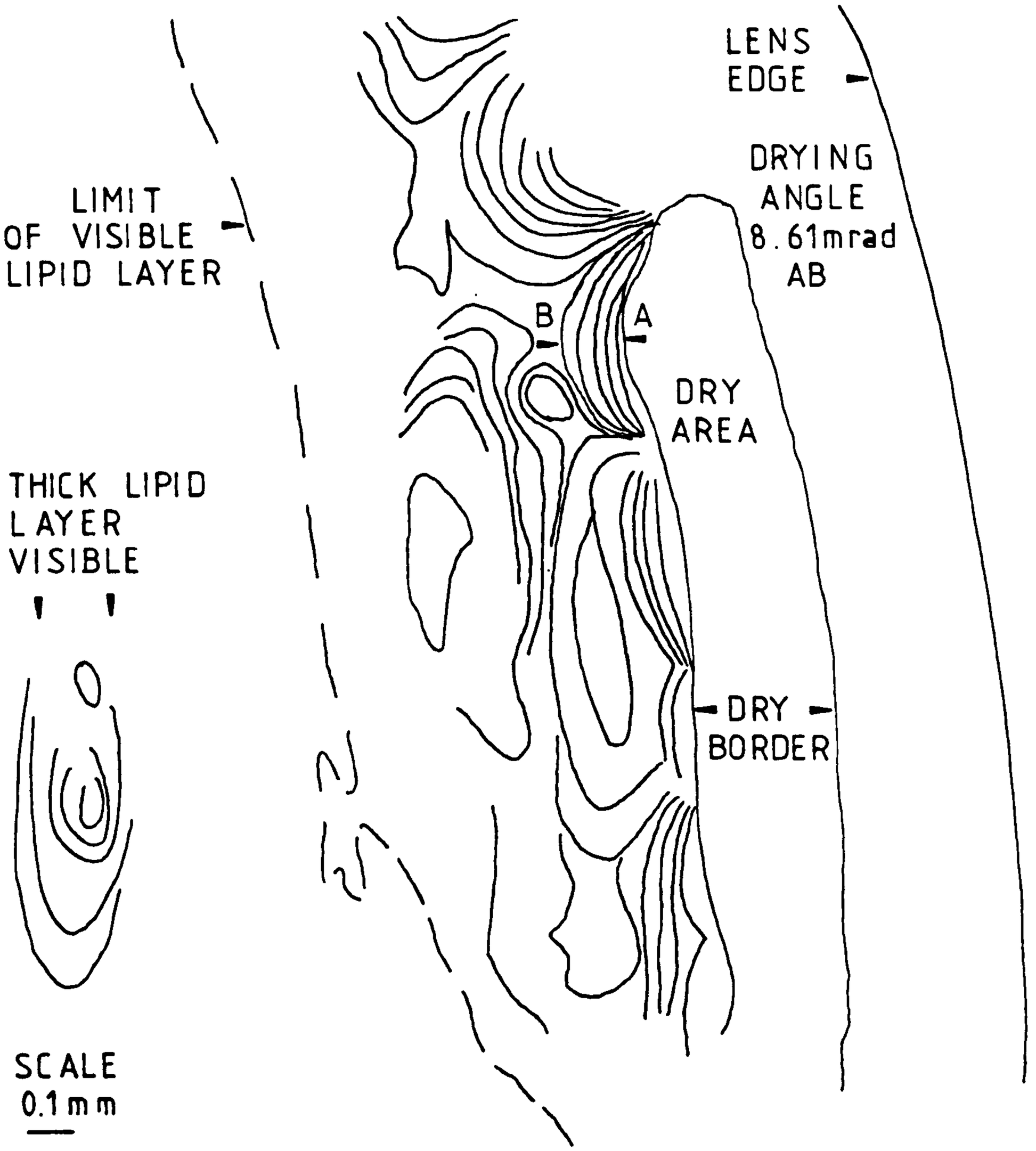

FIGURE 7.40
PRE-LENS TEAR FILM LOW WETTING ANGLE MATERIAL DRYING SEQUENCE PHASE 1: AQUEOUS AND LIPID COVERAGE

reaches 0.14µm and it is vary favourable to tear film formation on contact lenses.

A dry area is present on the lens near the edge.

Closely packed interference fringes near the dry border reveal a steep drying angle in aqueous phase of the pre-lens tear film. This value is of the same order as the PMMA lens and wetting solution: 9.60 mrad.

Further on the left, the main feature of the photograph is the presence of the visible lipid layer, a large grey regular area whose borders are drawn on Figure 7.40.

A thicker part of the lipid layer is also visible and its interference colours denotes a thickness of 0.22µm. Our observations have shown that this lipid layer moves over the lens in a similar fashion as it does as part of the pre-corneal tear film.

A rapid movement following the lid edge, followed by a slower vertical progression, the same area of the layer frequently being repositioned in the same place and thus visible in our narrow specular area even after a few blinks.

The thickness and amorphous nature of the superficial lipid layer present on the right of the photograph prevent the aqueous phase from being visible underneath. It indicates a thick aqueous phase.

PLTF Quantitative Evaluation. The drying angle between A and B has been calculated (Table 7.3).

A : Dry border - d = 0. microns

B : 7th fringe - d = 1.304 microns

AB: Projected distance : 13mm

Reference on Slide and Nature	Tear Film Thickness (μm)	Drying Direction (Distance mm)	Drying Angle (mrad)
A Dry border	0.000	-	-
B (p = 7)	1.304	AB = 141	8.61
Superior Region			
(p = 4)	0.783	-	-
(p = 5)	0.956	Sup 4-5 = 163	1.061
(p = 6)	1.130	Sup 5-6 = 177	0.983
(p = 7)	1.304	Sup 6-7 = 273	0.637
Inferior Region			
p = 4	0.783	-	-
p = 5	0.956	Inf 4-5 = 241	0.718
p = 6	1.130	Inf 5-6 = 201	0.866

TABLE 7.3
LOW WETTING ANGLE MATERIAL PHASE 1: TEAR FILM THICKNESS AND DRYING ANGLES

Real distance: 0.141mm = 7 interfringes

Interfringe : 0.02mm

Drying angle

$$\beta = \frac{0.465}{0.02 \times 2 \times 1.337} = 8.61 \text{ mrad}$$

b) Low wetting angle material

Drying pre-lens tear film Phase II

Because a large area was photographed (Fig 7.41)(2.7mm vertically x 3.4mm horizontally), two diagrams were traced representing adjoining areas (Figs 7.42 and 7.43).

On Figure 7.43, two smaller areas were chosen for observation at higher magnification (x900) in view of determining the possibility of refining the technique of fringe tracing and fringe counting in the case of rapidly thickening tear layer. The two areas are noted on Figures 7.44 and 7.45.

Figure 7.41 and Figure 7.43.

The lens edge is situated on the right, bordered by a dry area and a thick aqueous phase area with its visible interference colours and the sequence green-red-green-red enabling us to determine the position of the 1st blue fringe (p = 4).

The next few fringes are so packed that, at this magnification, the 10th fringe is barely visible.

This is the sign of increasing layer thickness at the centre of the photograph.

In this area a thin lipid layer of the marmoreal type is visible at the bottom and two 'lipid islands' of high reflectance are present further up.

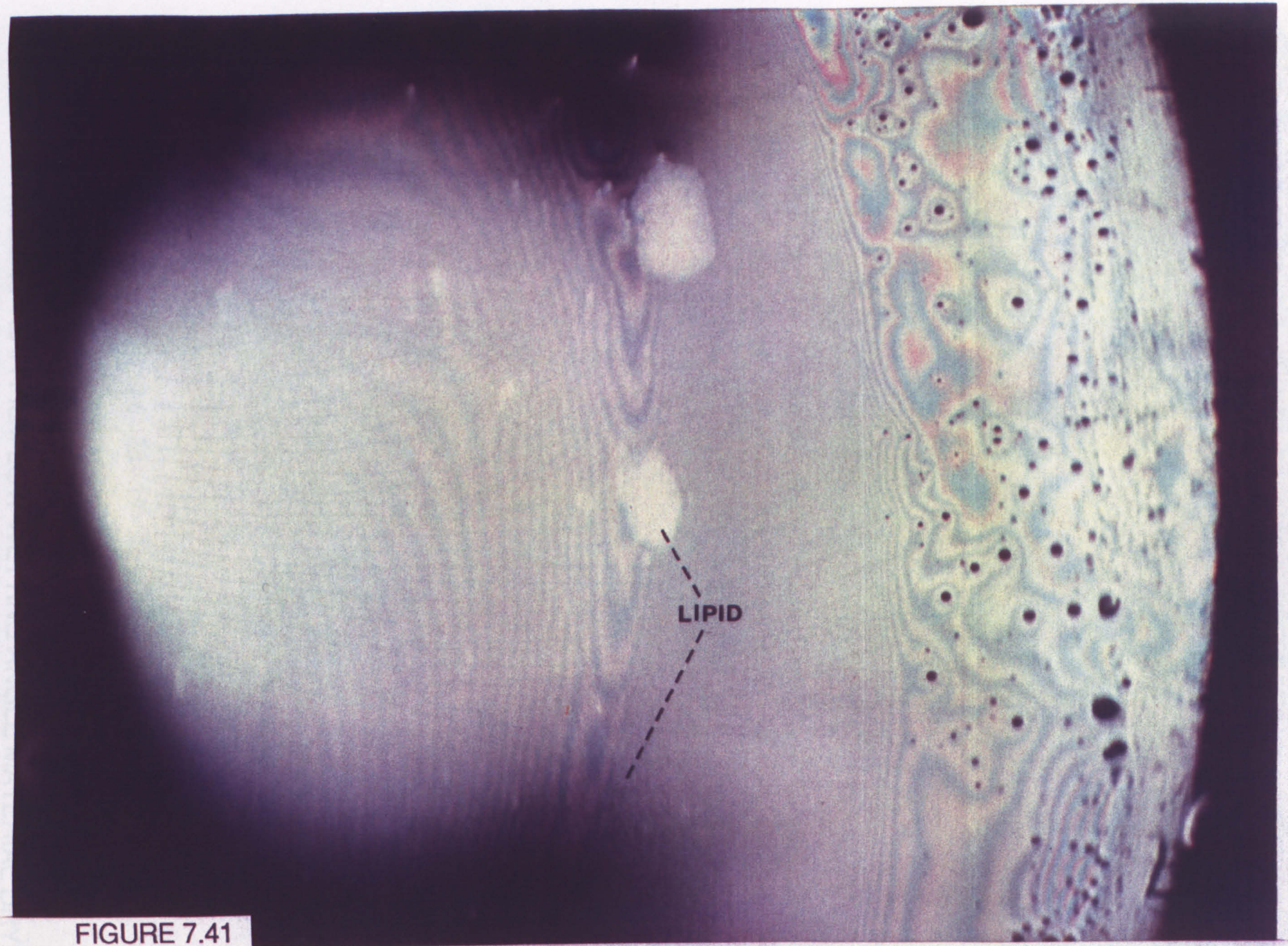

FIGURE 7.41
PRE-LENS TEAR FILM LOW WETTING ANGLE MATERIAL DRYING SEQUENCE PHASE 2
ORIGINAL MAGNIFICATION (X9.6) PHOTOGRAPH MAGNIFICATION (APPROX 95)

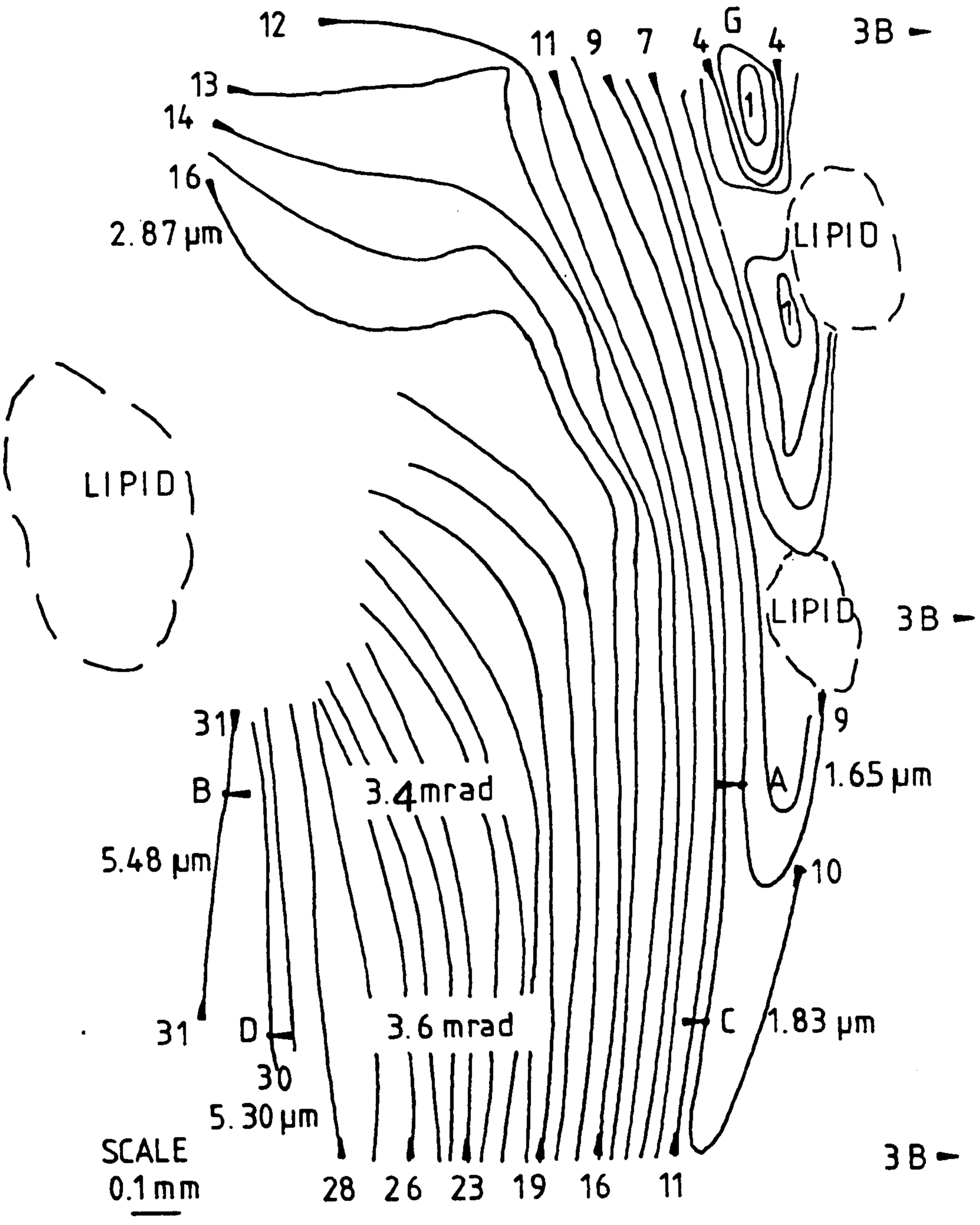

FIGURE 7.42 3 A

PRE-LENS TEAR FILM LOW WETTING ANGLE MATERIAL DRYING SEQUENCE PHASE 2: OUTLINE OF FRINGES 1 TO 31 AND LIPID OUTLINE LEFT SIDE OF PHOTOGRAPH

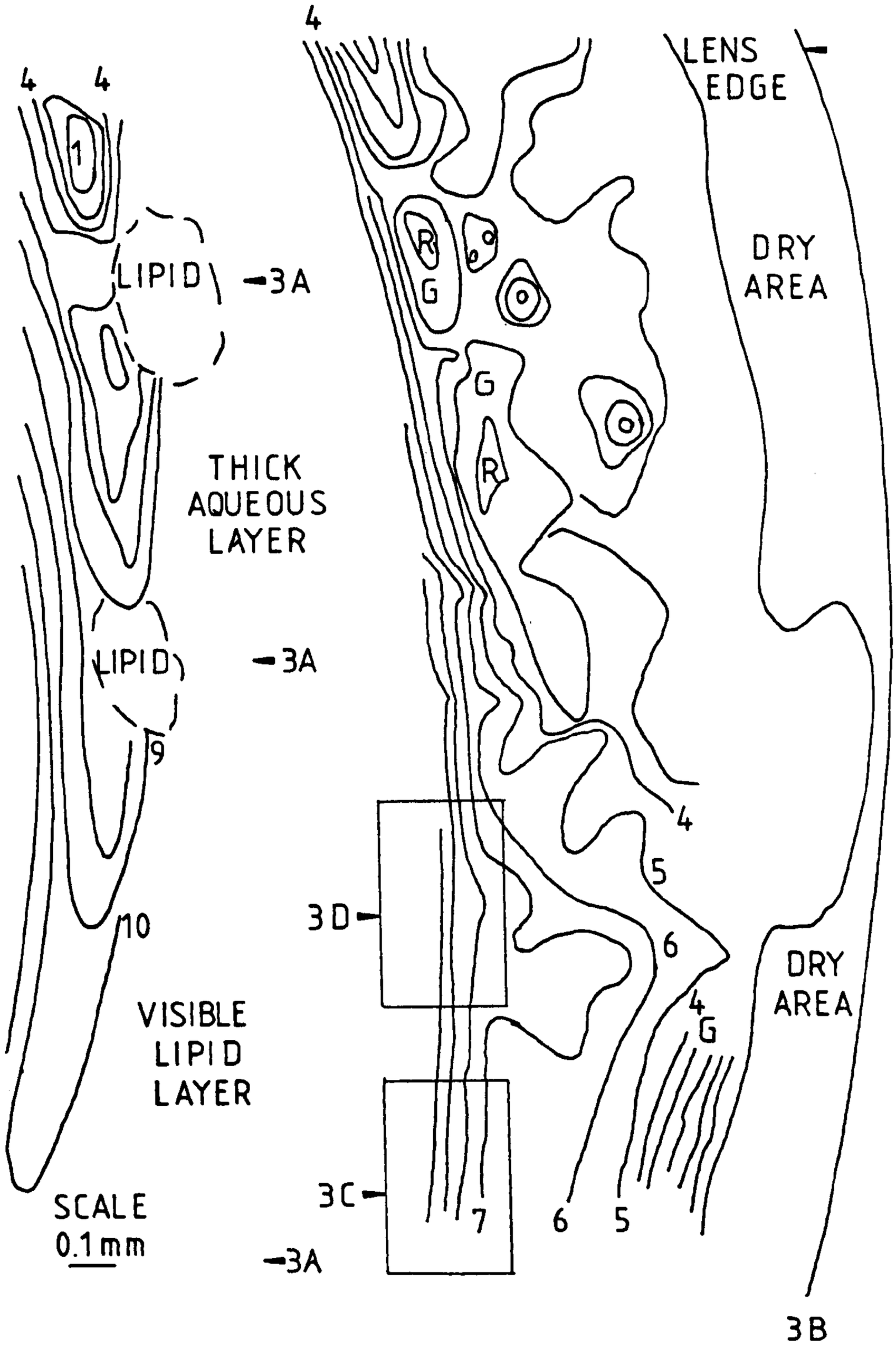

FIGURE 7.43
PRE-LENS TEAR FILM LOW WETTING ANGLE MATERIAL DRYING SEQUENCE PHASE 2: OUTLINE OF FRINGES AND LIPID LAYER RIGHT SIDE OF PHOTOGRAPH

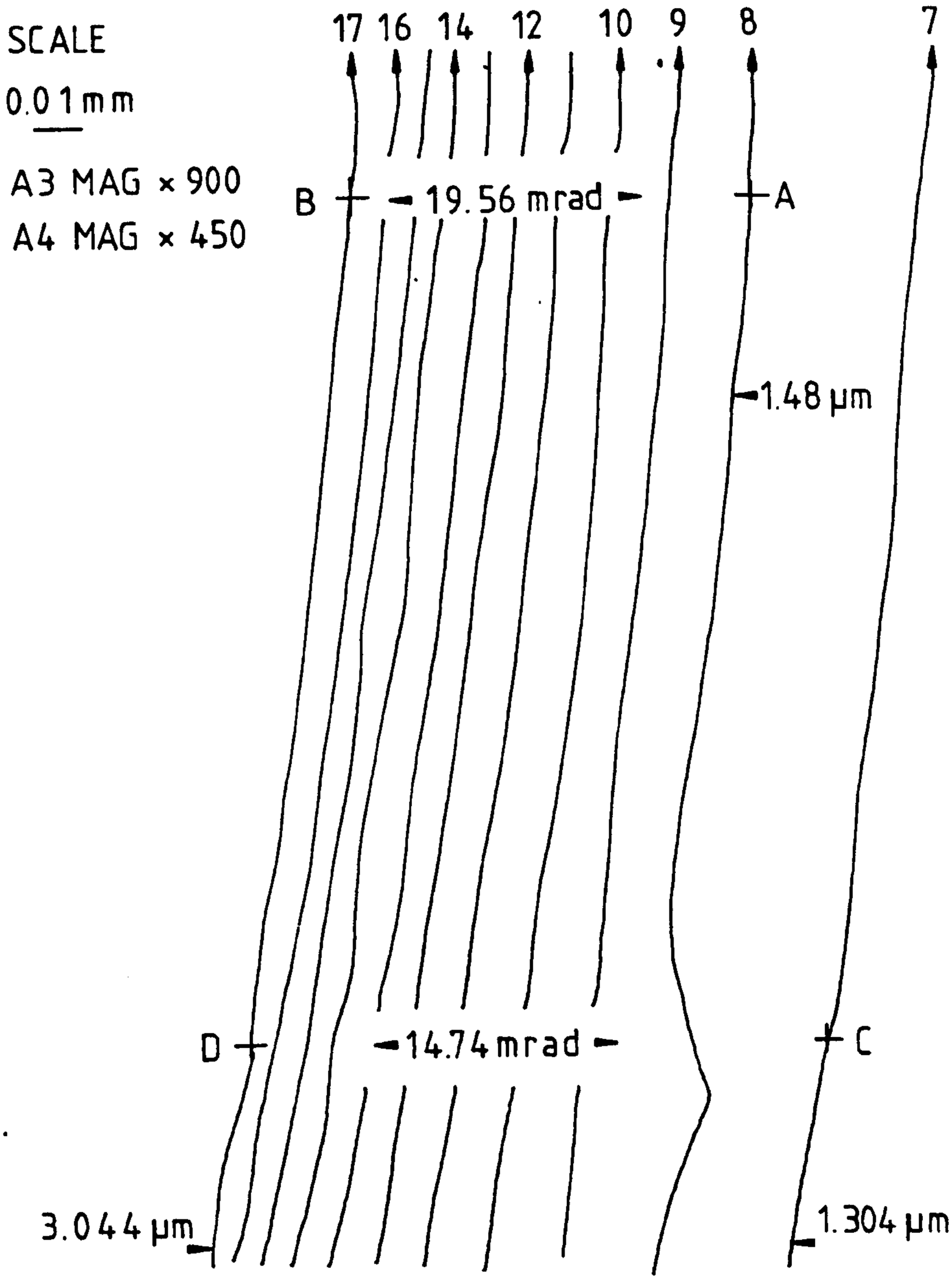

FIGURE 7.44
PRE-LENS TEAR FILM LOW WETTING ANGLE MATERIAL DRYING SEQUENCE PHASE 2: AREA C OF FIG 7.43: OUTLINE OF FRINGES 7 TO 17 AND RESULTS OF MEASUREMENT

3D

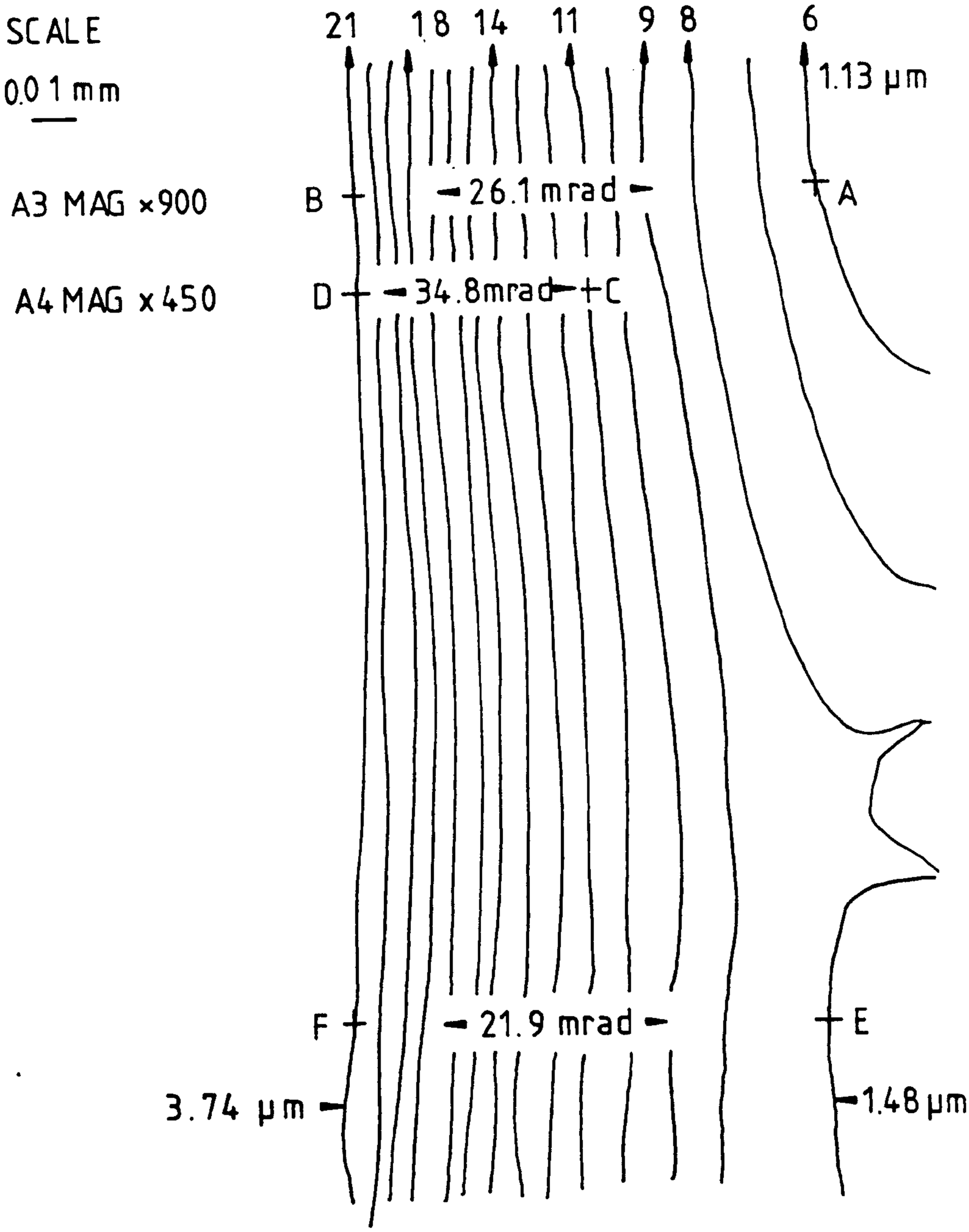

FIGURE 7.45
PRE-LENS TEAR FILM LOW WETTING ANGLE MATERIAL DRYING SEQUENCE PHASE 2: AREA D OF FIG 7.43: OUTLINE OF FRINGES 6 TO 21 AND RESULTS OF MEASUREMENT

Figure 7.42

Next to the 'lipid islands' the fringes reappear in the aqueous phase of the pre-lens tear film. Interference colours of the first order (noted I on the figure) are seen.

Fringe tracing in this area shows an aqueous phase thickness increasing to 2.87µm at the top and to 5.48µm at the bottom. Where the aqueous wedge angle was respectively 3.35 mrad between A and B and 3.60 mrad between C and D (Table 7.4).

This photograph (Fig 7.41) demonstrates very well different aspects of the photographic technique and its use for the analysis of the structures and measurements of tear layer thicknesses on rigid contact lenses.

1) The precision of the technique renders the 31st fringe of interference visible; this is due to the use of the polarising filters used in near crossed polarisation which effectively narrows the peak of emission of the strobe light and increases the length of coherence of the system (Section 6.4 3). From the centre to the left of the picture, it can be seen that the visibility of the aqueous fringes reduces with increasing layer thickness before merging as a white continuum.

2) The effect of the lipid layer on the visibility of the fringes can be seen:

- at the bottom of the picture a thin marmoreal layer is visible because the underlying aqueous phase is too thick to produce interference fringes of sufficient intensity. The steep aqueous wedge angle in that area narrows the separation of the fringes; over a very short

Reference on Slide and Nature	Tear Film Thickness (μm)	Drying Direction (Distance mm)		Drying Angle (mrad)
		-		-
A p = 9	1.652			
B p = 31	5.480	AB	= 1.141	3.350
C p = 10	1.826		-	-
D p = 30	5.306	CD	= 0.956	3.640
p = 7	1.304	-		-
p = 8	1.478	7-8	0.398	0.437
p = 9	1.652	8-9	0.363	0.479
p = 10	1.826	9-10	0.305	0.570
p = 11	2.000	10-11	0.314	0.554
p = 12	2.174	11-12	0.288	0.604
p = 13	2.348	12-13	0.294	0.582
p = 14	2.522	13-14	0.251	0.693
p = 15	2.696	14-15	0.328	0.530
p = 16	2.870	15-16	0.313	0.556
p = 17	3.044	16-17	0.325	0.535
p = 18	3.218	17-18	0.413	0.421
p = 19	3.392	18-19	0.440	0.395
p = 20	3.566	19-20	0.444	0.392
p = 21	3.740	20-21	0.487	0.357
p = 22	3.914	21-22	0.518	0.336
p = 23	4.088	22-23	0.458	0.380
p = 24	4.262	23-24	0.437	0.398
p = 25	4.436	24-25	0.471	0.369
p = 26	4.610	25-26	0.490	0.355
p = 27	4.784	26-27	0.401	0.434

TABLE 7.4
LOW WETTING ANGLE MATERIAL PHASE 2: TEAR FILM THICKNESS AND DRYING ANGLES

distance they cannot be discerned individually and this leads to the appearance of the whitish continuum.

- on the left of that area, the decreased aqueous phase thickness and the flatter aquous phase wedge angle produces interference fringes of wider separation, higher intensity and increased visibility. This makes them visible below a thin lipid layer (of probably 40nm in thickness).

- when that lipid layer thickness increases as seen on the big patch on the left of photograph, Figure 7.41 (L1); its intensity overcomes that of the fringes produced by the layer of increased aqueous thickness (3µm to 5.5µm).

- with further increase of lipid thickness (80 to 90nm) seen on the floating patches marked L2 and L3 the increase reflectivity can even overcome aqueous fringes of high intensity produced in the thin end of the wedge (1µm to 1,83µm).

A large 'lipid island' is noticeable on the left of the picture by its increased reflectivity.

Figure 7.44

This corresponds to area C of Figure 7.43. This small area has been projected to obtain a x900 magnification to enable us to discern the fringes which lie very close to one another. It was possible to outline fringes 7 to 17 corresponding to a layer increase from 1.304µm to 3.044µm.

The points A, B, C and D were chosen for angle calculation in that area (Table 7.4)(Fig 7.46).

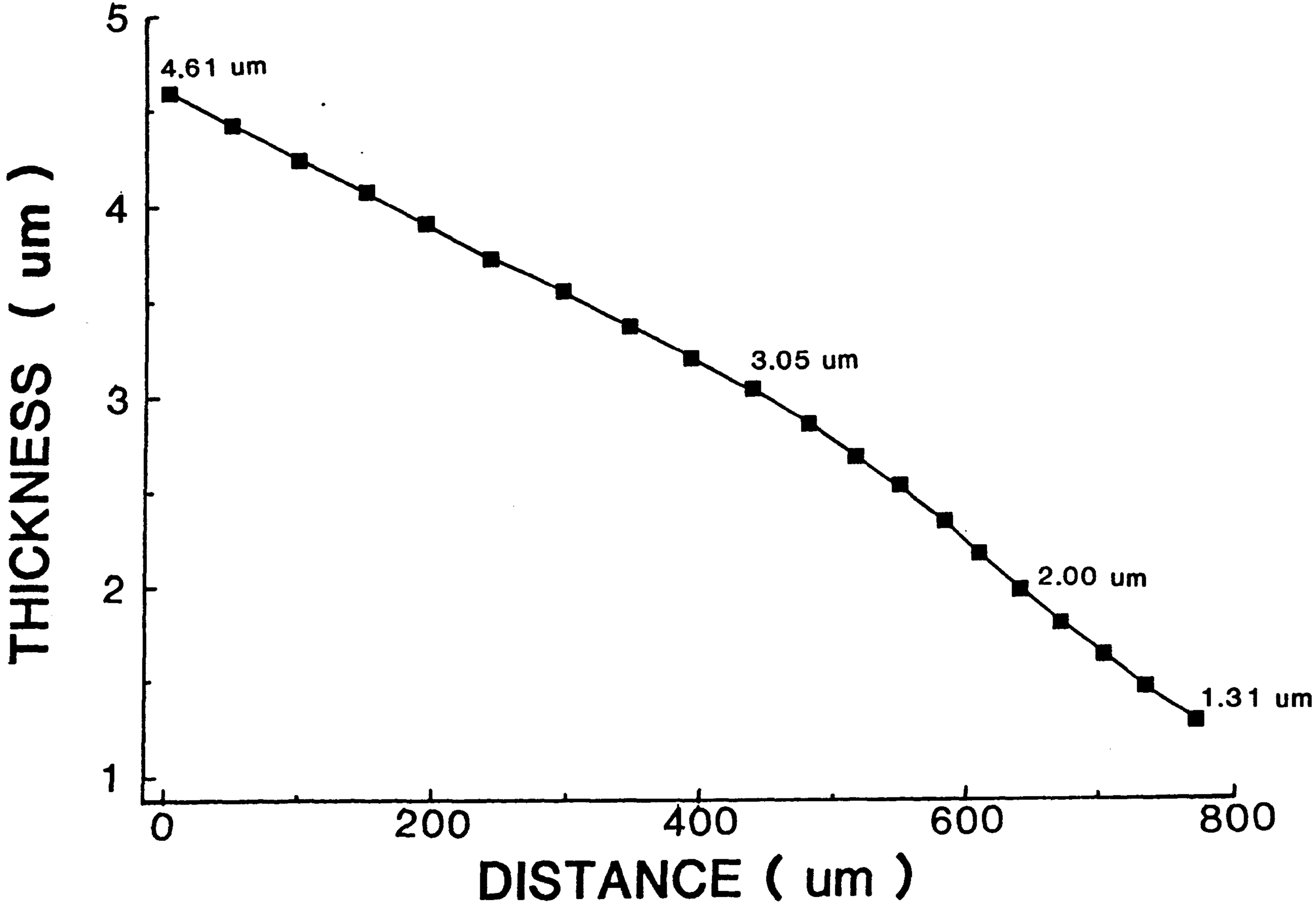

FIGURE 7.46
PRE-RIGID LENS TEAR FILM THICKNESS PROFILE 1: LOW WETTING ANGLE MATERIAL

The large value of the wedge angle in the area C and D chosen explains the quick disappearance of the fringes over a very short distance. This area corresponds to the junction zone of the contact lens between the front optic zone and the flattening lens edge. The change of curvature at that point produces local depression filled with the tear film which depth is measured by the aqueous wedge measurement.

c) Low wetting angle material

Drying pre-lens tear film Phase III

Figure 7.47 and Figure 7.48 correspond to 4 seconds after Figure 7.41.

PLTF Qualitative Assessment. The junction line is now visible following overall thinning of the PLTF.

- on the right of the junction a dry zone is present.

- as on the previous picture, the junction zone is covered by a layer of tear film where fringes are not visible.

- two small areas of wetting encroaches on the neighbouring drying zone. These small areas (arrowed on Figure 7.48) correspond to those previously covered superficially by the two lipid islands.

- the central drying area is covered by particles of greater size than those present when the covering PLTF is thinner (Figs 7.30, 7.32 and 7.34) they may be remnants of a thick basal mucin layer necessary to support a thicker and more stable PLTF.

- the aqueous phase on the left of the photograph has undergone further thinning, down to 4.4µm, since the

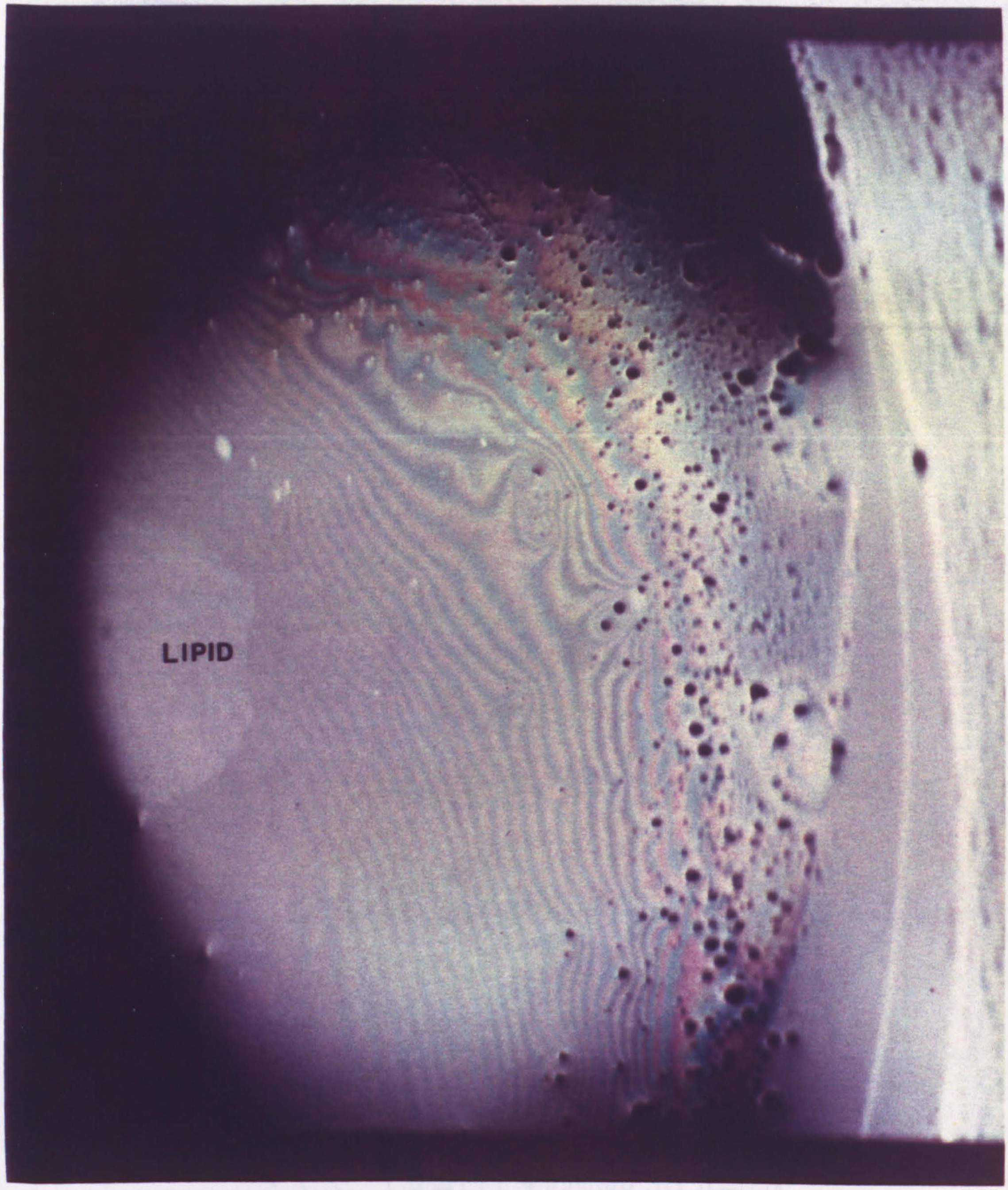

FIGURE 7.47
PRE-LENS TEAR FILM LOW WETTING ANGLE MATERIAL
DRYING SEQUENCE PHASE 3
ORIGINAL MAGNIFICATION (X9.6)
PHOTOGRAPH MAGNIFICATION (APPROX 95)

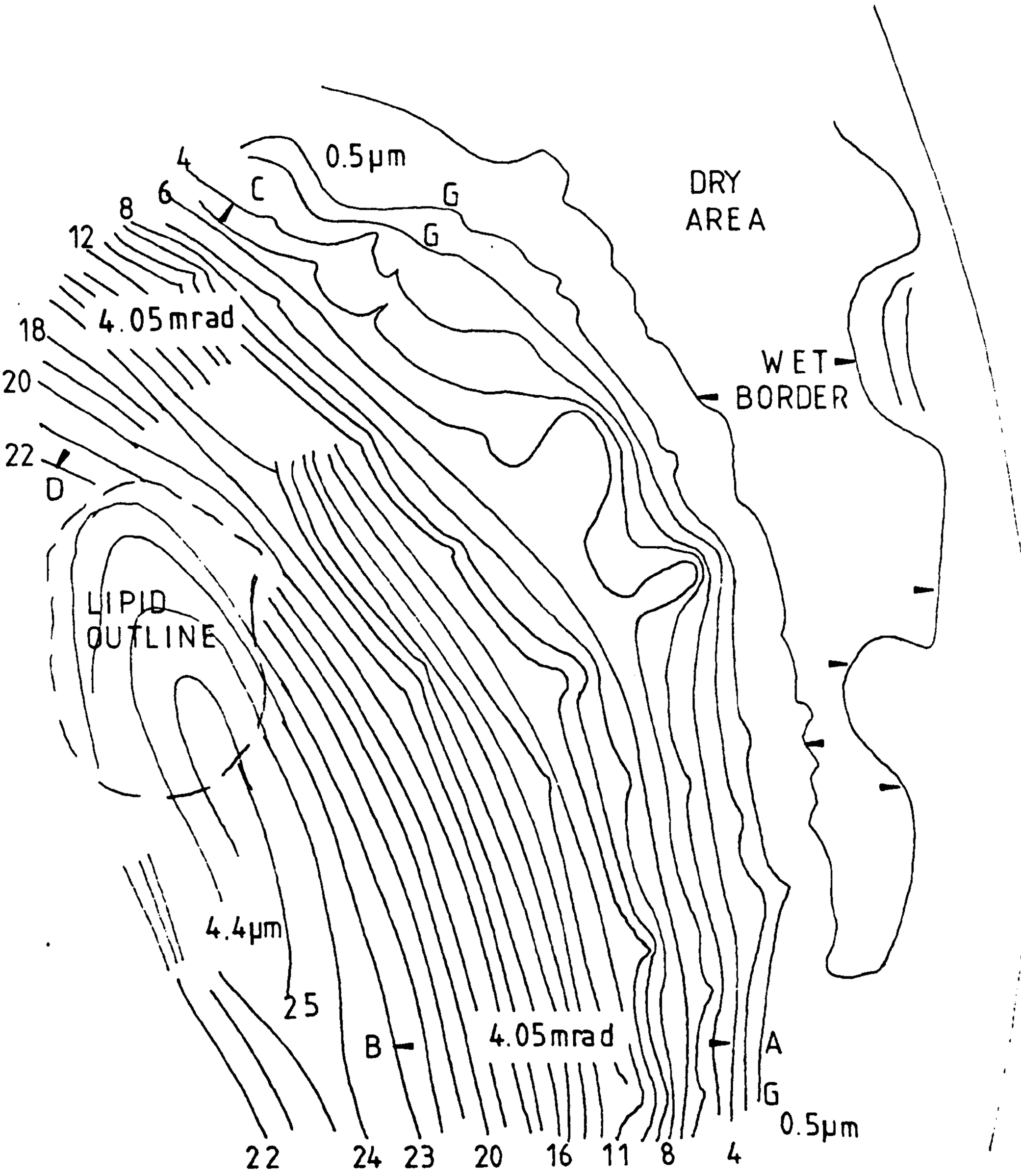

FIGURE 7.48
PRE-LENS TEAR FILM LOW WETTING ANGLE MATERIAL
DRYING SEQUENCE PHASE 3: OUTLINE OF FRINGES 1 TO 25
AND LIPID OUTLINE

previous photograph but the same remarks still hold true for the visibility of the aqueous fringe, in fact, some are now faintly visible below the large superficial lipid patch. With further drying the PLTF will continue to thin by the effect of evaporation and if blinking is prevented the whole of the lens surface will dry.

A blink will reform a new PLTF which will undergo again the same process of drying previously presented.

PLTF Quantitative Evaluation. The points A, B, C and D have been chosen for calculation of drying angles (Table 7.5 and Fig 7.49).

7.4 EXPERIMENTAL STUDY 4. MUCOUS LAYER PHOTOGRAPHY ON THE CORNEAL AND ON CONTACT LENS SURFACES

7.4.1 INTRODUCTION

The high and low magnification photography of the superficial layers have shown that the tear film displays a variety of structures according to the surface on which it spreads.

Only a brief glimpse of the basal mucous layer has been possible in the course of dry spot formation on the cornea and on contact lenses (7.2.3 and 7.3).

The present experimental study was set up to devise a technique to make this layer visible and investigate its appearance, structure and measure its thickness.

Reference on Slide and Nature	Tear Film Thickness (μm)	Drying Direction (Distance mm)		Drying Angle (mrad)
A p = 4	0.783	-		-
B p = 23	4.088	AB	= 0.815	4.055
C p = 4	0.783	-		-
D p = 22	3.914	CD	= 0.772	4.056
p = 7	1.304	6-7	0.404	0.431
p = 8	1.478	7-8	0.335	0.519
p = 9	1.652	8-9	0.316	0.551
p = 10	1.826	9-10	0.363	0.479
p = 11	2.000	10-11	0.324	0.537
p = 12	2.174	11-12	0.347	0.501
p = 13	2.348	12-13	0.350	0.497
p = 14	2.522	13-14	0.311	0.559
p = 15	2.696	14-15	0.297	0.586
p = 16	2.870	15-16	0.332	0.524
p = 17	3.044	16-17	0.363	0.479

TABLE 7.5
PRE-LENS TEAR FILM LOW WETTING ANGLE MATERIAL DRYING SEQUENCE PHASE 3

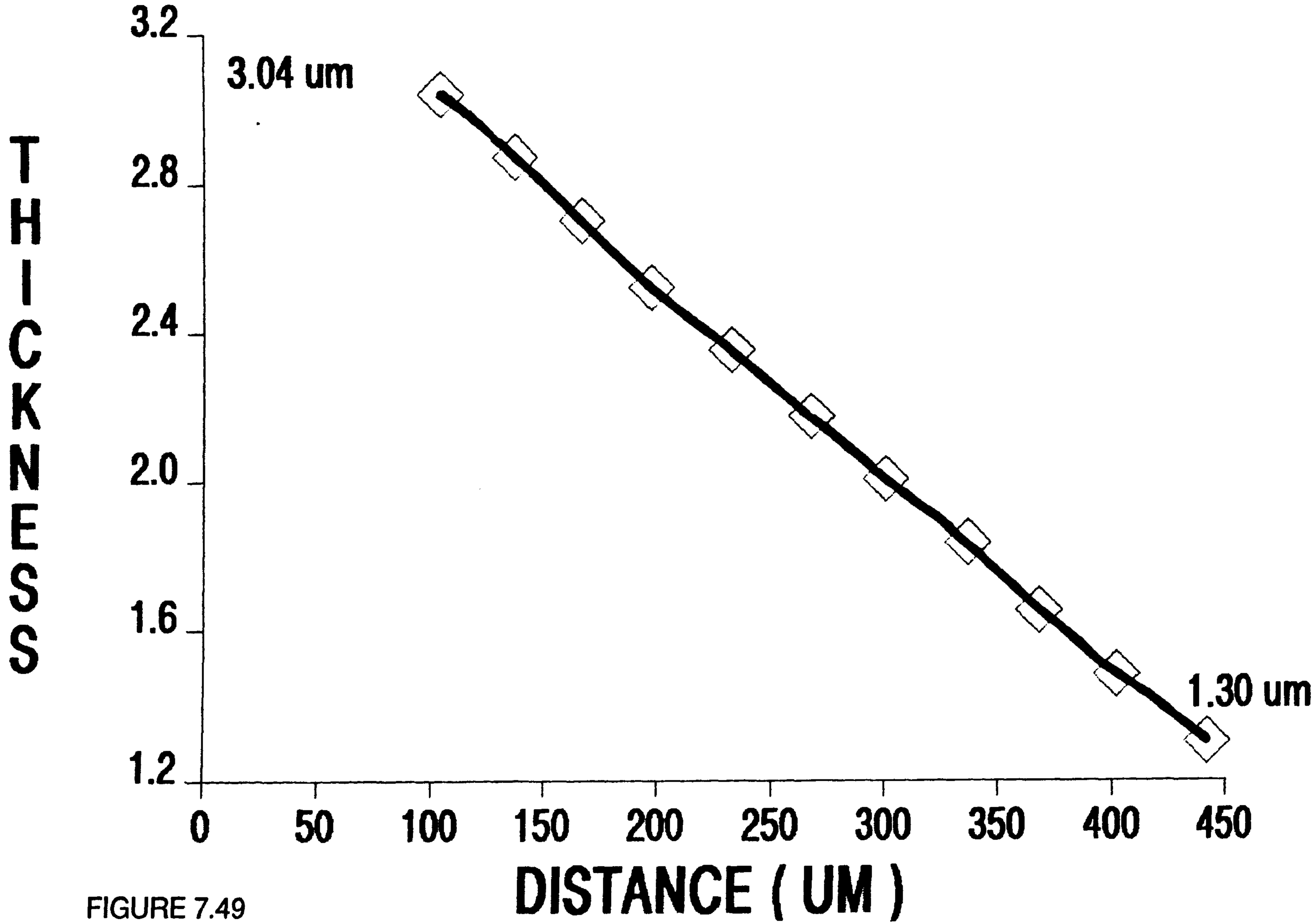

FIGURE 7.49
PRE-LENS TEAR FILM LOW WETTING ANGLE MATERIAL: SECTIONAL ANALYSIS OF THICKNESS AND DRYING ANGLES

7.4.2 MATERIAL & METHOD

The technique described in Chapter 5.4 has been applied to the study of the corneal surface of two normal subjects and one subject presenting dry eye symptoms. The observations were repeated on the two normal subjects after fitting with contact lenses of different materials.

i) Observation on the Cornea

The two subjects had a normal tear film. The pre-ocular tear film had been examined by the non-invasive techniques described previously and presented both a marmoreal pattern with limited amounts of surface particles. Their tear meniscus had a normal morphology and height and the break-up time measured by the non-invasive technique (NIBUT) was above 20 seconds. No corneal staining was present after fluorescein instillation.

The pre-ocular tear film was first examined and photographed with the Nikon biodifferential microscope and the routine for observation of the mucous layer was carried out as described in Chapter 5.5.

The observations were repeated on 3 different days and the best photographs taken at different stages of drying were analysed, one example is shown.

The same routine was applied to the cornea of one subject presenting dry eye symptoms. The subject had a history of subjective complaints of ocular dryness and grittiness, repeated failure with soft and rigid contact lenses directly linked to drying problems and a low NIBUT (right eye - 8 seconds: left eye - 7 seconds) but no

corneal staining was present following fluorescein instillation.

ii) Observations on Contact Lenses

At subsequent sessions, the subjects with normal tear films were fitted with contact lenses of the followimg materials and water contents.

Lenses	Water Content
Hydron Z6	38 percent
Permalens	75 percent
Collagen	90 percent
Saturn	Hybrid lens4

The best photographs taken at different stages of drying obtained were analysed and one example presented here. The discussion and conclusion will also be drawn from all the observations on all lenses.

7.4.3 RESULTS

i) Normal Tear Film

The photograph (Fig 7.50) is representative of the dry spot formation on the normal cornea as explained in Chapter 5.4.2. The tear film enclosed within a containing meniscus takes longer to break up and the surface of the ocular tear film was scanned until such a break occurred.

a) POTF drying sequence

A small area of thinning of the film is first noted. It took either the shape of an elongated depression or more commonly a circular shape. Throughout

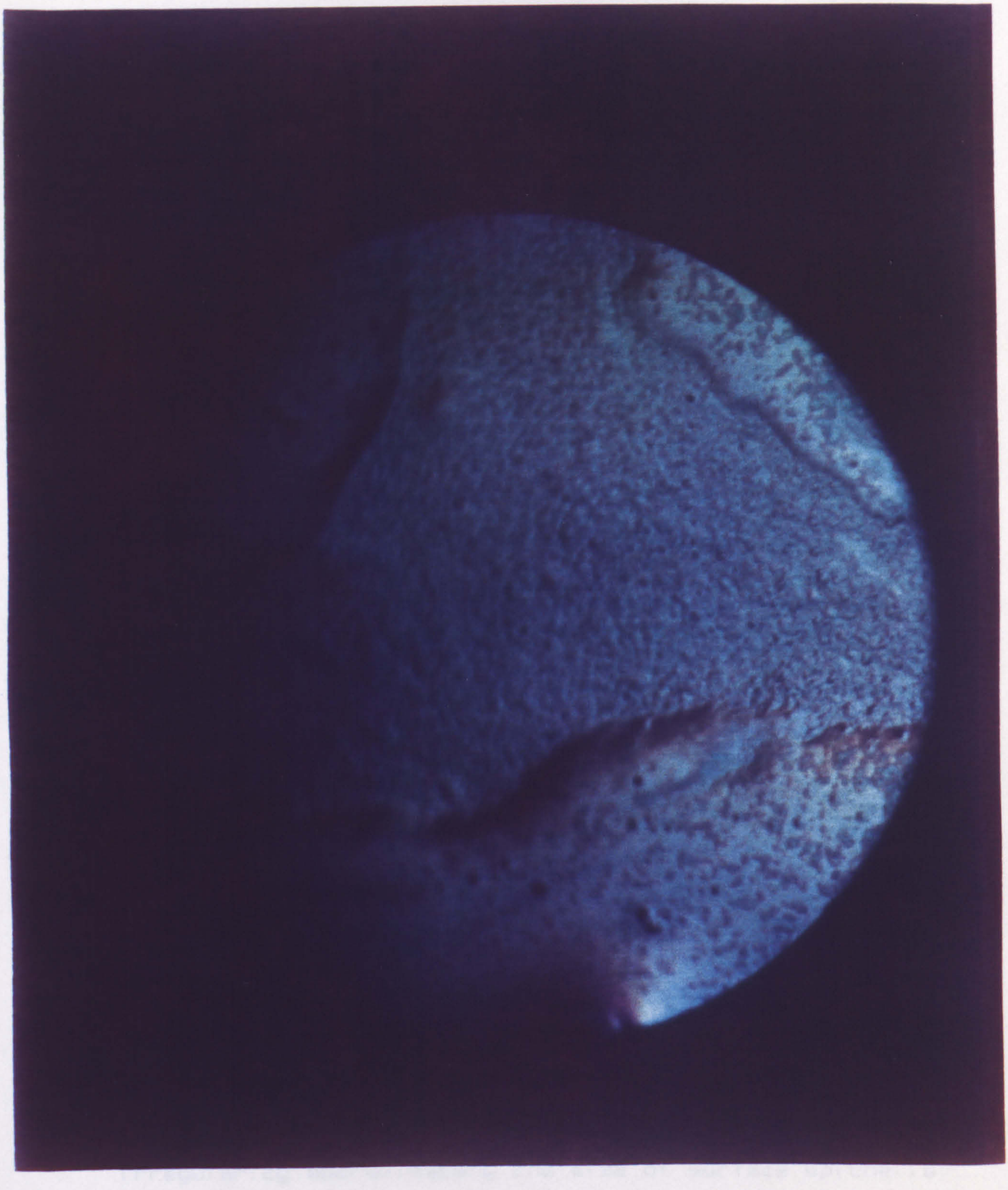

FIGURE 7.50
IN-VIVO PHOTOGRAPHY OF THE MUCOUS LAYER ON THE CORNEA
NORMAL EYE

the drying process the lipid layer was always visible but no interference fringes produced within the aqueous phase were ever seen. Even when that layer was very thin immediately before the appearance of the mucous coated corneal surface.

The intensity of interference fringes formed in very thin films is very high (Chapter 6), it was expected to be able to photograph some of the fringes in those conditions especially when the superficial lipid phase was marmoreal in appearance (40 to 70nm thick).

b) Qualitative analysis

Figure 7.50 shows one photographic example and Figure 7.51 its diagrammatic outline.

The tear film is visible in the periphery of the photograph. Its lipid layer interference colours reveal a thickness between 90nm (0.09µm)(whitish) to 220nm (blue). The edge of the film is curved effecting the in-vivo shape of the real receding contact angle of the tear film on the corneal surface in natural conditions.

The central drying area represents the corneal surface. Its coating has high reflectivity and possibly this is due to remnants of the thick lipid layer which has deposited on the underlying mucous phase.

The surface is not smooth but shows discrete irregularity approximately the size of surface epithelial cells (10 to 20 microns).

Continuous observation of the dry spot area showed an increase of the surface irregularity. This is possible if the mucous layer has a finite thickness and is hydrated. The micrometre latex spheres in aqueous

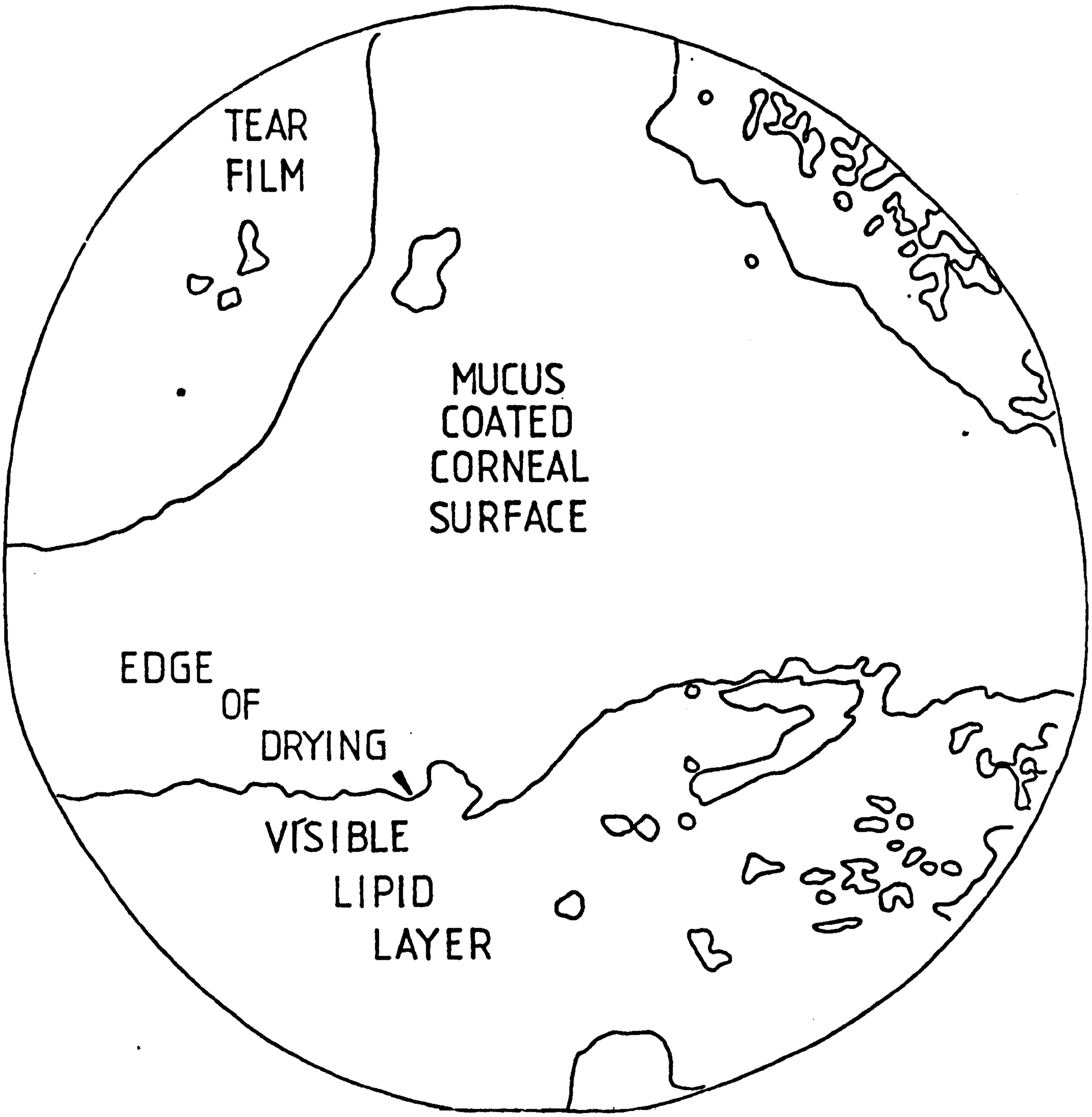

FIGURE 7.51
DIAGRAMMATIC OUTLINE OF IN-VIVO PHOTOGRAPHY OF THE MUCOUS LAYER ON THE CORNEA: NORMAL EYE

solution had been instilled for some observations, they floated at the surface of the film or rested at the surface of the dry spot and did not imbed themselves in the mucous layer. It was then not possible to assess the layer thickness by this method.

On removal of the scleral contact lens and following fluorescein instillation, no staining was noted in the central area that was under observation. This is only possible if the integrity of the epithelial surface and its mucous coating is respected. It is a good guide to the safety of the technique of in-vivo epithelial surface examination but also enhances the protective role provided by an integral mucous coating.

ii) Dry Eye Symptoms Subject

Figure 7.52 and 7.53 is a representative example of dry spot formation in a subject with dry eye symptoms, that can be classified as marginal dry eye and did not exhibit the gross epithelial signs present in dry eye syndromes.

The dry spot formation followed the same sequence as that seen in normal subjects. The receding tear film is seen at the periphery of the photograph (Fig 7.52). A lipid layer is present and its interference colours reveals a thickness between 90nm (whitish) and 220nm (blue). Interference fringes from the aqueous phase cannot be seen. The central drying area representing the corneal surface coating appears duller than in the normal case and the surface irregularities present are limited in number and more widely spaced apart.

FIGURE 7.52
IN-VIVO PHOTOGRAPHY OF THE MUCOUS LAYER ON THE CORNEA:
DRY EYE SYMPTOMS

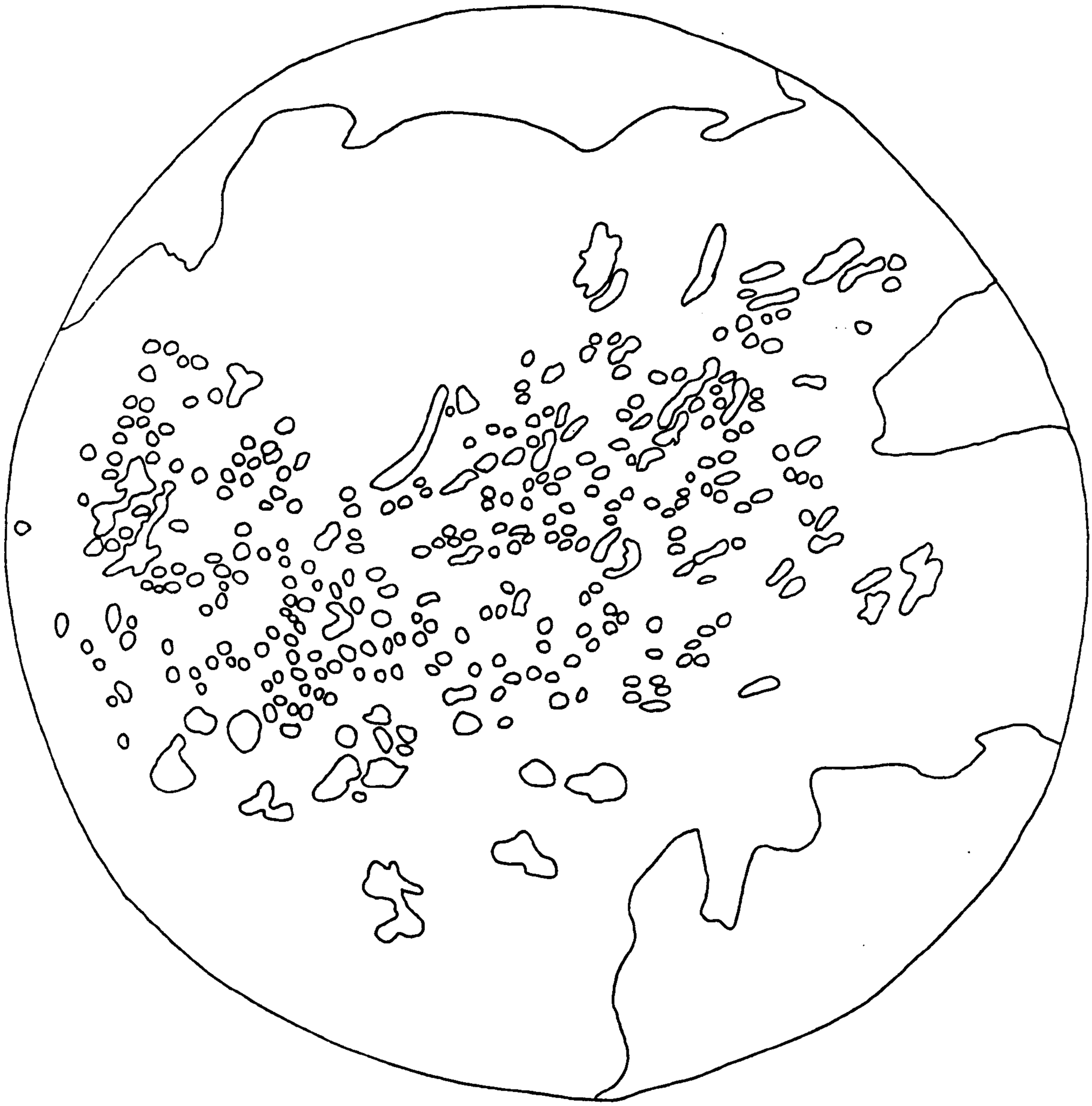

FIGURE 7.53
DIAGRAMMATIC OUTLINE OF IN-VIVO PHOTOGRAPHY OF THE MUCOUS LAYER ON THE CORNEA: DRY EYE SYMPTOMS

The continuous observation of the dry spot reveals only a small increase in the depth of those irregularities. This would be the case for a thin layer with reduced hydration where evaporation will have only a limited effect.

iii) Mucous Coating on Contact Lens Surface

The process of dry spot formation was studied with the same technique on a variety of contact lens surfaces. The photograph in Figure 7.54 and its diagrammatic representation (Fig 7.55) is representative of the situation in a low water content soft lens (eg. Hydron Z6; 38 percent water content).

a) PLIF drying sequence

A thin marmoreal lipid pattern was visible at the surface of the pre-lens tear film. As the localised thinning occurred the interference fringes formed within the aqueous phase could be faintly seen. Their intensity is much lower than those seen in front of rigid corneal lenses. The lipid layer receded faster than the aqueous phase and was not seen near the aqueous border. The receding aqueous phase revealed a smooth dull surface.

b) Qualitative analysis

The lower right part of the photograph denotes the interference fringes of the receding aqueous phase. This is part of a series of photographs showing the aqueous movement.

The smooth surface structure at the centre of the dry spot represents the mucous coating of the contact lens. This coating is not as compiete as in the case of

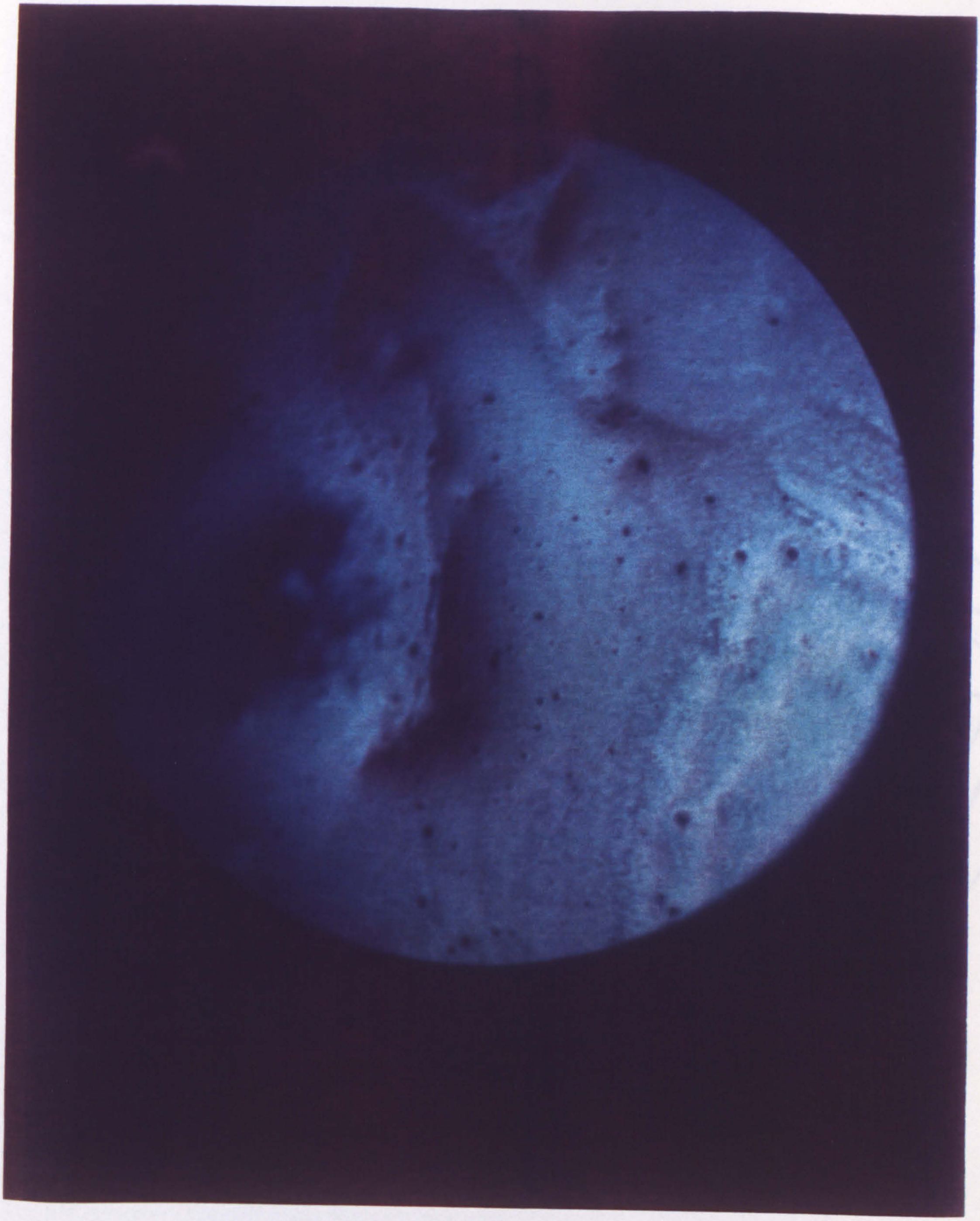

FIGURE 7.54
PHOTOGRAPHY OF THE MUCOUS LAYER ON SOFT CONTACT LENSES

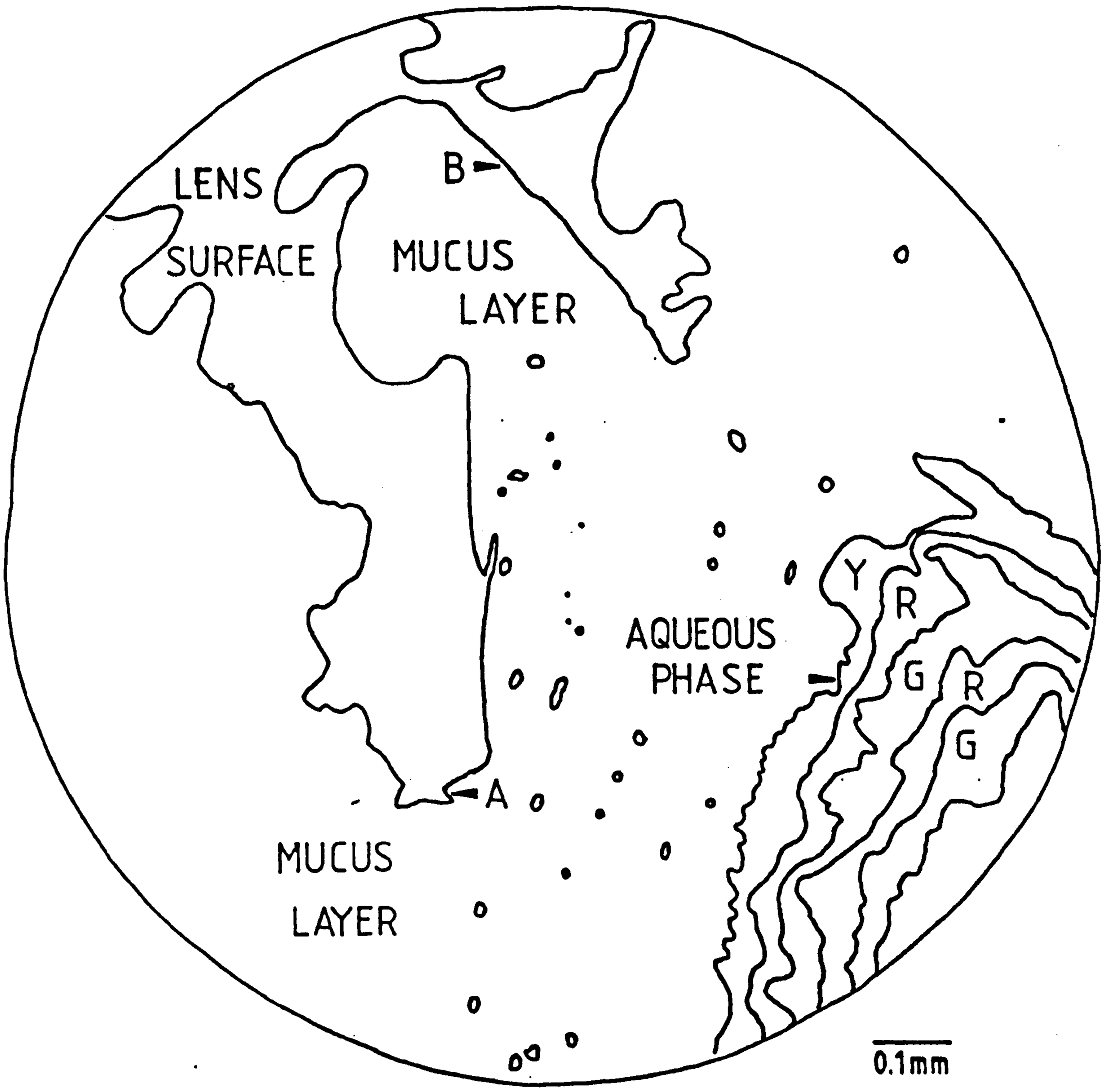

FIGURE 7.55
DIAGRAMMATIC OUTLINE OF PHOTOGRAPHY OF THE MUCOUS LAYER ON SOFT CONTACT LENSES

the corneal surface, the gentle slope delimits the area where the coating is thinnest. The appearance of ridges is a common feature in the area of dry spot formation on hydrophilic lenses and this may have induced the localised break-up.

The black dots resting at the surface of the mucous layer are the micrometre latex spheres that had been instilled in an effort to measure the thickness of the layer. The spheres floated at the surface of the lipid layer at first and when it receded stayed on top of the surface.

The continuous observation of the dry spot produced an increase and a deepening of the ridge formation while the rest of the smooth area remained unaffected.

CHAPTER 8

DISCUSSION

8.1 EXPERIMENTAL STUDY 1: PRE-OCULAR TEAR FILM LIPID LAYER

8.1.1 COMMON LIPID PATTERNS

i) Normal Marmoreal Pattern

Such a pattern was first observed by McDonald (1969) but only described, in detail, by Hamano et al (1979a), and can be considered as the normal lipid layer. It is encountered in approximately 89 percent of patients (Hamano et al, 1979b).

Functionally the marmoreal pattern is usually associated with a stable POTF. If contact lens fitting is attempted with either hard or soft contact lenses these patients are usually free of tear related problems.

ii) Contaminated Marmoreal Pattern

This is a particular problem with contact lens wear. The increased instability occurs as follows:

- excessive atmospheric or epithelial debris and/or mucous lumps deposit to the lens front surface.

- the lens front surface is no longer smooth and the normal tear film spreading and surface wetting becomes more difficult and dry areas appear at the zones of discontinuity.

- when mucous strands are found the matter is even worse, not only increased deposits are observed, but the

mucous strands affect the lipid layer and do not allow even lipid spreading.

One clinical implication is that of caution when fitting contact lenses to patients with contaminated marmoreal lipid pattern. A material known for its low deposit attraction should be selected and the patient informed of the possible problems. Cleaning procedures strictly adhered to and regular protein deposit removal is strongly advocated.

The presence of a contaminated marmoreal lipid pattern renders the tear film unstable. This is a particular problem with contact lens wear.

iii) Flow Pattern

This wavy pattern is probably due to the flow of lipids of different classes with poor mixing properties. However, one must not confuse this pattern with the phenomenon that normally occurs immediately after a blink, when the mucin and aqueous films first spread, followed a few tenths of a second later by the spreading of lipids (Brown & Dervichian, 1969; Holly, 1973a).

Hamano et al (1979a), were responsible for naming that type of pattern a Flow Pattern.

Patients exhibiting a flow pattern have usually a stable tear film and if fitted with contact lenses they are free of tear film related problems.

iv) Amorphous Pattern

The amorphous pattern was first described by Koby (1924) and later incorporated in the first lipid layer classification by Hamano et al (1979a).

The amorphous pattern is always associated with a very stable tear film, as this even and relatively thick lipid layer is very efficient at maintaining a low evaporation rate. Patients with an amorphous layer are good candidates for contact lens wear, with the exception of a small minority who exhibit lens greasing problems due to the large volume of lipids present. In such cases, hard gas permeable lenses may be the best option, with routine use of in-eye lens surface cleaners such as Blink N Clean or Clerz eye drops.

v) Coloured Fringe Pattern

These coloured interference fringes produced by the lipid layer were first described in detail by McDonald (1969).

Those patients are poor contact lens candidates in particular with regard to soft contact lenses, where large deposits rapidly form at the lens front surface.

As an unstable pre-lens tear film (PLTF) will be present, accompanied with a very short anterior surface drying time (ASDT) and symptoms of dryness, treatment of the underlying cause is necessary and visible improvement in the stability of the lipid layer will accompany the disappearance of symptoms.

8.1.2 OVERALL PRE-CORNEAL LIPID PATTERN

The figures 7.7 and 7.8 show well the potential of the low magnification method for routine clinical use. The area of observation covered by the instrument is dependent on its promixity to the eye surface. This in turn varies with the morphology of the patients face and

the presence of the nose impeding on the reflection cup positioning. Usually a 7.8mm circular area is covered.

i) Combination 1 (Figure 7.7)

The property of such a layer is a combination of the properties of its two components.

ii) Combination 2 (Figure 7.8)

Because of the presence of large volumes of lipids a stable film tends to form on the lens front surface but following its break-up, increased surface contaminants may occur and the patients complain of greasy lenses.

8.1.3 ABNORMAL LIPID PATTERNS

i) Lipid Clumping (Figure 7.9)

These patients usually have a low break-up time and are poor contact lens candidates.

ii) Localised Lipid Layer Break-Up

The photograph 7.10 shows only localised lipid break-up. In cases of severe tear film contamination produced by cosmetic products or oils migrating to the ocular surface, the break-up becomes total. The lipid gathers in isolated islands at the surface of the aqueous phase - the ensuing instability of the tear film induces reflex tearing action and the contaminated lipid must be removed by blinking before the reformation of a new and adequate tear coverage. When the contamination is present at the lid margin and has reached the Meibomian gland orifices, the process of break-up and renewal is repeated every few blinks. This contamination by cosmetic products is a common problem

for contact lens wearers as it induces accelerated drying and increased lens surface contamination, areas of non-wetting, and surface deposition. The use of water soluble products and the avoidance of oily (or petroleum based) creams and make-up removers is advocated.

8.1.4 LIPID LAYER PATTERN WITH REDUCED PALPEBRAL APERTURE (Figures 7.11, 7.12 and 7.13)

Norn (1979) has described a semi quantitative method of assessing the lipid layer thickness with cooperative patients using that method. He asks the patient to slowly close his/her eyes and notes the palpebral aperture corresponding to the appearance of the first interference fringes. A simple calculation allows us to estimate the normal tear lipid layer thickness. Because of the uneven lipid layer thickening during eye closure demonstrated in the pictures, this estimation is of limited value.

Contrary to the aqueous, the lipids are not washed away in large quantities at the puncti following each blink, but are squashed and respread at eye opening.

8.1.5 SEQUENTIAL ANALYSIS OF LIPID SPREADING

These photographs demonstrate that there is no immediate spreading and mixing of the secreted lipids, but that the process takes several blinks to be complete.

The spreading of the lipids is, in fact, complex and can be explained as follows:

- the tear flow per minute is of the order of 20 to 30 percent (Mishima et al, 1966) of the basal tear

volume. At each blink the main outflow channel is via the puncti and the aqueous forms the near totality of the tear eliminated that way.

- the lipid layer that is present at the front of the aqueous is compressed and thickens during eye closure as shown in Section 7.1.3 iv), then spreads again at the eye opening with a slight lag compared to the aqueous spreading as already described (Brown & Dervichian, 1969; Holly, 1973a; Benedetto et al, 1984). Only a very small portion of lipids is lost through the lacrimal passage at each blink, due to the long retention time (Benedetto et al, 1975).

- Meibomian gland secretion, contrary to aqueous secretion does not take place at every blink but more infrequently, approximately once every few blinks. When secretion occurs, the spreading process and mixing with the established lipid film takes time and follows the sequence described previously.

The following sequence is postulated with regard to the control of Meibomian gland secretion: when the lipid layer decreases in thickness and loses its stability, aqueous evaporation increases and a dry spot appears, this triggers aqueous secretion by the lacrimal gland.

The Meibomian secretion described does not occur simultaneously with the aqueous secretion, but with a small delay of a few seconds or a few blinks in the case of reflex tear production, triggered by irritation.

It is postulated that the delay is due either to a delayed secretion following the original reflex response

of the lacrimal gland, or to a slower secretion mechanism possibly due to a secretion rather slower than that of the lacrimal gland. Following eye irritation and profuse reflex lacrimation, large amounts of lipids are secreted but only after elimination of the excess volume of aqueous tears by the overflow or through the naso-lacrimal duct.

In these cases, a new lipid layer of increased thickness visible by its interference colours is seen spreading in a single blink but after a delay of a few seconds.

Excessive lacrimation results in a newly created tear film consisting of thicker than average aqueous and lipid phases to temporarily increase stability and subsequently induces recovery of the mucous coating on the epithelial surface.

8.1.6 EYE DROP INSTILLATION

In general, preservatives tend to reduce the eye drop in-vivo stability while wetting agents such as PVA increase the contact time.

The examination of the PDTF and the influence of eye drops and their components on the tear film stability can be efficiently carried out by the use of the low magnification instrument described in Chapter 5.

The measurement of non-invasive break-up time combined with the observation of the superficial lipid layer give in those cases a complete and precise representation of the stability and structure of the PDTF.

8.2 LIPID THICKNESS AND STRUCTURE EVALUATION

The thickness of the marmoreal pattern is difficult to evaluate by reflection photography as it lies in the range where no interference colours are produced. But within that range the lid edge forms a frame of varying surface within which the lipid layer is contained and regularly stretched and compressed during the blinking action.

The thickness of the layer is dependent on the palpebral aperture but as seen on Fig 7.11, Fig 7.12 and Fig 7.13, the increase is not linear but rather localised, the greater increase occurring in the vicinity of the lid margin.

The lipid layer thickness changes with the amount of lipid available. When a very small quantity is present it is stretched from lid to lid and probably decreases to the thickness (20 to 40 nanometers = 0.02 to 0.04μm) measured by Olsen (1985). Its visibility at low magnification is minimal and it may be only recognisable by its post blink movement at high magnification - this leads to the meshlike appearance commonly observed.

In the thickness range below 0.09μm the density of the meshwork pattern reflects the amount of lipid present. The more dense the meshwork the greater the volume and thickness of lipid.

With increased thickness, the meshwork appearance changes first to a wave type of pattern and then to an amorphous pattern effecting an even lipid coverage approaching 0.09μm in thickness. For greater thickness increase, interference colours are produced and a precise

thickness evaluation is possible up to 0.6μm by referring to Table 6.1A. All the colours described in Newton's range of interference colours are not visible. This is because some are restricted to a very small band range and will coalesce with neighbouring colours.

In the lipid layer, the first colour seen is a brown which is the combination occurring normally at a thickness of 0.143μm but in fact it encapsulates the range of yellow occurring between 0.09μm and 0.11μm. Only the colours that cover a wide enough range will be seen, the other will mix in the background.

In cases of Meibomian gland oversecretion, a globular formation as seen in Fig 7.17 is produced across the area of observation. The illuminating rays are reflected away from the observation axis and the specular reflection areas appear solely as a shiny black surface. The layer thickness assessment is not possible in this case.

In conclusion, the lipid layer appearance is very much linked to its thickness and it can be classified according to the following grading:

Grade 1	Open meshwork	≈0.02μm
Grade 2	Tight meshwork	to
Grade 3	Coloured wave and marmoreal	≈0.04μm
Grade 4	Amorphous	≈0.09μm
Grade 5	Combined amorphous and colour	>0.09μm to
Grade 6	Colour fringe appearance	<0.59μm
Grade 7	Globular appearance	>0.6μm

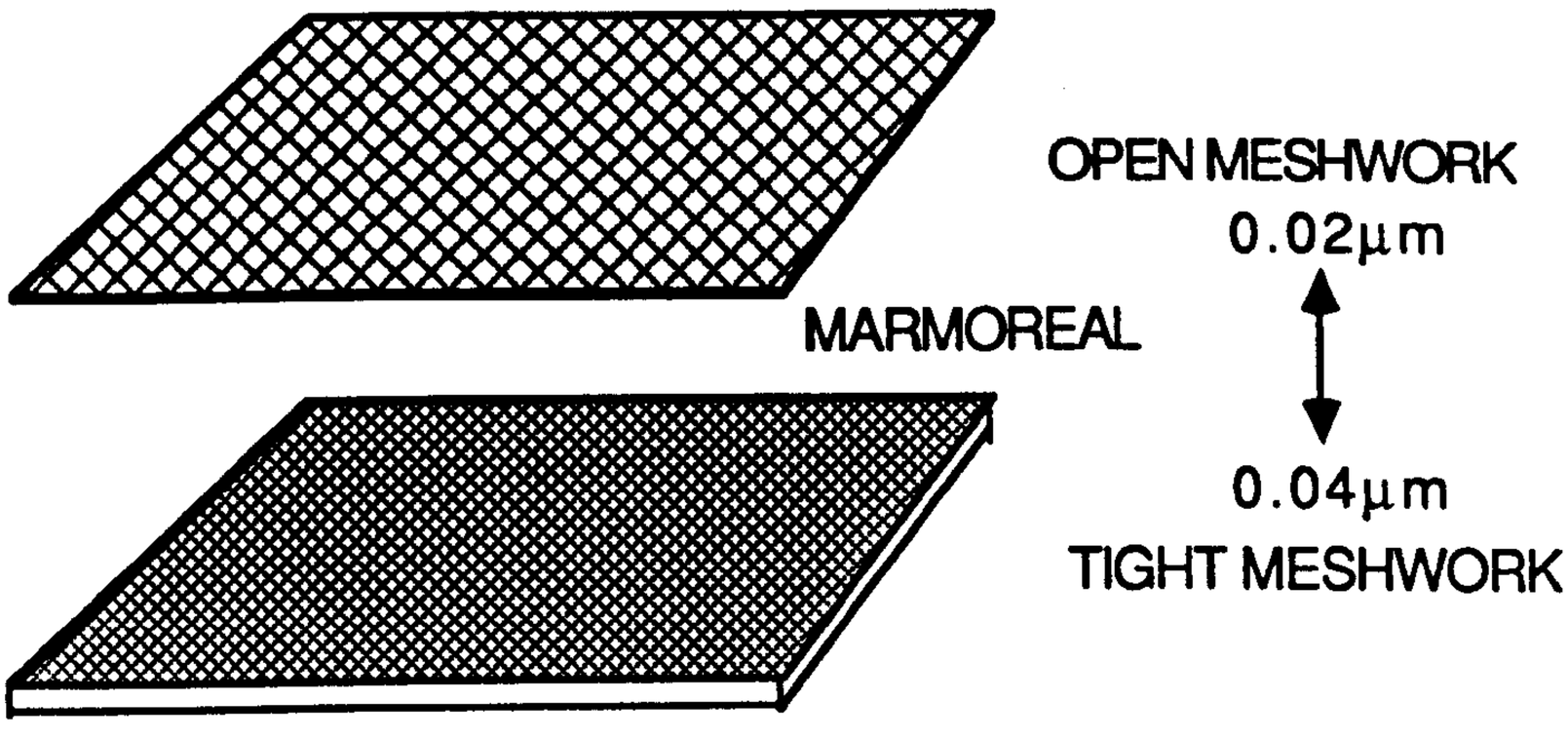

FIGURE 8.1
DIAGRAMMIC STRUCTURE OF LIPID LAYER
THICKNESS RANGE

These results are shown graphically in Figure 8.1.

In all cases, all interference colours are produced within the superficial lipid layer. Even when the lipid layer was missing no interference phenomena was produced within the aqueous phase of the pre-ocular tear film.

8.3 EXPERIMENTAL STUDY 2: PRE-SOFT LENS TEAR FILM

8.3.1 NORMAL PRE-SOFT LENS LIPID AND AQUEOUS LAYERS

As described the superficial lipid layer present at the surface of the pre-soft lens tear film is marmoreal in nature. When it is very thin it may be very difficult to see even at high magnification.

Occasionally an amorphous pattern is observed; in such a case the pre-lens tear film is very stable and the conditions are favourable for a successful soft contact lens wear. Exceptionally the lipid layer produces a coloured fringe pattern, this is always associated with tear lens greasing problem.

The visibility of the coloured interference fringes produced by the aqueous is regulated by the relative intensity of the light reflected at the interfaces of that layer. This intensity is influenced by a combination of factors, mainly the lens surface refractive index, the thickness of the aqueous phase, the presence and thickness of a superficial lipid layer. The observations indicate that the visibility of coloured interference fringes produced by the aqueous phase, is at its lowest in the following cases:

- when a thick, highly reflective lipid layer is present (as in the pre-ocular tear film) thus limiting the amount of transmitted light available for interference fringe formation in the aqueous layer and enhancing the intensity of its own interference colours.

- when a thick aqueous layer is present it induces a further decrease in the visibility of its fringes by spatial narrowing and by intensity loss through successive reflection and by destructive recombination of successive orders of interference.

- when the surface refractive index of the contact lens material is low as in high water content contact lenses and when surface quality is poor.

At the opposite the visibility of the coloured interference fringes produced by the aqueous phase is at its maximum when the contact lens surface quality is good as in spincast lenses and with low water content material such as Hema; both factors increase the contact lens surface reflectivity.

The description of the exact optical conditions and laws governing the visibility of the aqueous phase between the overlying lipid layer and the front surface of a soft contact lens is complex and detailed in Chapter 6. However, clinically four different situations were recorded with regard to lipid and aqueous film thickness and aqueous layer visibility.

- The aqueous film is not visible when the lipid layer is thick, 0.09µm and above.

- The aqueous layer is easiest to see when both the lipid layer (usually marmoreal) and aqueous layer (up to 1.5μm) are thin.

- The aqueous layer is moderately difficult to see in the following two conditions; either when the lipid layer has average thickness (just below 0.09μm) and the aqueous layer is thin (below 1.5μm) or when the opposite prevails, a thin lipid layer (marmoreal) with a thick aqueous layer (above 3μm). The results are graphically shown on Figure 8.2.

8.3.2 LIPID LAYER THINNING

The thinning process that takes place at the surface of the cornea or of a well fitting, wettable soft contact lens is very similar. Clinically, immediately after a blink we observe a thin marmoreal pattern. The pattern then stretches and becomes very difficult to see due to further thinning of the lipid layer and disappearance of its visible details even under high magnification observation. Increased evaporation leads to thinning of the aqueous phase evenly over large areas of the lens surface. This is seen as a rapid succession of interference colours in decreasing order of interference but increasing visibility specially for the last 2 or 3 orders. Areas of drying develop usually as a flat drying wedge along an horizontal median band across the lens surface, or from the edge of the lens with inward progression. This is seen by the disappearance of the interference fringe replaced by a greyish area due to

a phase change by specular reflection at the surface of denser medium than air.

Our observations have been that in general the pre-soft lens lipid film and its underlying aqueous phase are thinner than their pre-ocular tear film equivalent for the same patient regardless of lens material and design. Hence the drying sequence is usually shorter than the interblink period which may be a clinical problem in some cases.

8.3.3 LOCALISED DRY SPOT FORMATION

When the three layers are present in adequate amounts in the PLTF, their interaction ensure its stability which can be measured as the non-invasive anterior surface drying time (ASDT) but contrary to the case of the POTF whose mucous layer is actively anchored to the epithelial cell surface (Chapter 4) the stability of that layer in the PLTF relies solely on the spreading mechanism during the blink phase to set on the lens surface. This more limited attachment will render it less efficient to perform its function and this will be reflected in a shorter break-up time.

In the cases of thick pre-soft lens tear film, structurally more similar to the pre-ocular tear film, the evaporation is limited by the thick even lipid layer formed over the thicker than average aqueous phase.

In this case the increased stability of the whole pre-lens tear film structure and its larger volume leads to a longer tear film coverage. The drying sequence occurs mainly from localised minute dry spot formation

with a very steep aqueous drying wedge around the spot (Fig 7.21). The dry spot increases in size and coalesces with other neighbouring dry spots to form larger drying areas. This basal layer is only visible with our technique in those situations of localised drying of a PLTF possessing a thick aqueous phase with a thick superficial lipid layer.

8.3.4 EFFECT OF LENS MATERIAL, DESIGN AND FIT

Important differences have been noted during routine clinical observations with regard to the pre-soft lens tear film formation with various soft lens materials. PolyHema which is the most common soft contact lens material and has a water content of 38 percent has the most stable PLTF and is very similar in structure to the POTF. The film in front of Permalens lenses is slightly thinner, while the film in front of 'Duragel 75', 'Hydron 65' and 'Sauflon 70' is definitely thinner and somewhat unstable.

The lens geometry also affects the PLTF. For Hema lenses, standard thickness (centre thickness 0.12mm) and ultra thin lenses (centre thickness 0.06mm) such as 'Z6' (Hydron), 'U3' (B&L) have a thicker more stable film than hyperthin lenses such as 'Z4' (Hydron) and '03-04' (B&L) where the lipid layer is at times absent. When a very thin soft lens (centre thickness 0.04mm) does not support a stable tear film, an unprotected surface is present during most of the interblink period, evaporation of the tears from within the lens matrix may occur leading to lens surface drying and destabilisation at the level of

the corneal epithelium, resulting in superficial punctate staining. The fit and movement of the lens on the eye also influence the PLTF formation. An increase in lens movement will disrupt the formation of a stable PLTF: a more stable lens will favour it. Lens edge thickness is another factor; the thinner edges with a close conformation to the scleral shape favours the spreading across the lens border and the thicker edges of high minus lenses will be detrimental.

8.4 EXPERIMENTAL STUDY 3. PRE-RIGID CONTACT LENS TEAR STUDY

8.4.1 ANALYSIS OF INTERFERENCE FRINGE

The technique of specular reflection photography of interference fringes using crossed polarisation is an effective means of measurement of the tear layer thickness of the pre-rigid contact lens film.

When the tear film is very thin or at the end of a drying sequence, the thickness is assessed by comparison with the Newton's scale of colours adapted for the refractive index of the aqueous phase (Table 6.18).

Some colours described by Newton's are missing from the photographs. This is possibly due to the slightly irregular nature of the contact lens surface. It must be remembered that Newton fringes were produced between two highly polished glass surfaces free of irregularities. In our case, some colours present in Newton's experiment over only a few nanometers may be mixed with the stronger colours spread over a greater

distance and not influenced by the topographic irregularities. Further the difference in the spectral composition of the light used in the two experiments will influence the final composition of the wavelengths of light available for interference purposes. Their composition will vary to the extent that some colours will be entirely missing from some experiments according to the experimental conditions.

- the reflectivity of the surfaces, the refractive indices of the bordering media and that of the interference producing layer as well as the absorption characteristics of any intermediate layers all contribute to the final appearance and to the sequence of colours and their individual intensity.

- with different light sources the overlapping of interference orders will occur at a different rate thus potentially changing totally the final colour combinations.

The sequence of colours green-red-green-red starting at a thickness of 0.5μm is a constant feature of the drying pre-rigid lens tear film. When these are recognised and four extra blue fringes are seen it corresponds to a thickness of 1.1μm. Similarly, ten blue fringes are seen for a layer thickness of 2.00μm.

The photographic technique is effective up to 5.5μm of aqueous thickness where 31 fringes will be present. During normal observation, large numbers of fringes cannot be counted precisely as their appearance is changing during the drying sequence. But the apparent

movement of fringes will be a good guide to the speed of the drying process.

For research purposes, filming and frame by frame analysis should be an improvement on the photographic technique.

When using hard white light the fringes disappear after 4 or 5 orders of interference. The use of a polarising filter is necessary to achieve greater fringe sharpness and visibility. The use of white light source allows the easy recognition of the bright colours produced within the first three orders of interference and permits the easy recognition of the fringes of higher orders.

8.4.2 PRE-PMMA LENS TEAR FILM

The thin pre-lens tear film that forms at the surface of the PMMA lens undergoes rapid changes after eye opening.

The drying sequence reveals a thin layer (drying from 2.5µm) which does not present a visible superficial lipid layer.

An horizontal band of drying forms quite commonly near the median part of the lens suggesting a thicker PLTF towards the superior and inferior part of the lens, near the lid margins. This uneven spreading and irregular drying combined with the unstabilising effect of the lens meniscus 'black line', often leads to the appearance of 3 and 9 o'clock staining of the cornea and conjunctiva near the edge of corneal lenses.

The 'in-vivo' receding contact angle measurements are taken in the thicker part of the wedge which has approximate linearity. For thicknesses below 1µm the wedge angle flattens dramatically and measurements are less accurate, this change is possibly due to surface force.

This discrepancy in the tear layer spreading will lead to differences in the effect of evaporation in the first zone, a reduced volume of tears is spread over a large area and the effect of evaporation will be greater there than in the second zone where a greater volume of tears is confined to a more restricted space.

For thicknesses below 0.5µm a large number of particles are visible. As they disappear with drying, they are possibly the hydrated parts of the basal mucous coverage. It is evidently very thin and sparse, unlike the one present on the corneal and soft lens surface, this could explain the very short wetting time (approx 4 secs) found at the surface of rigid lenses (Lydon & Guillon, 1984a).

When a wetting solution is used, a greater pre-lens tear film thickness is achieved (3.32µm) over a small distance from the dry border.

The variation in wedge angle is interesting. A steep gradient (10.14 mrad) is present at the edge of the dry area. This is 84 percent increase compared to the steepest angle (5.52 mrad) measured before the use of the wetting solution.

Then a plateau is reached (0.38 mrad) followed by a further thickness increase at a lower rate (2.44 mrad).

The initial effect of the wetting solution seems to be limited to the increase in the thickness of the aqueous phase, 3.32µm compared to 2.52µm but the lack of superficial lipid layer and the presence of a large area of drying bordered by a steeper contact angle shows that the effect of the wetting solution on the limiting layer of the PLTF is limited. A wetting solution with mucomimetic properties should be more effective in those situations.

i) Low Wetting Angle Materiai

When material with improved wettability is used or increased tear layer thickness are achieved, a superficial very thin lipid layer is usually seen.

This lipid coverage, not only limits the effect of evaporation but also has a stabilising effect on the underlying tear film thus retarding localised break-up.

- the central drying area is covered by particles of greater size than those present when the covering PLTF is thinner. These particles are remnants of a thick basal mucin layer necessary to support a thicker and more stable PLTF.

In all cases of corneal contact lenses, the edge of the contact lens acts as a barrier to the spreading of an adequate pre-lens tear film. Especially it limits the formation of an adequate superficial lipid layer.

8.5 EXPERIMENTAL STUDY 4. MUCOUS LAYER PHOTOGRAPHY ON THE CORNEAL AND ON CONTACT LENS SURFACES

8.5.1 THE NATURE OF THE MUCOUS LAYER INTERFACE

In the aqueous phase of the POTF, the lack of visible interference fringes even at minimal thickness is probably due to the nature and morphology of the mucous interface which exhibits very low reflective properties. The formation and visibility of fringes is regulated by the intensity of the incident and reflected lights at successive interfaces. This depends on the thickness and reflectivity of the limiting layers which is a relative function of their refractive index.

In the pre-ocular tear film, the formation of interference fringes of high visibility in the aqueous layer depends on the physical characteristics of the underlying mucous layer, its homogoneity, its refractive index, and the nature of its surface.

At any interface, the light can be reflected, refracted or absorbed. The relative percentages will depend upon the homogeneity of the medium, the regularity of the surface and its definition.

The low reflective properties of the mucous interface is possibly due to the following:

- a high absorbtion of light by the medium. In that case the very reduced intensity of the light reflected at the mucous-aqueous interface is too low compared to the intensity of the light reflected at the aqueous-air interface to produce interference fringes.

- a lack of homogeneity of the mucous layer. If it is made up of various components of different reflective indices, this anisotropic medium will not fulfil the optical requirment of interfaces necessary for the production of interference fringes.

- a lack of uniformity of the mucous layer. This is possible if the interface is irregular, and the reflection will be scattered and not directed back to the observation system. This is what would happen in parallel sided plates with unpolished or scratched surfaces.

- the absence of a real interface. If the mucous layer is highly hydrated (90% water) its refractive index, n = 1.34 (J.M. Tiffany personal communication) will be very similar to that of the aqueous phase.

Such a low difference between the refractive indices will prohibit the formation of interference fringes.

8.5.2 MUCOUS LAYER MEASUREMENT

The lack of interference fringes in the mucous layer prevents us from applying our interferometric method of thickness measurement. The use of micrometric latex spheres did not prove to be a successful tool as they stayed in suspension and did not embed themselves in the mucous layer, as hoped. The effect of evaporation induces a certain amount of dehydration of the uncovered mucous layer and creates a more ragged surface.

The presence of such an hydrated structure will limit its effectiveness as an interface for interference

fringe formation but will increase its effectiveness as a wetting interface.

8.5.3 MUCOUS LAYER IN THE DRY EYE SYMPTOMS SUBJECT

The difference in appearance of the mucous coating suggests the presence of a thinner or less hydrated coating.

A highly hydrated and thick structure would in the experimental condition exhibit rapid changes of surface morphology such as furrowing. This is not the case in our observation. No other difference could be noted.

8.5.4 MUCOUS COATING ON CONTACT LENS SURFACE

The mucous coating on soft contact lenses differs from that on the cornea in two aspects:

- it acts as an optical interface, well enough to produce interference fringes within the aqueous phase it supports. It is not a perfect interface, the fringe intensity is limited and visible only over the very limited thickness (6 fringes). If rigid contact lens surface is more reflective (31 fringes visible for a thickness of 5.5µm.

- its morphology is different. Its thickness variation does not seem to providea regular surface coverage and will induce local variation in tear film stability.

On soft contact lens surfaces it is possible that the muco-proteinous coating is not evenly distributed as it relies solely on the spreading effect of the lids during blinking. The lack of the anchoring system

present on the ocular surface may produce an accumulation of material loosely bound to the lens surface as a paste-like structure. Both the presence, the thickness, the binding forces and the contamination of this layer will dictate the in-vivo wettability of the underlying soft lens surface.

On rigid contact lenses, a stable, thick mucous layer is not apparent. During the drying sequence observation only a few isolated globules were seen drying at the surface.

This minimal coating by mucous secretion could explain the limited wetting time which is a feature of rigid lens surfaces.

The proposed structure of the mucous layer on the cornea, on soft and rigid lenses in shown in diagrammatic form in Fig 8.2.

The proposed structure of the pre-soft lens tear film is shown diagrammatically in Fig 8.3 and that of the pre-rigid lens tear film in Fig 8.4.

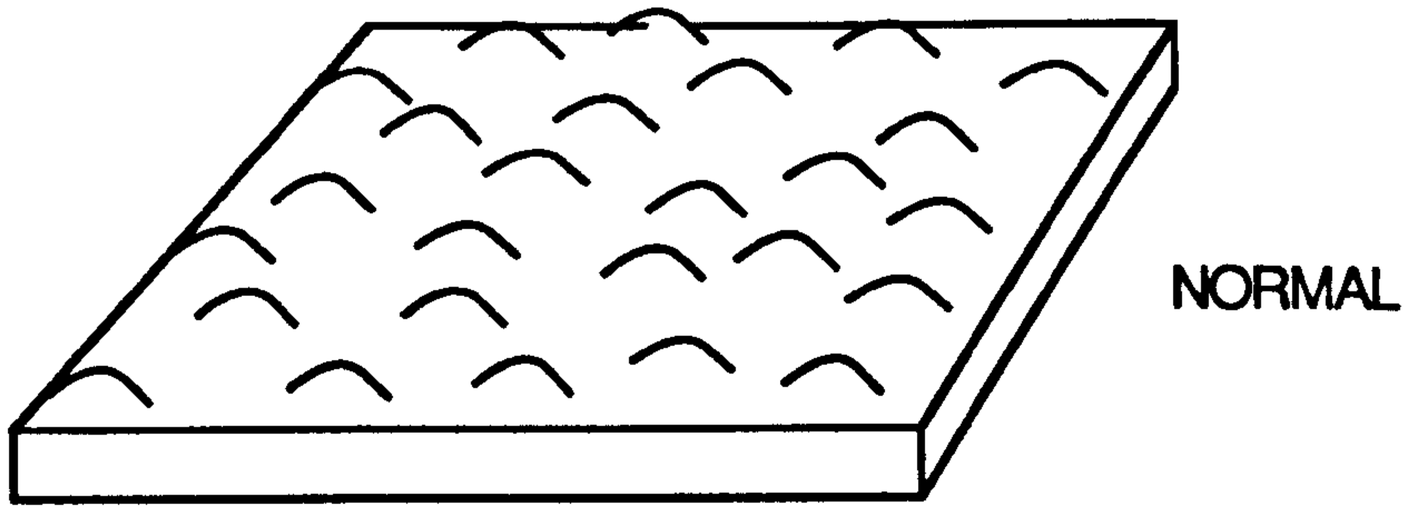

FIGURE 8.2
DIAGRAMMATIC STRUCTURE OF MUCOUS LAYER APPEARANCE

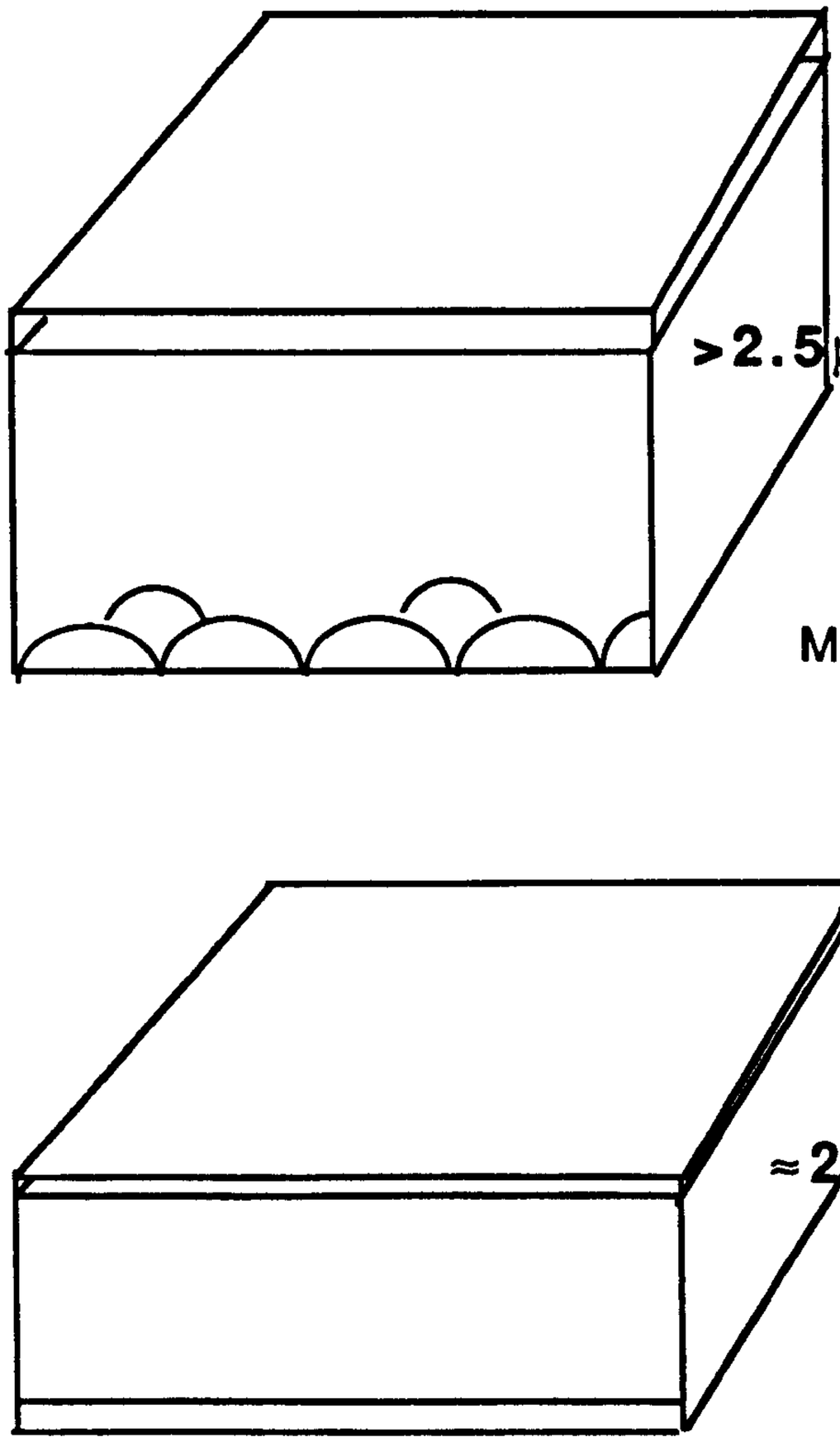

STRUCTURE	LAYER TYPE	INTERFERENCE FRINGES
	Combination or Amorphous Lipid	Visible
>2.5µm	Aqueous	Not Visible
	Mucous layer - thick paste-like mucous coating	
	Wave or Marmoreal	Visible
≈2.5µm		Not Visible
	Open Meshwork	Just visible
<1µm		up to 5 orders of interference
	Mucous	Thin coating

FIGURE 8.3
DIAGRAMMATIC STRUCTURE OF PRE-SOFT LENS TEAR FILM

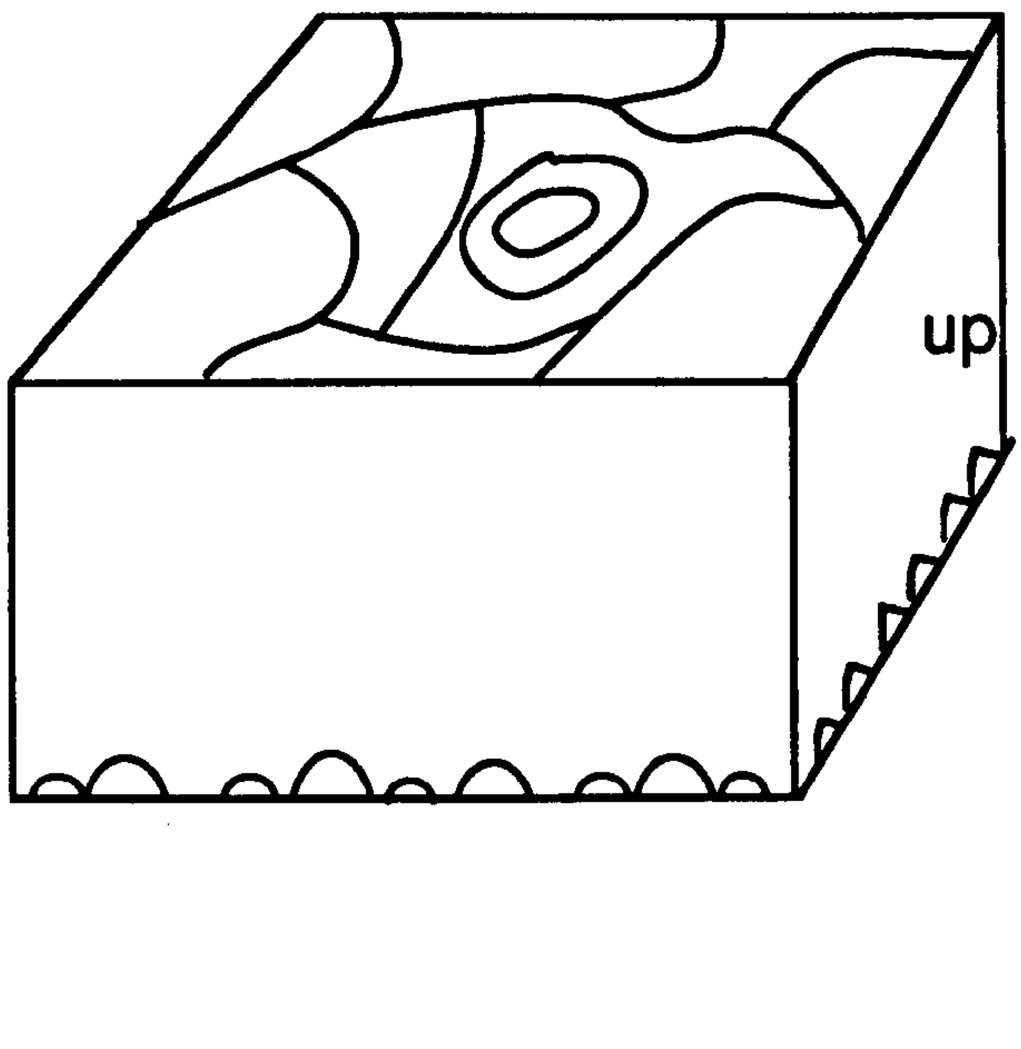

Lipid — Faint mesh lipid island

up to 5.5µm — up to 31 orders visible low intensity

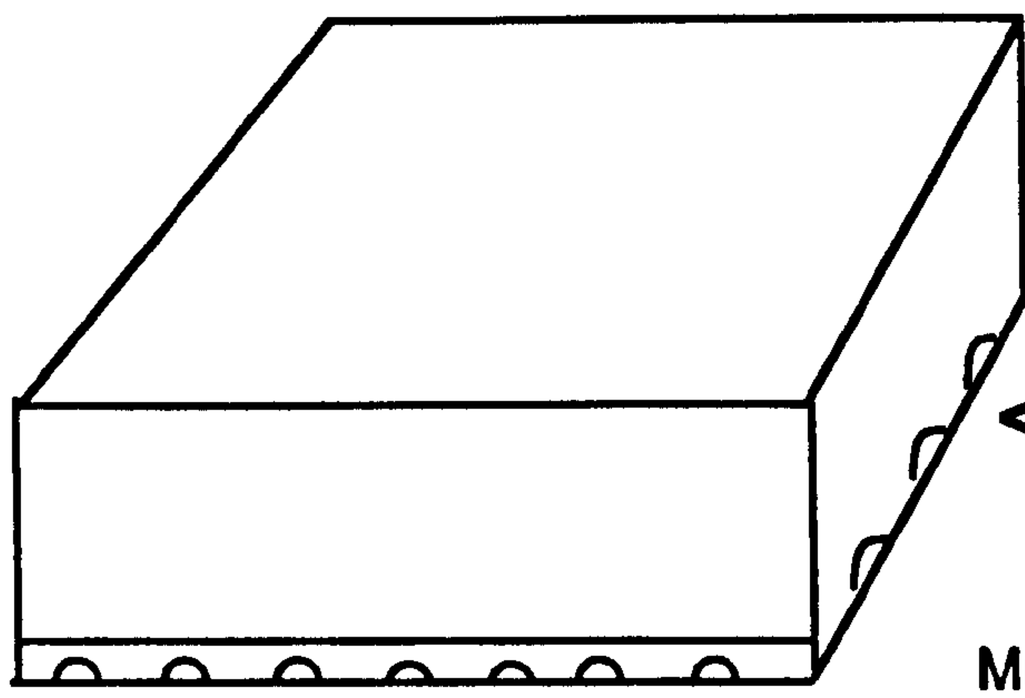

Sparce — Absent not visible

<2µm — bright fringes 10th order

Mucous — minimal

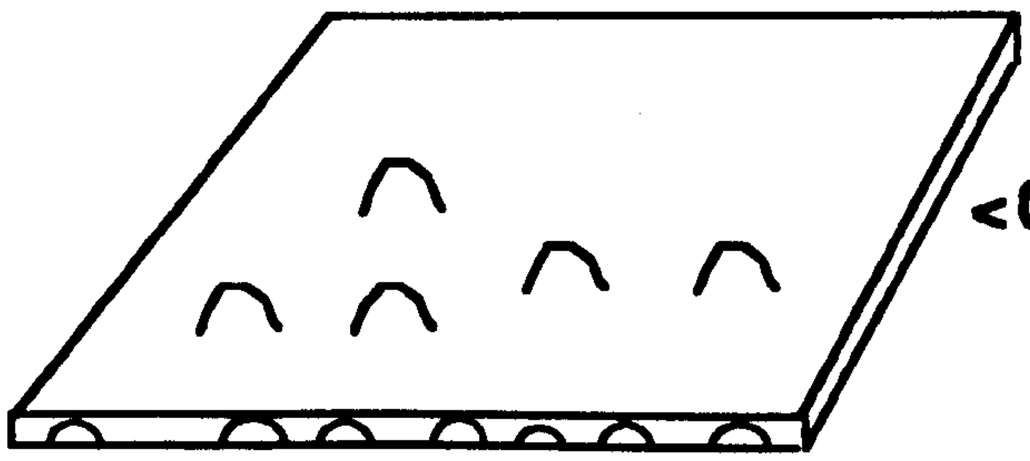

No lipids

<0.5µm — Aqueous

Large number of particles

FIGURE 8.4
DIAGRAMMATIC STRUCTURE OF PRE-RIGID LENS TEAR FILM

CHAPTER 9

CONCLUSION

As described previously a series of techniques has been designed specifically to allow the observation and photography of all the individual layers of the tear film. The techniques and analysis are an effective means of tear film assessment, both for the clinician and the researcher.

In the pre-ocular tear film, the lipid phase can be viewed under high magnification and low magnification. As a result of this work the appearance of the normal lipid layer of the pre-ocular tear film has been classified into 7 grades within a thickness range of 0.02µm to 0.58µm.

The observations of the lipid layer under high magnification are very useful but must be considered as the localised effect occurring within the frame formed by the superior and the inferior lids. It is therefore very important to be able to observe the overall behaviour of the lipid layer under low magnification over a large area of the ocular surface. It is easy to observe any irregularity or instability of the surface film and the formation of localised dry spots which can then be more closely examined under high magnification.

Use of the novel hand-held instrument allows the clinical measurement of tear film break-up time (BUT) and is particularly suitable for the tear film examination of the contact lens patient (Guillon & Guillon, 1988).

The mucous coverage of the epithelial surface can be observed after the tear film has receded following the formation of a dry spot, and it appears as a continuous undulated surface.

In the pre-lens tear films the lipid phase, the aqueous phase and the inner mucous coating of the surface can be individually observed.

On rigid contact lenses the presence of the lipid layer and aqueous phase can be detected separately. Their individual thickness can be measured from high magnification photography. The receding in-vivo wetting angle formed by the aqueous phase on the contact lens surface can also be calculated. The pre-PMMA rigid contact lens tear film rarely possesses a visible superficial lipid layer and its aqueous layer measured 1.5µm on average. Its basal mucous layer has only a sporadic occurrence.

The overall behaviour of the tear film covering the lens surface can be examined under low magnification. Its thickness decrease by evaporation and meniscus induced thinning can be related to the anterior surface drying time or lens surface break-up time.

The use of wetting solutions and supplementary eye formulation can be directly observed and measured by their effect on the pre-lens tear film thickness and stability. The wetting solution acts on the thickness of the aqueous phase which increases to 2.5µm and supports a minimal lipid layer.

The use of contact lens materials of better wettability permits the formation of films of increased thickness (up to 5.5µm) with a visible superficial lipid layer which was seen to stabilise the film and retard its drying.

The disturbing effect of lens deposits or coating and that of cosmetics can be assessed early by the abnormal features its creates at the tear surface. Adequate measure can be taken by the practitioner to improve the clinical picture and any improvement can be easily detected.

In soft contact lenses the same observations can be achieved. The pre-soft lens tear film usually possesses a thin superficial lipid layer and an aqueous phase of limited dimensions. Its mucous layer has a discontinuous distribution.

According to the observations the care regimen can be adjusted and include the use of protein removal tablets or supplementary eye drops if necessary. A more informed choice of lens can be achieved by assessing the

need for water content or improved in-vivo surface wettability.

On a research basis the ability to observe the mucous coating on the corneal surface will hopefully allow the differentiation of various corneal surface disturbances and a better understanding of the wetting mechanism achieved by looking directly at the 'trouble spot' where break-up occurs. In contact lens wear, the very high magnification observation of drying surfaces will allow us to assess the muco-protein coating and the behaviour of the fluid spreading over it. The study of the formation, structure and thickness of this inner layer made visible in-vivo for the first time on contact lenses should bring valuable information on its properties and effectiveness as a support to the aqueous phase and lipid layer.

REFERENCES

ABELSON, M. B. & HOLLY, F. J. (1977)
A tentative mechanism for inferior punctate keratopathy. *Am J Ophthalmol.* 83: 866-869.

ABELSON, M. B., SOTER, N. A., SIMON, M. A., DOHLMAN, J. & ALLANSMITH, M.R. (1977)
Histamine in human tears. *Am J Ophthalmol.* 83(3): 417-418.

ADLER, F. H. (1965)
The cornea. In: Physiology of the eye. 4th ed., *Editor*, (St. Louis: C.V. Mosby Co). Ch.22.

ALLANSMITH, M. R. (1973)
Immunology of the tears. In: The pre ocular tear film and dry eye syndromes. *Editors*, Holly, F. J. & Lemp, M. A. *Int Ophthalmol Clin.* 13(1): 47-72.

ALLANSMITH, M. R. (1986)
Comment les lentilles de contact attaquent la surface oculaire. *Contactologia.* 8: 42-45.

ALLANSMITH, M. R., KAJIYAMA, G., ABELSON, M. B. & SIMON, M. A. (1976)
Plasma cell content of main and accessory lacrimal glands and conjunctiva. *Am J Ophthalmol.* 82(6): 819-826.

ALLEN, M., WRIGHT, P. & REID, L. (1972)
The human lacrimal gland. A histochemical and organ culture study of the secretory cells. *Arch Ophthalmol.* 88: 493-497.

ANDRASKO, G. (1983)

Hydrogel dehydration in various environments. *Int Con Lens Clin.* 10(1): 22-28.

ANDREWS, J. S. (1973)

The Meibomian secretion. In: The pre ocular tear film and dry eye syndromes. *Editors*, Holly, F. J. & Lemp, M. A. *Int Ophthalmol Clin.* 13: 1-23.

von BAHR, G. (1941)

Könnte der Flüssigkeitsabgang durch die Cornea von physiologischer Bedeutung sein? *Acta Ophthalmol (Kbh).* 19: 125-134.

BALIK, J. (1952)

The lacrimal fluid in keratoconjunctivitis sicca. A quantitative and qualitative investigation. *Am J Ophthalmol.* 35: 773-782.

BAUM, J. L. (1973)

Systemic diseases associated with tear deficiencies. *Int Ophthalmol Clin.* 13: 157-184.

BELLDEGRUN, R., KENYON, K. R., REFOJO, M. F. & DUNCAN, J. E. (1985)

Aqueous tear evaporation in ocular surface disorders. *Proc VIIth Congress European Soc Ophthalmol* (Helsinki, 1985). Editor, Henkes, H. E.: 352-353.

BENEDETTO, D. A., CLINCH, T. E. & LAIBSON, P. R. (1984)

In vivo observation of tear dynamics using fluorophotometry. *Arch Ophthalmol.* 102(3): 410-412.

BENEDETTO, D. A., SHAH, D. O. & KAUFMAN, H. E. (1975)

The instilled fluid dynamics and surface chemistry of polymers in the preocular tear film. *Invest Ophthalmol & Vis Sci.* 14(12): 887-902.

BENJAMIN, W.J., PICCOLO, M. G. & TOUBIANA, H. A. (1984)
Wettability: a blink by blink account. *Int Con Lens Clin.* 11(8): 492-498.

BENJAMIN, W. J., YEAGER, M. D., DESAI, N. N. & CARMICHAEL, C. A. (1986)
In vivo analysis of contact angles. *Int Eyecare.* 2(3): 163-170.

BERGER, R.E. & CORRSIN, S. (1974)
A surface tension gradient mechanism for driving the pre corneal tear film after a blink. *J Biomechanics.* Z(3): 225-238.

BERGMANSON, J. P. G. & CHU, L. W. F. (1982)
Corneal repsonse to rigid contact lens wear. *Brit J Ophthalmol.* 66: 667-675.

BIER, N. & LOWTHER, G. E. (1977)
Preliminary investigation and initial examinacion. In: Contact lens correction. (London: Butterworth). Ch.6. 103-128.

BIOLOGICAL DATA HANDBOOK -TEARS (1974)
Physical properties and chemical composition of tears. 2nd Ed., 3. (Federation Am Soc Exp Biol)

BLODGETT, K. B. (1935)
Films built by depositing successive monomolecular layers on a solid surface. *J Am Chem Soc.* 5Z: 1007-1022.

BLUMCKE, S. & MORGENROTH, R. (1967)
The stereo ultrastructure of the external and internal surface of the cornea. *J Ultrastruct Res.* 18: 502-518.

BOTELHO, S. Y. (1964)

Tears and the lacrimal gland. *Sci Am.* 211: 78-86.

BRANDT, H.P. & FRITSCHE, G. (1967)

Klinische Erfarungen mit dem Tränenstreifen

Verdünungstest von Norn M.S. *Acta Ophthalmol*

(Kbh). 45: 166-176.

BRAUNINGER, G. E., SHAH, D. O. & KAUFMAN, H. E. (1972)

Direct physical demonstration of oily layer on the tear

film surface. *Am J Ophthalmol.* 73(1): 132-134.

BRON, A. J. (1985)

Prospects for the dry eye. *Trans Ophthalmol Soc UK.*

104: 801-826.

BRON, A. J., MENGHER, L. S. & DAVEY, C. C. (1985)

The normal conjunctiva and its responses to inflam-

mation. *Trans Ophthalmol Soc UK.* 104: 424-435.

BROWN, M., CHINN, S., FATT, I. & HARRIS, M. G. (1973)

The effect of soft and hard contact lenses on blink

rate; amplitude and length. *J Am Optom Assoc.*

44: 254-257.

BROWN, S. I. & DERVICHIAN, D. G. (1969)

Hydrodynamics of blinking. In vitro study of the

interaction of the superficial oily layer and the

tears. *Arch Ophthalmol.* 82(10): 541-547.

CALLANDER, M. & MORRISON, P. E. (1974)

A quantitative study of human tear proteins before and

after adaptation to non-flexible contact lenses.

Am J Optom & Physiol Opt. 51(12): 939-945.

CARNEY, L. G. & HILL, R. M. (1976)

Human tear pH. Diurnal variations. *Arch Ophthalmol.*

94: 821-824.

CARNEY, L. G. & HILL, R. M. (1979)

Human tear buffering capacity. *Arch Ophthalmol.* 97: 951-952.

CARNEY, L. G. & HILL, R. M. (1984)

Variation in blinking behaviour during soft lens wear. *Int Con Lens Clin.* 11(4): 250-253.

CARNEY, L. G. & JACOBS, R. J. (1984)

Mechanisms of visual loss in corneal oedema. *Arch Ophthalmol.* 102: 1068-1071.

CLARK, B. A. J. (1973)

Some experiments in corneal interferometry. *Aust J Optom.* 56: 448-453.

CLARK, B. A. J. & CARNEY, L. G. (1971)

Refractive index and reflectance of the anterior surface of the cornea. *Am J Optom.* 48: 333-343.

COCHET, P. & AMIARD, H. (1962)

Methods for evaluating lacrimal secretion. *Int Ophthalmol Clin.* 9(2): 280-296.

COLLINS, M., HERON, H., LARSEN, R. & LINDNER, R. (1987)

Blinking patterns in soft contact lens wearers can be altered with training. *Am J Optom & Physiol Opt.* 64(2): 100-103.

COPE, C., DILLY, P. N., KAURA, R. & TIFFANY, J. H. (1986)

Wettability of the corneal surface: a re-appraisal. *Curr Eye Res.* 5(10): 777-785.

CORDREY, P. (1984)

What the papers say. *J Brit Con Lens Assoc.* 7: 48.

CUCKLANZ, H. D. & HILL, R. M. (1969)

Oxygen requirements of contact lens systems. *Am J Optom.* 46(3): 228-230.

DAMATO, B. E., ALLAN, D., MURRAY, S. B. & LEE, W. R. (1984)
Senile atrophy of the human lacrimal gland: the contribution of chronic inflammatory disease. *Brit J Ophthalmol.* 68: 674-680.

DICKINSON, F. (1973)
A new hydrophilic hard contact lens. *NZ J Optom.* 5: 6.

DICKINSON, F. (1978)
Corneal respiration: some observations on the comparative performances of PMMA and CAB materials. *Con Lens J.* 6: 16.

DILLY, P. N. (1986)
Conjunctival cells, subsurface vesicles, and tear film mucus. In: The Preocular Tear Film in Health, Disease, and Contact Lens Wear, Ch.61: 677-687. *Editor,* Holly, F. J. (Lubbock, Texas: Dry Eye Instit)

DILLY, P. N. & MACKIE, I. S. (1981)
Surface changes in the anaesthetic conjunctiva in man with special reference to the production of mucous from non-goblet cell source. *Br J Ophthalmol.* 65: 833-842.

DOANE, M. G. (1980)
Interaction of eyelids and tears in corneal wetting and the dynamics of human eyeblink. *Am J Ophthalmol.* 89: 507-516.

DOUGHMAN, D.J. (1977)
Basic and clinical considerations of tear film stability. *Con Lens J.* 10(4): 25-31.

DUKE-ELDER, W. S. (1938)

Textbook of ophthalmology Vol II. (London: Henry Kimpton)

EDMUND, J. (1951)

The corneal gloss. *Thesis: Danish Science Press, Copenhagen*

EHLERS, N. (1965)

The pre corneal tear film. Biomicroscopical, histological and chemical investigations. *Acta Ophthalmol suppl.* 81: 5-136.

EHLERS, N. (1967)

A calculation of the average tear flow. *Acta Ophthalmol (Kbh).* 45(3): 273-274.

EHLERS, N., KESSING, S. V. & NORN, M. S. (1972)

Quantitative amounts of conjunctival mucus secretion in tears. *Acta Ophthalmol.* 50: 210-214.

FARRIS, R. L., KUTOTA, Z. & MISHIMA, S. (1971)

Epithelial decompensation with corneal contact lens wear. *Arch Ophthalmol.* 85: 651-660.

FATT, I. (1984)

Contact lens wettability - myths, mysteries and realities. *Am J Optom & Physiol Opt.* 61(7): 419-430.

FATT, I. & BIEBER, M. T. (1968)

The steady state distribution of "oxygen and carbon dioxide" in the in-vivo cornea. I. The open eye in air and the closed eye. *Exp Eye Res.* 7(1): 103-112.

FATT, I. & HILL, R. M. (1970)

Oxygen tension under a contact lens during the blinking. *Am J Optom & Am Acad Optom.* 47: 50-55.

FINNEMORE, V. M. & KORB, J. E. (1980)
Corneal oedema with polymethylmethacrylate versus gas-permeable rigid polymer contact lens of identical design. *J Am Optom Assoc.* 51(3): 271-272.

FISCHER, F. P. (1928)
Uber die Darstellung der Hornhaut - Oberfläche und ihrer Veränderung im Reflexbild. *Arch Augenheilk* 98: Ergänzungheft 1-84.

FISCHER, F. P. (1931)
Erhährung und Stoffwechsel der Gewebe des Auges. *Ergebn Physiol.* 31: 507-591.

FISCHER, F. P. (1940)
In: Modern trend in ophthalmology. *Editors.* Ridley, F. & Sorsby, A. (London: Butterworth & Co Ltd).

FOLCH, J., LEES, M. & SLOANE STANLEY, G. H. (1957)
A simple method for isolation and purification of total lipids from animal lipids. *J Biol Chem.* 226: 497-509.

FORD, L. C., DELANGE, R. J. & PETTY, R. W. (1976)
Identification of a nonlysozymal bactericidal factor (Beta Lysin) in human tears and aqueous humour. *Am J Ophthalmol.* 81(1): 30-33.

FORST, G. (1976a)
Experiments with the tear film BUT. *The Optician suppl.* Jan.

FORST, G. (1976b)
Nachweis des Pumpeffektes bei Kontaklinsen. *Die Kontaklinsen.* 10(5): 8-20.

FORST, G. (1978)
Stabilitá della pellicola lacrimale e tollerabilitá di una lente a contacto. *L'ottico.* 178: 16-25.

FORST, G. (1981)

Movement and centering of a contact lens on the eye. *Contacto*. Sept: 6-18.

FRANCOIS, J. & NEETENS, A. (1973)

Tear flow in man. *Am J Ophthalmol*. 76(3): 351-358.

FRANKLIN, R. M., KENYON, K. R. & TOMASI, T. B. (1973)

Immunohistologic studies of human lacrimal gland. *J Immunol*. 110: 984-992.

FRIEDLAND, B. R., ANDERSON, D. R. & FORSTER, R. K. (1972)

Nonlysozyme antibacterial factor in human tears. *Am J Ophthalmol*. 74(1): 52-59.

FURUKAWA, R. R. & POLSE, K.A. (1978)

Changes in tear flow accompanying aging. *Am J Optom & Physiol Opt*. 55(2): 69-74.

GILBARD, J. P., FARRIS, R. L., SANTAMARIA, J. (1978)

Osmolarity of tear microvolumes in keratoconjunctivitis sicca. *Arch Ophthalmol*. 96(4): 677-681.

GOLDING-WOOD, P. H. (1954)

The ocular effect of autonomic surgery. *Proc Roy Soc Med*. 52: 494-497.

GORDON, G. (1951)

Observations upon the movements of the eyelids. *Br J Ophthalmol*. 35: 339-351.

GREINER, J. V., KENYON, K. R., HENRIQUEZ, A. S., KORB, D. R., WEIDMAN. T. A. & ALLANSMITH, M. R. (1980)

Mucus secretory vesicles in conjunctival epithelial cells of wearers of contact lenses. *Arch Ophthalmol*. 98: 1843-1846.

GREINER, J. V., KORB, D. R., COVINGTON, H. I., PEACE, D. G. & ALLANSMITH, M. R. (1982)
Human ocular mucus. Scanning electron microscope study. *Arch Ophthalmol (Chicago).* 100(10): 1614-1617.

GUILLON, J-P. (1982)
Tear film photography and contact lens wear. *J Brit Con Lens Assoc.* 5(2): 84-87.

GUILLON, J-P. (1985)
Le film lacrymal. *L'optometrie.* 31(10): 8-12.

GUILLON, J-P. (1986)
Tear film structure and contact lenses. In: The Preocular Tear Film in Health, Disease, and Contact Lens Wear, *Editor*, Holly, F. J.
(Lubbock, Texas: Dry Eye Instit). Ch.85: 914-939.

GUILLON, J-P. & GUILLON, M. (1984)
The tear surface. *Paper presented at 5th International Contact Lens Congress*, Surfers Paradise, Australia, August 1984.

GUILLON, J-P. & GUILLON, M. (1988)
Tear film examination of the contact lens patient. *Contax.* May: 14-18.

GUILLON, M., LYDON, D. P. M. & SAMMONS, W. A. (1983)
Designing rigid gas permeable contact lenses using the edge clearance technique. *J Brit Con Lens Assoc.* 6(19): 22-26.

HABERICH, F. J. (1982)
The stability of the precorneal tear film. Extract of lectures. *15th Contact Lens Congress Aschaffenburg.* March 1982: 17-45. (Aschaffenburg: Titmus Eurocon Kontaktlinsen Gmbh & Co.)

HABERICH, F. J. & LINGELBACH, B. (1981)
Eine optische methode zur darstellung von inhomogenitäten des Tränenfilms mit demonstration des verwendeten Schlierenopticschen Verfahrens. *Vortrag 14 Aschaffenburger Kontaktlinsen Tatung.* (Referatem 55-14) 3: 26-28.

Van HAERINGEN, N. J. (1981)
Clinical biochemistry of tears. *Surv Ophthalmol.* 26(2): 84-95.

HAMANO, H., MITSUNAGA, S. (1982)
Clinical examinations and research on tears. In: Menicon 30th Anniversary Special Compilation of Research Reports, *Editors*, Tanaka, K., Anan, N. & Mikami, M. (Japan: Tokyo Con Lens Co; Tokyo). Ch.2.

HAMANO, H., HORI, M., KAWABE, H., UMENO, M. & MITSUNAGA, S. (1979a)
Bio differential interference microscopic observations on anterior segment of eye. (First report: Observations of pre corneal tear film). *J Jap Con Lens Soc.* 21: 229-238.

HAMANO, H., HORI, M., KAWABE, H., UMENO, M. & MITSUNAGA, S. (1979b)
Bio differential interference microscopic observations on anterior segment of eye. (Third report: Observation of surface states of contact lenses on eye). *J Jap Con Lens Soc.* 21: 264-270.

HAMANO, H., HORI, M., KAWABE, H., UMENO, M., MITSUNAGA, S., OHNISHI, Y. & KOMA, I. (1980a)
Clinical applications of bio differential interference microscope. *Con & Intraoc Lens Med J.* 6(3): 229-235.

HAMANO, H., HAMANO, T., HAMANO, T., HORI, M., MITSUNAGA, S., OHNISHI, Y. & KOMA. I. (1980b) Breakup of the pre corneal tear film on a dendritic keratitis. *Fol Ophthalmol Jap.* 31: 1071-1074.

HAMANO, H., HORI, M. & MITSUNAGA, S. (1980c) Application of an evaporimeter to the field of ophthalmology. *J Jap Con Lens Soc.* 22(2): 101-107.

HAMANO, H., KAWABE, H. & MITSUNAGA, S. (1982) Even field bio-differential interference microscope. *Fol Ophthalmol Jap.* 33: 383-388.

HANNA, C. & O'BRIEN, J. E. (1960) Cell production and migration in the epithelial layer of the cornea. *Arch Ophthalmol.* 64(10): 536-539.

HARRIS, M. G. & MANDELL, R. B. (1969) Contact lens adaptation: osmotic theory. *Am J Opt.* 46(3): 196-202.

HAYASHI, T. T. & FATT, I. (1980) Forces retaining a contact lens on the eye between blinks. *Am J Optom Physiol Opt.* 57: 485-507.

HENRIQUEZ, A. S. & KORB, D. R. (1981) Meibomian gland dysfuntion and contact lens wear. *Brit J Ophthalmol.* 65(2): 108-111.

HILL, R. M. (1975) Osmotic oedema associated with contact lens adaptation. *J Am Optom Assoc.* 46(9): 897-899.

HILL, R. M. (1981) Laboratory studies. In: Complications of Contact Lenses. *Editors*, Miller, D & White, P. F. *Int Ophthalmol Clin.* 21(2): 223-236.

HILL, R. M. & BAILEY, N. J. (1978)

Can oxygen pass through PMMA? *Int Con Lens Clin.* 5(1): 48-50.

HILL, R. M. & CARNEY, L. G. (1984)

The effect of hard lens wear on blinking behaviour. *Int Con Lens Clin.* 11(4): 242-248.

HILL, R. M. & FATT, I. (1963)

Oxygen uptake from a reservoir of limited volume by the human cornea in vivo. *Science.* 142: 1295-1297.

HILL, R. M., SCHULTS, J. E. & THAYER, G. R. (1973)

Can a 'hard' contact lens material transmit adequate oxygen? *Am J Optom & Am Acad Optom.* 50: 949-951.

HILL, R. M. & UNIACKE, N. P. (1969)

Tear chemistry of a new contact lens wearer. *J Am Optom Assoc.* 40(3): 295-296.

HOLLY, F. J. (1973a)

Formation and stability of the tear film. In: The pre ocular tear film and dry eye syndrome. *Editors,* Holly, F. J. & LEMP, M. A. *Int Ophthalmol Clin.* 13(1): 73-96.

HOLLY, F. J. (1973b)

Formation and rupture of the tear film. *Exp Eye Res.* 15: 515-525.

HOLLY, F. J. (1978a)

Surface chemical evaluation of artificial tears and their ingredients. I. Interfacial activity. *Con & Intraoc Lens Med J.* 4(2): 14-31.

HOLLY, F. J. (1978b)

The pre ocular tear film. *Con & Intraoc Lens Med J.* 4(4): 135-142.

HOLLY, F. J. (1979)

Protein and lipid adsorption by acrylic hydrogels and this relation to water wettability. *J Polym Sci Polym Symp.* 66: 409-417.

HOLLY, F. J. (1980)

Tear Film physiology. *Am J Optom & Physiol Opt.* 57(4): 252-257.

HOLLY, F. J. (1981a)

Tear film physiology and contact lens wear. I. Pertinent aspects of tear film physiology. *Am J Optom & Physiol Opt.* 58(4): 324-330.

HOLLY, F. J. (1981b)

Tear film physiology and contact lens wear. II. Contact lens tear film interaction. *Am J Optom & Physiol Opt.* 58(4): 331-341.

HOLLY, F. J. & LEMP, M. A. (1971a)

Wettability and wetting of the corneal epithelium. *Exp Eye Res.* 11: 239-250.

HOLLY, F. J. & LEMP, M. A. (1971b)

Surface chemistry of the tear film: implications for dry eye syndromes, contact lenses and ophthalmic polymers. *J Am Con Lens Soc.* 5: 12-19.

HOLLY, F. J. & LEMP, M. A. (1973)

The preocular tear film and dry eye syndrome. *Int Ophthalmol Clin.* (Boston: Little, Brown & Co.).

HOLLY, F. J. & LEMP, M. A. (1977)

Tear physiology and dry eyes. *Surv Ophthalmol.* 22: 69-87.

HOLLY, F. J., PATTEN, J. H. & DOHLMAN, C. J. (1977)
Surface activity determination of aqueous tear components in dry eye patients and normal. *Exp Eye Res.* 24: 479-491.

HOLM, S. (1949)
Keratoconjunctivitis sicca and the sicca syndrome. *Acta Ophthalmol suppl.* 27(33): 1-230.

IWATA, S., LEMP, M. A., HOLLY, F. J. & DOHLMAN, C. H. (1969)
Evaporation rate of water from the pre-corneal tear film and cornea in the rabbit. *Invest Ophthalmol.* 8: 613-619.

JANSSEN, P. T., MUYTJENS, H.L. & Van BIJSTERVELD, O.P. (1984)
Non lysozyme antibacterial factors in human tears, (fact or fiction)? *Invest Ophthalmol Vis Sci.* 25: 1156-1160.

JENSEN, O. A., FALBE-HANSEN, I., JACOBSEN, T. & MICHELSEN, A. (1969)
Mucosubstances of the acini of the human lacrimal gland (orbital part). I. Histochemical identification. *Acta Ophthalmol (Kbl).* 47(3): 605-619.

JONES, L. T. (1966)
The lacrimal secretory system and its treatment. *Am J Ophthalmol.* 62(1): 47-60.

JONES, L. T. (1973)
Anatomy of the tear system. In: The pre ocular tear film and dry eye syndromes. *Editors*, Holly, F. J. & Lemp, M. A. *Int Ophthalmol Clin.* 13(1): 3-22.

JORDAN, A. & BAUM, J. (1980)

Basic tear flow: does it exist? *Ophthalmology (Rochester)*. 87: 920-930.

JOSEPHSON, J. E. (1983)

Appearance of the pre ocular tear film lipid layer. *Am J Optom & Physiol Opt*. 60: 883-887.

KAME, R. T., TAKEMURA, R. K. & MUKAI, G. T. (1976)

Tear break up time and the Schirmer tear test. *Am J Optom Assoc*. 47(12): 1535-1538.

KEITH, C. G. (1967)

Seborrhoeic blepharo-kerato-conjunctivitis. *Trans Ophthalmol Soc UK*. 87: 85-103.

KESSING, S. V. (1967)

A new division of the conjunctiva on the basis of X-ray examination. *Acta Ophthalmol (Kbh)*. 45: 680-683.

KESSING, S. V. (1968)

Mucous gland system of the conjunctiva. A quantitative normal anatomical study. *Acta Ophthalmol (Kbh) suppl*. 95: 1-33.

KIKKAWA, Y. (1970)

The mechanism of contact lens, adherence and centralization. *Am J Optom*. 47(4): 275-281.

KILP, H. (1985)

Tear film changes in dry eyes. *Trans Ophthalmol Soc UK*. 104: 450-451.

KILP, H., SCHMID, E. & VOGEL, A. (1982)

Tränenfilm Untersuchungen in Spiegelbezirk. *Klin MBL Augenheilk*. 180: 49-52.

KIRCHNER, C. (1964)

Untersuchungen über das Ausmass der Tränensekretion beim Menschen. *Klin Mon Augen.* 144: 412-417.

KLEIN, M. (1949)

The lacrimal strip and the pre corneal film in cases of Sjögren's syndrome. *Brit J Ophthalmol.* 33: 387-388.

KLINE, L. N., DE LUCA, T. J. & FISHBERG, G. M. (1979)

Corneal staining relating to contact lens wear. *J Am Optom Assoc.* 50(3): 353-357.

KNOLL, H. & WALTERS, H. (1985)

Pre-lens tear film specular microscopy. *Int Con Lens Clin.* 12(1): 30.

KOBY, F. E. (1924)

Microscopie de l'oeil vivant. (Paris: Masson et Cie). : 47-58; 85-89.

KOETTING, R. A. (1976)

Tear film break-up time as a factor in hydrogel lens coating. A preliminary study. *Contacto.* 20(3): 20-23.

KOHLER, J. & FLANAGAN, G. (1985)

Clinical dehydration of extended wear lenses. *Int Con Lens Clin.* 12(3): 152-161.

KORB, D. R. & HENRIQUEZ, A. S. (1980)

Meibomian gland dysfunction and contact lens intolerance. *J Am Optom Assoc.* 51(3): 243-251.

KRESS, J. A. (1978)

Comparison of different hard oxygen permeable lenses. *Ophthalmol Opt.* 18(11): 413-414.

LAMBERTS, D. W., FOSTER, C. & PERRY, H. P. (1979)
Schirmer test after topical anaesthesia and the tear meniscus height in normal eyes. *Arch Ophthalmol.* 97(6): 1082-1085.

LAMBLE, J. W., GILBERT, D. & ASHFORD, J. J. (1976)
The break-up time of artificial preocular films on the rabbit cornea. *J Pharm Pharmacol.* 28: 450.

LANGMUIR, I. (1934)
Mechanical properties of monomolecular films. *J Franklin Instit.* 218: 143-171.

LEE, W. R., MURRAY, S. N., WILLIAMSON, S. & McKEAN, D. C. (1981)
Human conjunctival surface mucins: a quantitative study of normal and diseased (KCS) tissues. *Graefes Arch Ophthalmol.* 245: 209-221.

LEMP, M. A. (1976)
Cornea and sclera. *Arch Ophthalmol.* 94(3): 473-490.

LEMP, M. A. & HAMILL, J. R. (1973)
Factors affecting tear film break up in normal eyes. *Arch Ophthalmol.* 89(2): 103-105.

LEMP, M. A. & HOLLY. (1970)
Recent advances in ocular surface chemistry. *Am J Optom & Am Acad Optom.* 47(9): 669-670.

LEMP, M. A., DOHLMAN, C. H. & HOLLY, F. J. (1970a)
Corneal desiccation despite normal tear volume. *Ann Ophthalmol.* 2: 258-261.

LEMP, M. A., HOLLY, F. J., IWATA, S. & OOHLMAN, C. H. (1970b) The pre corneal tear film. I. Factors in spreading and maintaining a continuous tear film over the corneal surface. *Arch Ophthalmol*. 83: 89-94.

LEVENSON, O. S. (1983) Change in corneal curvature with long term PMMA contact lens wear. *The CLAO J*. 9(2): 121-125.

LIOTET, S., COHEN, M. & SAINTE-LAUDY, J. (1980) Un antibiotique naturel des larmes: la lactotransferrine. *J Fr Ophthalmol*. 3(3): 159-163.

LOWTHER, G. E. (1981) Comparing corneal thickness changes with Silcon resin lenses to the changes with PMMA, CAB and polycon lenses. *Int Cont Lens Clin*. 8(3): 25-29.

LOWTHER, G.E. & HILBERT, J. A. (1975) Deposits on hydrophilic lenses: differential appearance and clinical causes. *Am J Optom Physiol Opt*. 52: 687-692.

LOWTHER, G. E. & HILL, R. M. (1967) Fluid forces associated with contact lens systems. *J Am Optom Assoc*. 38(10): 847-850.

LOWTHER, G. E. & HILL, R. M. (1968) Sensitivity threshold of the lid margin in the course of adaptation to contact lenses. *Am J Optom*. 45(9): 587-594.

LOWTHER, G. E. & PARAMORE, J. E. (1982) Clinical comparison of Silcon resin lenses to PMMA, CAB and polycon lenses. *Int Con Lens Clin*. 9(2): 106-118.

LYDON, D. P. M. & GUILLON, J-P. (1984a)

The integrity of the pre lens tear film. In: The Frontier of Optometry. *Trans of the First International Congress of the British College of Optometrists*. April 11-14: 106-135.

LYDON, D. P. M. & GUILLON, M. (1984b)

Effect of centre thickness variations on the performance of rigid gas permeable contact lenses. *Am J Optom & Physiol Opt*. 61: 23-27.

McCLELLAN, B. H., WHITNEY, C. R., NEWMAND, P. L. & ALLANSMITH, M. R. (1973)

Immunoglobulins in tears. *Am J Ophthalmol*. 76(1): 89-101.

McCULLEY, J. P. & SCIALLIS, G. F. (1977)

Meibomian keratoconjunctivitis. *Am J Ophthalmol*. 84(6): 788-793.

McDONALD, J. E. (1968)

Surface phenomena of tear films. *Trans Am Ophthalmol Soc*. 66: 905-939.

McDONALD, J. E. (1969)

Surface phenomena of the tear film. *Am J Ophthalmol*. 67(1): 56-64.

McDONALD, J. E. & BRUBAKER, S. (1971)

Meniscus induced thinning of tear films. *Am J Ophthalmol*. 72(1): 139-146.

McEWEN, W. K. (1962)

Secretion of tears and blinking. In: The Eye, Vol 3. *Editor*, Davson, H. (New York: Academic Press Inc) 3: 271-305.

MACKIE, I. A. (1970)

Factors influencing corneal contact lens centration.

Brit J Physiol Opt. 25(2): 87-103.

MANDELL, R. B. (1977)

Theory of contact lenses. In: Contact Lens Practice.

Hard and flexible lenses, 2nd ed. Ch.6: 133-165.

(Springfield, Illinois: Charles C Thomas).

MANDELL, R. B. (1981)

Gas permeable lenses. In: Contact Lens Practice,

3rd Ed. *Editor*, Mandell, R. B. (Springfield,

Illinois: Charles C Thomas). Ch.10.

MANDELL, R. B. (1982)

Corneal physiology and permeable materials. *Contacto.*

26(2): 4-8.

MANDELL, R. B. & FARRELL, R. (1980)

Corneal swelling at low atmospheric oxygen pressures.

Invest Ophthalmol & Vis Sci. 19(6): 697-702.

MANDELL, R. B. & HARRIS, M. G. (1968)

Theory of the contact lens adaptation process. *J Am*

Optom Assoc. 39(3): 260-261.

MARQUARDT, R. (1982)

Untersuchungen zur Tranenfilmstabilitas. *Chronische*

Conjunctivitis Trockenes Auge. Springer-verlag,

Wien-New York.

MARQUARDT, R. (1986)

Histological studies of goblett cell counts in the

human conjunctiva. In: The Preocular Tear Film in

Health, Disease and Contact Lens Wear, *Editor*, Holly,

F. J. (Lubbock, Texas: Dry Eye Instit): 312-318.

MARQUARDT, R., STODTMEISTER, R. & CHRIST, T. (1986)
Modification of tear film break up time test for increased reliability. In: The Pre Ocular Tear Film in Health, Disease and Contact Lens Wear. *Editor*, Holly, F. J. (Lubbock Texas: Dry Eye Institute): 57-63.

MARTIN, D. K. & HOLDEN, B. A. (1983)
Variations in tear fluid osmolarity, chord diameter and movement during wear of high water content hydrogel contact lenses. *Int Con Len Clin.* 6: 332-341.

MARX, E. (1921)
De la sensibilite et du dessechement de la cornee. *Ann Oculist.* 158: 774-789.

MASNICK, K. B. (1979)
Newer hard contact lens materials. *Aust J Optom.* 62: 138-142.

MASNICK, K. B. & HOLDEN, B. A. (1972)
A study of water content and parametric variation of hydrophilic contact lenses. *Aust J Optom.* 55: 481-487.

MASTMAN, G. J., BALDES, E. J. & HENDERSON, J. W. (1961)
The total osmotic pressure of the tears in normal and various pathological conditions. *Arch Ophthalmol (Chicago).* 65: 509-513.

MAURICE, D. M. (1962)
The cornea and sclera. In: The eye, Vol I. *Editor*, Davson, H. (New York: Acad Press) : 289-368.

MAURICE, D. M. (1973)
The dynamics and drainage of tears. In: The pre ocular tear film and dry eye syndromes, *Editors*, Holly F. J. & Lemp, M. A. *Int Ophthalmol Clin.* 13(1): 103-116.

MAURICE, D. M. (1980)

Structures and fluids involved in the penetration of topically applied drugs. *Int Ophthalmol Clin.* 20: 7-20.

MEESMANN, A. (1927)

Die mikroskopie des lebenden Auges an der gullstrandschen Spaltlampe mit Atlas typischer Befunde. (Berlin & Weimar: Urban & Schwarzenberg): 33-37.

MEIBOMIUS, H. (1666)

(latinised version of Meibom)

De vasis palpebrarum novis epistola. Müller, Helmstädt.

MENGHER, L. S., BRON, A. J., TONGE, S. R. & GILBERT, D. J. (1985a)

A non-invasive instrument for the clinical assessment of the pre-corneal tear film stability. *Curr Eye Res.* 4: 1-8.

MENGHER, L. S., BRON, A. J., TONGE, S. R. & GILBERT, D. J. (1985b)

Effect of fluorescein instillation on the pre-corneal tear film stability. *Curr Eye Res.* 4: 9-11.

MILLODOT, M. (1981)

Corneal sensitivity. In: Complications of Contact Lenses. *Editor*, Miller, D & White, P. F. *Int Ophthalmol Clin.* 21: 47-54.

MISHIMA, S. (1965)

Some physiological aspects of the pre corneal tear film. *Arch Ophthalmol.* 73: 233-241.

MISHIMA, S., GASSET, A., KLYCE, S. D. & BAUM, J. L. (1966)
Determination of tear volume and tear flow.
Invest Ophthalmol & Vis Sci. 5(3): 264-276.

MISHIMA, S., KUBOTA, Z. & FARRIS, R. L. (1971)
Tear flow dynamics in normal and keratoconjunctivitis sicca cases. In: Ophthalmology proceedings of the XXI International Congress, Mexico, 8-14 March 1970. *Editor*, Solanes, M. P. *Excerpta Medica (Amsterdam)*. (2): 1801-1805.

MISHIMA, S. & MAURICE, D. M. (1961a)
The oily layer of the tear film and evaporation from the corneal surface. *Exp Eye Res.* 1: 39-45.

MISHIMA, S. & MAURICE, D. M. (1961b)
The effect of normal evaporation on the eye.
Exp Eye Res. 1: 46-52.

NICHOLS, B. A, CHIAPPINO, M. L. & DAWSON, C. R. (1985)
Demonstration of the mucous layer of the tear film by electron microscopy. *Invest Ophthalmol & Vis Sci.* 26(4): 464-473.

NICOLAIDES, N. (1986)
Recent findings on the chemical composition of the lipids of steer and human Meibomiam glands. In: The Preocular Tear Film in Health, Disease and Contact Lens Wear, *Editor*, Holly, F.J. (Lubbock, Texas: Dry Eye Instit): 570-596.

NORN, M. S. (1960)
Cytology of the pre corneal tear film. *Acta Ophthalmol (Kbh).* 38: 67-71.

NORN, M. S. (1963)

Foam at the outer palpebral canthus. *Acta Ophthalmol (Kbh).* 41: 531-537.

NORN, M. S. (1965)

Tear secretion in normal eyes. *Acta Ophthalmol.* 43(4): 567-573.

NORN, M. S. (1969a)

Mucous flow in the conjunctiva: Rate of migration of the mucin thread in the inferior conjunctival fornix towards the inner canthus. *Acta Ophthalmol (Kbh).* 47: 129-146.

NORN, M. S. (1969b)

Desiccation of the pre corneal film. I. Corneal wetting time. *Acta Ophthalmol.* 47(4): 865-880.

NORN, M. S. (1972)

Vital staining of the cornea and conjunctiva. *Acta Ophthalmol (Kbh) suppl.* 113: 9-66.

NORN, M. S. (1979)

Semi quantitative interference study of fatty layer of pre corneal film. *Acta Ophthalmol (Kbh).* 57: 766- 774.

NORN, M. S. (1983)

Studies of surface phenomena. In: External eye: methods of examination, 2nd Ed., (Copenhagen: Scriptor): 80-92.

NORN, M. S. (1985)

Meibomian orifices and Marx's line. Studied by Triple Vital Staining. *Acta Ophthalmol.* 63: 698-700.

NOVER, A. & JAEGER, W. (1952)

Kolorimetrische Methode zur Messung der Tränensekretion (Fluoreszein-Verdünnungstest). *Klin Mbl Augenheilk.* 121: 419-425.

OLSEN, T. (1985)

Reflectometry of the pre corneal film. *Acta Ophthalmol.* 63: 432-438.

PATEL, S., MURRAY, D., McKENZIE, A., SHEARER, D. S. & McGRATH, B. D. (1985)

Effect of fluorescein on tear break up time and on tear thinning time. *Am J Optom & Physiol Opt.* 62(3): 188-190.

POLSE, K. A. & MANDELL, R. B. (1970)

Critical oxygen tension at the corneal surface. *Arch Ophthalmol.* 84(4): 505-508.

POSTER, M. G. (1964)

Hydro-dynamics of corneal contact lenses. *Am J Optom.* 41(7): 422-425.

POSTER, M. G. & SKOLINK, A. (1974)

Effects of pH and tonicity change on some parameters on the soflens. *J Am Optom Assoc.* 45: 311-314.

POSTER, M. G., GLEFER, D. & GOODERMAN, S. (1978a)

Measuring the contact lens wetting angles in a simulated in vivo environment. *Int Con Lens Clin.* 5(1): 32-36.

POSTER, M. G., GELFER, D. & GOODERMAN, S. (1978b)

Wetting angles of hard contact lenses as related to soaking solutions. *Int Con Lens Clin.* 5(1): 166-170.

RECORDS, R. E. (1979)

Tear film. In: Physiology of the human eye and visual system. (Hagerstown: Harper & Row).

RENGSTORFF, R. H. (1974)

The pre corneal tear film: break-up time and location in normal subjects. *Am J Optom & Physiol Opt.* 51: 765-769.

RENGSTORFF, R. H. (1981)

Post wear refrative changes. In: Complications of Contact Lenses. *Editor*, Miller, D. & White, P. F. *Int Ophthalmol Clin.* 21: 85-93.

RIDLEY, F. (1928)

An antibacterial body present in great concentration in tears and its relation to infection of the human eye. *Proc Roy Soc Med.* 21: 1495.

RIDLEY, F. & SORSBY, A. (1940)

Modern trends in ophthalmology. *Editors.* (New York: Hoeber Inc).

ROLANDO, M. & REFOJO, M. F. (1983)

Tear evaporimeter for measuring water evaporation rate from tear film under controlled conditions in humans. *Exp Eye Res.* 36: 25-33.

ROLANDO, M., REFOJO, M. F. & KENYON, K. R. (1983)

Increased tear evaporation in eyes with keratoconjunctivitis sicca. *Arch Ophthalmol.* 101: 557-558.

ROLANDO, M., BALDI, F. & CALABRIA, G. A. (1986)

Tear mucous ferning test in keratoconjunctivitis sicca.

In: The Preocular Tear Film in Health, Disease and

Contact Lens Wear, *Editor*, Holly, F. J. (Lubbock,

Texas: Dry Eye Instit). Ch.18: 203-210.

RUBEN, C. M. (1975)

Contact lens practice: visual, therapeutic and

prosthetic. (London: Baillière Tindall).

RUSKELL, G. L. (1968)

The fine structure of nerve terminations in the

lacrimal glands of monkeys. *J Anat.* 103: 65-76.

RUSKELL, G. L. (1969)

Changes in nerve terminals and acini of the lacrimal

gland and changes in secretion induced by autonomic

denervation. *Z Zellforsh Mikroskop Anat.* 94: 261-281.

RUSKELL, G. L. (1971)

The distribution of autonomic postganglionic nerve

fibres to the lacrimal glands in monkeys. *J Anat.*

109: 229-242.

RUSKELL, G. L. (1976)

Motor control of lacrimal secretion. *The Optician.*

Nov 26: 13-16.

SAPSE, A. T., BONAVIDA, B., STONE Jr, W. & SERCARZ, E. E.

(1968)

Human tear lysozyme. III. Preliminary study on

lysozyme levels in subjects with smog eye irritation.

Am J Ophthalmol. 66: 76-80.

SARVER, M. D., BROWN, L. R. & RIGGERT, R. (1977)

Corneal oedema with several hard corneal contact

lenses. *Am J Optom & Physiol Opt.* 54: 231-235.

SCHIRMER, O. (1903)

Studien zur Physiologie und Pathologie der Tränenabsonderung und Tränenabfuhr. *Graefes Arch Ophthalmol.* 56: 197-291.

SCHMIDT, P. P., SCHOESSLER, J. P. & HILL, R. M. (1977)

Effect of hard contact lenses on the chloride ion of the tears. *Am J Optom.* 51(2): 84-87.

SCHULLER, W., YOUNG, W. & HILL, R. M. (1972)

Clinical measurements of the tears: viscosity. *Am J Optom Assoc.* 43: 1358-1361.

SMELSER, G. K. & OZANICS, V. (1952)

Importance of atmospheric oxygen for maintenance of the optical properties of the human cornea. Science. 115: 140.

SORENSEN, T. & JENSEN, F. (1976)

Determination of tear flow using a radioactive tracer. *Exp Eye Res.* 22: 297.

SORENSEN, T. & JENSEN, F. (1977)

Methodological aspects of tear flow determination by means of a radioactive tracer. *Acta Ophthalmol (Kbh).* 55: 726-737.

SORENSEN, T. & JENSEN, F. (1979)

Tear flow in normal human eyes. Determination by means of radioisotope and gamma camera. *Acta Ophthalmol (Kbh).* 57: 564-580.

STODTMEISTER, R., KESSLER, K. F. & SCHLÖRER, J. (1983)

Die Tränenfilmaufreißzeit bei Unterschiedlicher Anfärbung. *Klin Mbl Augenheilk.* 183: 110-114.

SZMYT, J. (1958)

Lacrimation tests. *Klin Oczna.* 28: 195-201.

TAKAKUSAKI, I. (1969)

Fine structure of the human palpebral conjunctiva with special reference to the pathological changes in vernal conjunctivitis. *Arch Histol Jap.* 30: 247-282.

TAYLOR, H. R. (1980)

Studies on tear film in climatic droplet keratopathy and pterygium. *Arch Ophthalmol.* 98: 86-88.

TERRY, J. E. (1984)

Eye disease of the elderly. *J Am Optom Assoc.* 55: 23-29.

TERRY, J. E. & HILL, R. M. (1978)

Human tear osmotic pressure: diurnal variation and the closed eye. *Arch Ophthalmol.* 96(1): 120-122.

THAYSEN, J. H. & THORN, A. T. (1954)

Excretion of urea, sodium, potassium and chloride in human tears. *Am J Physiol.* 178: 160-164.

TIFFANY, J. M. (1986)

Refractive index of Meibomian and other lipids. *Curr Eye Res.* 5(11): 887-889.

TIFFANY, J. M. (1988)

Tear film stability and contact lens wear. *J Brit Con Lens Assoc.* 11: 35-38.

TIFFANY, J. M. & BRON, A. J. (1978)

Role of tears in maintaining corneal integrity. *Trans Ophthalmol Soc U.K.* 98: 335-338.

TOMASI, T. B. (1967)

The Gamma A globulins. *Hosp Pract.* 2(7): 26-31; 34-35.

TOWNSLEY, M. (1972)

Tear layer hydraulics. *Contacto.* 2(16): 4-10.

TRIPATHI, R. C. (1975)

Applied physiology and anatomy. In: Contact lens practice; visual, therapeutic and prosthetic, Ch. 3: 24-55. *Editor*, Ruben, M. (London: Bailliére Tindall).

VANLEY, G. T., LEOPOLD, I. H. & GREGG, T. H. (1977)

Interpretation of tear film break up time. *Arch Ophthalmol*. 95: 445-448.

VOGT, A. (1921)

Atlas der Spaltlampenmikroskopie des lebenden Auges. (Berlin: Springer Verlag): 26-31.

WALKER, P. J. C. (1982)

But what about the other properties of oxygen permeable hard lens materials. *J Brit Con Lens Assoc*. 5: 98-106.

WECHSLER, S., JOHNSON, M. H., BUSINGER, U. (1983)

In vivo hydration of Hydrogel lenses - the first hour. *Int Cont Lens Clin* 10(6): 349-352.

WHITE, P. F. & MILLER, D. (1981)

Corneal oedema. In: Complications of Contact Lenses. *Editors*, Miller, D. & White, P. F. *Int Ophthalmol Clin*. 21: 3-12.

WHITNALL, S. E. (1932)

Anatomy of the human orbit and accessory organs of vision. 2nd Ed. (New York: Oxford): 209-214.

WHITWELL, J. (1958)

Denervation of the lacrimal gland. *Brit J Ophthalmol*. 42: 518-525.

WOLFF, E. (1946)

The muco-cutaneous junction of the lid margin and the distribution of the tear fluid. *Trans Ophthalmol Soc UK.* 66: 291-308.

WOLFF, E. (1954)

Anatomy of eye and orbit. 4th Ed: 207-209. (New York: Blakiston Co)

WRIGHT, P. (1971)

Diagnosis and management of dry eyes. *Trans Ophthalmol Soc UK.* 91: 119-128.

YORKE, H. C. (1971)

Determination of forces retaining a contact lens on the eye. *Brit J Physiol Opt.* 26(1): 75-87.

ZANTOS, S. G. & HOLDEN, B. A. (1978)

Ocular changes associated with the continuous wear of contact lenses. *Aust J Optom.* 61: 418-426.